THE EFFECTS OF PRIMARY ORIFICES AND OCCLUDERS ON PROSTHETIC HEART VALVE FLUID MECHANICS

by

VINH TRAN VAN

B.Sc.(Hons), 1985

A thesis submitted for the degree of Master of Engineering

in the Department of Mechanical Engineering

UNIVERSITY OF ADELAIDE

November 1995

TABLE OF CONTENT

LIST OF FIGURES

1. CHAPTER ONE

2. CHAPTER TWO

3. CHAPTER THREE

4. CHAPTER FOUR

5. CHAPTER FIVE

ABSTRACT

The use of prosthetic heart valves, to replace defective aortic or mitral natural valves, is common practice in surgery. However, implantation of these valves can cause problems for patients. Some of these problems are directly related to the nature of the blood flow through the valves. Haemolysis, arterial wall damage, thrombus formation, tissue overgrowth and high pressure drops are the most frequently observed problems. This study aims to provide haemodynamic information about prosthetic heart valves and to give an aid for future valve design and further investigation through the determination of velocity profiles, shear stresses, and pressure drops through primary orifices. The study concentrates on the influence of primary orifices and occluders on heart valve flow.

This work was carried out experimentally using Laser Doppler Anemometry (LDA). LDA has become the most popular method in recent years for the determination of turbulent phenomena through heart valve prostheses such as shear stress, velocity profile, and the extent of stagnation and recirculation regions. Pressure taps and flow meters were used for determining pressure drops, regurgitant flow and energy losses through heart valves.

Two empirical equations were established; the first deals with the estimation of pressure losses through heart valves, and second with calculation of the effective orifice area of heart valves.

In the region downstream of a valve or orifice, jet-flow can be observed with a plug-flow velocity profile, and corresponding fourth order shear stress profile. In the fully developed jet-flow region the shear stress profile is second order. Shear stress distribution depends on flow régime, and velocity profile, whereas the magnitude of shear stress is a function of axial velocity gradients and its r.m.s. component. Maximum shear stress and mean absolute shear stress occurs at the same downstream measuring plane - in the transition flow region.

Pressure losses and effective orifice area of the Jellyfish valve were calculated using the equations developed to within a 5% error as compared with experimental data.

The major conclusions are:

- The orifice area is the most important factor in the causation of shear stress, pressure drops and the extent of stagnation and recirculation regions.
- The valve can be optimised by increasing the ratio of orifice area to sewing area *(r_A):* the result of this study shows that as r_A increases from 0.4 to 0.75, pressure drop and shear stress reduces 10 and 70 fold, respectively. However, it is often infeasible to increase r_A due to the limitation of the valve size and sewing ring requirements: hence r_A must be optimised, whilst maintaining flow area, by adapting the orifice shape and the occluder type and position.
- The comparison of maximum velocity gradient and shear stress in heart valve prostheses at a fixed position is not practical. Mean absolute shear stress should be compared within the transition flow region of the valves.

SIGNED STATEMENT

This work contains no material which has been accepted for the award of any other degree or diploma in any university or other tertiary institution and, to the best of my knowledge and belief, contains no material previously published or written by another person, except where due reference has been made in the text.

I give consent to this copy of my thesis, when deposited in the University Library, being available for loan and photocopying.

Vinh Tran

ACKNOWLEDGMENT

Firstly, I would like to thank and express my sincere gratitude to Dr. G. D. Tansley, my supervisor and director of studies. He has helped and encouraged me very much during this study, especially during the times when I had difficulties. He has provided a great deal of guidance and direction for this project. I appreciate very much the effort and time which he has devoted to me to finished this project. Thanks also to Mrs E. Tansley for help in proof reading my thesis.

I am grateful to Professor M. Zockel for useful advice in designing test equipment and to all the staff of Mechanical Engineering for providing laboratory space, equipment, technical support and finances.

I am grateful to all the technical staff for technical support, most especially, Mr H. Bode, Mr. G. Osborne and Mr. M. Bethune for assistance with experimentation, Mr. A. Mitler, Mr. S. De Ieso and Mr. J. May for support with computational equipment, and Mr. R. Jager and Mr. C. Price for the manufacture of test equipment.

I would like to thank The G.K. Williams Cooperative Research Centre for Extractive Metallurgy at The University of Melbourne for use of their LDA, especially, Mr. Wei Yung and Mr T Berrigan, and also Associate Professor Y. Morsi at The Swinburne University of Technology. Without the use of this LDA, I would not have finished my project in time. I appreciate very much the time Mr. Wieng Wand. has spent for me.

Many thanks also go to my friends and colleagues, especially, Mr. K C Ang and Mr Ninh Nguyen who have encouraged and helped me during this study.

Thanks must go to my family, my parents, my wife and children who have encouraged and supported me and I really appreciate their tolerance, especially my wife's, whilst I was studying in Australia.

I also acknowledge, with thanks, the financial support of the Australian Government through the *Aus*AID programme. Without this I would not have had a chance to study and finish this work.

AIMS

There are many studies in literature which have investigated fluid mechanics of prosthetic heart valves. Therefore, this study focuses on investigating primary orifice flow with aims as follow:

- To investigate prosthetic heart valves and the effects of primary orifices on prosthetic heart valve fluid mechanics using experimental techniques.
- To establish how much of the disturbance in heart valve flow is due to orifice configuration (different area, shapes and positions of the primary orifices).
- To establish empirical equations to determine effective orifice area and pressure losses through heart valve prostheses.
- To establish the relationship between pressure drops, velocity and shear stress fields.
- To investigate the Jellyfish heart valve with measured and calculated data to check the accuracy of the model found in this study and to establish the effects of the occluder type on flow phenomena.
- Finally, to find and explain what causes the most significant disturbance in heart valve flow and give an aid for future heart valve design and recommendations for future work.

NOMENCLATURE

Symbol	Meaning	Unit
A	sewing ring area	cm^2
A_0	tube area	cm^2
A_{Actual}	actually measured orifice area	cm^2
$A_{Effective}$	effective orifice area	cm^2
$A_{Effective\ concentric}$	effective orifice area of concentric orifices	cm^2
$A_{Effective\ eccentric}$	effective orifice area of eccentric orifices	cm^2
A_{Real}	effective orifice area (A_{Actual}) corrected via calculation	cm^2
C_s	the mean (flow parameter)component of a segment	
C_i	the instantaneous components contained within a segment	
C	discharge coefficient	
$C_{Position}$	position coefficient, measured and calculated	
C_{Shape}	shape coefficient	
C_P	pressure coefficient	
C_{PE}	pressure coefficient dependent primarily on eccentricity	
C_{Pr}	pressure coefficient dependent primarily on area ratio	
C_{PR}	pressure coefficient dependent primarily on Reynolds number	
$C_{P\ Shape}$	Pressure coefficient dependent primarily on shape	
D	tube diameter	mm
D	ball occluder diameter	mm
d	distance from lens to windows *Equation 3-6*	mm
d	orifice diameter	mm
d	sensor diameter	µm
d_f	laser fringe spacing	µm
E	eccentricity percentage	
E	hydraulic efficiency	
$E\%$	relative energy loss	

f	Darcy friction factor	
$f(\pi_i)$	transformation functions	
F	focal distance	mm
i	counter: 1, 2, ..., n	
k	exponential constant in dimensionless products	
L	tube length	mm
L_{max}	maximum length of the initial jet-flow	mm
l	mixing length	mm
l	length (generally along axial axis)	mm
l	hot-wire sensor length	mm
m	number of measured cycles	
n	number of measured data points	
N	refractive index	
P	wetted perimeter (Equation 5-13)	mm
P	pressure	Pa
PI	performance index	
$P_{Downstream}$	static pressure in the downstream region	Pa
P_d	dynamic pressure	Pa
$P_{Maximum}$	upper limit of pressure transducer range	kPa
P_s	static pressure	Pa
P_t	total pressure	Pa
$P_{Upstream}$	Static pressure in the upstream region	Pa
Q	flowrate	m^3/s
Q	flow volume in pulsatile flow	m^3
q	flowrate in pulsatile flow	m^3/s
$Q_{Regurgitant}$	regurgitant flow volume	m^3
$Q\%$	relative regurgitant flow	
r	pertaining to the radial direction	
r	correlation factor	
r	radial position	mm
r_A	ratio of orifice area to tube area	
Re	Reynolds number	

S	slope of ΔP and Q^2/d^4 relationship; *Equation 2-2*	
t	thickness of the window	mm
T	time of a cycle	s
T_1	time of period of forward flow (systole)	s
T_2	time of period of closing phase	s
T_3	time of period of closed phase	s
TI	turbulence intensity	
U	time averaged velocity	m/s
U	mean axial velocity	m/s
u	instantaneous axial velocity	m/s
u'	fluctuating axial velocity	m/s
u'_1 and u'_2	fluctuating velocities measured at ±45° relative to axial direction	m/s
v	instantaneous tangential velocity	m/s
v'	fluctuating tangential velocity	m/s
V	mean tangential velocity	m/s
w	instantaneous radial velocity	m/s
w'	fluctuating radial velocity	m/s
W	mean radial velocity	m/s
x	distance in axial direction	m
x	pertaining to axial direction	
α	half angle of two laser beams intersection	
α	angle of laser beam with normal direction of a surface	
δ	partial differential	
$\delta\%$	accuracy of pressure transducers	
δP	absolute error of pressure transducers	kPa
Δ	denotes a difference or gradient	
ΔE	energy loss	W
ΔP	pressure drop	Pa
ΔP_0	overall pressure loss	Pa
θ	pertaining to the tangential direction	

Φ_{Shape}	shape factor	
λ	wavelength of laser light	nm
μ	dynamic viscosity	Pa s
ν	kinematic viscosity	m^2/s
π_d	dependent dimensionless product	
$\pi_1, \pi_2, \ldots, \pi_n$	independent dimensionless products	
ρ	density	kg/m^3
σ_U	axial velocity standard deviation	m/s
σ_V	tangential velocity standard deviation	m/s
τ	shear stress	Pa

1. CHAPTER ONE: INTRODUCTION

1.1 General introduction

The human heart is the organ in the human body which plays the most important role in circulating blood around the body. The heart in conjunction with heart valves causes the blood to flow in one direction and dysfunction of the heart or heart valves can be fatal. Open heart surgery is common practice in remediation of these conditions - where the heart or valves may be replaced or repaired. Minor cardiac surgery and heart valve remediation have been practiced for seventy years or so; the first successful heart treatment was dilation of a stenotic mitral valve using the fingers. This was performed by Souttar in 1925. Following the advent of heart-lung bypass machines, open heart surgery enabled heart valve replacement and donor organs transplantation. The first prosthetic heart valve was implanted successfully in humans by Starr and Edwards in 1960 (Starr and Edwards, 1961) and nowadays, prosthetic heart valve implantation is widespread and common clinical practice in medical centres and nearly 75,000 prosthetic heart valves are implanted in humans annually throughout the world.

Though prosthetic heart valves have been used for a long time, cardiac patients still continue to suffer from numerous pathological problems. These problems are directly related to the fluid dynamics of artificial heart valves. For example, high shear stresses cause haemolysis and endothelial damage (Hellums *et al.* 1977), stagnation, recirculation regions and low shear rate may lead to thrombus formation and tissue overgrowth, and high pressure gradients cause high energy loss and may lead to dysfunction of the heart (Hanle *et al.* 1989). In these cases, fluid dynamics plays a very important role in understanding and analysing the pathological problems of these prostheses.

The presence of the prosthesis disturbs the flow of blood producing areas of high shear stress, high wall stress and separated flow regions, which cause pathological problems to the valve's recipient. The sewing ring and occluder are the two main components of a prosthesis which cause the greatest stenosis and obstruction. The intensity of flow disturbance through heart valves strongly depends on structure and geometry of the sewing ring and occluder.

It is evident, that investigating the fluid dynamics of heart valve flow is a very important stage in designing a heart valve. There are two major methods for investigating fluid dynamics of heart valve prostheses, viz computational and experimental. The computational techniques can provide a full picture and relatively good approximations of velocity and stress distributions in a flow field. However, the limited memory capacity of contemporary computers impedes them in giving accurate results, especially in complicated flows and flows in intricate geometries. Measurements using experimental techniques, especially using Laser Doppler Anemometry (LDA) techniques in heart valve flow, provide much valuable and accurate information of flow through heart valves in both steady and pulsatile flow conditions. However, such experimental techniques can not provide a full picture of the flow or the distribution of turbulent flow phenomena.

This study was carried out using experimental techniques. Heart valve flow was examined by investigating primary orifice flows. The effects of the orifice area, orifice shape, and orifice and occluder position on velocity and shear stress fields and pressure drops across heart valves were investigated. Pressure drops across orifices were measured using pressure taps, and analysed using dimensional analysis to establish empirical equations such as pressure coefficient and effective orifice area for comparison of several heart valves. Instantaneous velocities were measured using LDA, from which shear stresses and turbulence intensities were calculated.

The aims of this study were to:

- investigate prosthetic heart valves and the effects of primary orifices on prosthetic heart valve fluid mechanics using experimental techniques
- establish how much of the disturbance is due to orifice configuration (different area, shapes and positions of the primary orifices)
- establish empirical equations to determine effective orifice area and pressure losses through heart valve prostheses
- establish the relationship between pressure drops, velocity and shear stress fields
- investigate the Jellyfish heart valve with measured and calculated data to check the accuracy of the model developed in this study and to establish the effects of the occluder type on flow phenomena
- explain what causes the most significant disturbances in heart valve flow and give an aid for future heart valve design and recommendations for future work.

1.2 Description of the human heart and its valves

The heart is a very important organ functioning as a pulsatile synchronous pump which beats about 72 times each minute and transports about 6 l/min of blood at rest to about 25 l/min during extreme exertion. The heart with the lungs provides the oxygen requirements of the human body by maintaining the circulation of blood. There are two separate circulations, a greater or systemic circulation through the body, and a lesser or pulmonary circulation through the lungs. The purpose of the systemic circulation is to carry oxygen and nourishment to all parts of the body and to remove carbon dioxide and other waste products of metabolism from tissues. The purpose of the lesser circulation is to carry deoxygenated blood from the right ventricle to the lungs where its carbon dioxide is liberated and oxygen absorbed (see Figure 1-1).

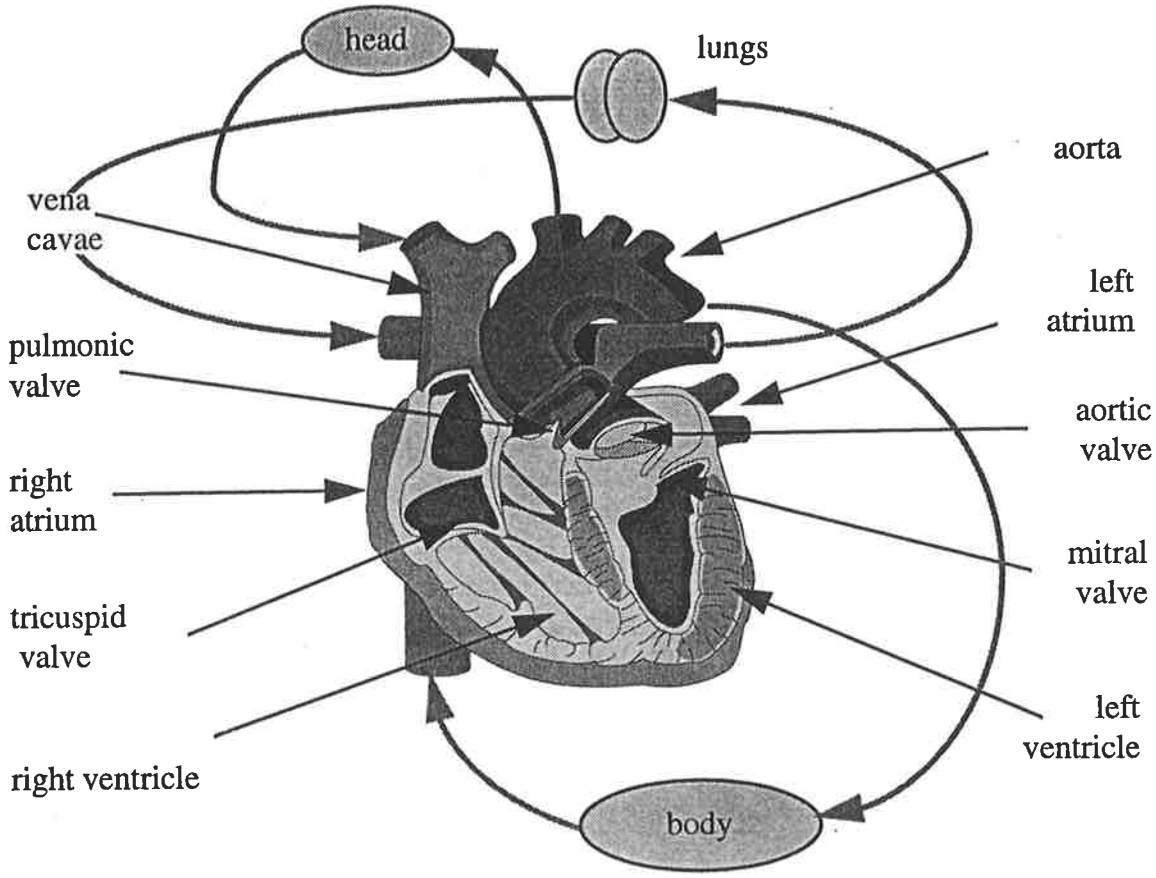

Figure 1-1 Human heart with two circulations

The heart has four chambers: two ventricles and two artria. The two ventricles are pumping chambers and the two artria are receiving chambers. Corresponding to the four chambers, the human heart has four valves: aortic, mitral, tricuspid and pulmonary. The action of these four heart valves within the heart restricts blood flow to one direction and prevents substantial backflow.

Blood returning from the body is deoxygenated and flows through the venae cavae to the right atrium. This blood flows further through the tricuspid valve into the first pumping chamber called the right ventricle. Blood in the right ventricle is pumped through the pulmonary valve and the pulmonary artery into the lungs where the blood becomes oxygenated. Blood then flows into the left atrium, then fills the left ventricle through the mitral valve. This filling phase of the cardiac cycle is called diastole. When the diastolic cycle is finished, the left ventricle contracts abruptly, the mitral valve closes and blood is pumped through the aortic valve. This phase of the cardiac cycle is called ventricular systole. Left and right ventricular systole occur simultaneously as do left and right diastole. Pressures on the left side are 5 times greater than those on the right side, hence the left hand valves (mitral and aortic) fail more readily. As a result, both mitral and aortic incompetence are common valvular defects (a valve is incompetent when it fails to close properly, producing a jet of blood to flow retrogradely through the valve when it should be shut). Another common valve defect is stenosis. This is a narrowing of the valve which impedes forward flow of blood through the valve. Both of these conditions are indications for valve replacement.

In the natural heart, the valve leaflets open at the centre to allow unobstructed central flow. The aortic and pulmonary valves are outlet valves, each consisting of three cusps attached to a fibrous tissue ring on the inner walls of the aorta and pulmonary artery respectively. Both outlet valves have similar dimensions. The mitral and tricuspid valves are inlet valves, the tricuspid valve has three similarly sized cusps whereas mitral valve has one major leaflet and one minor leaflet.

1.3 Outline of the present study

This study focuses on the disturbance caused by primary orifices in prosthetic heart valve fluid flow and the effects of the structure of the orifice and occluder on the fluid dynamics of the valve. Chapter One presents the most general introduction, the aims of this study, the human heart, heart valves and their functions in the human body.

In Chapter Two, the literature is reviewed. Details of heart and heart valve prostheses can be observed, such as the most commonly used heart valves, the history and development of heart valve prostheses, and surgery. Problems related to heart valve fluid dynamics are analysed briefly in *section 2.4* to impress the importance of investigating heart valve fluid dynamics for the development of future valve design. Furthermore, orifice and heart valve flows are reviewed, *in-vitro* measurements made by several investigators of flow through different heart valves are analysed and compared in terms of fluid dynamics, and in conjunction with the structure of each valve. This leads to the conclusion that the valve configuration is an important factor to affect fluid flow downstream of the valve. The review of orifice flows and their further investigations may explain the disturbance caused by the presence of different valve configurations in blood flow. Finally, conclusions leading to objectives of this study are drawn and presented.

Chapter Three is concerned with the methodology and instrumentation which were needed for this study. Firstly, several methods are reviewed and compared allowing the choice of the one which was the most appropriate for this study. Experimental methods using LDA (Laser Doppler Anemometry) pressure and flow measurement techniques were chosen for this study. LDA has recently become the most commonly used technique for measuring turbulence phenomena in fluid flow, especially in heart valve flow. Several experimental set-ups and instruments which were used for this study are presented and described.

Data analysis in this study is a vital stage in presenting and clarifying the work, as this study was carried out experimentally. Chapter Four mentions some analysis techniques and equations used to analyse pressure drop, LDA velocity measurements and their products in both steady and pulsatile flows, eg. a 5° binning analysis was used for pulsatile flow data to calculate mean and fluctuating components; dimensional analysis was used for pressure drop measurements to generate empirical equations. Furthermore, some equations for calculating shear stresses, regurgitant flow and energy losses are presented.

Chapter Five presents the results and discussions of this study. Firstly, pressure drop data are analysed and discussed, two empirical equations are established for valve design and comparison. The effects of the orifice area, orifice shape and position on pressure drops, velocity and shear stress fields are analysed and established.

Furthermore, a valve prototype called the Jellyfish valve is investigated to establish the effects of the occluder type on pressure drops, velocity and shear stress fields. The effects of the occluder oscillation and the presence of the struts on pressure drops, velocity and shear stress fields are also established.

The conclusion, recommendations and clinical significance of this study for further heart valve design and investigation in terms of fluid dynamics are given in Chapter Six. The verification of experimental techniques is also presented in this chapter to validate the results of this study. The last two sections contain appendixes and a reference list. In the first appendix, the index-matching box, test section and orifice designs are shown. Papers published by the author are attached in *Appendix 2*. Results with raw and analysed data such as pressure drops and LDA velocity measurements across orifices are attached in *Appendixes 3* and *4*.

2 CHAPTER TWO: LITERATURE REVIEW

2 .1 Introduction

This chapter will go through the main aspects of prosthetic heart valves. Firstly, the history of valve surgery and replacement is presented with the development of prosthetic heart valves. It looks at the description of different heart valves, especially commonly used heart valves. Secondly, pathological complications are discussed which are directly related to fluid dynamics such as haemolysis, thrombus formation, tissue overgrowth and endothelial damage. A review of orifice flow is necessary, as well as of the valves, since stenotic orifice flow causes problems related to fluid dynamics. This chapter also introduces details and results of the tests and evaluation of prosthetic heart valves with a historical perspective. Furthermore, some criteria for good prosthetic heart valves are presented which all valve designs should exhibit if they are to yield reliable performance and patient safety. Finally, conclusions leading to objectives of this study are presented.

2 .2 History of valve surgery and replacement

Experimental cardiac transplantations were carried out in animals from the beginning of this century. In 1905, the first cardiac transplant was performed by Carrell and Guthrie, in dogs, at the University of Chicago. The best survival period for a dog was two hours. Along with others, Mann in 1933 and Demikhove in 1956 carried out their experiments in animals and reported survival durations were 8 and 32 days, respectively. Much later, in 1980, Reitz and Shumway reported their experiments in monkeys with 311 day survival (Lansman *et al.* 1990).

The first clinical surgery was successfully performed by Souttar in 1925 who used his finger to dilate a stenotic mitral valve, this practice continued until 1959 when the transventricular dilator was introduced (Mazumdar 1992).

In 1953 the first prosthetic heart valve (the caged ball type) located in the descending aorta of patients was implanted by Hufnagel (Hufnagel *et al.* 1954) without the use of a heart - lung machine. Unfortunately, this surgery was not successful because the valve was not able to prevent regurgitant flow from the aorta and was also prone to a high incidence of thrombus formation.

In 1960, the first prosthetic heart valve was successfully implanted in humans by Starr and Edwards using the caged ball valve in the position of the mitral valve (Starr and Edwards 1961). Since then, heart valve surgery and prosthetic heart valve implantation have become common clinical practice in medical centres throughout the world.

2 .3 Prosthetic heart valves

Prosthetic heart valves were introduced in the early 1950s; the caged ball type was the first to be designed. In the late 1950s and early 1960s, Hufnagel, Bahnson, McGoon, Kay, Muller and many others developed new valve designs with the occluder of flexible leaflets for implantation within the heart, but clinical use of these valves was limited (Harken *et al.* 1960 and 1962). Tissue fabricated valves have also been introduced, which aim to duplicate the flow behaviour of natural valves. These valves are good for short term use, but for long term are not satisfactory due to the valve failure through calcification, leaflet degeneration, material fatigue, structural deterioration and eventual valve stenosis. However, this valve type (eg. pericardial and porcine tissue heart valves) are closer to the natural form and show advantages over mechanical heart valves in that patients with tissue valve do not need to use anticoagulant therapy (Chandran *et al.* 1984; Bortolotti *et al.* 1987; Reul *et al.* 1990; Purinya *et al.* 1993 and Chew *et al.* 1993). The calcification of the valves may be eventually solved by biological and chemical intervention (Pathak *et al.* 1990). Mechanical failure of the valves may be reduced by modification of the stent and cusp geometries (Krucinski *et al.* 1992).

Because of the problems associated with the material of the flexible leaflets used as valve occluders, Starr and Edwards developed prosthetic heart valves with rigid components, returning to the caged ball principle. However, the caged ball showed a disadvantage as its central occluder requires a lot of space which leads to anatomical complications in some recipients (Thalassoudis 1987). In an attempt to overcome the problems of the ball valve (eg. improve haemodynamics and reduce weight), the caged disc valve was introduced in 1965 (Hufnagel and Conrad 1965) but this valve type proved the most obstructive of all prosthetic valves. The problems were associated with the occluder of the valve, consequently a new valve design, the tilting disc valve, was introduced and several developments of this type have been made since most of them showing improvements.

In 1977 St. Jude Medical Inc. introduced a bileaflet pivoting valve which consists of two similarly sized semicircular leaflet occluders: it exhibited the least obstructive flow (Hanle *et al.* 1989). This valve type has become very successful and there are numerous references to it in the literature. All the mechanical heart valve prostheses are more durable and their performance is more predictable than bioprosthetic valves. However, the flow patterns produced by mechanical heart valves is an unnatural form, thus they are more prone to thrombosis and patients usually require long-term anticoagulant therapy (Chew *et al.* 1993).

Since 1960, about 50 different cardiac valves have been introduced, many of them have been discarded due to lack of clinical success. The most commonly used basic types of prosthetic valves at present are: (1) caged ball; (2) tilting disc; (3) bileaflet pivoting disk, and (4) tissue bioprosthesis (Hanle *et al.* 1989). A typical mechanical prosthesis consists of four basic components: (1) occluder; (2a) cage, (2b) strut or (2c) hinge; (3) sewing ring, and orifice ring (see *Figure 2-1*).

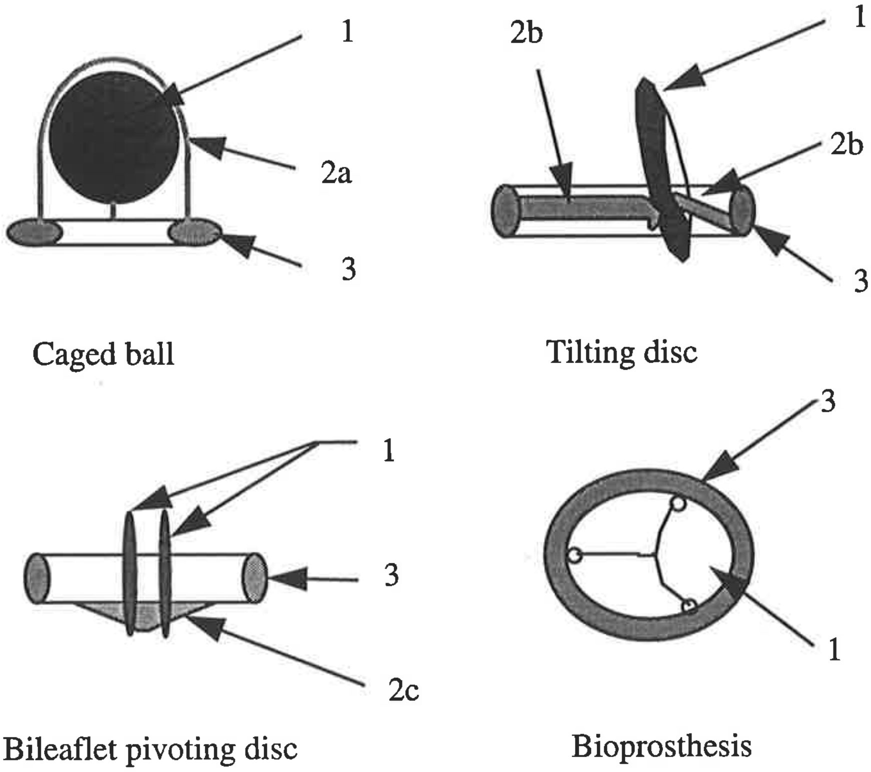

Figure 2-1 The most commonly used basic types of heart valve prostheses

The occluder, with the orifice ring, takes the role within the heart of allow forward flow when the valve is open and prevent substantial backflow when the valve is closed. The cage, strut, or hinge retains and guides the motion of the occluder in a fixed condition. The cage, strut or hinge and sewing ring are attached to the orifice ring in which the occluder moves under action of blood flow. Blood flows through the orifice when the valve opens and is sealed by the occluder in conjunction with the orifice ring, when the valve closes. The presence of these elements such as the sewing and orifice rings cause a stenosed section and leads to higher pressure gradients across the prosthesis. Having such a ring also induces larger blood shear stresses which will increase haemolytic potential. The presence of the occluder causes jet issue especially in mechanical valves, impingement, stagnation and eddy regions will occur which promote thrombus formation and tissue overgrowth (Tansley 1988).

As can be seen from the literature, all artificial heart valves show drawbacks related to fluid dynamics. These drawbacks depend on the structure and geometry of the valves (Hanle *et al.* 1989). For example, caged ball heart valves show high pressure drops, high shear stresses and a large stagnation region in the near vicinity downstream of the heart valve. Because the ball occludes the central flow region it causes a small orifice area. The occluder is relatively heavy so that it causes high pressure drops and energy loss. Furthermore, the ball causes a large stagnation and recirculation region which leads to a large ratio of maximum velocity to average velocity (ie. high velocity gradients) and correspondingly high shear stresses (Hanle *et al.* 1989).

The tilting disc heart valves have two regions of unequal area available for forward flow viz the major and minor flow orifices. These cause very eccentric velocity profiles in the near vicinity downstream from the valve, which generates a large wake behind the disc occluder and causes high velocity gradients. These imply that high shear stresses and pressure drops are produced in the near vicinity downstream of the valve (Hanle *et al.* 1989). The flow performance of the tilting disc valves is considerably worse than that of caged ball valves, on an equal orifice basis (Gentle 1977). Furthermore, because of the eccentric flow downstream of the valve, the extent of the turbulent phenomena depend on the orientation of the valve, as a result, this valve should be orientated during implantation (Chandran *et al.* 1984 and Walker *et al.* 1989).

On the other hand, St. Jude bileaflet valves have two similar semicircular leaflets, when it opens the leaflets rotate out to an angle of 85° leaving an orifice that is 85-90% free from obstruction to flow. These leaflets divide the base ring orifice of the valve into three regions. Two of these regions are themselves roughly semicircular in shape and represent about 80% of the area available for forward flow, the third region is located in the centre. This valve induces minimal occlusion, small velocity gradients and symmetrical velocity profiles and leads to small pressure drops and shear stresses (Hanle *et al.* 1989).

The occluders of the three above-mentioned heart valves are different and generate different flow patterns. The tilting disc heart valves generate the highest mean and fluctuating velocity gradients and also generate the highest shear stresses. These are attributed to the considerable eccentricity of the forward flow generated by the tilting disc. The ball occluder produces a large central obstruction leading to small orifice flow, large pressure drops and high wall shear stresses. Whereas bileaflet occluders have some advantages over other two occluder types - such as minimal obstruction leading to large orifice area, low pressure drops and shear stresses and near axial flow patterns.

2 .4 Pathological complication

Though heart valve prostheses have been used for several decades, the problems associated with these prostheses have not been totally eliminated. The most serious problems and complications associated with heart valve prostheses are: (a) thromboembolism; (b) tissue overgrowth; (c) infection; (d) tearing of sewing sutures; (e) red cell destruction; (f) valve failure due to material fatigue or chemical change; (g) damage to the endothelial tissue; (h) large pressure gradient across the valve, and (i) leaks caused by failure of the valve to close properly. Problems (a), (b), (e), (g), and (h) are directly related to the fluid dynamics (Woo *et al.*, 1983) and will be discussed in detail in the next sub-sections.

2 .4 .1 Haemolysis

Haemolysis is red blood cell damage due to mechanical forces acting within the fluid. Blood cells in a region where shear stresses are elevated within the surrounding fluid will experience a distribution of shear stress over their entire membrane. Consequently, the blood-cell membrane will be stretched and may suffer irrevocable changes harmful to its essential function. Sub-haemolytic injury, or damage to blood cells occurs commonly in prosthetic valve recipients. Haemolysis occurs due to disturbance of the valve causing high shear stresses.

Shear stresses are used to indicate the propensity of a valve to damage the blood (Hanle *et al.* 1989; Woo *et al.* 1983 and Tiederman *et al.* 1986). *Table 2-1* shows the effects of shear stresses on blood cells and endothelium by experimental observations of several investigators.

Estimates for shear induced in-bulk haemolysis threshold values have varied widely, from 150 to 4000 Pa (Leverett *et al.* 1972 and Tansley *et al.* 1988). Leverett *et al.* in 1972 considered shear stress and exposure time to be the two primary determinants for in-bulk haemolysis. Blood trauma does not occur when blood is exposed for a very short duration even to very high stresses; but exposure for a long duration with much lower stress levels can cause lysis. Furthermore, blood trauma can occur at values as low as 150 Pa in heart valves as flight-time through valves allows sufficient exposure to take cells beyond their lysis threshold (Leverett *et al.* 1972 and Tansley *et al.* 1988).

Table 2-1. The effects of shear stresses on blood cells and endothelium

shear stress	Result
40 Pa	Damage to endothelial cells (Fry 1968)
90 Pa	Erosion of endothelial cells (Fry 1968)
150 - 4 000 Pa	Damage to red blood cells (Leverett *et al.* 1972; Hellums and Brown 1977; Lutz and Barras 1983 and Tansley *et al.* 1988)

2 .4 .2 .Thrombosis

Thrombosis is defined as the formation of a blood coagulum within a vessel or the heart. The presence of prosthetic heart valves in blood flow produce thrombus formation (Yoganathan *et al.* 1981), eg. the downstream side of an occluder type valve, such as caged disk and caged ball, is a region of potential thrombus formation. The low velocity and recirculation regions increase the probability of thrombus formation. The incidence of thrombus formation from prosthetic heart valves, especially from mechanical heart valves represents a major threat to patients. Consequently, intense anticoagulation therapy is mandatory with any mechanical valve implant (Hanle *et al.* 1989 and Chew *et al.* 1993). High shear stress and turbulence are also triggers of thrombus formation (Huang *et al.* 1994).

The complications that can arise from thrombosis of a prosthetic valve are:

- thrombotic stenosis - when a thrombus blocks the prosthesis partially thus inhibits the valve's performance
- thromboembolic events - when a part of the thrombus breaks off the main thrombus body and is carried by the blood into the small arteries of a vital organ such as the heart, kidney or brain causing temporary or permanent damage (Mazumdar 1992).

2.4.3 Tissue overgrowth

Yoganathan and his co-workers in 1981 observed tissue overgrowth and thrombus formation on a caged ball valve during autopsy. The presence of cage, strut and sewing ring increases the probability of thrombus formation and tissue overgrowth. Tissue overgrowth occurs due to valve stenosis and high pressure drops across the valve.

Low velocity regions of blood flow generally favour tissue overgrowth. This phenomenon is still not understood, however, high blood flow and the associated effects of blood scouring may play a role in limiting or preventing tissue overgrowth (Thalassoudis 1987). Generally in prosthetic heart valves, the occluder, sewing ring and supplementary elements produce a high disturbance in the blood flow, where separation and recirculation occur. The flow stagnation and low shear stress regions are more prone to thrombus formation and tissue overgrowth than areas of high shear stresses (Yoganathan *et al.* 1981 and Huang *et al.* 1994).

2.4.4 Endothelial damage

The endothelium is the wall membrane of the aorta, blood vessels and body cavities. Endothelial damage occurs due to high wall shear stresses and also increases the potential for thrombus formation (Hanle *et al.* 1989 and Huang *et al.* 1994). Generally, the presence of the orifice ring with the occluder (caged-ball, caged disc or tilting disc) causes a significant increase in velocity gradients in the proximal portions of the aorta. This implies that higher wall shear stress can be observed along the wall of the aorta. In 1968, Fry indicated experimental measurements to determine threshold wall shear stress at which damage and erosion of endothelial cells occurs (see *Table* 2-1).

2.5 Test and evaluation of prosthetic heart valves

Test and evaluation of prosthetic heart valves is one of the most important stages in heart valve design. It assesses the valve's performance and whether or not the valve can be implanted in humans, when the valve is implanted what effects can be attributed to the presence of the valve?

Many researchers have made *in-vitro* measurements of prosthetic heart valves. Firstly, they have judged the fluid mechanical performance of the prosthetic heart valves by measuring the pressure drops and retrograde flow rates across them and by observing the flow pattern around them using flow visualisation. Flow visualisation techniques were applied first to heart valve assessments by Weiting in 1969, Duff in 1970. Following these early investigations, researchers have used visualization techniques to investigate the flow characteristics of valves. These techniques can provide only qualitative information which is useful but not necessary for the comparison of the various designs and modifications of the prosthetic valves (Woo *et al.* 1983). Pressure drop in steady flow is the first indication of acceptability of prosthetic heart valves (Reul *et al.* 1987) and can give an aid for future valve design (Gentle 1977). Therefore, many investigators have focused on pressure drop measurements eg. Forrester *et al.* (1969); Kaster *et al.* (1970); Gentle (1977); Yoganathan *et al.* (1978); Knoch *et al.* 1988; *Hanle et al.* (1989) and many others.

In 1978, Yoganathan and his co-workers measured *in-vitro* velocity profiles and wall shear stresses in the near vicinity of prosthetic aortic heart valves using a Laser Doppler Anemometer (LDA), later the same group (Yoganathan *et al.* 1979a, 1979b and 1979c) measured and compared the different kinds of aortic prostheses and their modifications (for example, since 1960 the Starr-Edwards valves have had several modifications leading to models: Starr-Edwards 1200; 1260; 2320 and 2400). Chandran *et al.* (1985a and b) measured turbulent flow phenomena in caged ball and tilting disc valves in pulsatile flow using LDA. Nandy and Tarbell (1988) measured wall shear stress of a trileaflet valve using hot film anemometer. Hanle *et al.* (1989) compared the most four commonly used heart valve types, especially the effects of the occluder of these valves on velocity and shear stress fields. Teijeira and Mikhail in 1992 investigated flow phenomena of different valves, especially regurgitant flow and energy losses. Other researchers eg. Sergio *et al.* (1985), Thalassoudis (1987), Tansley (1988), Huang *et al.* (1994) and many others studied the same parameters using Computational Fluid Dynamics (CFD). These works have focused on:

- Pressure drops - high pressure drops favour tissue overgrowth and cause large energy loss which may lead to malfunction of the heart and heart valves. Teijeira and Mikhail (1992) considered pressure gradients to be the most important factor to be considered during the design of a valve.
- Shear stresses - high shear stresses cause haemolysis and the threshold level of shear stresses for haemolysis in a free jet is around 400-500 Pa. But blood trauma can occur at a value of 150 Pa when subjected to prolonged exposure (Hellums and Brown 1977; Leverett *et al.* 1972; Lutz and Barras, 1983 and Tansley *et al.* 1988).

- Velocity profiles - jets forming downstream of a prosthetic heart valve are deleterious to a valve's proper functioning. Stagnation and separation regions could lead to thrombus formation and tissue overgrowth (Woo *et al.* 1983 and Huang *et al.* 1994).
- Shear rates - low shear rates increase thrombus formation and can lead to valve dysfunction or embolism (Tansley 1993).

2 .5 .1 In-vitro measurements and comparisons of prosthetic heart valves

The comparison of the hydrodynamic *in-vitro* with the *in-vivo* measurements of the normal human valves is very problematical, as it is very difficult to measure *in-vivo* exactly enough for comparison with the *in-vitro* results (Heiliger 1987). However, *in-vitro* measurements and prediction using computational and experimental techniques of flow parameters of different valves can be compared with each other to chose the best valve.

The use of different blood analogue solutions as the medium for *in-vitro* tests could lead to some differences, especially in laminar and low velocity flow regions. However, aspects of non-Newtonian blood flow in prosthetic valve studies and the use of different analogue solutions in the prediction of flow parameters in highly turbulent and complex flow regimes should lead to accurate representations of the *in-vivo* situation (Tansley 1993). As a result, many studies have focused on *in-vitro* measurements using experimental techniques with analogue solutions for the purpose of comparison of different heart valves for pressure drops, velocity and shear stress fields, regurgitant flow and energy losses.

2.5.1.1 *Pressure drops*

Pressure drops measurements under both steady and pulsatile flow conditions are widely reported in literature. Pressure drops in steady flow were compared for different valves with the same size, whereas pressure drops in pulsatile flow were used for calculating energy losses and mean systolic pressure gradients to correlate steady data. Pressure drop measurement is one of the most important stages in assessing heart valve prostheses. Thus many investigators have focused on this component measurement eg. Forrester *et al.* (1969) measured pressure drops through fifteen different types of aortic prostheses under steady flow condition, Kaster and his co-workers (1970) compared the Lillehei-Kaster pivoting disc aortic valve with four other prosthetic heart valves under pulsatile flow conditions, Yoganathan *et al.* (1979a) measured and compared pressure drops across ten different prosthetic aortic heart valves under both steady and pulsatile flow conditions. Many other researchers have measured pressure drops, eg: Yoganathan *et al.* (1981); Heiliger (1987); Hanle *et al.* (1989).

Pressure drops were also compared to determine the effects of different viscosities on the results eg. pressure drops across ten prosthetic heart valves were measured under both steady and pulsatile flow conditions using two different Newtonian liquids having different viscosities and results showed no differences caused by the use of different liquids as test media (Yoganathan *et al.* 1979a).

Generally, pressure drops were measured and analysed for effective orifice area using the Gorlin and Gorlin (1951) formula and valves were compared for effective orifice area and efficiency index (Chandran *et al.* 1984); Heiliger 1987 and Hanle *et al.* (1989). A more complete comparison could be afforded by applying a constant of linear proportionality between pressure drop and square of flowrate/unit area as suggested by Gentle (1977). He condensed pressure drop versus square of flowrate/unit area (Q^2/d^4) and linear regression revealed a slope. The efficiency of the valves was defined as the ratio of the slope of an ideal orifice to that of the valves (Gentle 1977). Pressure drops across an ideal orifice are condensed in the following form:

$$\Delta P = 1775\frac{Q^2}{d^4} \qquad \textit{(Equation 2-1)}$$

where Q is flowrate in l/min and

d is the orifice diameter in mm.

In a similar form, condensed pressure drops of any valve types are follows:

$$\Delta P = S \times \frac{Q^2}{d^4} \qquad \textit{(Equation 2-2)}$$

where S is the slope of the ΔP and Q^2/d^4 relationship of the valves.

The hydraulic efficiency E of the valves can be written as:

$$E = \frac{1775}{S} \times 100\%. \qquad \textit{(Equation 2-3)}$$

As mentioned before, the comparison between *in-vitro* and *in-vivo* results is very difficult. However, the Gentle method can give an ideal not only for the comparison of valve against valve, but also against a theoretical value. This procedure can give an aid for future valve design.

2.5.1.2 Velocity profiles

Low velocity and recirculation flow regions increase the probability of thrombus formation (Figliola and Mueller 1981), stagnation and separation regions could lead to thrombus formation and tissue overgrowth and jets forming downstream of a prosthetic heart valve are deleterious to a valve's proper functioning (Woo *et al.* 1983). High velocity gradients imply high shear stresses (Hanle *et al* 1989). Furthermore, shear stress measurements stem from velocity measurements as velocities can be divided into two components, mean and fluctuating; two orthogonal fluctuating components are used for calculating turbulent shear stresses which cause effect on blood cell. The mean velocities are plotted to determine the stagnation and recirculation regions which promote thrombus formation and tissue overgrowth and may lead to dysfunction of the valves. This need for heamodynamic information has lead to velocity profiles in heart valve prostheses being investigated extensively and comparisons made with similar studies.

Velocities of flow through heart valve prostheses have been measured under both steady and pulsatile flow conditions and generally using hot-wire anemometry and LDA techniques. Yoganathan *et al.* (1981) compared velocity profiles of the Starr-Edwards aortic ball valve with the ball occluder tied and untied using LDA and found that the oscillation of the occluder reduced the extent of the stagnation and recirculation region, however, shear stress and pressure drops were increased. This region could encourage thrombus formation and tissue overgrowth on the apex of the cage and along struts of the ball valve. Hasenkan *et al.* (1988) compared velocity fields downstream of six mechanical aortic valves in a pulsatile flow model using a hot-film anemometer probe. Hanle *et al.* (1989) measured and compared velocity profiles of four valve types using LDA. These valves had the same orifice diameter, but different occluders so that they had different effective orifice areas. The tilting disc valve generated very high mean velocity gradients because of the considerable eccentricity of the forward flow generated by the tilting disc. Whereas the St. Jude Medical bileaflet valve produced the lowest mean velocity gradients due to having the highest effective orifice area and concentric forward flow. On the other hand, bioprosthetic valves generated the highest velocity gradients due to the triangular shape of the valve when the valve was fully open (see *Table* 2-2).

2.5.1.3 Shear stresses

The presence of a prosthetic heart valve in blood flow produces disturbances and high shear stresses which lead to blood trauma in valve recipients. Therefore, many studies in literature have focused on shear stress measurements. Yoganathan (1979a) measured *in-vitro* velocities in the near vicinity of the Björk-Shiley aortic prosthesis using LDA. The Reynolds shear stresses were calculated from u' and v', the axial and tangential fluctuating components, respectively. The maximum shear stress was estimated to be 100 Pa. Later, the same group (Yoganathan *et al* 1979b and c) made measurements of the Starr-Edwards aortic ball valve and reported a maximum shear stress of 175 Pa from u and v components.

Woo *et al.* in 1983 investigated *in-vitro* fluid dynamic characteristics of the Abiomed trileaflet heart valves (Number 25 and 21 valves) and reported maximum shear stresses of 220 and 450 Pa in the immediate vicinity of the number 25 and 21 valves, respectively. These values exceed the threshold shear stress value of 150 Pa for blood trauma.

In 1985 Walburn and Stein measured flow parameters in a Hancock porcine bioprosthetic aortic valve under pulsatile flow condition, the instantaneous shear stresses were calculated from u'_1 and u'_2 components where u'_1 and u'_2 are the fluctuating velocities measured at $\pm 45^{\circ}$ relative to the direction of the mean flow in the horizontal plane; in other words, shear stresses are calculated from u' and w' components, axial and radial, respectively. They reported a maximum shear stress of 254 Pa.

Hanle and his co-workers in 1989 measured and compared four different types of prosthetic valves such as the Björk-Shiley (tilting disc valve), Smeloff-Cutter (double-caged ball valve), St. Jude Medical (bileaflet valve) and Ionescu-Shiley (bioprosthesis). They reported the bileaflet valve having smallest turbulent shear stress of 76 Pa and bioprosthesis valve having highest shear stress of 128 Pa in comparison with those of other three valves (see *Table 2-2*).

2.5.1.4 *Backflow and energy losses*

Backflow occurs during the closing and closed phase of the valves' cycle. Leakage gaps may lead to increased haemolysis because of higher shear stresses within the gap flow and within the turbulent mixing region of the backflow jet. The leakage jet velocities are about 3 to 5 times higher than the peak velocities during systole (Knott *et al.* 1988). For example, the tilting valves exhibit 3 leakage jets which correspond to the one central and two peripheral gaps. No such leakage jets were observed with the ball valves since, in the closed position, there are no gaps between the silastic ball and the housing rim. Woo *et al.* (1983) measured regurgitant flow and energy losses of two Abiomed valves (size number 21 and 25) and reported regurgitant flow of 0.7% and 2.8% of total cardiac output. These values are small in comparison with 8.4% and 14% of the Björk-Shiley and St. Jude Medical mechanical valves, respectively.

Energy loss is the product of flowrate and pressure drop, and occurs in three distinct stages. For example, in the aortic position, these three energy losses are: (a) resistance of forward flow during systole; (b) reverse flow during closing and (c) leakage flow during the closed phase (Teijeira and Mikhail 1992). Knott and his co-workers (1988) considered leakage flow and energy loss to be the most serious source of cell damage and thrombus formation. *In-vitro* energy losses indicate that as much as 10% of the ventricular energy can be lost by each mechanical prosthesis. Energy losses in the first stage by mechanical heart valve prostheses is always larger than those in other two stages and ranks from 40 to 60% of total energy losses (Teijeira and Mikhail 1992).

2 .6 Review of orifice flow

The orifice is one of the oldest known devices for measuring and regulating the flow of fluids, chiefly water. It is known that when fluid flows through an orifice a pressure gradient can be observed, this pressure drop is proportional to the velocity of the flow or flowrate through the orifice. This effect is used for measuring fluid flow by devices known as an orifice meter.

Flow is measured by recording pressure drops across the orifice as the presence of the orifice in the flow causes pressure gradients between up and downstream of the orifice. *Figure 2-2* shows static pressure distribution along a tube into which an orifice is installed. Close to the inlet of the orifice, the static pressure in the pipe increases slightly and reaches its maximum value at the entrance to the orifice. The pressure of fluid drops abruptly as it flows through the orifice and, on the outlet side, the pressure continues to decrease.

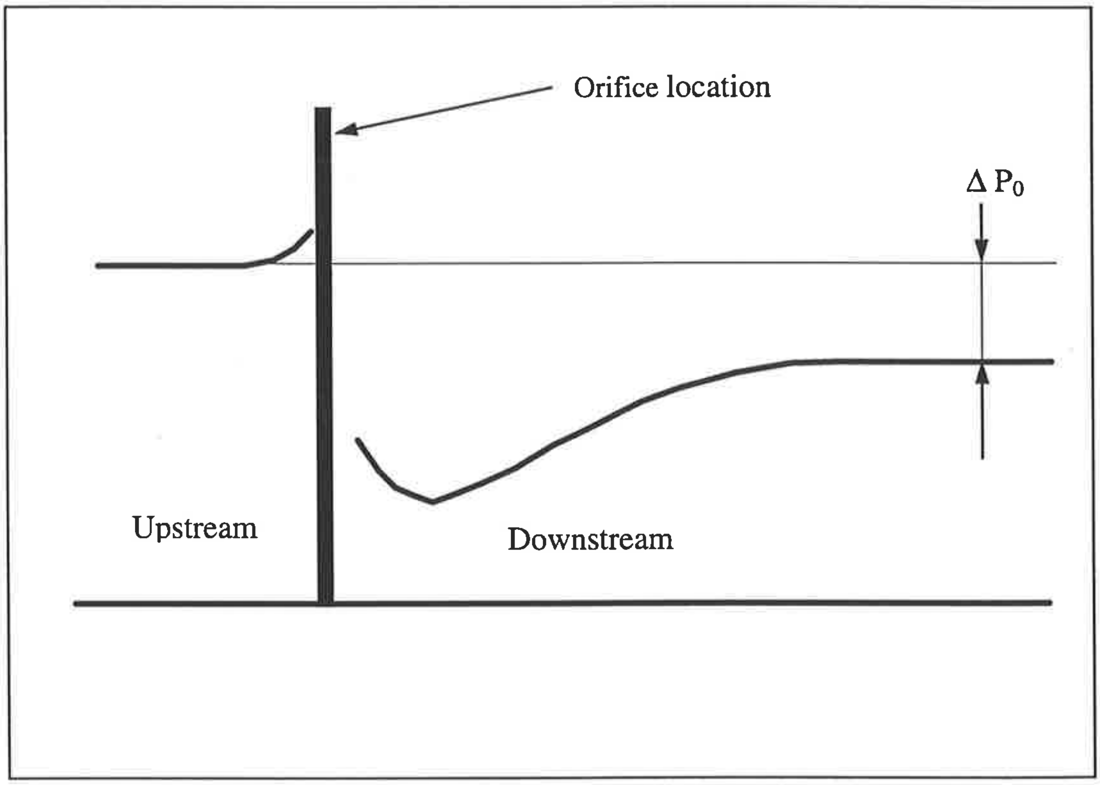

Figure 2-2. Static pressure distribution through an orifice

The minimum value of static pressure is reached at a short distance from the outlet side of the orifice. Beyond this minimum point the static pressure increases again, at first slowly, then rapidly and reaches the second point of maximum value several diameters downstream of the orifice plate, this phenomenon is referred to as pressure recovery. Consequently, ΔP_0 is the overall pressure loss, which is less than the non-recovered pressure drop. This point is called as the point of the maximum pressure restoration. For all the concentric orifices, the point of maximum pressure restoration occurs at a distance of 4 pipe diameters downstream of the orifice, and for the special orifices eg. eccentric and segmental, the maximum restoration of the pressure occurs at the distance of no less than 5 pipe diameters from the plane of the orifice (Horace *et al.* 1916).

Pressure gradients through orifices strongly depend on the orifice-to-pipe diameter ratio and flowrate (Gerhart and Gross 1985). The more the diameter ratio increases, the less pressure gradient can be observed. However, for the same diameter ratio but for different orifice types such as the Venturi tube; the concentric thin-plate orifice, and the eccentric and segmental orifice the pressure drop exhibits different values. The overall pressure loss through the eccentric orifice is largest and the pressure drop through the thin-plate orifice is somewhat larger than through the Venturi tube (ASME 1959). This may mean that the eccentric and segmental orifice causes more disturbance in the flow downstream of the orifice than the concentric orifice does. Furthermore, pressure drops depend on the roughness of the orifice and the tube surface (Clark, 1965). The flow régime upstream of the orifice (eg with or without straightener, the position of the straightener and elbow in the test configuration), and the position of the orifice installed in the pipe also caused effects on flow measurements (ASME 1935, Scott *et al.* 1993, and Scoot and Lewis 1994).

In conclusion, there are many investigators in literature who have studied pressure drops and losses across orifices. None of them have focused on velocity and shear stress fields and the relationship between pressure drops, shear stress and velocity fields in the vicinity downstream of the orifices. Therefore, this study shall investigate the effects of the primary orifices on pressure drops, velocity and shear stress fields in the vicinity downstream of the orifices and to apply these effects on heart valve fluid flow.

2 .7 Criteria of a good prosthetic heart valve

In order to allow a prosthetic valve to satisfy long-term effectiveness in clinical application, Henze *et al.* (1973) considered that a good prosthetic valve to must fulfil the following design criteria:

- It must be fabricated of chemically inert materials that are tissue compatible, reasonably atraumatic to blood elements, and nonthrombogenic.
- It must be durable enough to retain physical and geometric properties over many years of usage.
- It must present minimal obstruction to the forward flow of blood in the open position.
- It must open and close quickly in response to alterations in pressure gradient, and be relatively competent in the closed position.
- Its permanent fixation must be technically feasible, safe and secure over many years.
- The valve should not annoy the patient by being noisy and it should not require the patient to modify his or her lifestyle appreciably.

2 .8 Conclusion and objectives

Table 2-2 shows Hanle *et al.'s* work from 1989, and as can be seen the occluder plays a very important role in determining flow patterns and flow characteristics of the valve. The ball valve presents the most obstructive area in comparison with those of the three other valve types, it leads to the highest pressure drops, but shear stresses are not the highest.

The tilting disk and tissue valves show the highest shear stresses as the tilting valve produces eccentric flow, whereas tissue valves generate the highest velocity gradient due to the triangular shape of the orifice when the valve is fully open. Pivoting disk valves have the largest flow area producing the lowest pressure drops, shear stresses and velocity gradients.

Table 2-2. Dependence of flow phenomena on flow configuration. From Hanle et al (1989)

Valve types	Effective area (cm^2)	Pressure drops (kPa)	Shear stresses (Pa)	Velocity gradients (m/s)
Ball	2.17	Highest (2.2)	78	Lowest (1.2)
Tissue	2.57	1.3	Highest (128)	Highest (2.4)
Tilting	2.71	1.4	112	1.6 and low region
Pivoting	3.00	Lowest (1.0)	Lowest (76)	1.4

In conclusion, orifice area can reduce dramatically the flow turbulent phenomena such as pressure drop, velocity gradient and shear stress. Furthermore, the orifice shape and position are important factors in reducing such effects on blood flow through valves. Pressure gradient does give enough information about shear stress. Eccentric flow and high velocity gradient imply high shear stress which are unaccounted for (or not predicted) by pressure gradient. In terms of orifice flow, the effects of several factors such as diameter ratio; roughness of the orifice surface; upstream régime and structure; and orifice types on pressure drop and flow measurements were investigated carefully. However, none of the orifice studies have focused on velocity and shear stress fields and the relationship between pressure drops, shear stress and velocity fields in the vicinity downstream of the orifices.

2 .9 Directions for this study

The above discussion lends direction to this study, which focuses on two major topics:

- Investigation of the effects of the orifice area, shape and position; and occluder position on fluid dynamics of the valves by measuring velocity profiles and pressure drops across different orifices.
- Investigation of a newly designed valve called the Jellyfish valve, to establish the effects of the occluder on pressure drops, velocity and shear stress fields (the Jellyfish valve has a special occluder which is a flexible membrane attached to the centre of the orifice ring).

3. CHAPTER THREE: METHODOLOGY AND INSTRUMENTATION

This chapter deals with two major themes: firstly, different techniques which may be used for investigating heart valve flow, are reviewed to select suitable techniques for this study; and secondly, instruments and experimental set-ups which were used as major techniques in this study are described.

3.1 Review of possible techniques

The success of a given prosthetic heart valve design is based on many criteria. One important set of criteria is the fluid mechanical characteristics of the valve design. There are many approaches used for solving flow problems in heart valves. These approaches fit into three broad categories: numerical, analytical and experimental; each approach has distinct advantages and unique disadvantages. In the sections which follow, some techniques which may be used for investigating fluid flows in valves are described.

3.1.1 Computational Fluid Dynamics

Numerical and analytical methods are referred to here as Computational Fluid Dynamics. These methods are based on algebraic equations, These methods usually lead to a vast number of finite-difference or finite-element equations which are solved by computer.

The Navier-Stokes equations describing fluid flow are partial differential equations. These equations cannot be solved by analytical methods as these methods can only be applied to simple flow configurations. Such flow situations do not occur in prosthetic heart valve flow. Heart valve flow is either undeveloped-laminar or turbulent (Tansley 1988). As a result, the use of analytical methods in heart valve flow is very restricted.

Numerical methods offer solutions to differential equations to solve problems in fluid flow of prosthetic heart valves. Detailed understanding of flow characteristics at every point of the flow field in heart valve prostheses can be obtained by numerical simulation (Huang *et al.* 1994). Unfortunately, the standard computational numerical methods are restricted in their ability to solve turbulent fluid flow, especially pulsatile flow because the requirements of excessive storage space and run time make it impractical in existing computers (Tansley 1988). However, CFD can offer some advantages over experimental methods as follows:

- In small space where experimental techniques are impossible to access.
- In real blood and near to the wall or occluder surface where results gained experimentally are influenced.
- A full picture of the flow field in heart valve prostheses can be obtained.
- CFD is relatively cheap and time saving for valve design.

3.1.2 Experimental techniques

An extremely important and (potentially more) reliable approach is experimentation which is able to deal with different flow problems and flows in complicated geometries. However, experimental techniques are not capable of providing a full picture of a flow field, they can only give information where the probe was inserted and measurements taken. Due to the limitation of experimental apparatus and the structure of prosthetic heart valves, it is very difficult to experimentally measure flow parameters in the immediate vicinity of the valves (Huang *et al.* 1994). Nevertheless, experimental methods are usually used as a tool for assessing heart valve flow; sufficient care is needed so that results are valid and that measurement processes do not unduly affect the fluid mechanics being observed. Experimental methods also find application in verifying computational methods; the two different approaches are complimentary with CFD filling in gaps in measured data and experimental results verifying correctness of computational models.

Since prosthetic heart valves have been used clinically, many investigators have investigated the fluid mechanical performance of valves. Firstly, flow visualisation technique was applied for observing the flow patterns around valves. Pressure drop and retrograde flowrate measurements across valves have been carried out since the late 1960s. These techniques were good but not able to provide all of the necessary information for comparison of various valve designs (Yoganathan *et al.* 1978). Consequently, since the 1970s many fluid dynamical measuring techniques have been adapted to measuring velocities and determining shear stress fields in the near vicinity of prosthetic valves eg. hot-wire anemometers or hot-film anemometers (Figliola 1976); Laser Doppler Anemometers (LDA) (Wang 1977 and Yoganathan. 1978) and Doppler ultrasound anemometers (Jorgensen *et al.* 1973). All of these techniques are still used to investigate fluid flow in heart valves. In order to elaborate further, some experimental techniques are discussed, in the following sections, for their limitations and capabilities.

3.1.2.1 Flow visualisation

Patterns of fluid flow in heart valves can be observed using flow visualisation techniques, eg streaklines, wherein small tracer particles such as powders, emulsions, gas bubbles or beads are seeded into the flow. As these tracers pass through an illuminated section the paths they prescribe are recorded by photographic film or video. Flow visualisation experiments in Woo *et al.* (1983) were performed to provide a good qualitative description of the flow field of heart valve prostheses. Moreover, by, observing the whole flow field of the valve it was possible to decide where to conduct the detailed quantitative LDA measurements. However, the flow visualisation technique can provide only qualitative information of the flow. This information is very useful but not good enough for comparison of flows of various valves (Yoganathan *et al.* 1978 and Yoganathan *et al.* 1979c). Many flow visualisation techniques are applicable to the assessment of heart valve flow and the reader is referred to JSME, 1988 for more details.

3.1.2.2 Pressure drop measurements

Pressure tappings are made in the side of the test section wall, one upstream and one or more downstream of the valve. Pressure measuring devices such as U-tube and pressure transducers are connected to the taps to measure directly either pressure difference across the valve or gauge pressure above atmospheric, then pressure drops across the valve are calculated from the difference between upstream and downstream static pressures. In this study, piezoresistive strain-gauge transducers were used for measuring up and downstream static pressures. Energy loss measurements are calculated as the product of pressure drop and flowrate measurements.

Pressure drop measurements are still used as the definitive classifier of the valve haemodynamic performance. These techniques are very cheap and simple to apply for static pressure gradient and pressure recovery information. However, pressure drop measurements alone are not enough for providing information about haemolysis, thrombus formation and tissue overgrowth caused by the presence of the valve in the flow. Thus, velocity measurement techniques were introduced to produce more information of the valve haemodynamic performance.

3.1.2.3 Velocity measurements

The major techniques commonly used for velocity measurements in the literature are: Pitot-static tube; thermal (hot-film and hot-wire) anemometry; Laser Doppler Anemometry (LDA) and Ultrasound Doppler. These are briefly discussed below.

3.1.2.3.1 Pitot Static Tube

The Pitot tube is the most traditional velocity measuring instrument, its mode of operation is based on Bernoulli's equation:

$$P_t = P_s + P_d = P_s + \rho \frac{U^2}{2}$$ *(Equation 3-1)*

where P_t : is total pressure

P_s is static pressure

P_d is dynamic pressure

ρ is the density of the flow medium

U is the (axial mean) velocity to be assessed.

Static and total pressures are obtained by a probe called a Pitot-static tube, which is placed into the flow field. Static and dynamic pressures are gained by nozzles 1 and 2, respectively (see *Figure 3-1*). The difference between these two pressures is proportional to ½ ρ U^2.

When a Pitot-static tube is used for measuring velocities, some conditions must be considered such as: (a) the tube should be aligned within about $\pm 10^{\circ}$ of the flow direction; (b) the root mean square intensity of turbulence in the stream should be smaller than 5% of the mean velocity; (c) the total pressure does not change more than 1 to 2 % across the tube diameter; (d) the probe is not too near to the wall, (d) the probe size is not so large as to interfere with the flow velocity significantly (Bradshaw 1975).

Velocity fluctuations cannot be measured with a Pitot-static tube, but Pitot-static tubes are generally used as calibration references because the accuracy of these measurements is about 0.25% and higher than other techniques eg. hot-wire and LDA.

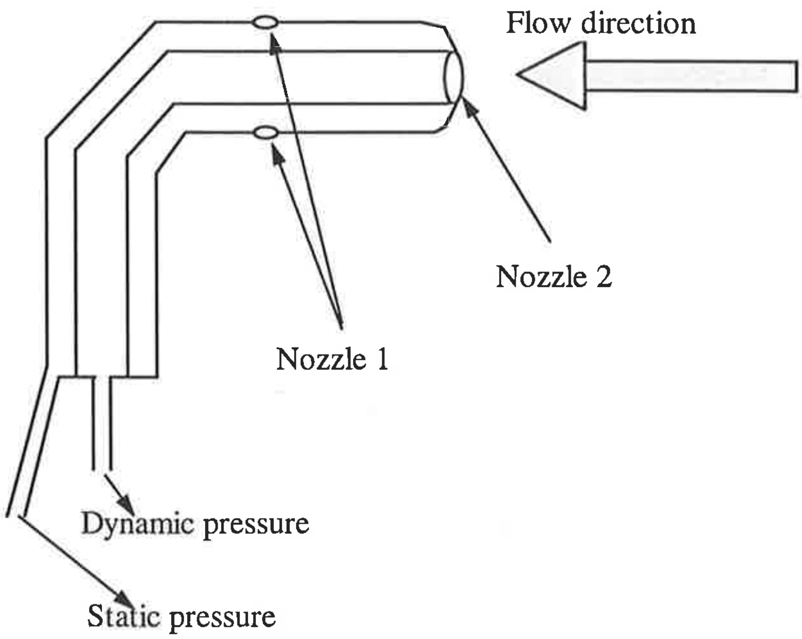

Figure 3-1. Pitot static tube

3.1.2.3.2 Hot-wire or hot-film anemometers

Hot-wire or hot-film anemometers rely on a heated body. The temperature of a heated body in a flow depends on the velocity of the flow into which the heated body is inserted, so that velocity can be measured by calibrating in terms of temperature. Early hot-wire probes suffered the disadvantages that they could not be used in liquid or in fact in any flow environments more hostile than a standard laboratory wind tunnel. This problem has now overcome by the introduction of coated probes or hot-film probes (Lomas 1986).

Figure 3-2 shows a typical hot-wire probe. It consists of a wire sensor whose ends are welded onto the tips of two support needles. These two support needles are supported by the probe body. The wire sensor is usually made of Tungsten or Platinum, about 1 mm long *(l)* and 5 µm in diameter *(d)*. Generally, the ratio of *l* to *d* is between 200 and 400. The diameter is limited by the need for an adequate electrical resistance and by the need for the wire to respond to rapid fluctuations in heat transfer due to changes in velocity.

The sensors of hot-film probes are usually made of Nickel or Platinum deposited in a thin layer onto a backing material, such as Quartz, and connected to the electronics package by leads attached to the ends of the film. A thin protective coating of Quartz is deposited over the film to prevent damage by chemical reaction.

There are three types of electronics packages (Lomas 1986) which are used to control the sensor heating current in different modes. Firstly, the most common is the constant temperature anemometer which supplies a heating current that varies with the fluid velocity to maintain constant sensor resistance, thus constant sensor temperature. Secondly, and less often used, is the constant current anemometer which supplies a constant heating current to the sensor, this type has the disadvantage of suffering from thermal inertia. The third type is the pulsed wire anemometer which measures velocity by momentarily heating a wire to heat the fluid around it.

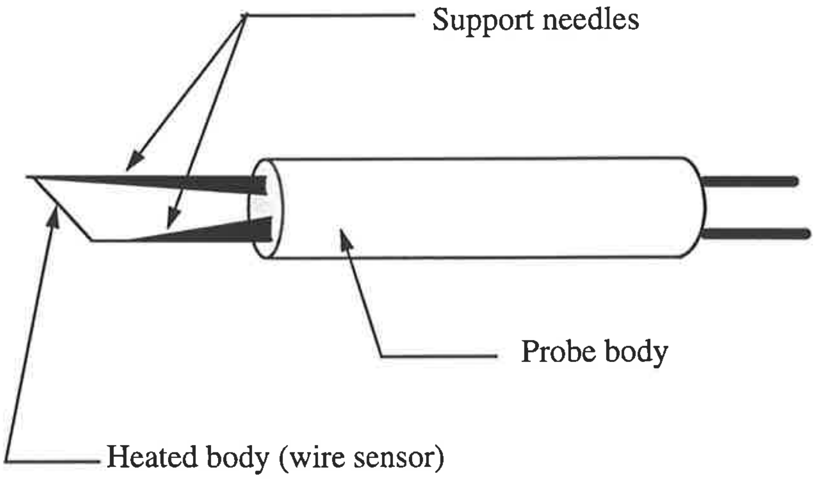

Figure 3-2. Typical hot wire probe

Hot-wire or hot-film anemometry can be used for measuring not only the velocity, but also the direction of the flow and fluctuations. This technique is very well established, widely accepted and relatively cheap to install. It is a simple technique and can be used in opaque media. The technique will yield velocity and Reynolds shear stresses and wall shear stresses. However, there are some disadvantages such as the sensor is sensitive to dust in air and slime in liquid, so that frequent recalibration is necessary; and the probe insertion complicates the test section geometry. Furthermore, the probe insertion into the flow channel perturbs the flow and may lead to erroneous results.

3.1.2.3.3 Laser Doppler Anemometer (LDA)

Laser Doppler anemometry is based on the Doppler effect; which is caused by moving the source of the light or the receiver. This effect can be used for measuring particle velocity. When a particle moves and passes through the light, it represents the moving receiver and causes the Doppler effect. This Doppler effect is detected and analysed to calculate the particle velocity.

LDA relies on the scattering of light by microscopic particles in the fluid flow. The most popular LDA system uses the two beam correlation method. Two laser beams cross and cause an intersection and fringes (see *Figure 3-5*). As a particle moves through the region of interference fringes it will scatter light, whose intensity will vary according to the light intensity variations inside the bisector of the two beams. The returned signal contains a varying amplitude superimposed on to a high frequency signal, the frequency of which is inversely proportional to the velocity of the particle These light intensity variations are detected by a photodetector and processed by signal processing system.

Figure 3-3 and *Figure 3-4* show two typical optical configurations and their basic components in back- and forward-scatter mode, respectively. An LDA system, in back- or forward-scatter mode, always consists of five main components: a laser source; beam-splitter; frequency shifter; photodetector; and signal processor. A beam from the laser source passes through the beam-splitter to become two beams which then cross each other to make the intersection in the flow channel (the measurement volume). A frequency shifting system is mounted next to the beam-splitter and is used to: reduce the percentage of frequency change in highly turbulent flows; optimize frequency, reduce fringe bias and increase the accuracy of measurements. The frequency shift system is designed to increase the application range of LDA by shifting the frequency of the laser light; this permits the measurement of: reversing flows; low velocity convective flows; vortex and recirculation flows; pulsatile flows; and velocity components perpendicular to the mean flow direction. This system consists of two separate components, namely the an acousto-optic cell (called a Bragg cell) and a downmix circuit (TSI incorporated 1986).

The last two components are the photodetector and signal processor. Two types of detectors are commonly used, photodiodes and photomultipliers. For high light level and small band width laser sources, photodiode detectors are the most satisfactory. Photodiodes have the advantage of being small in size and relatively inexpensive; they do not require any high-voltage power supply as do photomultiplier tubes and are usually used under daylight conditions without any optical screening. At low light levels and wide band width in high speed-flow measuring situations, photomultipliers are superior (Durrani and Greated 1977). The photodetector's function is that of collecting Doppler signals to the signal processor where the signals are filtered, amplified and processed to calculate mean velocities, turbulence intensities and shear stresses.

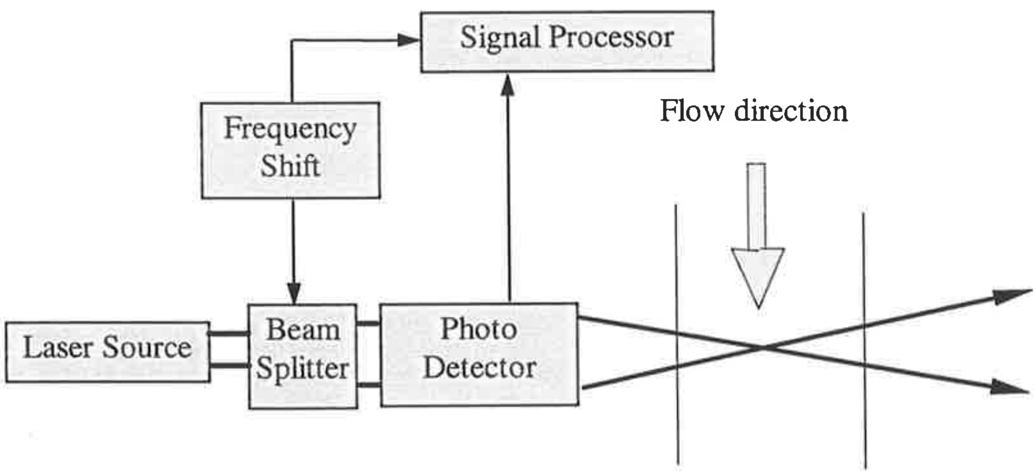

Figure 3-3. Typical back scatter mode optical configuration and basic components

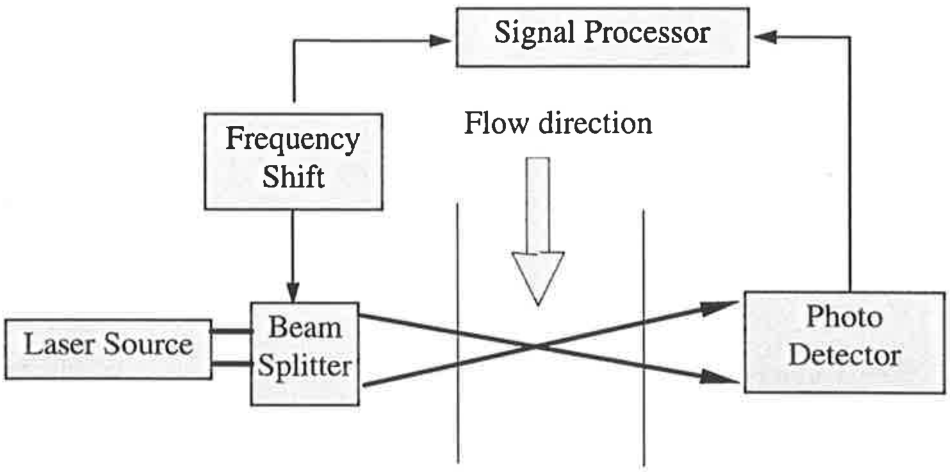

Figure 3-4. Typical forward scatter mode optical configuration and basic components

There are two basic types of signal processors: counters and Burst Spectrum Analysers (BSA). Counter-type signal processors work by counting the number of cycles in a fixed time or measuring time at a preselected number of cycles. BSA is a simple method of analysing signals from LDA systems, at which Doppler signals are analysed by direct spectral analysis (Durrani and Greated 1977).

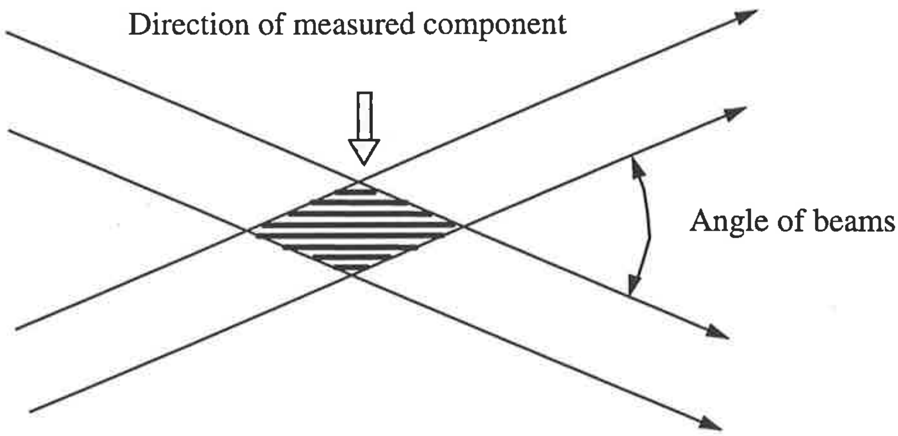

Figure 3-5. Two beam intersection

LDA has many advantages over other techniques, however, accurate flow measurements strongly depend on the following conditions: particle concentration and size in the fluid; quality of optical systems; the sensitivity of photodetectors; the signal processor; and the alignment of the optics (TSI incorporated 1985).

In order to get accurate flow measurements with LDA, the conditions of particles in the fluid are as follows:

- The particle is spherical and small in size compared with the smallest wave-length of the fluid motion.
- The pathlines of the particle and fluid coincide, no over-shooting takes place.
- The flow is not perturbed by the presence of the particle (Durrani and Greated 1977).

LDA can be used for measuring velocities, shear stresses and turbulence intensities in both steady and pulsatile flow conditions. Furthermore, these measurements can be established in three dimensions in coincidence windows. However, LDA cannot easily be used to measure fluid velocities in opaque media (Stern 1985). Distortion of the control volume by refractive index mismatching can occur leading to either measuring in the wrong place or false results.

LDA can be used for measuring fluid velocities in opaque media eg. blood flow by introducing the self-mixing effect technique (Slot *et al.* 1992 and Mito *et al.* 1993). Like ultrasound Doppler, fibre-optic LDA using the self-mixing effect technique can be used for *in-vivo* measurements due to the small size of fibres. LDA has a high spatial resolution in comparison with other techniques eg. ultrasound Doppler. However, one of the shortcomings of this technique when measuring in blood flow, is the fact that LDA using the self-mixing effect measures invasively, whereas for example ultrasound Doppler anemometers can measure noninsavely (Slot *et al.* 1992).

3.1.2.3.4 Ultrasound Doppler

Like LDA, this technique relies on the Doppler principle, as particles pass through the reference beam a Doppler shift is created in the reflected beam. The magnitude of the shift is proportional to the velocity of the particles. Unlike LDA, the beam is of ultrasound waves. This technique can be used for yielding information about heart valve flow *in-vivo*. However, a major disadvantage of ultrasound Doppler method compared to the other techniques is poor spatial resolution, because the size of the control volume yielded by ultrasound Doppler is very large, consequently, the results are very noisy and inaccurate; and due to a lot of the smaller scale turbulence information, velocity profiles cannot be accurately assessed (Hughes and How 1994).

In conclusion, the LDA technique offers many advantages over other techniques: (a) it requires no probes to be inserted into the flow channel; (b) requires no calibration whatsoever; (c) has a high signal/noise ratio and therefore can be used with good accuracy to measure velocities in highly disturbed flow fields like in heart valve flow; (d) can be used with good accuracy to measure velocities close to prosthetic valves and to the walls of flow channel; (e) has a high frequency response (at least 10^5 Hz); (f) can distinguish between forward and reverse flow directions (Yoganathan *et al.* 1979b) and (g) Reynolds stresses can be obtained through the use of coincidence of two orthogonal velocity component measurements. Like other techniques, such as hot-film anemometry and ultrasound Doppler anemometry, LDA using the self-mixing effect can be used for measuring blood flow both *in-vitro* and as well *in-vivo*.

3.1.2.4 Flow metering

Flowrate through prosthetic heart valves is measured under both steady and pulsatile flow conditions. There are three popular flow meter types applied to prosthetic heart valve flow measurements, these are floating, turbine and electro-magnetic flow meters. Floating and turbine meters are suitable for measuring steady flow, whereas electro-magnetic meters are suitable for measuring in both steady and pulsatile flows.

The floating meter (Rotameter) is the most basic flow meter type consisting of a body, which is floated in a conical tube at a level proportional to the flowrate through the tube. The turbine flow meter relies on the movement of a turbine inserted into the flow. This movement is proportional to flowrate through the turbine which is then converted into flowrate electrically or mechanically. The electro-magnetic meter works by the Hall effect where an electrically conducting fluid, passing through a field of magnetic flux, generates an EMF proportional to flowrate through the meter.

3.1.3 Summary of measurement techniques

After viewing the different approaches for solving fluid flow problems, experimental methods seem to be the most suitable for prosthetic heart valve flow; as the flow through heart valve prostheses is complicated and the geometry is not simple for modeling and solving flow problems using CFD. Therefore, this study was carried out using experimental techniques such as LDA for measuring velocities, shear stresses and turbulence intensity; pressure taps and flow meters for measuring pressure losses, flowrate and energy losses.

3.2 Experimental set-up and instrumentation

In the next sections, some experimental set-ups and instruments used in this study are presented. Laser Doppler anemometry, pressure transduction and flow meters were used as the major research tools throughout this study.

3.2.1 Steady flow circulatory system

Steady flow generated by two small centrifugal pumps circulated through artificial valve and orifices and was returned, via a floating flow meter to an open sump. Flow was also straightened by a flow straightener installed at about 30 tube diameters upstream of valve or orifice location, so that the flow before entering the valve or orifice was fully developed, turbulent tube flow (see *Figure 3-6*). Valves and orifices were inserted into a plain acrylic tube of internal diameter of 19 mm which was placed in the refractive index matching box (*see Figure 3-8,* or for more detail see *Appendix 1*). A blood analogue fluid of water-saline solution was used in all the *in-vitro* experiments.

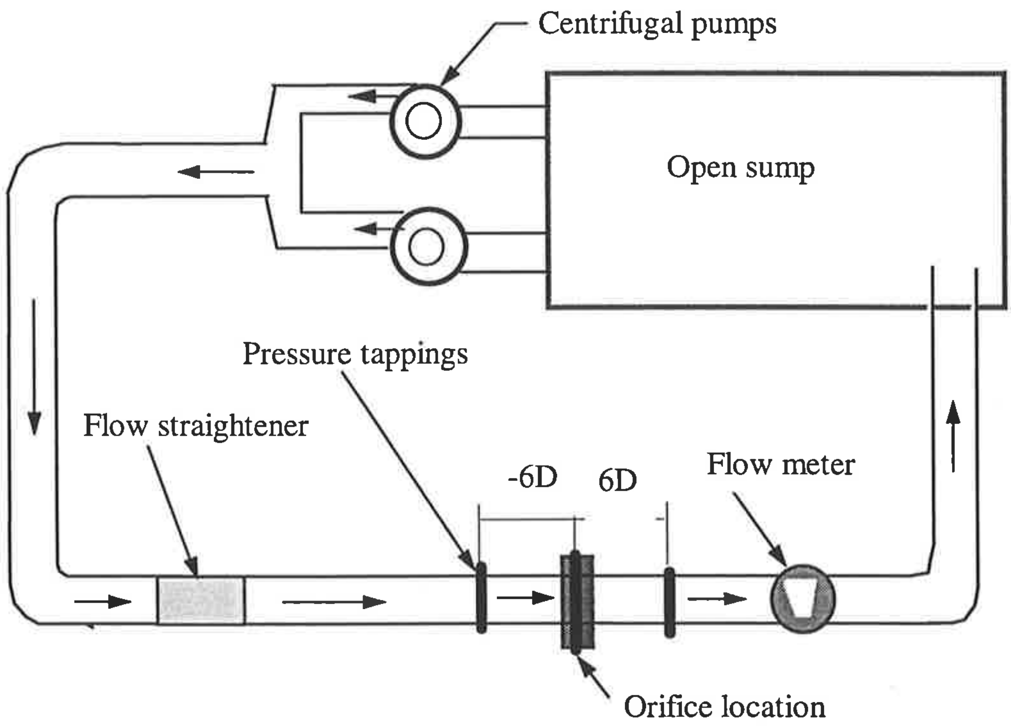

Figure 3-6. Schematic of steady flow measurement

In order to reduce the error in pressure drop measurements, static pressures were kept as low as possible, because pressure drops were calculated from the difference between the two static pressures in upstream and downstream regions and each static pressure was measured above atmospheric pressure (see *sub-section 3.2.4*). Thus, two small pumps were installed in parallel to increase flowrate up to 500×10^{-6} m^3/s (30 l/min)and maximum static pressure of around 16 kPa (120 mm Hg). Steady flow measurements such as pressure drops were made at flowrates of between 100 and 417×10^{-6} m^3/s (6 to 25 l/min), whereas velocities were carried out at only one constant flowrate of 417×10^{-6} m^3/s.

3.2.2 Pulsatile flow circulatory system

Pulsatile measurements were conducted through the Jellyfish valve (no pulsatile measurements were made through the orifices) in a mock loop based on the *vi-vitro* system (Leefe *et al.* 1986) with an in-house fabricated ventricle (heart duplicator) and flow elements. The pulse duplicator and mock loop were used for generating pulsatile flow for cyclic flow tests. This duplicated heart outflow allowed for the control of variables such as cardiac output, aortic pressure and heart beat rate. The ventricle consisted of a chamber and in its inlet a prosthetic heart valve was installed. Blood analogue was contained inside the ventricle chamber separated from the piston pump by a polymeric membrane. The frequency of the pump could be regulated by a VSI pump frequency controller. The cardiac output was controlled by adjusting the stroke length of the piston inside the cylinder pump; adjusting throttle and aortic pressure. The required aortic pressure was adjusted by relieving air from or pumping air into the compliance chamber or changing the free surface height within this chamber (see *Figure 3-7*). In order to achieve a required aortic pressure and cardiac output, firstly pump frequency was set, then all adjustable components such as the stroke length; adjusting throttle and compliance chamber settings were regulated in sequence.

Velocities, pressure drops and flowrate in pulsatile flow were measured over eight cycles and then analysed for mean and fluctuating values using a 5° binning analysis (see *section 4.2*). Pulsatile velocities across the valve were measured using an LDA system . Pressure drops were measured using pressure taps (see *sub-section 3.2.4*) and volumetric flow measurements were made in pulsatile flow using an electro-magnetic flow meter[1] rigidly attached 250 mm downstream of the valve base ring. All tests were conducted at a heart rate of 1.2 Hz (72 beats/min) with aortic pressure set at 10.26/16 kPa (80/120 mmHg) and a cardiac output of 93.3×10^{-6} m^3/s (5.6 l/min). with the Jellyfish valve located in (the in-vitro equivalent of) the aortic position.

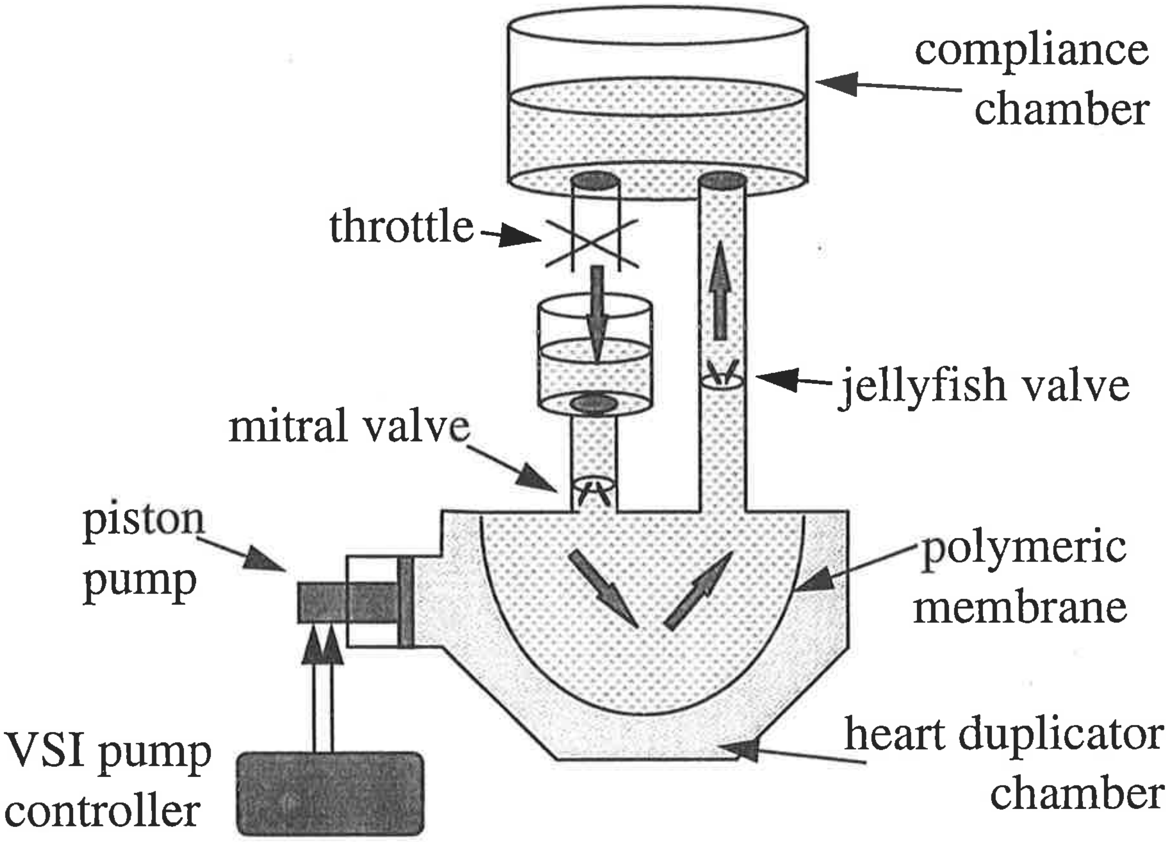

Figure 3-7 Heart duplicator and schematic pulsatile flow channel

The 5° binning analysis used is introduced in *section 4.2*. The accuracy of the mean values depended on the number of cycles measured, the size of the bins, and the extent of flow turbulence (Reynolds number). In order to gain a satisfactorily converged mean value (a good average with minimum standard deviation) of each measuring point in cyclic flow, the above parameters such as the number of cycles

[1] Zepeda Instruments (Seattle, Washington) SWF5 Electromagnetic square wave flowmeter of 19 mm diameter

measured and the size of the bins were chosen (see *section 4.2*) using results found from previous studies (Schoephoerster and Chandran 1991; and Jin and Clark 1994). In this study, a bin size of approximately 12 ms (corresponding to 5° of each cycle) and number of measured cycles of 8 were selected giving the convergence of mean data with correlation factor of 98%.

3.2.3 Turbulence phenomena determination using LDA

The laser Doppler anemometers used were two-beam systems operated in the back-scatter mode. Two systems were employed, one at The University of Adelaide and the other at The University of Melbourne. The system in Adelaide was used in pulsatile flow tests to determine velocity profiles and shear phenomena in the flow through the Jellyfish valve. The LDA system in Melbourne was used in steady flows through orifices as the major technique of this study to determine flow turbulence phenomena.

The Adelaide's system comprised 488 nm and 514.5 nm beams from a 5 W Spectra Physics 165 argon-Ion laser driving a TSI 9100-7 laser Doppler anemometer. Optics included two Bragg cells, a beam expander (to 82.5 mm beam spacing) and a 450 mm lens mounted on TSI 9400 traverse. Signal processing was achieved by TSI 1990C counters, data to which was phase resolved by interrupting the hand-shaking between the counters and controlling PC by an in-house built device. This hand-shaking interruption allowed for the 5° binning analysis. Unlike the system in Adelaide, the LDA system in Melbourne possesses fibre-optics with a beam intersection half angle of 4.35°. The laser source is a Spectra-Physics Stabilite 2017 Argon-Ion laser. The probe traverse system in Melbourne is fully automatic, this reduced the time needed to measure one data set from three days (measured manually in Adelaide) to a maximum of four hours. The LDA seeding particles used were 11 μm metallic coated spheres and the signal processor used was a Burst Spectrum Analyser (BSA).

Artificial heart valves and orifices were inserted into a plain acrylic tube (refractive index 1.48 and internal and external diameter of 19 and 25 mm, respectively) which was then placed in an index matching box (see *Appendix 1* and *Figure 3-8*) filled with medical grade paraffin to reduce refraction. Index matching was necessary as the laser beams passed from air into a curved acrylic tube and finally into the water flow medium. A small degree of optical malalignment was present even after index matching and the two control volumes were slightly displaced with respect to each other, the amount of received reflected light was also diminished.

LDA measurements through different windows (incidence points on the tube walls) also changed the intersection angle (two half angles) between the beams. however, the change of this angle did not change the fringe spacing *(d_f)* as the wavelength also changed according to the refractive index of the test medium (TSI incorporated 1994) as follows:

The path of alight beam crossing from one medium to another one is described Snell's law:

$$N_1 \sin\alpha_1 = N_2 \sin\alpha_2 \qquad \text{(Equation 3-2)}$$

where N is the refractive index of the medium

α is the angle between beam and the surface normal.

Fringe spacing, if measured in air without any window, is:

$$d_f = \frac{\lambda_A}{2\sin\alpha_A} \qquad \text{(Equation 3-3)}$$

where λ_A is the wavelength of laser light in μm

d_f is fringe spacing in μm

α is the half angle of the two intersection beams.

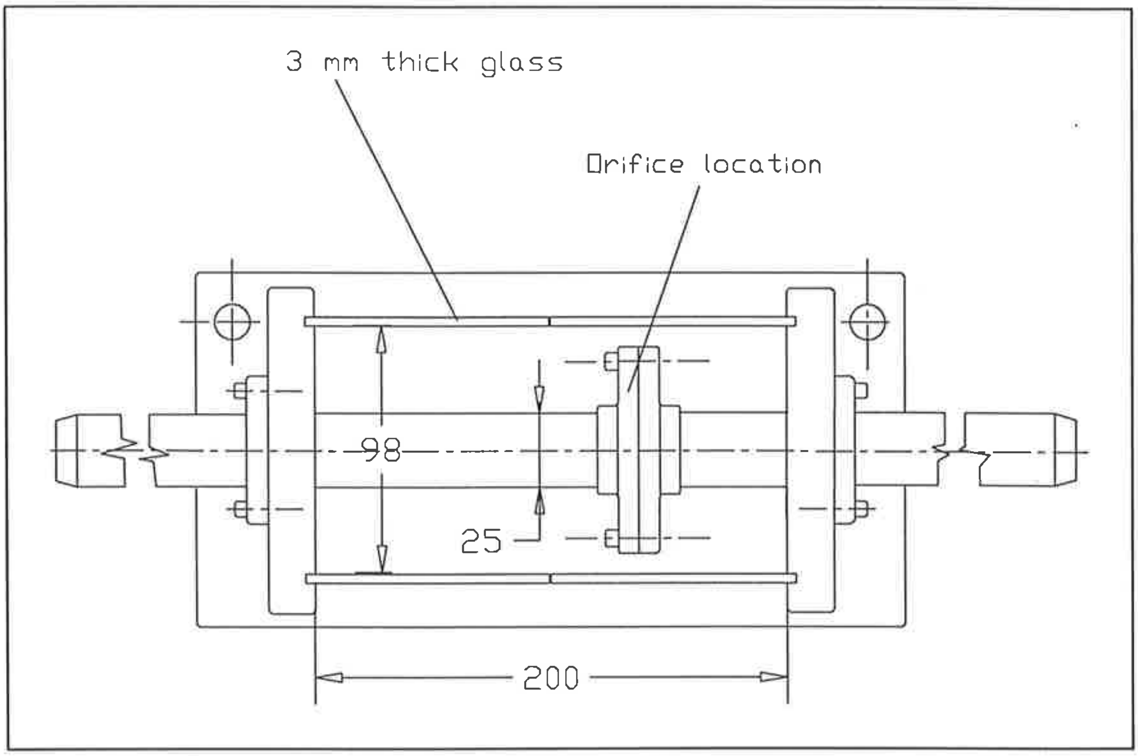

Figure 3-8 Index matching box

The wavelength in the new medium is:

$$\lambda_f = \frac{\lambda_A}{N_f} \qquad \textit{(Equation 3-4)}$$

thus, fringe spacing for new medium is established from *Equations 3-2, 3-3* and *3-4* as follows:

$$d_{f\ A} = \frac{\lambda_f}{2\sin\alpha_f} = \frac{\dfrac{\lambda_f}{N_f}}{\dfrac{2\sin\alpha_A}{N_f}} = \frac{\lambda_A}{2\sin\alpha_A} \qquad \textit{(Equation 3-5)}$$

This value remains unchanged and means that the magnitude of velocity measured through different windows (ie. for a change in optical medium) does not change.

This does not mean that the change in optical medium is entirely aproblematic: (a) the location of measurement volume is not correct leading to measuring in wrong place and (b) measurement volumes of horizontal and vertical beams are located in different places due to laser beams passing through different geometries within the test section and leading to erroneous results for shear stresses. Except Chew *et al.*'s study (1993), all the heart valve studies using LDA in literature up to date, did not mention how to solve and compensate for these problems. In order to solve these problems, the geometry of the test sections was analysed as follows:

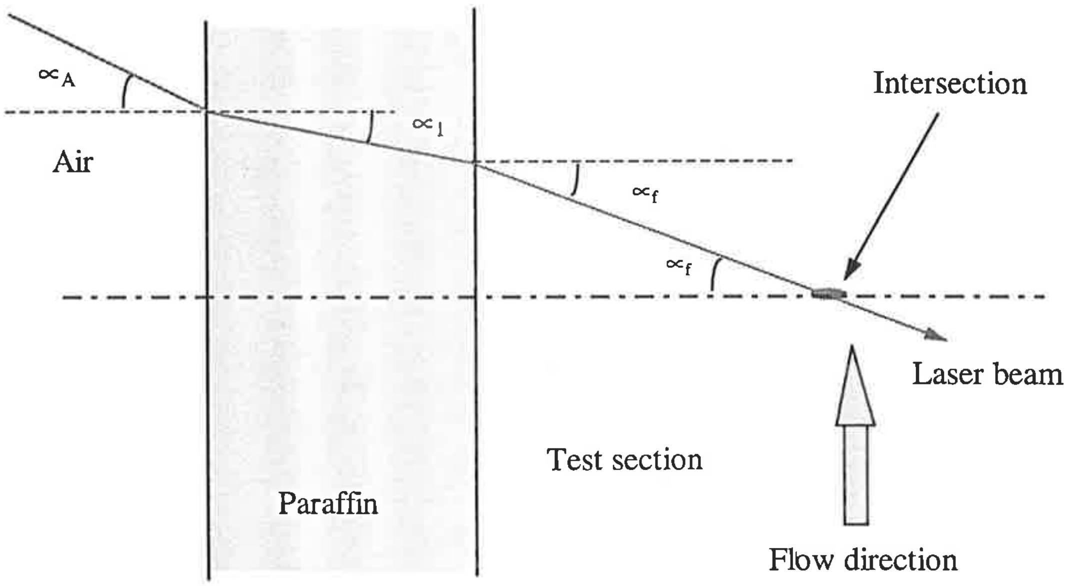

Figure 3-9 Horizontal beams through index matching windows

The horizontal beams were used for measuring axial velocities. These beams were not affected by the curved window, however they passed through the index matching box so that the location of measurement volume changed due to the variation of refractive indexes. The actual focal distance F_a was calculated using *Equation 3-6* (TSI incorporated 1994).

$$F_a = F \times \frac{\tan\alpha_A}{\tan\alpha_f} + t\left(1 - \frac{\tan\alpha_w}{\tan\alpha_f}\right) + d\left(1 - \frac{\tan\alpha_A}{\tan\alpha_f}\right) \qquad \textit{(Equation 3-6)}$$

where F_a is the actual focal distance in mm

F is the given focal distance of lens in mm

t is the thickness of window in mm

d is the distance from lens to window in mm.

As can be seen from *Equation 3-6* and the maximum tolerance on the location of the horizontal beams measurement volume occurred at the far side tube wall.

The vertical beams were used for measuring tangential velocities, these beams were affected not only by the index matching windows, but also by the curved window (see *Figure 3-10*). As a result, the location of this measurement volume changed differently from the location of measurement volume of the horizontal beams. This phenomenon impacted on shear stress measurements as shear stress calculations were based on coincident velocities.

In order to reduce these problems, such as the movement of the correct measurement volume and the difference of the location of the two measurement volumes, medical grade paraffin was filled in the index matching box and the actual movement of probe was calculated using *Equation 3-6*. The actual movement of the probe of 0.8 mm was decided for measuring axial velocities exactly at every 1 mm in test sections as axial velocity profile is dominant over tangential velocity in investigating heart valve flow. Measurement volume of the horizontal beams was exactly adjusted for measuring axial velocities in the correct positions. However, the location of vertical beam measurement volume was still different from the location of the horizontal measurement volume. The difference between the two locations was calculated using equations found in previous study (Chew *et al.* 1993). Maximum alteration of 2.5 mm was calculated in the centre of tube, this causes affects on the result of shear stresses. However, shear stress does not change very much because (a) maximum alteration of 2.5 mm is of the same order of magnitude as the measurement volume (1.5 mm), (b) tangential velocities and their fluctuations do not change significantly along radial position, (c) axial velocities plays a dominant role over tangential velocities (see *Equation 5-20*) in calculating shear stresses, and (d) axial velocities were measured in correct positions.

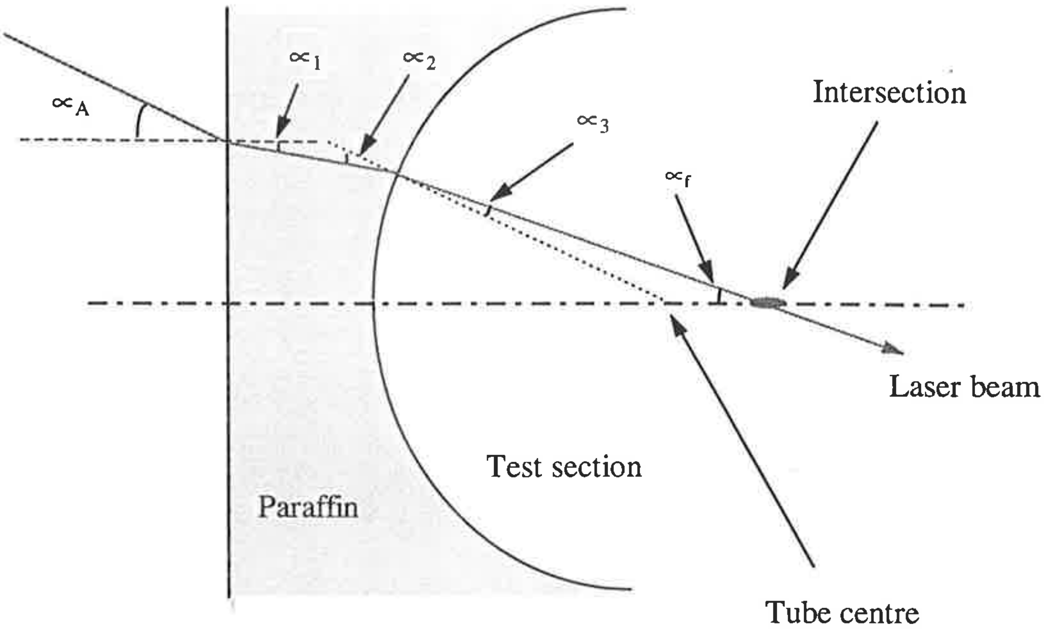

Figure 3-10. Vertical beams through curved window

Two velocity components (*U* and *V*, axial and tangential, respectively) and stress measurements were recorded at five planes in the upstream and downstream region of the valves and orifices eg. at 1 diameter (19 mm) upstream of the valve seating ring or orifice plate location, and at four positions downstream: 1, 2, 3 and 6 diameters. At each measuring plane, 18 data points from 1 mm to 18 mm radially (within the 19 mm internal diameter tube) were recorded, in. 1 mm radial steps. This provided a good picture of the structure and subsequent development of the flow (see *Figure 3-11*). This constituted one velocity data set.

LDA velocities were measured under both steady and pulsatile flow conditions then analysed for mean and fluctuating velocity components. The mean velocity components were plotted to determine flow properties such as velocity profile, vorticity, stagnation and recirculation regions which are known to promote thrombus formation and tissue overgrowth. The fluctuating components were used for calculating Reynolds shear stresses which cause lysis effects on blood cells. In this study, steady flow shear stresses were calculated from maximum of 6000 coincident data points collected in each of the two orthogonal directions and then plotted versus radial position to compare shear stress fields of different orifices. Pulsatile velocities in the Jellyfish valve were measured over 8 cycles then analysed for shear stresses (see *sub-section 3.2.3*)

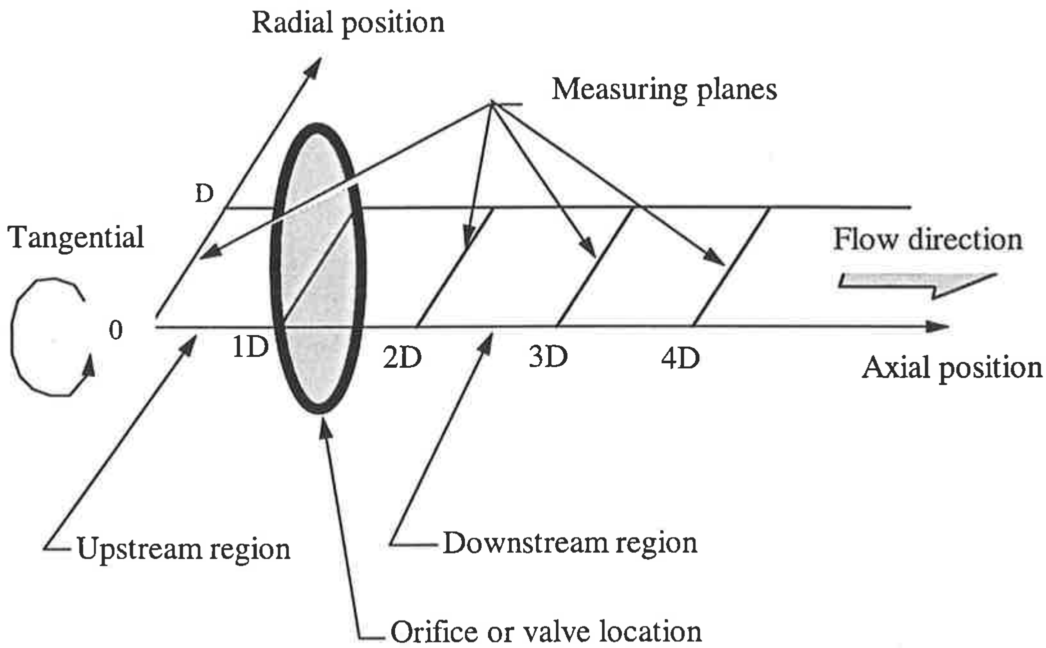

Figure 3-11. Velocity measuring planes

3.2.4 Pressure drop and volumetric measurements

Pressure drops across orifices were measured only under steady flow conditions at flowrates of 100 to 417×10^{-6} m^3/s (25 l/min). Whereas pressure drop measurements across the Jellyfish valve were made under the steady and pulsatile flow conditions described in *sub-sections 3.2.1* and *3.2.2*.

All pressure measurements were made using wall pressure taps located ±6 diameters downstream and upstream of the location of valve or orifices. According to ASME (1959) these pressure drops are actually pressure losses caused by the obstruction of orifices. Pressure taps consisted of four holes around the tube wall (see *Appendix 1*) so that average static pressures were measured representing upstream or downstream static pressures. Pressure drops were the difference between upstream static pressures and downstream static pressures.

$$\Delta P = P_{Upstream} - P_{Downstream} \qquad (Equation\ 3\text{-}7)$$

where ΔP is the Pressure drop (kPa)

$P_{Upstream}$ is the static pressure in the upstream region

$P_{Downstream}$ is the static pressure in the downstream region.

In this case, the error of pressure drop measurements caused by instruments is calculated as follows:

$$\delta P = P_{Maximum} \times \delta\% \qquad (Equation\ 3\text{-}8)$$

where δP is the absolute error (kPa)

$P_{Maximum}$ is the upper measuring limit of the of pressure the transducers (kPa)

$\delta\%$ is the accuracy of pressure transducers.

As indicated by *Equation 3-8,* in order to reduce the error of pressure drop measurements, the measuring range of pressure transducers was reduced. This was possible only when the measured static pressures were kept as low as possible, hence two small pumps were installed in parallel (see *sub-section 3.2.1*).

In steady flows, pressure drop measurements across orifices were analysed for empirical equations to calculate pressure coefficient (Cp) and effective area of orifices. In pulsatile flows, pressures and flowrates were measured over eight cycles in the Jellyfish valve then analysed using 5° binning analysis (see *section 4.2*) for mean values. Pressure drops, regurgitant flow and energy losses of the valve were calculated using *Equations 4-11, 4-12* and *4-16,* respectively. All pressure transducers used in this study were disposable, physiological blood pressure transducers[2]. The strain gauge conditioners fabricated at The University of Adelaide.

[2] PVB 2-PDPT-3003S

Steady pressure drops and flowrates across different orifices were presented in *section 5.1.* Pulsatile pressure drops and flowrates were measured only across the Jellyfish valve and their analysis and discussions were shown in *section 5.5.*

4. CHAPTER FOUR: DATA ANALYSIS

This study was carried out using experimental techniques which usually deal with complicated flow problems. In experiments, data analysis plays a very important role in making experimental data become useful and meaningful. The role of different data analysis techniques is to package and transmit experimental information efficiently from an experimenter to other researchers. As an example, LDA measures instantaneous velocities over a period of time. These velocity data themselves do not say any thing about heart valve flow characteristics: instead, data needs to be analysed to yield mean velocities, turbulence intensities and shear stresses to enable flow comparisons between heart valves. This illustrates the importance of the data analysis role. Chapter Four presents some techniques for analysing LDA velocity and pressure drop data.

4.1 LDA velocity data analysis

In this study, LDA was used for measuring axial and tangential velocities, which are instantaneous and can be divided into two components as follows:

$$u = U + u' \qquad \textit{(Equation 4-1)}$$

where u is the instantaneous velocity component

U is the time averaged mean velocity component

u' is the fluctuating velocity component.

The instantaneous velocity component *(u)* itself does not say anything about the flow characteristics of heart valve flows; whereas the axial, time averaged mean velocity component *(U)* is important as it provides information about stagnation and recirculation regions which promote thrombus formation and tissue overgrowth, and on velocity profiles which indicate jetting. High turbulence intensity and Reynolds shear stresses in blood flow indicate haemolysis; these are derived from the fluctuating velocity components following analysis by Reynolds algebra. Methods for extracting mean velocities, turbulence intensities and Reynolds shear stresses are developed here for use as predictors of haemodynamic parameters.

Time averaged mean velocities are calculated from n instantaneous data points gathered in a fixed time period:

$$U = \frac{\sum_{i=1}^{n} u}{n} \qquad \textit{(Equation 4-2)}$$

Turbulence intensity is calculated as follows:

$$TI = \frac{\sigma_u}{U} \times 100 \qquad \textit{(Equation 4-3)}$$

where $\sigma_u = \frac{\sum_{i=1}^{n} (u^2 - U^2)^{0.5}}{n}$ is the velocity standard deviation.

Haemolysis is red blood cell damage due to mechanical forces acting within the blood, especially in a region where high Reynolds shear stresses are acting. The mechanisms of haemolysis are stretching of the blood cell membrane and irrevocable changes harmful to the cell's essential function. Reynolds shear stresses can be calculated from any orthogonal fluctuating components (Stevensohn *et al.* 1985). For example:

$$\tau_{x\theta} = \rho \ \overline{u'v'} \qquad \textit{(Equation 4-4)}$$

where u' and v' are axial and tangential fluctuating components, respectively.

ρ is the density of fluid.

In this study, Reynolds shear stresses in steady flow are calculated from n coincident data points collected in each of the two orthogonal directions, axial and tangential, (yielding the u and v velocity components) by the following equations:

$$\tau = \frac{1}{n} \rho \sum_{1}^{n} (u - U)(v - V) \qquad \textit{(Equation 4-5)}$$

where n data points were measured over a period of time

u and v are the instantaneous velocity components

U and V are time averaged mean values calculated from n data using *Equation 4-2*.

Analysed data, such as mean velocities, turbulence intensity and shear stresses are plotted versus radial positions to provide graphical flow field data for the various orifices, so that these parameters might be easily compared between orifices.

Analysing LDA velocity, pressure drop and flowrate measurements in pulsatile flow is more difficult because measured data are dependent on the time of cyclic flow. Consequently, time averaged mean, fluctuating values, turbulence intensity and shear stresses are not able to be produced directly from *Equations 4-2, 4-3, 4-4* and *4-5*. In order to gain these parameters in cyclic flows, 5° binning analysis is introduced in the next section.

4.2 The 5° binning analysis

Experimental data viz: velocities, flowrates, and pressure drops were measured under both steady and pulsatile flow conditions. Data in steady flow at each point was taken over a period of time, from this instantaneous data, time averaged mean and fluctuating components were calculated as simple arithmetic averages. From these averages, turbulence intensity and shear stresses can be calculated (see *section 4.1*). On the other hand, pulsatile flow parameters are dependent on low frequency cycles, thus time averaged mean and fluctuating values are not easily gained. In order to ascertain these values, data from pulsatile flow, such as velocities, pressure drops and flowrate, was measured over several cycles and then analysed for time varying mean and fluctuating components imposed on a low (carrier) frequency using a 5° binning analysis.

In the 5° binning analysis, data from each cycle is divided into 5° segments which were compiled into bins with corresponding data from subsequent (360°) cycles and averaged to yield fluctuating and mean components (see *Figure 4-1*).

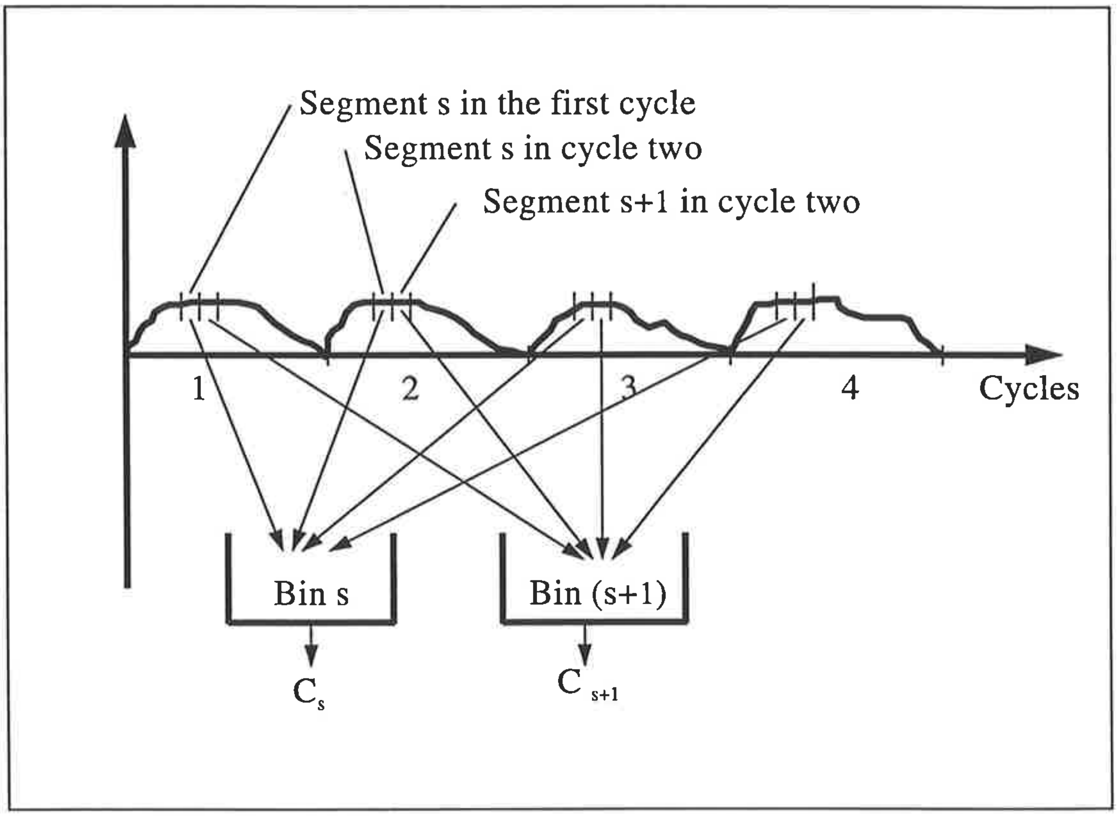

Figure 4-1. 5° binning analysis

Mean components over several cycles can be manipulated into one representative cycle as follows:

$$C_s = \frac{\sum_{i=1}^{n} \sum_{j=1}^{m} C_{ij}}{nm} \qquad \textit{(Equation 4-6)}$$

where C_s is the mean component of segment s

C_i are the instantaneous components contained within a segment of the cycle

n is the number of data points in a segment

m is the number of cycles measured.

As can be seen from *Equations 4-1* and *4-2,* time averaged mean and fluctuating values in steady flow become more accurate if the amount of measured data or measuring time is increased. However, in pulsatile flow, time increases lead to a spread of values and a smoothing of essential data; the quality of the averaged mean and fluctuating values depend on the size of the bins, the number of cycles measured and Reynolds number or turbulent intensity (Jin and Clark 1994). The number of cycles required for calculating the average value should be large and the size of the bins should be small enough so that the average value converges to a single value with a minimal standard deviation. Furthermore, the convergence of the mean value in pulsatile flows is quicker when the Reynolds number in the flow is smaller (Jin and Clark 1994). The bin size of around 15 ms and the number of data points of 100 to 300 was chosen in the previous study (Schoephoerster and Chandran 1991). In the more recent study Jin and Clark (1994) suggested to calculate the number of cycles measured with a fixed correlation factor so that a minimal standard deviation of the mean value in cyclic flows could be obtained.

In this study, pulsatile data such as pressure drops, flowrates and velocities were measured at maximum Reynolds number of 27,000. Data was taken over 8 cycles with a bin size of 11.57 ms corresponding to 5° in a 1.2 Hz (72 beats/min) cycle; this yielded average values with a correlation factor of 98%.

4.3 Dimensional analysis

Dimensional analysis is a packaging or compacting technique used to reduce the complexity of experimental programmes and at the same time increase the generality of experimental information. Data from steady flow tests eg. pressure drops are analysed using dimensional analysis techniques to give the most essential formulae to describe pressure losses through prosthetic heart valves. According to Buckingham's Π (Pi) theory (Gerhart and Gross 1985, Barenblatt 1987), any physical system can be expressed by a dimensionally homogeneous equation of the following form:

$$\pi_d = k \times f(\pi_1) \times f(\pi_2) \times \cdots \times f(\pi_n) \qquad \textit{(Equation 4-7)}$$

where $f(\pi_i)$	are transformation functions
$\pi_d, \pi_1, \pi_2, \ldots, \pi_n$	are terms of a complete set of dimensionless products
π_d	dependent dimensionless product
$\pi_1, \pi_2, \ldots, \pi_n$	independent dimensionless products
k	exponential constant dependent on the values of the respective dimensionless products.

The concept of the component equations can be applied to obtain the prediction equation in the form of the *Equation 4-7.* Data obtained from a set of experiments in which only one π-term was varied while keeping all the other π-terms constant can be used to find a component equation in the following form:

$$\pi_d = a_i \pi_i^{k_i} \qquad \textit{(Equation 4-8)}$$

where a_i and k_i are constants dependent on the experimental results and the other π-terms were held constant. *Equation 4-8* can be rewritten in the following form:

$$\pi_d = k_i \times f(\pi_i) \qquad \textit{(Equation 4-9)}$$

It can be seen from *Equation 4-9* that the transformation function $f(\pi_i)$ can be obtained by plotting the experimental data of π_d versus π_i in each set of experiments designed by the concept of component equations as mentioned above and the standard curve fitting procedures are applied here to find out component equations.

In this study, pressure drops across orifices and occluders were collapsed for pressure coefficient using dimensional analysis. Firstly, all the variables such as flowrate, orifice area, orifice and occluder position and orifice shape were taken into dimensionless terms (independent dimensionless products) such as Reynolds number (Re*),* ratio of orifice area to tube area *(r_A),* eccentricity percentages *(E)* and shape factors *(Φ_{Shape}).* Secondly, pressure coefficient (the dependent dimensionless product) was plotted versus each of the independent variables which were gained experimentally. Thirdly, standard curve fitting procedures were applied to these plots to establish five component equations. Finally, the five component equations were combined in the form of *Equation 4-9* to establish pressure coefficients across any orifices. The k_i constants were determined from each set of experiments in which only one π-term was varied while keeping all the other π-terms constant. The mean value of different constants k_i was the constant of the complete equation determined from experiments (for more detail, see *section 5.1*).

4.4 Pressure drops - effective orifice area

Pressure drops across prosthetic heart valves do not say very much about valve performance or lend much to comparisons between various valves. The introduction of effective orifice area and performance index of heart valves has made the valve comparison more complete. The effective orifice area of a heart valve can be calculated using Gorlin and Gorlin's (1951) formula:

$$A_{effective} = \frac{Q}{C \times 44.5 \times \sqrt{\Delta P}} \qquad \textit{(Equation 4-10)}$$

where C is the discharge coefficient

ΔP is the pressure drop across the valve in cm of H_20

Q is the flowrate in cm^3/s.

and $$\Delta P = P_{Upstream} - P_{Downstream} \qquad \textit{(Equation 4-11)}$$

where $P_{Upstream}$ and $P_{Downstream}$ are static pressure in the upstream and downstream region, respectively.

The valve performance index is defined as the ratio of effective orifice area to the valve ring area (Woo et al. 1983 and Heiliger 1987).

$$PI \equiv \frac{A_{Effective}}{A}$$

where $A_{Effective}$ is the effective orifice area of the valve

A is the valve ring area.

Generally, prosthetic heart valves are compared for effective orifice area and efficiency index. In this study, pressure drops were measured across different orifices and effective orifice areas were calculated using *Equation 4-10* to establish the effects of the orifice shape and position on effective orifice area of valves.

4.5 Energy losses and regurgitant flow

Regurgitant flow and energy losses indicate a valve's proper functioning. Large energy loss may lead to dysfunction of the heart; high regurgitant flow implies the valve's incompetence (failure to close properly), and large leakage produces very high retrograde velocities and a high shear stress region which may damage red blood cells. Regurgitant flow and energy losses are investigated carefully in recent studies eg. Teijeira and Mikhail (1992).

Regurgitant flow includes both backflow (during the closing phase) and leakage-flow (in the closed phase) over a cycle and can be calculated as follows:

$$Q_{Regurgitant} = \frac{1}{n} \int_{0}^{T_2+T_3} q \, dt \qquad \textit{(Equation 4-12)}$$

where q is the flowrate through the valve

n is number of cycles measured

T is the time of a cycle and the cycle is divided into three distinct phases:

T_1 is the time period of forward flow (systole)

T_2 is the time period of closing phase; and

T_3 is the time period of closed phase, then:

$$T = T_1 + T_2 + T_3 . \qquad \textit{(Equation 4-13)}$$

Total flow for one cycle is:

$$Q_{Total} = \frac{1}{n} \int_{0}^{T} q \, dt \qquad \textit{(Equation 4-14)}$$

Relative regurgitant flow is defined as follows:

$$Q\% = \frac{Q_{Regurgitant}}{Q_{Total}} \times 100\% \qquad \textit{(Equation 4-15)}$$

Energy loss is the product of flowrate and pressure drops, and this occurs in three distinct stages. For example, in the aortic position, these three energy loss stages are: (a) resistance of forward flow during systole; (b) reverse flow during closing and (c) leakage flow during the closed phase. Energy losses are calculated using the following equation:

$$\Delta E \quad = \frac{1}{n} \int_0^T \quad q\Delta P \quad dt \qquad \textit{(Equation 4-16)}$$

where ΔP is pressure drop across the valve

ΔE is average energy loss over a cycle.

Relative energy loss is defined as the ratio of energy loss ΔE to total energy:

$$E\% = \frac{\Delta E}{E_{Total}} \times 100\% \qquad \textit{(Equation 4-17)}$$

where $E_{Total} = \frac{1}{n} \int_1^T q \times P_{Upstream} \; dt$ is total energy.

In this study, a prosthetic heart valve prototype called the Jellyfish valve was investigated. Relative regurgitant flow and energy losses across this valve were calculated using *Equations 4-15* and *4-17* to indicate the valve functioning and then were compared with those of other prosthetic heart valves. Generally, regurgitant flows and energy losses are from 6-12 % for mechanical valves (Teijra and Mikhail 1992) and 1-4% for bioprostheses (Woo *et al.* 1983). Maximum regurgitant flow of 4% and energy loss of 3.5% was observed in the Jellyfish valve.

5. CHAPTER FIVE: RESULTS AND DISCUSSIONS

The use of prosthetic heart valves, to replace defective aortic or mitral natural ones, is a common practice in surgery. However, implantation of these valves may causes problems for some patients. Some of these problems are directly related to the nature of the blood flow through the valves. Haemolysis, red blood cell damage, arterial wall damage, thrombus formation and high pressure drop are the most frequently observed problems. This chapter presents and discusses pressure drops, velocity profiles and shear stress fields in light of experimentation conducted as part of this study.

5.1 Steady flow pressure drops

Pressure drop measurement is one the most important factors in comparing and evaluating the insufficiency of heart valve prostheses; it can be used to compare relative performances of different valves or as an aid to future valve design (Gentle 1977 and 1984). Furthermore, from pressure drop measurements, effective orifice area and performance index can be calculated using the Gorlin and Gorlin formula (Gorlin - Gorlin 1951). Heiliger in 1987 investigated five different heart valves in a mock circulation during pulsatile flow conditions and found that the mean orifice area determined by him and the effective orifice area calculated using the Gorlin formula was in disagreement; he does not postulate reasons for this. Steady state pressure drop versus flow rate measurements were shown by Yoganathan *et al* 1979a to correlate well with mean cyclic pressure drops versus r.m.s. flowrate during systolic ejection from pulsatile flow data. In 1984, Swanson compared pressure drop results from different investigators, and he found that pressure drops were significantly different, which he attributed to:

- different geometries in the test regions into which the valves were inserted,
- different approach flow conditions,

- different placement of pressure measurement taps and
- different methods of pressure measurement.

This section simply focuses on pressure losses caused by the presence of valves in a smooth tube by modeling different orifices. This procedure may simplify or even replace the need to measure pressure drops through prosthetic heart valves and compare different heart valve types without any differences just by measuring geometries of the valves.

Four pressure drop measurement tests were carried out through different orifices to establish the effects of orifice area, position and shape and the occluder position on pressure drops. Pressure drops are a function of orifice areas, flowrate, orifice shapes and orifice or occluder positions. Dimensional analysis was used to aid analysis of collected data. All variables were changed to dimensionless products eg. pressure drop becomes pressure coefficient and so on.

For pressure drops:

$$C_P = \frac{\Delta P}{\rho \frac{U^2}{2}}$$

For flowrates:

$$Re = \frac{UD}{\nu}$$

For orifice areas:

$$r_A \equiv \frac{A_1}{A_0}$$

where A_1 is orifice area and A_0 is the tube area.

And finally for eccentricities:

$$E = \frac{\text{Eccentricity (mm)}}{\text{D (mm)}} \times 100\%$$

where E is the percentage eccentricity

D is the internal diameter of the tube; or the diameter of the ball occluder.

So pressure coefficient can be written in the following form:

$$C_P = f(r_A, \mathrm{Re}, E) \qquad \textit{(Equation 5-1)}$$

where C_p is the dependent dimensionless product and r_A,, Re and E are independent dimensionless variables. Using *equations 4-4 and 4-5,* C_p can be rewritten as follows:

$$C_P = k \times f(r_A) \times f(\mathrm{Re}) \times f(E) \qquad \textit{(Equation 5-2)}$$

where f are empirical equations. These equations are obtained by plotting the experimental data for C_p versus each independent dimensionless variable in each set of experiments, called component equations, these are shown in *Figures 5-2, 5-4, 5-6* and *5-8*. Standard curve fitting procedures are applied to these figures to establish their component equations.

5.1.1 The effects of the orifice area on pressure drops

Firstly, steady flow pressure drops measurements were conducted for flow through different circular orifices with flowrate range of 100 to 417 $\times 10^{-6}$ m^3/s (6 - 25 l/min) corresponding to the peak systolic flowrate of cardiac output of 33.3 to 91.7 $\times 10^{-6}$ m^3/s (2 - 5.5 l/min). These circular orifices had the same geometric characteristics but different areas. The ratio of orifice area to tube area (r_A) was chosen to be in the range 0.4 to 0.75 corresponding to the ratio of orifice area to sewing ring area of the most commonly used heart valve prostheses (the ball valve is the most obstructive and has a ratio of orifice area to sewing area of 0.4, and the bileaflet valve is the least obstructive and its ratio is about 0.75).

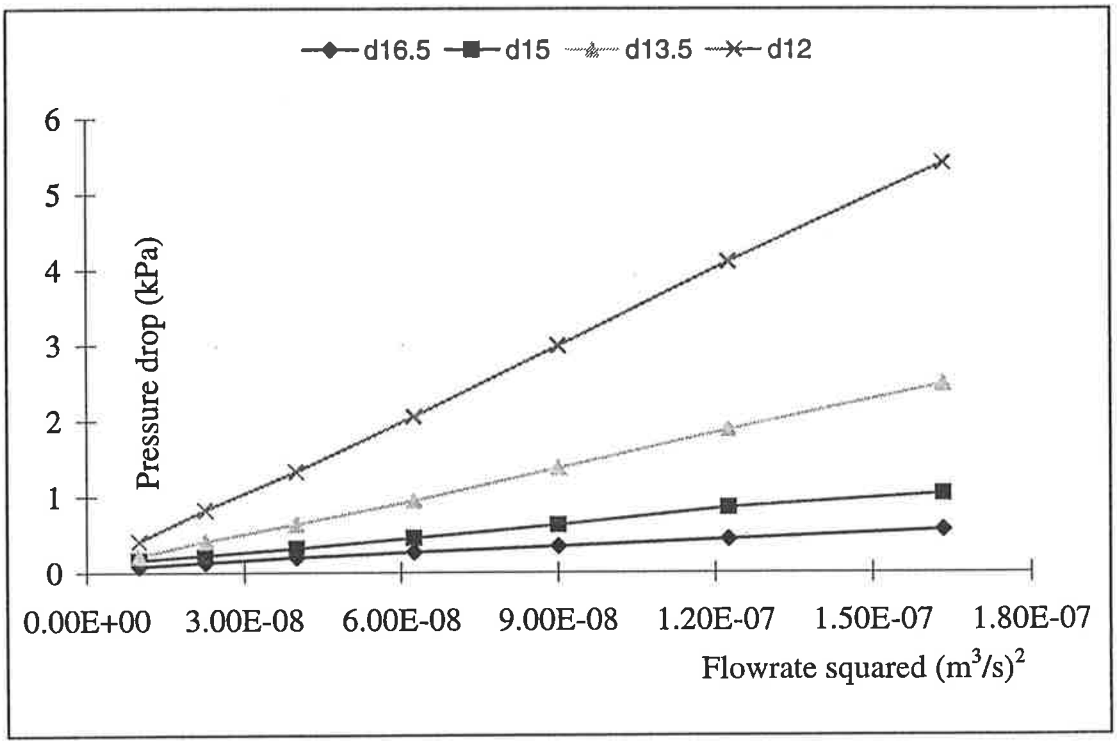

Figure 5-1. Pressure drop versus flowrate squared for flow through circular, concentric orifices of diameters 16.5, 15, 13.5 and 12 mm

Pressure drops in kPa are plotted versus the square of flowrates. Data points from each orifice are on a straight line, this agrees with other investigators' work eg. Gentle (1977). As can be seen, *Figures 5-1, 5-3, 5-6* and *5-4* show that pressure drop decreases when orifice area or r_A increases. Pressure drops change dramatically when r_A changes from 0.4 to 0.75. At a flowrate of 417×10^{-6} m^3/s (25 l/min) this change is 1000% (from 5.4 to 0.56 kPa). This means that the flow area of prosthetic heart valves is a very important factor in reducing or increasing pressure losses through orifices, and hence prostheses.

Furthermore, data points were condensed (collapsed) against Q^2/d^4, where Q is flowrate and d is the orifice diameter. As can be seen from *figure 5-2*, data points of this study were not on a straight line and gave a disagreement with Gentle's 1977 and 1984 studies; in which pressure drops were measured across a type of valve with different sizes, and data points were collapsed against Q^2/d^4 giving a straight line. This lead to an expectation that in this study, pressure drops versus Q^2/d^4 of a circular orifice with different sizes should lie on a straight line; this was not the case. The main reason which caused the difference between two studies, is the fact that the pressure drop across orifices in this study was measured in tube, whereas Gentle was mounting the valve between two relatively large chambers. So that most of the pressure drop was caused by dissipation of the velocity head of the jet issuing from the valve and then slowing down in the downstream chamber. (Gentle, 1995). This shows the gross differences between viscous, boundary layer flow (in the tube) and relatively inviscid, potential flow (between large vessels).

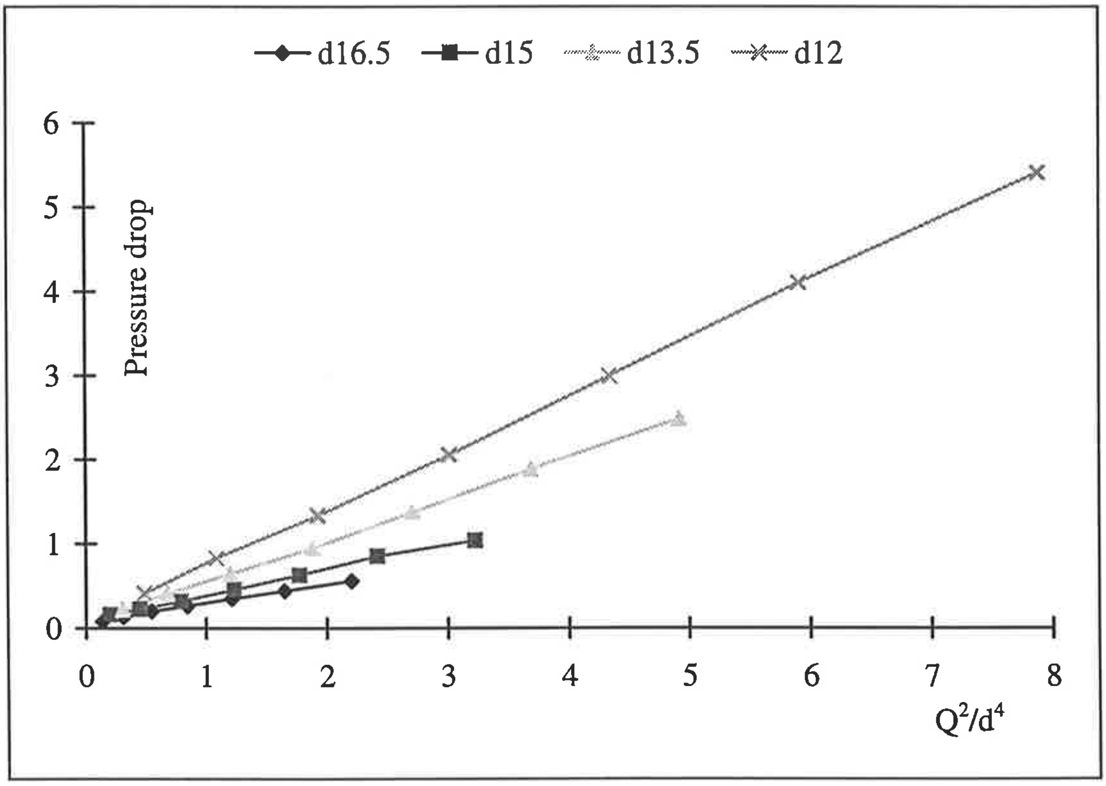

Figure 5-2. Condensed pressure drops across circular orifices for flow through circular, concentric orifices of diameters 16.5, 15, 13.5 and 12 mm

As can be seen from *Figure 5-1,* pressure drops depend greatly on the orifice area and flowrate or, in other words, on the r_A and Reynolds number. *Figures 5-3* and *5-4* show pressure coefficient C_p versus r_A and Reynolds number, respectively. Pressure drop increases, whereas pressure coefficient reduces with increasing Reynolds number. Pressure coefficient at low Reynolds numbers reduces quickly then slow down; at high Reynolds numbers it seems to be steady (see *Figure 5-4*).

Pressure coefficient reduces dramatically from 5.9 to 0.6 when r_A changes from 0.4 to 0.75 (see *Figure 5-3*).

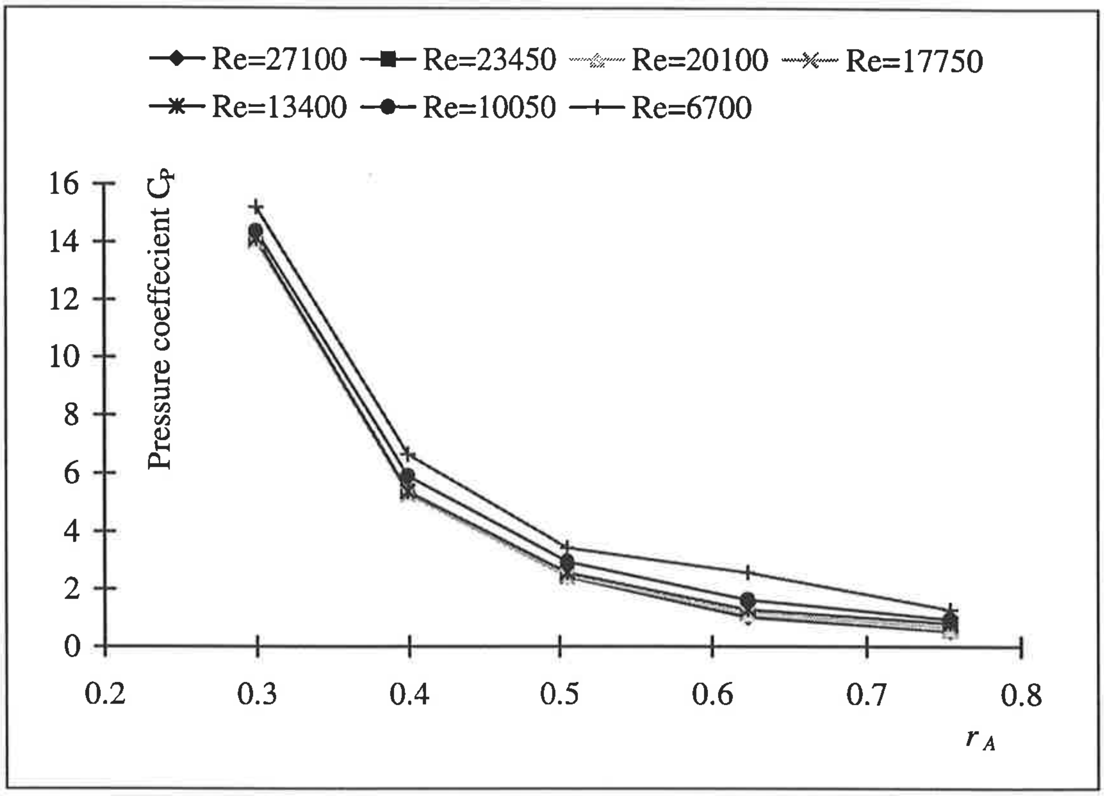

Figure 5-3. Pressure coefficient versus r_A for various Reynolds numbers of flow through circular, concentric orifices

The first component equation is the function of r_A which can be obtained from *Figure 5-3*. As can be seen from *Figure 5-3*, the pressure coefficient increases exponentially when r_A reduces from 0.75 to 0.4. In order to get a better curve, a boundary condition should be inserted here: when $r_A = 1$; this corresponds to pressure loss in flow through a 19 mm internal diameter tube. This value was calculated from Darcy-Weisbach equation, pressure loss and pressure coefficient are as follows:

pressure loss:

$$\Delta P_L = f \times (\frac{L}{D}) \times (\frac{\rho U^2}{2}) \qquad \textit{(Equation 5-3)}$$

and pressure coefficient:

$$C_P = \frac{\Delta P_L}{\frac{1}{2}\rho U^2} = f \times (\frac{L}{D})$$ *(Equation 5-4)*

where L: is tube length

D: is tube internal diameter

f: is the Darcy friction factor for smooth and fully developed turbulent flow.

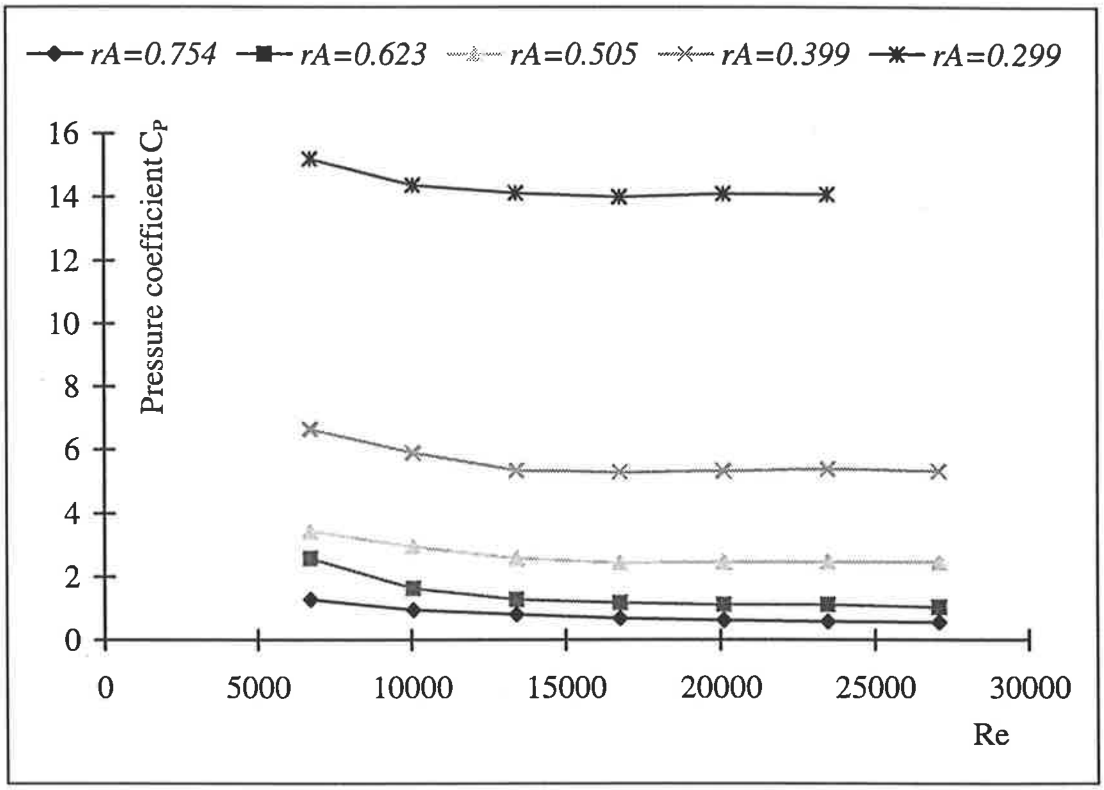

Figure 5-4. Pressure coefficient versus Reynolds number for varying area ratios of circular, concentric orifices in tube flow

The friction factor (f) can be expressed as a function of Reynolds number in a smooth tube as follows:

$$f_{Smooth} = 0.3164\ \mathrm{Re}^{-1/4}$$ *(Equation 5-5)*

Using *equations 5-3, 5-4* and *5-5*, $C_p = 0.3126$ can be calculated as $r_A = 1$ and then using curve fitting procedure on *Figure 5-3*, the first component equation can be determined as:

$$C_{Pr} = 0.473249 + 270.05902 \times e^{(\frac{-rA}{0.1002386})} \quad \textit{(Equation 5-6)}$$

the correlation factor r of this equation is:

$$r_1^2 = 0.999068$$

The second component equation is of the function of Reynolds number, the pressure coefficient seems to have an exponential relationship with Reynolds number. This equation can be obtained from *Figure 5-4* using the curve fitting procedure:

$$C_{pR} = 5.294376 + 10.382888 \times e^{\frac{-Re}{3302.9157}} \quad \textit{(Equation 5-7)}$$

and the correlation factor r is:

$$r_2^2 = 0.972834$$

5.1.2 The effects of the orifice position on pressure drops and effective orifice area

Secondly, pressure drop measurements were conducted through a circular orifice mounted within the tube with differing degrees of eccentricity. The circular orifice was positioned by a screw within the orifice housing to introduce the eccentricities (see *Appendix 1*). These eccentricity was adjusted in 0.5 mm steps from 0 (centre line of the tube) to 3.5 mm off the centre line providing a very good picture of pressure drops caused by eccentricity

$$E = \frac{\text{Eccentricity (mm)}}{\text{Tube diameter}} \times 100\% \quad \textit{(Equation 5-8)}$$

Pressure drops were plotted versus the square of flowrate dependent on eccentricities. Larger eccentricities caused larger pressure drops, and pressure drops increased by 23% (from 5.4 to 6.6 kPa) at a flowrate of 417×10^{-6} m^3/s (25 l/min) when E increased from 0% to 30% (see *Figure 5-5*). As can be seen from these measurements, eccentricity does not affect pressure drops as much as the orifice area and orifice shape do. *Figure 5-6* shows pressure coefficient C_p versus eccentricity percentage E. The coefficient of pressure, C_p, increased with increasing eccentricity: at the first stage, when the eccentricity is small, the pressure coefficient increases slowly; later this increases more rapidly and it seems to have a second-order relationship with E. Here again, pressure coefficient reduces with the increasing of Reynolds number.

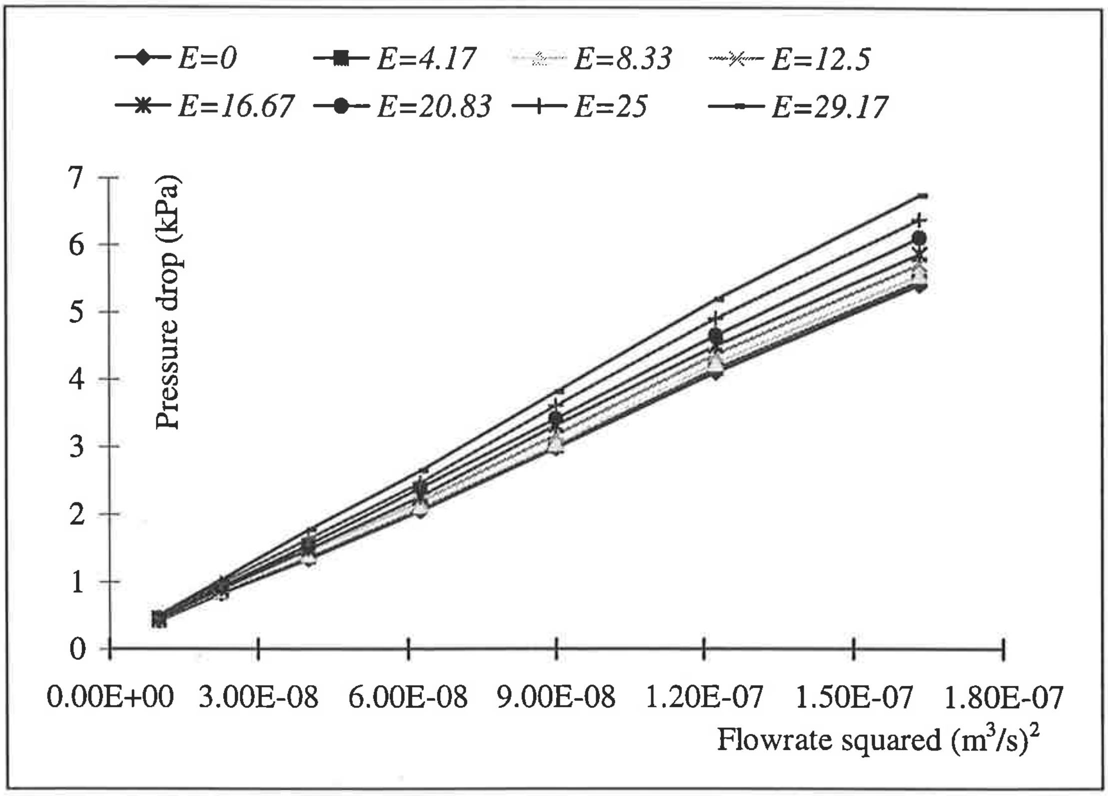

Figure 5-5. Pressure drop versus flowrate squared for various eccentricities of an orifice of 12 mm diameter (r_A = 0.4)

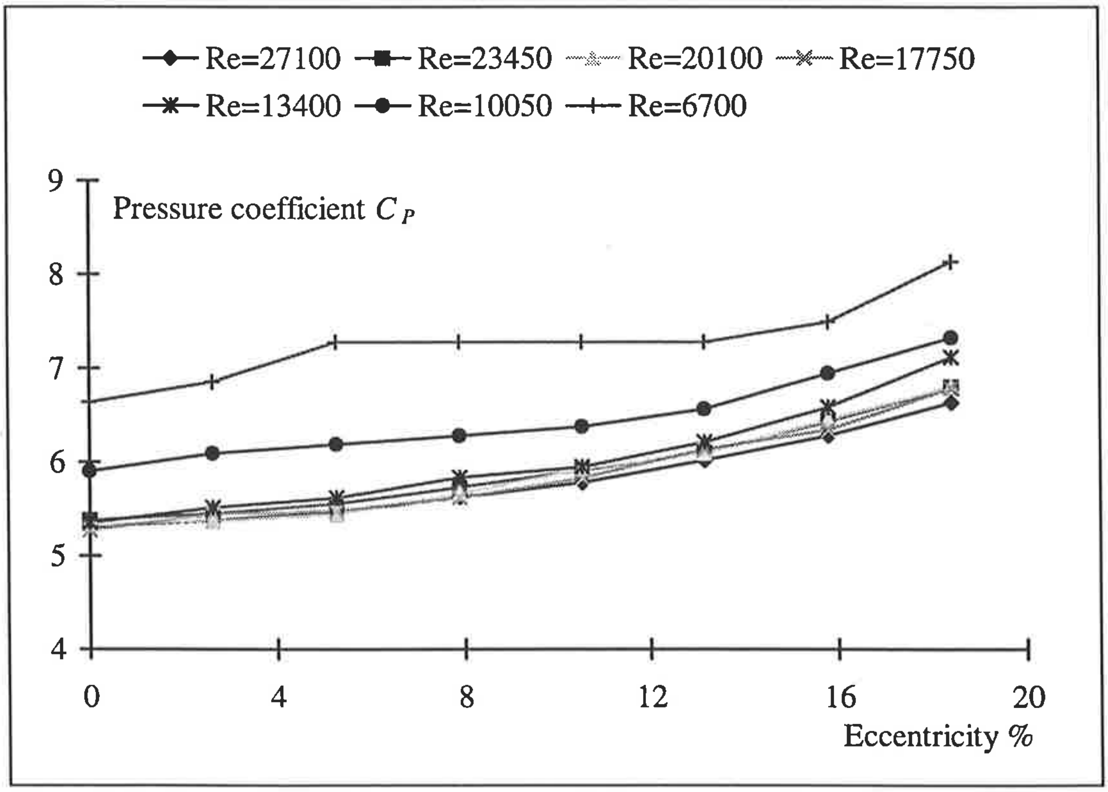

Figure 5-6. Pressure coefficient versus eccentricity percentage for various eccentricities of an orifice of 12 mm diameter (r_A = 0.4)

The third component equation is the function of the eccentricity percentage *E*, this equation can be obtained from *Figure 5-6* using the curve fitting procedure:

$$C_{PE} = 5.371233 + 0.004281 \times E^2 \qquad \textit{(Equation 5-9)}$$

The correlation factor *r* is:

$$r_3^2 = 0.993978$$

Effective orifice area of a circular orifice located with different eccentricities (different positions) was calculated after Gorlin and Gorlin (1951) *(Equation 4-6)*. For comparison, C, the discharge coefficient was considered to be 1. The results were calculated and are shown in *Table 5-1*.

Table 5-1. Effective orifice area of an eccentric orifice of constant diameter (12 mm)

E	0	2.63	5.26	7.89	10.53	13.16	15.79	18.42
$A_{Effective}$ (cm^2)	1.19	1.18	1.17	1.15	1.14	1.12	1.10	1.06
$C_{Position\ measured}$	1.00	0.989	0.979	0.966	0.954	0.939	0.917	0.888

As can be seen from this table the real orifice was unchanged, because measurements were carried out across only one orifice, but the orifice position was changed with eccentricities of 0 to 3.5 mm, consequently, pressure drop changed. Due to changing of pressure drops across the orifice, effective orifice area changed as well. The position coefficient is defined as a ratio of effective orifice area at any position of the orifice to effective orifice area of central flow orifice as:

$$C_{Position} = \frac{A_{Effective\ eccentric}}{A_{Effective\ concentric}} \qquad \textit{(Equation 5-10)}$$

The position coefficient seems to be a function of the eccentricity percentage *E* of the orifice and can be established from *Table 5-1* using the curve fitting procedure:

$$C_{Position} = 0.987672 - 0.000290 \times E^2 \qquad \textit{(Equation 5-11)}$$

with correlation factor

$r^2 = 0.996993.$

5.1.3 The effects of the occluder position on pressure drops and effective orifice area

Thirdly, the effects of the occluder position on pressure drops when a 14.5 mm ball occluder was inserted into a 19 mm tube. The ball was moved within the tube to make different eccentricities (different occluder positions). Five positions of the ball were created in 0.5 mm steps from 0 (the centre line of the tube) to 2 mm off the centre line (for more detail see *Appendix 1*). Again here, pressure drops were measured in a flowrate range of 100 to 417×10^{-6} m^3/s (6 - 25 l/min) then plotted versus the square of flowrate *(Figure 5-7)*, the pressure coefficient was plotted versus eccentricity percentage *E (Figure 5-8)* where:

$$E = \frac{\text{Eccentricity (mm)}}{\text{Ball diameter (mm)}} \times 100\% \qquad \textit{(Equation 5-12)}$$

The third component equation *(Equation 5-9)*, the function of the eccentricity percentage *E* caused by the eccentricity of the orifice, can be applied to describe the relationship between coefficient of pressure and eccentricity of the occluder. This equation was obtained from *Figure 5-6* and represents the data from *Figure 5-8* within 5% error (see *Appendix 3*). *Figure 5-8* shows the pressure coefficient measured through the ball of different eccentricities versus percentage eccentricity *E.*

The results show that the position of occluders and the position of orifices cause the same pressure drops and the third component equation can be used for all the orifice and occluder positions. From the last two measurement sets it can be seen that any eccentricity (of orifice or occluder) causes eccentric flow patterns downstream of the valve thus increasing pressure drops. This probably explains why pressure drops through the tilting valve is high in comparison with those of other valves with the same orifice diameter (Hanle *et al.* 1989). The tilting valve in an open position causes an eccentric flow downstream of the valve in the form of a major and a minor orifice flows. This increases pressure drops through the valve even though the effective orifice area of this valve is relatively large.

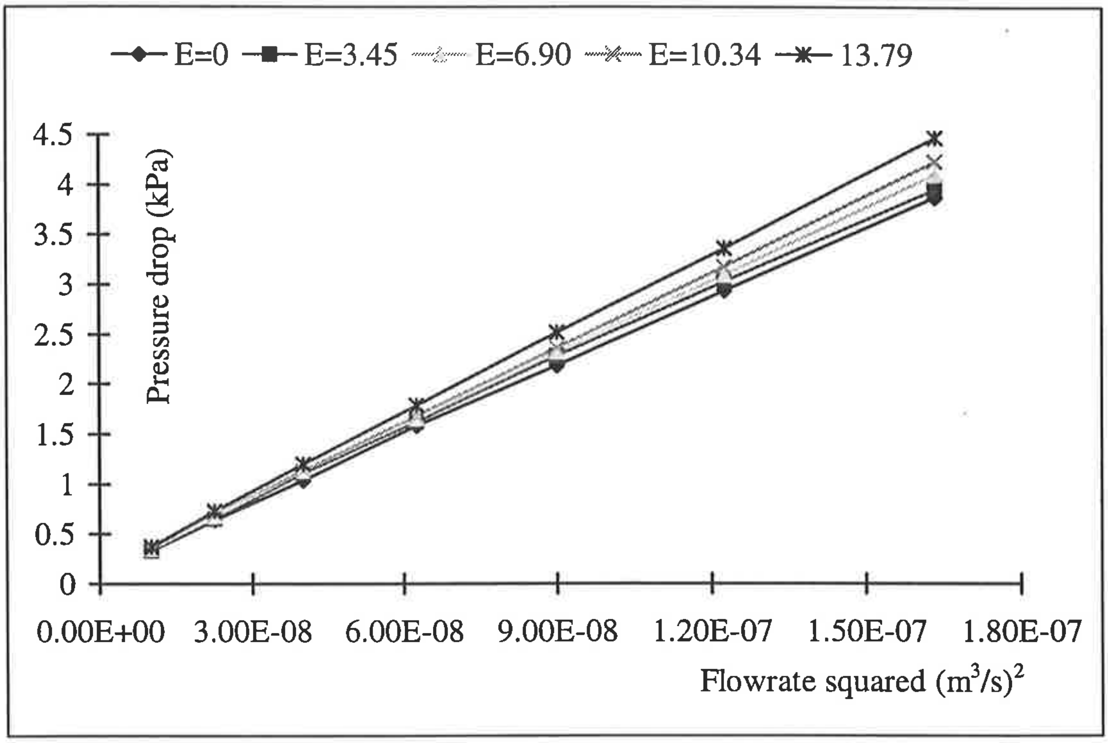

Figure 5-7. Pressure drop of the occluder position versus flowrate squared for a ball occluder mounted with various eccentricities

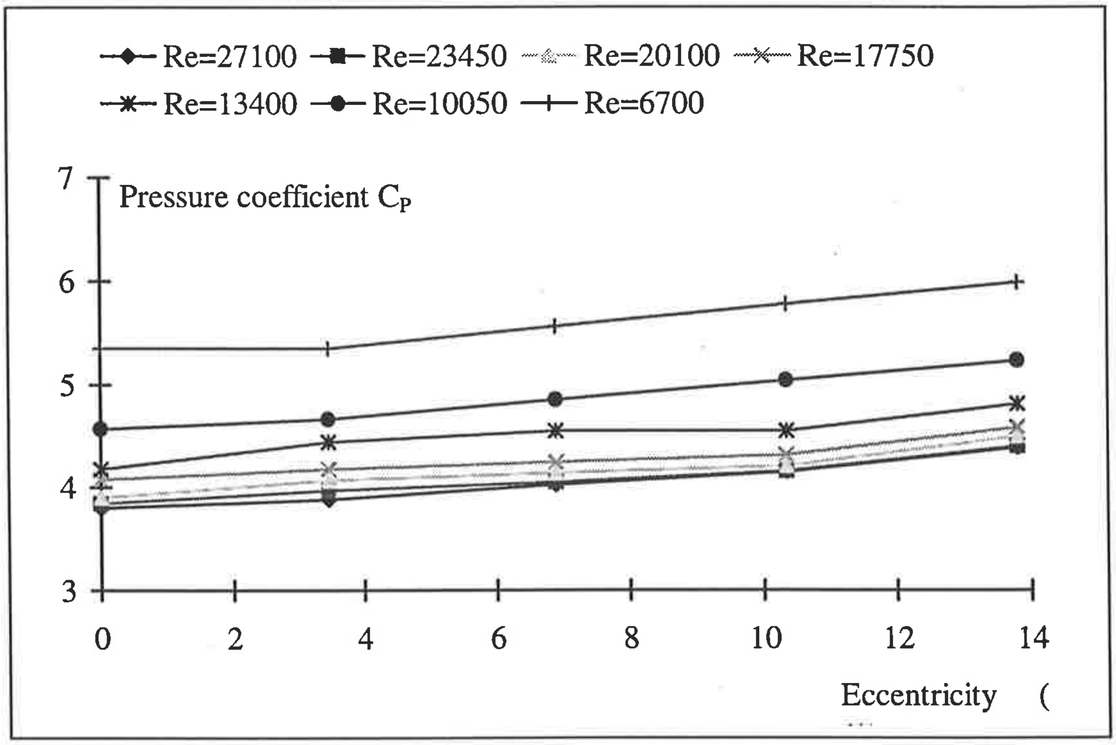

Figure 5-8. Pressure coefficient for occluder position versus eccentricity for a ball occluder mounted with various eccentricities

Like the effects of the orifice position, the occluder position also affects the effective orifice area. In the same way, effective orifice area of a constant area orifice in different positions of the occluder can be calculated and a function of occluder position coefficient on eccentricities can be established.

Table 5-2. Effective orifice area and position coefficient of an eccentric occluder orifice

E (%)	0	3.45	6.9	10.34	13.79
$A_{Effective}$ (cm^2)	1.38	1.36	1.34	1.32	1.29
$C_{Position\ measured}$	1	0.985	0.972	0.961	0.935
$C_{Position\ calculated}$	0.988	0.984	0.974	0.957	0.933

Equation 5-11 found in *sub-section 5.1.2* was applied to calculating the position coefficient of the occluder position, and the results indicated a maximum error of 1.2% in the predictive quality of *Equation 5-11*. Furthermore, *tables 5-1* and *5-2* show that effective orifice area not only depends on the orifice or occluder position, but also the orifice shape. Effective orifice area of an annular orifice is much larger than the real orifice area, thereby, it is worth investigating the orifice shape in the next section.

5.1.4 The effects of the orifice shape on pressure drops and effective orifice area

Finally, pressure drops were measured through constant area orifices with different shapes such as circular, triangular, square and annular. These shapes are similar to the shapes of the most commonly used heart valve prostheses when they are fully open. For example, the ball valve has an annular orifice shape, the bileaflet valve orifice is approximately circular and bioprosthetic and natural valves have orifices which may be approximated by triangular (trileaflet valves) or square (bileaflet) shapes.

Again, flowrates were varied from 100 to 417×10^{-6} m^3/s (6 - 25 l/min) and orifices were inserted into a 19 mm tube. Results from this measurement set are shown in

Figures 5-9 and *5-10*. Pressure drops were not dependent on the hydraulic diameters of the differently shaped orifices as might be expected. According to Gerhart and Gross, hydraulic diameters of different duct shapes can be calculated by the following equation:

$$D_h = \frac{4A}{P} = \frac{4 \times (\text{Duct cross} - \text{sectional area})}{\text{Wetted perimeter}} \qquad \textit{(Equation 5-13)}$$

The annular orifice had the smallest hydraulic diameter of the four different shape orifices but pressure drops across the annular orifice were shown to be lowest. Whereas the triangular orifice had a smaller hydraulic diameter in comparison with the square and circular orifices, but the pressure drops were higher. This means that pressure drops do not depend on the hydraulic diameter, but on the orifice shape, or possibly, *Equation 5-13* cannot be applied for calculating hydraulic diameter of annular orifices.

Figure 5-9 shows pressure drops versus the square of flowrate, the data points of each measurement are on a straight line. Pressure drops depend on the orifice shape; except for the annular orifice, the pressure drop reduces with increasing hydraulic diameter of the different shaped orifices (with increasing hydraulic diameter orifice shape tends towards circular). As can be seen from *Figure 5-9* the best shape is the annular shape, and pressure drop at a flowrate of 417×10^{-6} m^3/s (25 l/min) changes 200% from the annular shape to the triangular shape (from 3.8 to 7.4 kPa, respectively). From these measurements it is shown that the shape of valves when they are fully open is the second most important factor after the orifice area and before the eccentricity. In fact, orifice area is a limiting condition: due to the valve size limitation, orifice area cannot increase easily and infinitely, but the shape of valves can be changed for better shapes more easily in order to reduce pressure drops. This could explain why pressure drops through the bioprosthetic valve are higher than those of the tilting and bileaflet valves (Hanle *et al.* 1989), because bioprosthetic valves, when open, create a triangular orifice and this shape induces higher pressure drops.

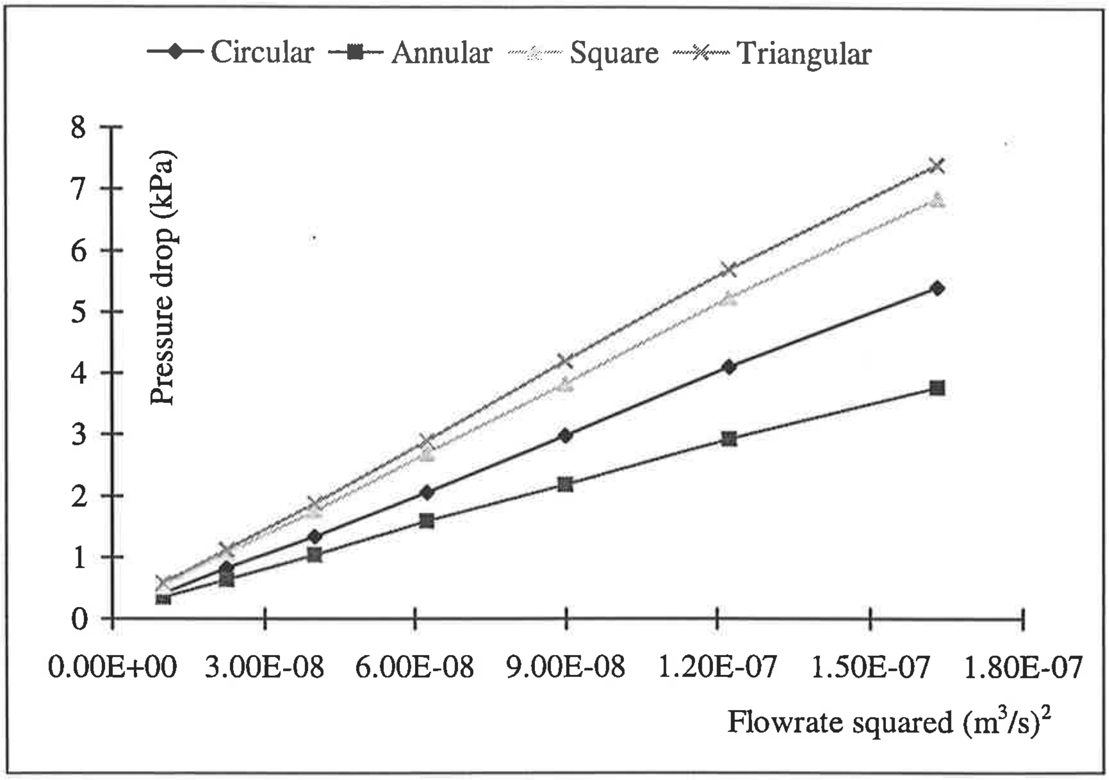

Figure 5-9. Pressure drop versus flowrate squared for orifices of equal area but different shape.

Figure 5-10 shows pressure coefficient versus Reynolds number for different orifice shapes. The pressure coefficient for the triangular orifice is the largest and that of the annular orifice is the smallest. Furthermore, the trend of the pressure coefficient versus Reynolds number of different shapes looks the same. At low Reynolds number, pressure coefficients reduce rapidly, then slow down. At high Reynolds number, they seem to remain steady (see *Figure 5-10*). As mentioned above, the pressure drop is not a function of the hydraulic diameter, but is dependent on the orifice shape. This study introduces a shape factor (Φ_{Shape}) which is used instead of the hydraulic diameter in the description of heart valve orifice configuration.

Pressure coefficient across any orifices are calculated based on a circular orifice with equivalent area then multiplied with shape factor as follows:

$$C_P = C_{P\,circular} \times \Phi_{Shape} \qquad \textit{(Equation 5-14)}$$

where Φ_{Shape} is the shape factor and $C_{P\,circular}$ is the pressure coefficient of a circular orifice with equivalent area. The shape factor is defined as ratio of pressure coefficient measured from experiments of any shape orifice to circular orifice with equivalent area as:

$$\Phi_{Shape} \equiv \frac{C_{P\,shape}}{C_{P\,circular}}$$

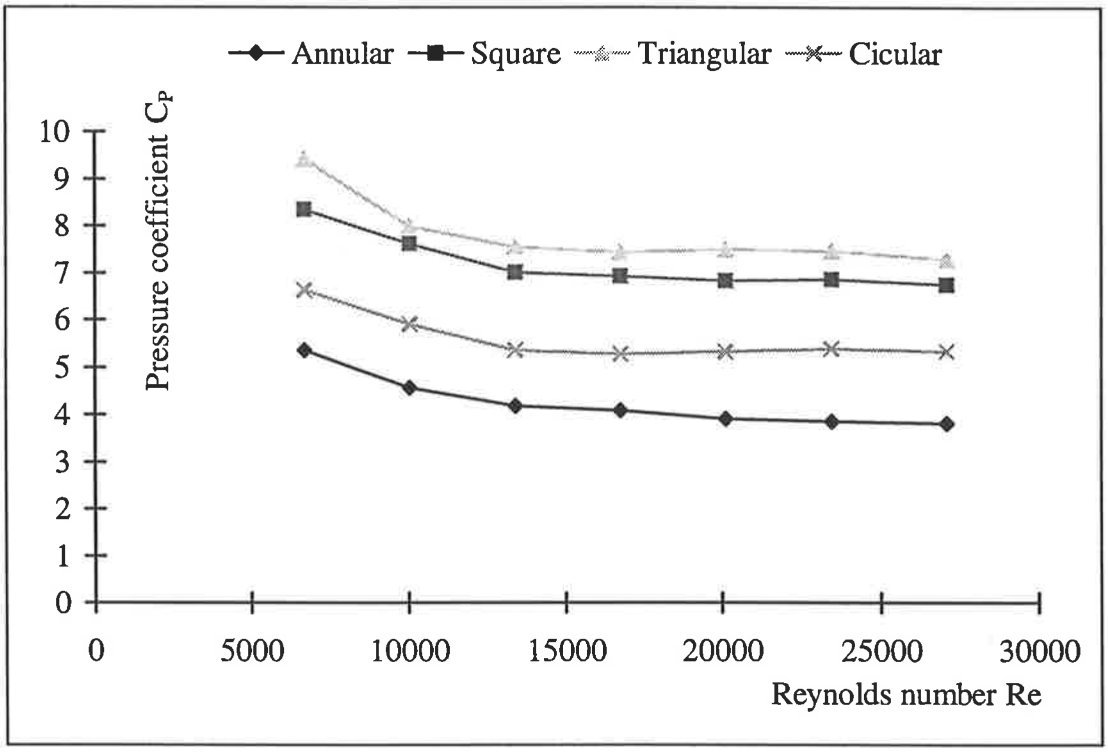

Figure 5-10. Pressure coefficient versus Reynolds number for orifices of equal area but different shape.

and the shape factor can be established from *Figure 5-10* by averaging from 7 data points. For annular orifices the shape factor is:

$$\Phi_{Annular} = 0.756$$

for square orifices the shape factor is:

$$\Phi_{Square} = 1.285$$

and finally, the shape factor of triangular orifices is:

$$\Phi_{Triangular} = 1.394$$

The actually measured orifice area of the four different shape orifices is the same and equal to 1.13 cm^2. The effective orifice area of these orifices can be calculated using Gorlin and Gorlin formula (1951) (re: *Equation 4-10*).

For comparison, the discharge coefficient for each orifice was considered to be unity ($C = 1$), and the effective orifice area of the different shape orifices was calculated. The actual discharge coefficient C of these orifices is calculated from the ratio of the calculated to the measured area and now is defined as the shape coefficient C_{Shape}.

Table 5-3. Effective orifice area and shape coefficient of different shaped orifices

Shape	Triangular	Square	Annular	Circular
$A_{Effective}$ (cm^2)	1.01	1.05	1.37	1.19
C_{Shape}	0.89	0.93	1.22	1.06

As can be seen from these results, due to the difference of pressure drops the calculated effective orifice area is significantly different from the theoretical orifice area (A_{Actual} =1.13 cm^2 for each shape). Discharge coefficients of the annular and circular orifice are larger than 1, here the discharge coefficient of the circular orifice is larger by 6% (see *Table 5-3*) probably due to the error in the instruments and the position of pressure taps along the tube (see *Figure 2-2*). The discharge coefficient of the annular orifice is equal to 1.22 which much larger than 1, this is due to its annular shape. This result is unexpected, because the discharge coefficient through any orifices were expected to be ≤ 1 (Gorlin and Gorlin 1951, ASME 1959). Discharge coefficients depend on the orifice shape as does the relationship between the effective orifice area and the actual orifice area. These results can imply that the comparison of calculated effective orifice area with the actually measured area obtained from an autopsy or during operation may lead to mis-evaluating discharge coefficient C. This is because the valve shape is different post-mortem or under open heart surgery compared with its shape under normal conditions. This is especially true for the patients with a prosthetic heart valve. For example, Horstkotte *et al.* (1983) calculated the mean value of effective orifice area of Björk-Shiley SD valves implanted in patients in the mitral position using the Gorlin and Gorlin formula and this value was 14% larger than the mean orifice area measured by Heiliger (1987) using a fibre-optic camera. This difference may be caused by the fact that the Gorlin and Gorlin formula did not take the orifice area of the Björk-Shiley valve as a annular orifice into account.

5.1.5 Summary of pressure-flow relationships

Finally, an equation of pressure coefficient through any primary orifices with flowrates of 100 to 417×10^{-6} m^3/s (6 - 25 l/min) can be established from *Equations 5-6, 5-7, 5-9* and *5-14* as follows:

$$C_P = \frac{C_{Pr} \times C_{PR} \times C_{PE}}{29.21423} \times \Phi_{Shape} \qquad \text{(Equation 5-15)}$$

with correlation factor r is:

$$r^2 = 0.98156$$

where C_{Pr}, C_{PR} and C_{PE} are from the component equations determined above

Φ_{Shape} is the shape factor, in case of circular orifice $\Phi_{Shape} = 1$.

As can be seen from *Equation 5-15*, the effective orifice area of any orifice or heart valve calculated from the Gorlin and Gorlin formula is dependent on the orifice shape, orifice position, Reynolds number and the location of pressure taps, as pressure coefficient is a function of all of these variables. This study advises a method to calculate the real orifice area of valves based on the Gorlin and Gorlin formula (1951), this is developed in the following paragraphs.

Firstly, discharge coefficient is considered to be unity (C = 1), so that the formula becomes:

$$A_{Effective} = \frac{Q}{44.5 \times \sqrt{\Delta P}}$$ (Equation 5-16)

Secondly, use *Equation 5-16* to calculate the mean effective orifice area, as the effective orifice area varies with the change of Reynolds number corresponding to flowrate of 100 to 417×10^{-6} m^3/s (6 to 25 l/min).

Thirdly, the real orifice area is established considering the orifice shape and position coefficient determined in *sub-sections 5.1.3* and *5.1.4* and the calculated real orifice area now can be written in the following form:

$$A_{real} = \frac{A_{Effective}}{C_{Position} \times C_{Shape}}$$ (Equation 5-17)

5.2 Velocity profiles

The blood flow through the natural valve is smooth and bathes the entire valve wall, reducing thrombus formation. The closing is perfect and the central opening does not alter the flow pattern, energy being a minimum. On the other hand, in the prosthetic valve, the occluder element and supplementary elements such as strut, hinge and cage produce a high disturbance in the blood flow, creating regions of accelerated flow, where separation and recirculation occur. The low velocity and recirculation regions increase the probability of thrombus formation (Figliola and Mueller, 1981). It is evident, therefore, that velocity profiles should be investigated carefully.

In previous studies, steady flow velocity measurements were generally conducted at flowrates of about 167 and 417×10^{-6} m^3/s (10 - 25 l/min). These steady flowrates correspond to the peak systolic flowrate for cardiac outputs between about 33.3 and 91.7×10^{-6} m^3/s (2 - 5.5 l/min) (Yoganathan *et al.* 1979a, b and c). In this study, velocity measurements through different orifices using LDA were conducted at a flowrate of 417×10^{-6} m^3/s (25l/min) only, and then presented to investigate the effects of flow area, flow shape and occluder position on velocity profiles.

Orifices were inserted into a 19 mm internal diameter tube creating two distinct flow regions, upstream and downstream. In the upstream region, the flow pattern is a fully developed tube flow and in the downstream region, the orifice as stenosis in the entrance disturbs the fully developed flow, and causes jet-flow in the vicinity downstream of the orifice producing different turbulence phenomena.

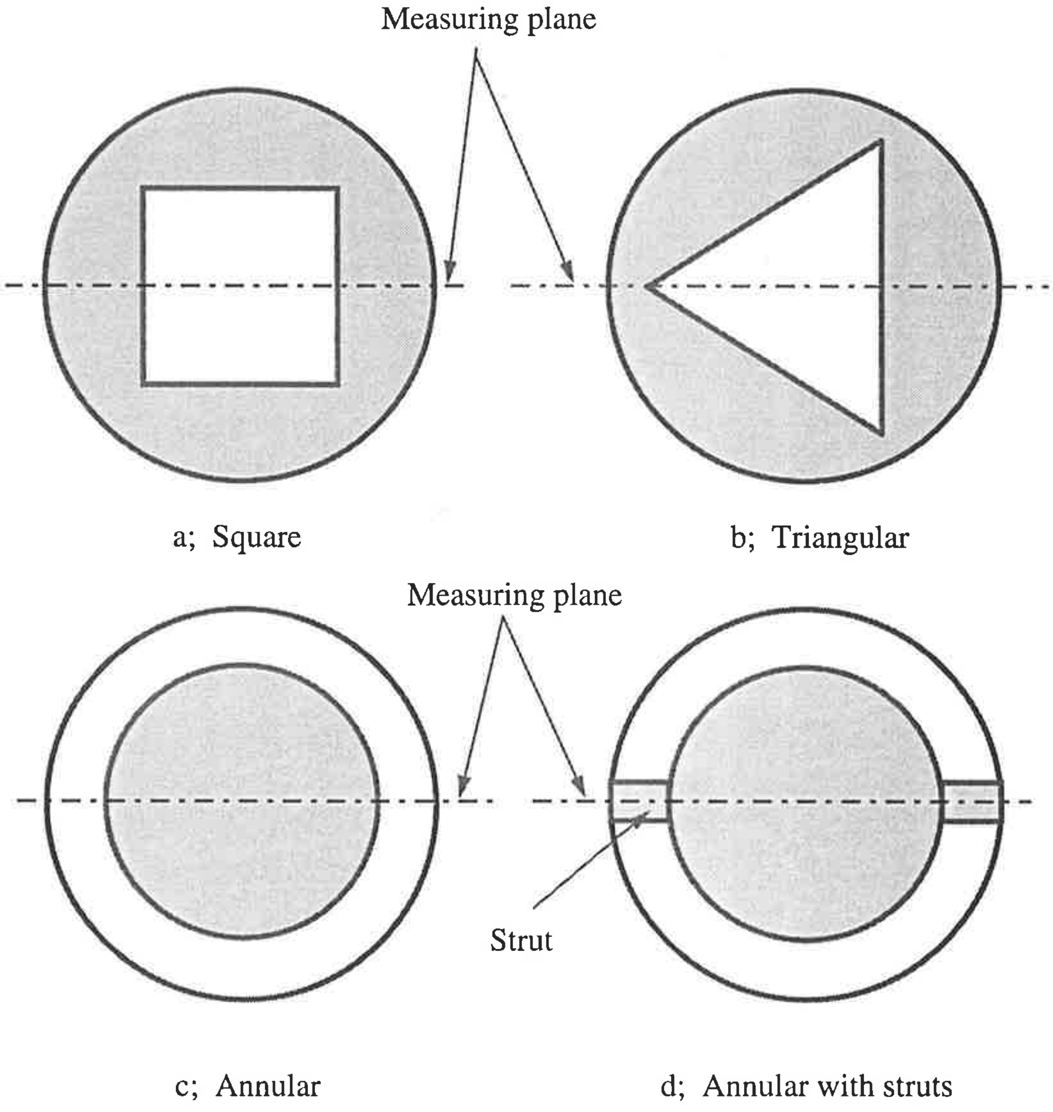

Figure 5-11. Measuring planes across some orifice cross-sections.

Velocity measurements through each orifice called 1 measurement set were carried out at five positions such as 1D up-stream, 1D, 2D, 3D and 6D downstream in the horizontal plane through the centre line of the tube. At each measuring plane, velocities were measured every 1 mm increasingly along the radial position, providing a good picture of the velocity profiles of each orifice. Furthermore, measuring planes through each of the orifice types were chosen to coincide with the critical plane, where the most disturbed velocity profiles should be found, therefore the largest shear stresses can be observed (see *Figure 5-11*).

5.2.1 The effects of the orifice area on velocity profiles

The first measurement set was conducted through four circular orifices with different areas corresponding to r_A = 0.4 to 0.75. As can be seen from the results, upstream profiles are the same, symmetrical, fully developed and with low turbulence intensities, because entrance flow followed a flow straightener. The turbulence intensities here were always under 20% (for more detail see *Appendix 4.1*).

The flow structures downstream of different orifices appears to have been greatly affected by the orifice area. The four different area orifices can be compared with respect to velocity results obtained 19 mm downstream from the orifices during forward flow. The 12 mm diameter orifice (smallest area orifice) generated the highest mean velocity gradients (4.14m/s) in the centre line of the tube and was the only one to generate regions of separated and recirculated flow near to the tube wall, which could be seen in the plane data at 1D downstream (see *Figure 5-12*). Root mean square (r.m.s.) axial velocities were minimal on the centre line and got larger near to the tube wall. Tangential velocities got larger when the radial position moved further from the centre line. The 12 mm orifice generated the highest r.m.s. axial and tangential velocities of the four orifices. The mean axial velocity, r.m.s. axial velocity and tangential velocity through the 13.5 , 15 and 16.5 mm diameter orifices were getting smaller and the turbulence intensities reduced in size when the orifice diameter was enlarging. Maximum axial velocity in the 16.5 mm diameter orifice was only 1.86 m/s in comparison with the maximum velocity of 4.14 m/s in the 12 mm orifice.

Maximum velocity 2D downstream of the 12 mm diameter orifice was still very high (3.05 m/s) and the velocity profile at 6D downstream became flat, whereas the velocity profile at 6D downstream of the 15 mm diameter orifice was getting redeveloped and the 16.5 mm diameter orifice had already become fully developed. Consequently, pressure drops and shear stresses became very low with increasing orifice size, because lower disturbance produced lower pressure drops and shear stresses (Hanle *et al.* 1989).

As can be seen from *Figure 5-12*, in the first stage of the downstream region is plug flow, the length of this plug flow depends on the orifice diameter. The diameters of plug flows 1D downstream were 5, 6, 7 and 8 mm across for the 12, 13.5, 15 and 16.5 mm orifices, respectively. Plug flow length for the 12 and 13.5 mm orifices ended somewhere between the 1D and 2D positions, this length for the 15 mm orifice was about 2D, whereas the plug flow diameter for the 16.5 mm orifice was still about 3 mm at 2D downstream, this length ended somewhere between the 2D and 2.5D positions. These points indicate the end of the initial region of jet-flow. Beyond these points, the flow becomes fully developed jet-flow, this stage ended, when the velocity profile became flat. The fully developed jet-flow length depends inversely on the orifice diameter. For example, the fully developed jet-flow of the 12 and 13.5 mm orifices ended at 6D downstream, whereas for the 15 and 16.5 mm orifices it ended somewhere between 3D and 6D downstream (for more detail see *Appendix 4.2*).

As can be seen that large orifice flow area produces many advantageous haemodynamic characteristics, but the fact is that the flow area of prosthetic heart valves is not easy to increase due to the limitation of the valve size, and structure of the sewing ring. This gives an ideal to optimise the flow with different shapes of a given area in the next section.

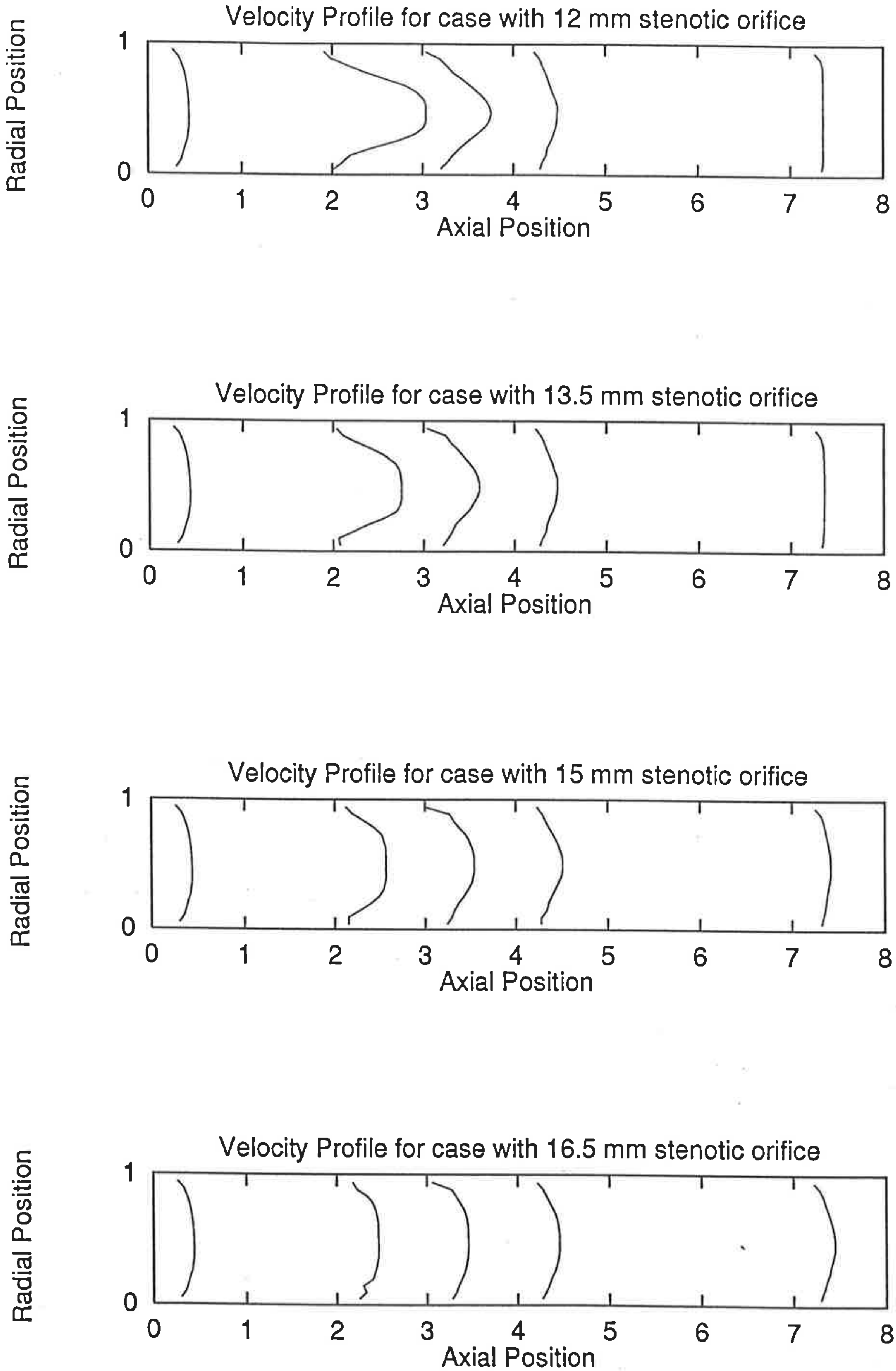

Figure 5-12. Velocity profiles through four circular orifices.

5.2.2 The effects of the orifice shape on velocity profiles

Secondly, velocity measurements were conducted through four orifices with the same area but different shapes, such as circular, square, triangular and annular, again at a flowrate of 417×10^{-6} m^3/s (25l/min). As before, upstream flow was fully developed turbulent tube flow, turbulence intensities were under 20% and peaked near to the tube wall.

Like pressure drop, the maximum velocity change through the annular orifice was the lowest of all orifice configurations (with a value of 3.01 m/s, 1D down stream). For flow through the circular, square, and triangular orifices at 1D downstream, this value was 4.14, 4.44 and 4.02 m/s, respectively. The velocity gradient of the annular orifice was low, but velocity jetting was occurring very near to the tube wall. This may lead to very high wall shear stress which can damage the aorta wall.

The length of the recirculation region of the triangular orifice was the longest, as can be seen from velocity profiles at 1D downstream. Velocities of the triangular and circular orifice near to the tube wall were negative, whereas those of the other two orifices were zero or positive. Here the result was unexpected, when the velocity gradient through the annular orifice was the smallest and through the triangular was smaller than those through the square and circular orifice. This can be explained by firstly, the r.m.s. of axial velocity through the triangular orifice was very high (1.07 m/s in comparison with 0.27 m/s through circular orifice and 0.46 m/s through square orifice of maximum velocity point) and the results thereby were affected and led to an unexpected value. Secondly, as mentioned in *sub-section 5.2.1* the length of the initial flow region depends on the orifice diameter, specifically hydraulic diameter, so that the comparison of velocity profiles at fixed distance was not very practical.

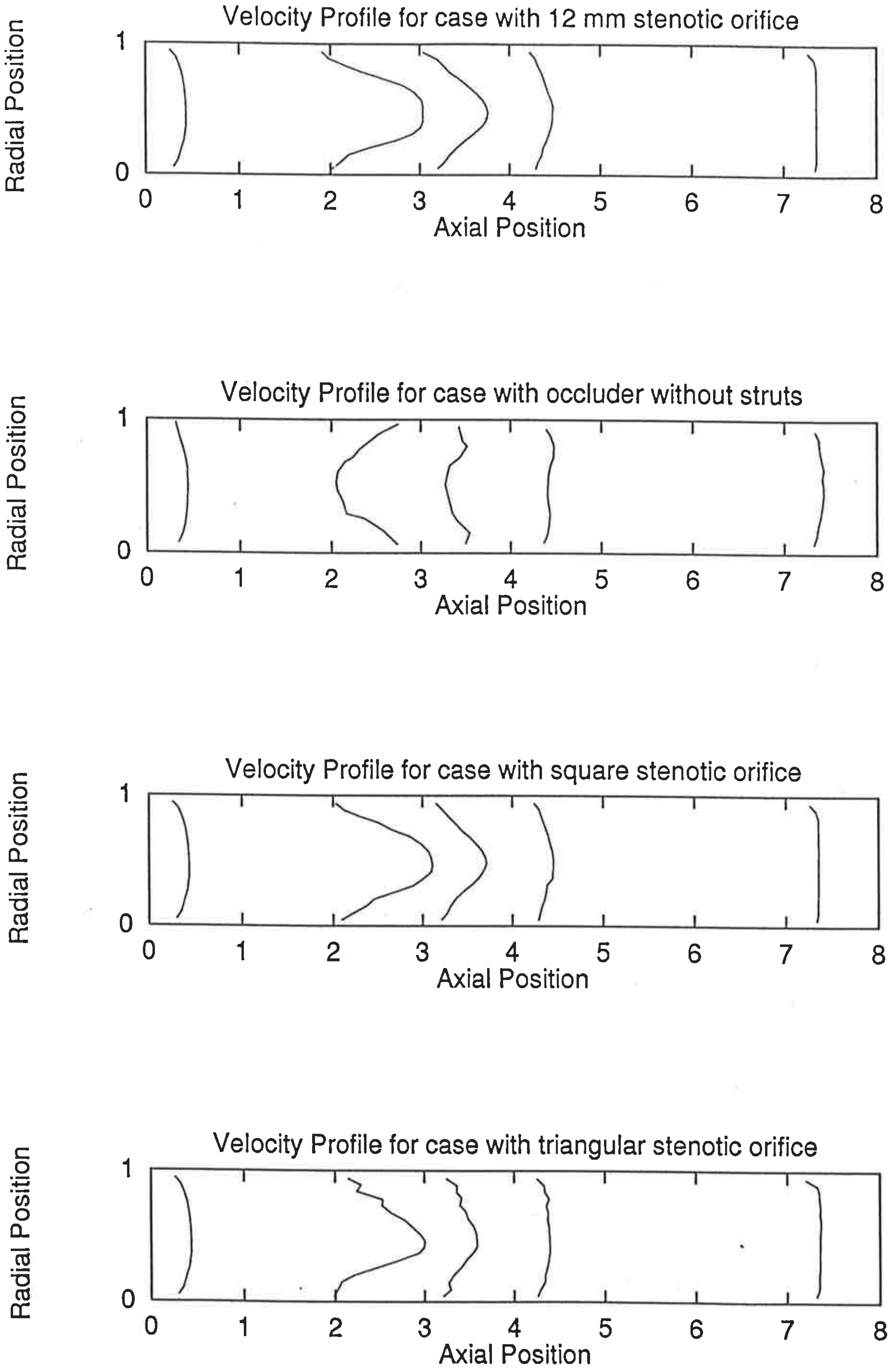

Figure 5-13. Velocity profiles through four different shape orifices for a constant flow rate

Figure 5-13 shows the velocity profiles across four shape orifices, the first stage (plug flow) of the triangular and annular orifices was not observed as it ended at a position less than 1D downstream, and the nearest measuring plane to the orifice location was located at 1D downstream. The initial jet-flow of the square orifice just ended at 1D downstream and the circular orifice ended somewhere between 1D and 2D downstream.

In the second stage, the flow becomes fully developed jet-flow and the result here is unexpected like in the pressure drop measurements. The flow through the annular orifice became fully developed jet-flow somewhat quicker than those of the three other orifices, even though the annular orifice had the smallest hydraulic diameter. Velocity profile through the annular orifice became flat somewhere between 3D and 6D downstream, and at 6D downstream the flow has already become redeveloped turbulent tube flow, whereas the velocity profiles through the triangular, square and circular orifices became flat only at around 6D downstream. In fact, the velocity profile through the circular orifice became flat somewhat quicker than those of the square and then the triangular orifices and seems to depend inversely on the hydraulic diameter. These results can imply that the hydraulic diameter of annular orifices does not work for pressure drop measurements or velocity fields.

As can be seen from these results, the triangular orifice produced the highest r.m.s. axial and tangential velocity and then the annular orifice. The circular orifice generated the lowest r.m.s. axial and tangential velocity. A region of separation and circulation can be observed at 1D downstream of the circular orifice and triangular orifice, between the wedge of the triangle and the tube wall. Furthermore, mean tangential velocity through the annular orifice was the highest and at 1D downstream this maximum value was 0.45 m/s in comparison with 0.14 m/s of the triangular; 0.08 m/s of the square and 0.06 m/s of the circular (for more detail see *Appendix 4.3*). This means that the orifice shape as the shape of prosthetic heart valves when they are fully open is a very important factor in affecting and disturbing the flow downstream of valves, and creating the regions of stagnation and recirculating flow -

which promote thrombus formation and tissue overgrowth. Moreover, the shape dictates the magnitude of the r.m.s. velocities which also imply higher shear stresses.

5.2.3 The effects of the occluder position on velocity profiles

Velocity measurements were conducted for flow around a 14.5 mm ball inserted inside a 19 mm internal diameter tube to investigate the effects of the occluder position (eccentricity) on velocity profiles. The ball was located in three positions (see *Appendix 1*). Firstly, in the centre of the tube then it moved from the centre line to 1 and 2 mm off the centre line to make eccentricities. Like previous measurements, the velocities were recorded at a flowrate of 417×10^{-6} m^3/s (25 l/min) and in 5 measuring planes - at 1D upstream, and at 1, 2, 3, and 6D downstream.

When the ball was located eccentrically, the orifice had two regions of unequal area available for forward flow , these are called the major and minor flow orifices. Due to the major and minor flow structure of these orifices, the flow fields, which are shown in *Figure 5-14* were very eccentric and dependent on the eccentricity of the ball.

When the ball was located at a maximum eccentricity of 2 mm, it caused the highest eccentric flow field in comparison with those of other measurement sets. A region of stagnation and recirculation was observed behind the ball which was approximately the same size as the 14.5 mm diameter ball. This region was still evident 1D downstream with a size of 3 mm on one side of the tube and in another side of the tube, a new stagnation and recirculation region was being created with a size of 5 mm because of the eccentric jet-flow downstream of the ball. This region reduced further from the orifice location and became zero at 2D downstream.

As eccentricity was reduced smaller stagnation and recirculation regions were generated. No further stagnation and recirculation regions were found at distances between 1 and 2D downstream of the 0 and 1 mm eccentrically positioned occluder.

The recirculation region within 1D downstream of the concentric occluder was somewhat smaller than that of the 1 mm eccentric orifice (see 2D downstream velocity profiles of the 0 and 1 mm eccentric orifices). The velocity profile of the 0 eccentric orifice became flat somewhere between 3 and 6D downstream of the orifice and started becoming redeveloped at 6D downstream. Whereas, the velocity profiles of the 1 and 2 mm eccentric orifices at 6D downstream were still affected by the eccentric flow or in other words, affected by the major and minor flow orifices. The direction of the jet-flow changed from the near-side of the tube wall to the far-side. At 6D downstream of the orifice, velocity fields of the 1 and 2 mm eccentric orifices had not become flat and still remained asymmetrical (see *Figure 5-14*).

The velocity gradient and r.m.s. axial velocity of the 1 mm eccentric orifice at 1D downstream was somewhat higher than that of the 2 mm eccentric orifice, 1 and 0.9 m/s for mean axial velocity and 1.7 m/s and 1.67 m/s for r.m.s. axial velocity, respectively. According to Hanle *et al.* (1989), the high velocity gradients imply high shear stresses, so that shear stress here should be higher than those in the 0 and 2 mm eccentric orifices and results agreed with expectations (see *sub-section 5.3.3*). However, the results were unexpected, because the velocity gradient, r.m.s. axial velocities and shear stresses of the 1 mm eccentric orifice were larger than those of the 2 mm eccentric orifice. These results imply that the comparison of velocity profiles across heart valve prostheses at a fixed distance may lead to mis-evaluating turbulent phenomena of the valve, because different heart valves as well as different occluders produce different jet-flows downstream and their flow regions such as plug flow and fully developed jet-flow ends and starts at different positions. Thereby, velocity measurements at some planes cannot imply the whole turbulent phenomena of the valve, but it can show clearly the region of stagnation and recirculation flow, which promotes thrombus formation and tissue overgrowth. Furthermore, the magnitude of velocity gradient and its r.m.s value can also indicate the magnitude of shear stresses in that measuring plane only.

Though the velocity measurements were conducted for only three positions of the occluder, the tendency of the development of velocity fields is clear. Larger eccentricity of the occluder induces larger stagnation and recirculation region and higher pressure drops which promote thrombus formation and tissue overgrowth, this agreed with Hanle *et al.'s* work (1989).

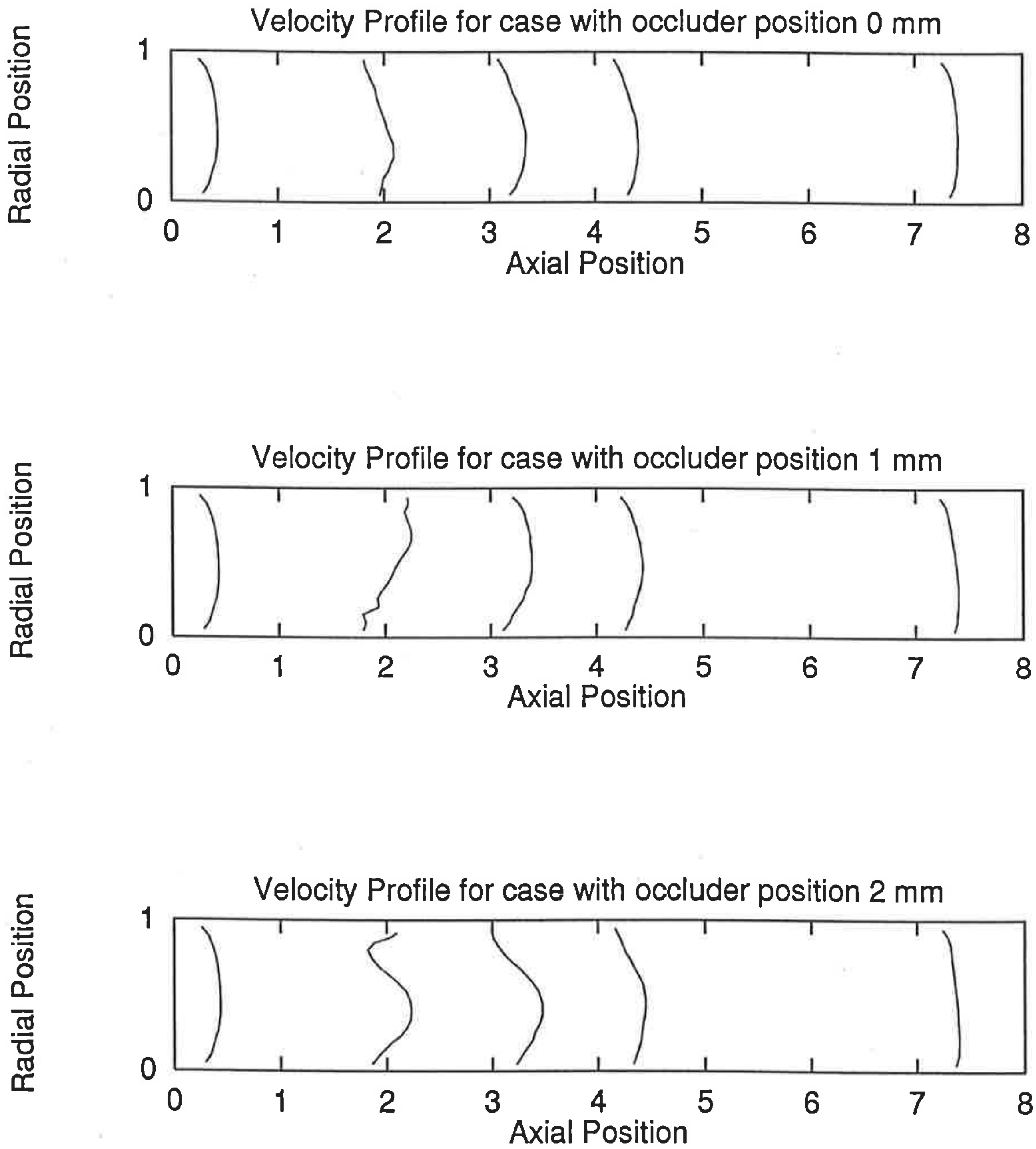

Figure 5-14. Velocity profiles through different occluder positions

5.2.4 Summary of velocity fields

The flow downstream of the orifices or valves is jet-flow, which consists of three stages; initial jet flow region, fully developed jet-flow and finally, redeveloped turbulent flow. At the first stage, plug flow can be observed, which separates at the edges of the orifice. Flow which is very close to the orifice (flow at the nozzle of the orifice) is simply a jet of uniform mean velocity separated from the surrounding fluid by a vortex sheet. With increasing distance from the orifice this vortex sheet is diffused by the action of molecular viscosity, and the region of plug velocities is tending to zero. Beyond this point, the rate of increase of thickness of the mixing length of the mixing layer is larger, and at several orifice diameter lengths the two mixing layers merge with each other and a fully developed jet-flow is established. At this point, plug flow disappears. This agrees with the theory of turbulent jets (Abramovich 1963).

According to Abramovich (1963) the maximum length of a jet in order to become a fully developed jet flow is :

$$L_{max.} = 3d$$

where d is orifice diameter.

As can be seen from the results of this study, this length is about $2d$, where d is the hydraulic diameter of orifices. Initial regions of the annular and triangular orifices cannot be observed in the results, because the closest velocity profile downstream of the orifice could not be located at the position less than 1D (19 mm), as the laser beams were obstructed by the orifice housing (see *Appendix 1*).

The second stage is the fully developed jet-flow, where no further plug flow can be found and mean velocity gradients became smaller further from the orifice location. The region between the end of the initial jet-flow and the beginning of the second stage is called a transition region. At the end of this stage the flow pattern again became plug flow and the velocity profiles became flat across the whole tube diameter; this occurred at about 3 to 7D downstream of the orifice, dependent on the hydraulic diameter, and the orifice and occluder position. Except in the concentric annular orifice, the length of the second stage flow depended inversely on the hydraulic diameter of orifices. Beyond this point, the flow pattern became redeveloped turbulent tube flow and this is the third stage.

As can be seen, three stage flows were observed downstream of orifices or heart valves and each stage occurred and ended at different positions downstream of their location. Comparison of velocity profiles of heart valves at the fixed positions such as 1 and 2D downstream can provide only the information of stagnation and recirculation region, otherwise it leads to incompatible practice, especially in the comparison of shear stresses.

5.3 Shear stress fields

For the determination of the effectiveness of artificial heart valves, not only pressure drops and velocity profiles, but also shear stress fields have to be taken into account. Reynolds shear stresses can be calculated from any orthogonal fluctuating components (Stevensohn *et al.* 1985):

$$\tau_{x\theta} = \rho \, \overline{u' v'} \qquad \textit{(Equation 5-18)}$$

where u' and v' are axial and tangential fluctuation components, respectively.

ρ is the density of fluid.

$$u' \approx \pm \delta U \approx \pm \frac{\partial U}{\partial r} \times \delta r \qquad \textit{(Equation 5-19)}$$

Furthermore, the mixing model assumes that the fluctuating velocities can be calculated (Gerhart and Gross, 1985) by:

$$\text{and} \quad u' \approx v' \approx -l \times \left(\frac{\partial U}{\partial r}\right) \qquad \textit{(Equation 5-20)}$$

where l is the mixing length and

U is the axial time average velocity of one point.

As can be seen from *Equation 5-18,* Reynolds shear stress is a function of r.m.s of axial and tangential velocities. Furthermore, *Equations 5-19* and *5-20* show that shear stress is dependent on the mixing length and mean axial velocity gradient. Larger r.m.s. velocities and larger velocity gradient imply larger shear stress. In this section, shear stresses were calculated from two measured velocity fluctuation components, axial and tangential, using LDA through different orifices to establish the effects of the orifice area, orifice shape and occluder position on shear stress fields. This procedure is necessary, because high shear stress induced by the disturbance of the presence of heat valves causes haemolysis and red blood cell damage.

5.3.1 The effects of the orifice area on shear stress fields

Velocities were measured using LDA through four circular orifices as mentioned in *5.2.1 sub-section* and shear stresses were calculated using *Equation 4-5,* as measured data was instantaneous, with coincidence windows of 6 μs and maximum data size of 6000 data points.

As mentioned above, the presence of the orifice as stenosis in the flow created two distinct flow regions, up- and downstream. In the upstream region, the flow was fully turbulent tube flow, and the results showed that fluctuating velocities and shear stresses were functions of radial position. These increased, with the radial position getting close to the tube wall, minimum values of fluctuations and shear stresses were evident at the centre line and maximum shear stresses of about 1 Pa in the regions near to the tube wall were observed. This result gave good agreement with Longwell's work (1966). Downstream, the flow was divided into three stages and the shear stress distribution of each measuring plane depended on its mean axial velocity profile, or the flow pattern of each flow stage. Velocity profiles of four circular orifices were clearly observed in the first two stages, the third stage was redeveloped turbulent flow and this was not very clear. The third stage could be observed only at 6D downstream of 16.5 mm orifice, hence only the first two shear stress phases are discussed in the following sections.

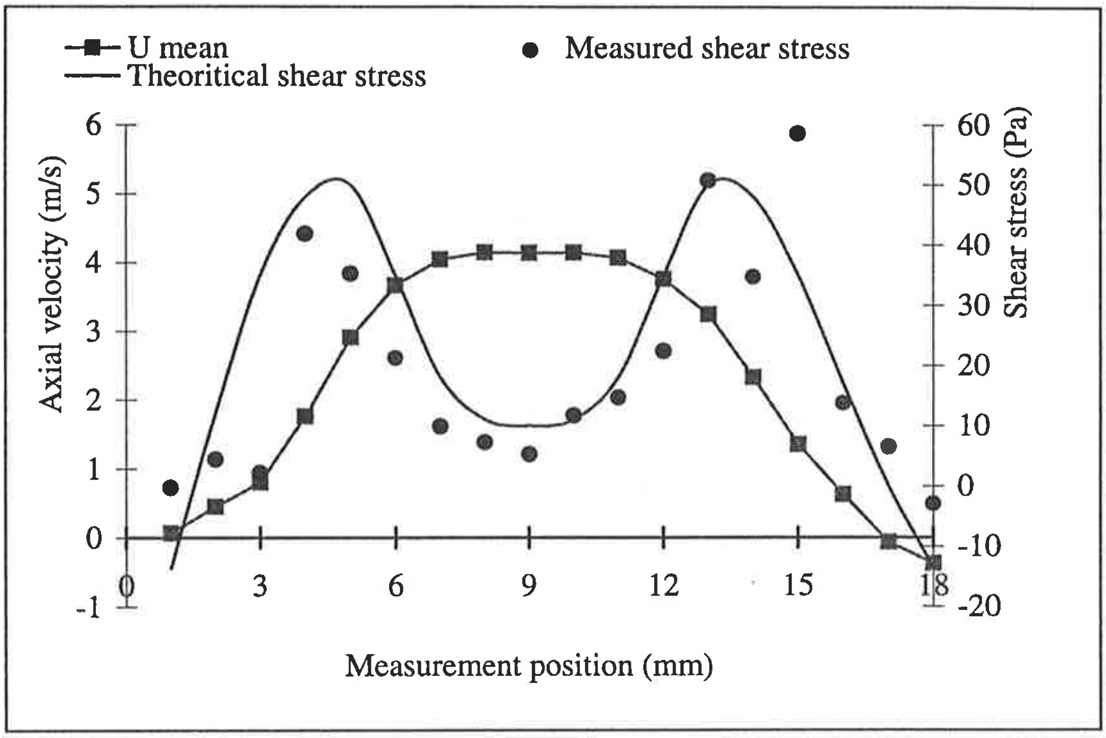

Figure 5-15. The relationship between velocity and shear stress field in initial jet flow region

The first shear stress distribution belongs to the first stage, initial jet-flow. The shear stress distribution of this stage seems to have fourth order function relationship with radial positions. In the centre, where plug flow was observed, axial fluctuating velocities and velocity gradients were minimal and so shear stresses were down as well. Shear stresses had peak values at two points, where axial velocities were increasing to attain the plug flow velocity value (see *Figure 5-15*). This shear stress distribution can be observed at 1D downstream of the 12 and 13.5 mm orifices and at 1 and 2D downstream of the 15 and 16.5 mm orifices.

The second shear stress distribution seems to be second order function with radial positions and this belongs to the second stage flow, fully developed jet-flow. Shear stresses were minimal at the place near to the tube wall and were at peak value at the centre of the tube (see *Figure 5-16*). The second shear stress distribution can be found at 2, 3 and 6D downstream of the 12 and 13.5 mm orifices and at 3 and 6D downstream of the 15 and 16.5 mm orifices.

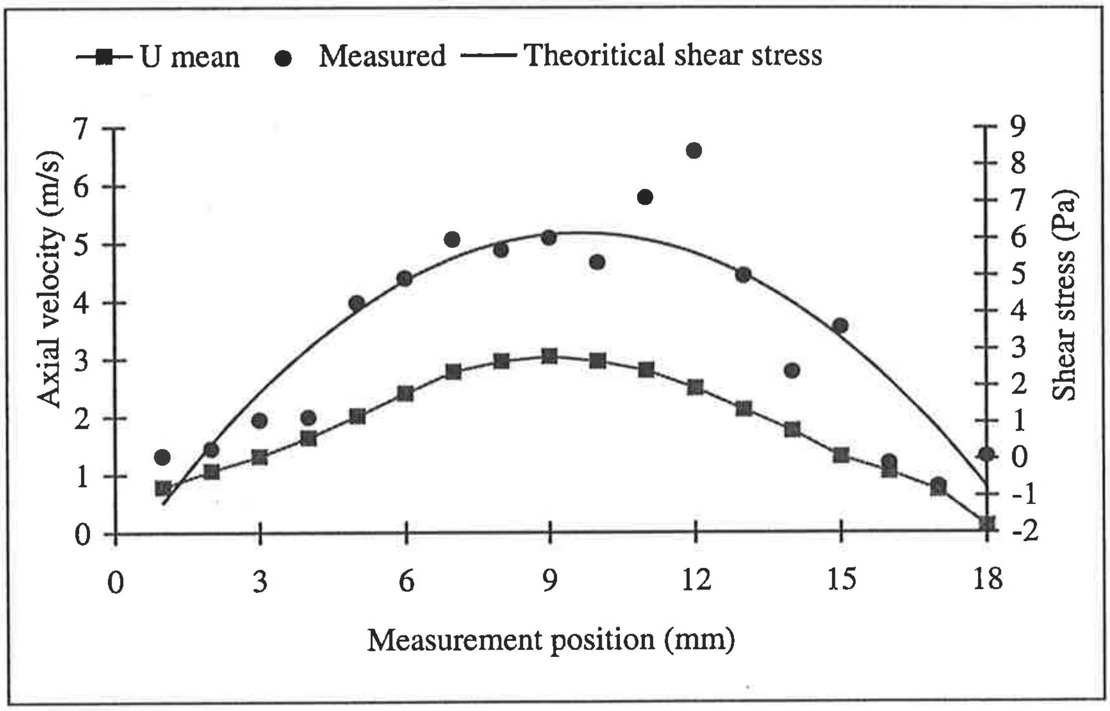

Figure 5-16. The relationship between velocity and shear stress field in fully developed jet-flow region

As can be seen from the shear stress results of four circular orifices, maximum shear stress value did not occur at 1D downstream of the orifice as expected, but did occur at different places from the orifice location dependent on the orifice area. This depended on the flow pattern downstream of orifices as well as prosthetic heart valves. Maximum shear stress of 83 and 45 Pa for the 12 and 13.5 mm orifices occurred at 2D downstream, respectively. Maximum shear stress of 8.6 Pa for the 15 mm orifice occurred at 2D and 3D downstream positions, however, mean absolute value (4.4 Pa) of 3D downstream measuring plane was larger than that (3.6 Pa) of 2D downstream measuring plane. This meant that velocity 2D downstream was still plug flow. Furthermore, maximum shear stresses of about 1 Pa for the 16.5 mm orifice were found at every measuring plane and these were very small in comparison with the error of the instrumentation (for more detail, see *Appendix 4.2*).

As can be seen from the results of shear stresses in the 15 and 16.5 mm orifices, maximum shear stress values were not distinct due to the error of measurements, however, mean absolute shear stress value was more suitable for the purpose of the comparison of shear stresses. It is evident, therefore, that shear stresses are better to be compared for mean absolute value of each measuring plane to avoid the error of experiments.

$$\tau_{mean} = \frac{\sum_{i=1}^{n} |\tau_i|}{n} \qquad \textit{(Equation 5-21)}$$

Maximum mean absolute value of each orifice occurred at the same measuring plane as the maximum value. The 12 mm orifice (the smallest area orifice) produced the highest shear stress of 83 Pa with an absolute mean value of 34.4 Pa at 1D downstream. Whereas the 13.5, 15 and 16.5 mm orifices had maximum mean absolute shear stresses of 19.9, 4.4 and 0.6 Pa, respectively.

It can be summarised, firstly, the magnitude of shear stresses depended on the ratio of orifice diameter to tube diameter *(r_A)*. Maximum mean absolute shear stresses changed significantly from 34.4 to 0.6 Pa when r_A changed from 0.4 to 0.75.

Secondly, mean absolute shear stress at the beginning of the initial jet flow region was minimal, then it increased when the measuring plane moved further from the orifice location and was at a peak value at the transition region, where the initial jet-flow ended and fully developed jet-flow started. In this stage, the rate of the increase of thickness of the mixing length of the two mixing layers was larger with the increasing distance from the orifice, it led to larger shear stresses. In the fully developed jet-flow region, the mean absolute shear stress reduced when the measuring plane was moved further from the orifice location (see *Figure 5-17*). The mean axial velocity gradient and its r.m.s. velocities also reduced. This result gave an agreement with other works (Schwarz *et al.* 1988).

Thirdly, shear stress had a very close relationship with axial velocity and its r.m.s. velocities, these flow parameters determined shear stress distribution downstream of valves. This result agreed with the assumption of the mixing model (Gerhart and Gross, 1985).

Fourthly, maximum shear stress and maximum mean absolute shear stress of the orifice occurred at the same measuring plane within the transition flow region and the position of this region was dependent on the orifice diameter or orifice area.

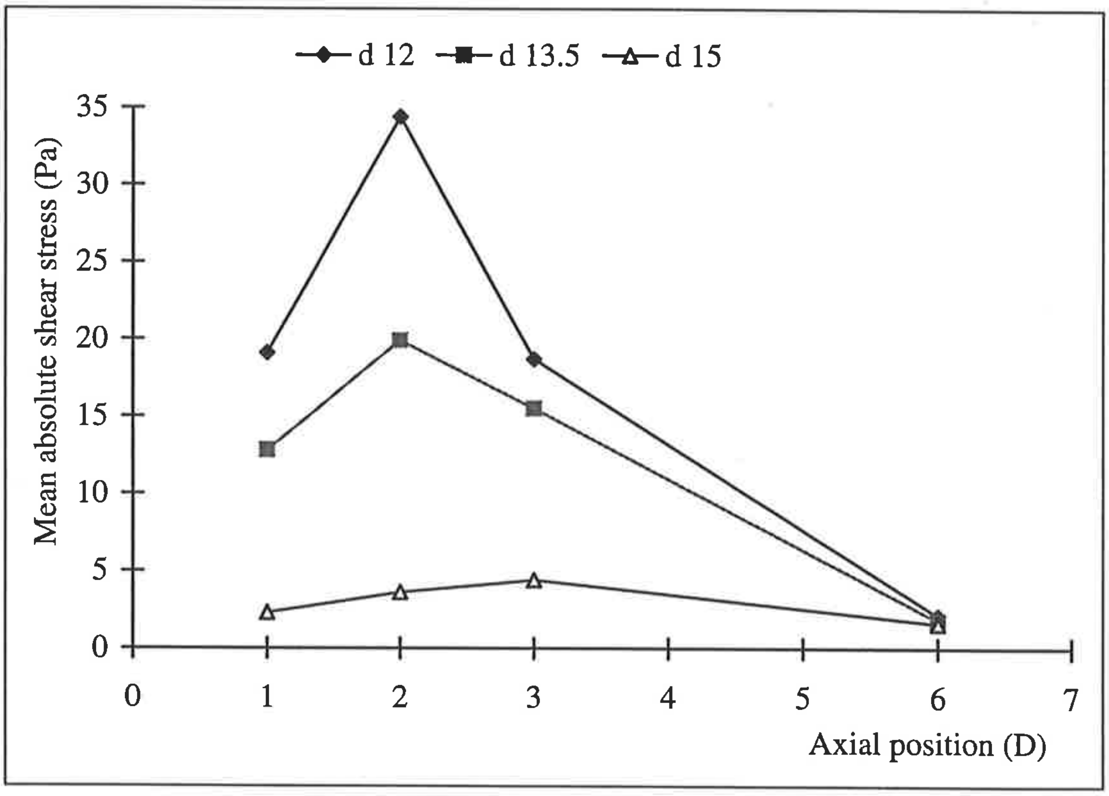

Figure 5-17. Mean absolute shear stress distribution with axial position

5.3.2 The effects of the orifice shape on shear stress fields

As mentioned in *sub-section 5.2.2*, velocities were measured through four differently shaped orifices with equivalent areas. Fluctuating velocity components of these results were used for calculating shear stresses using *Equation 4-5*.

The maximum shear stress point and maximum mean shear stress of the circular orifice occurred at the 2D downstream measuring plane, whereas those of the triangular, annular and square orifices occurred at the 1D downstream plane. This can be explained by the triangular, annular and square orifices having smaller hydraulic diameters than that of the circular orifice of 12 mm. As can be seen from velocity profiles of the square orifice, the initial jet-flow region just ended at the 1D downstream measuring plane. The triangular and annular orifices had hydraulic diameters of 8.5 and 4.5 mm, respectively. Consequently, plug flow was not observed at 1D downstream and only the second stage flow (fully developed jet-flow) was observed in the downstream region of these two orifices. As a result, the maximum shear stress point and maximum mean absolute value for these orifices occurred somewhere less than 1D downstream, so that the shear stress at 1D downstream of the triangular, square and annular orifices was larger than those at 2, 3 and 6D downstream measuring planes.

The triangular orifice produced the highest shear stress and mean absolute value of 230.7 and 104 Pa, respectively. Whereas, the annular orifice with the smallest hydraulic diameter of only 4.5 mm produced the maximum shear stress and mean absolute value of 155 and 90 Pa, respectively. These values were larger than those of the square and circular orifices (for more detail, see *Appendix 4.3*). This result can imply that again *Equation 5-13* is also not valid for calculating hydraulic diameter of annular orifice for shear stresses. The circular orifice generated the lowest shear stress and mean absolute value of 83 and 34.4 Pa, respectively as it had largest hydraulic diameter of four orifices.

As can be seen from these results, the orifice shape (as the valve shape when open) is a very important factor which affects the shear stress fields in the downstream region of valves. Maximum shear stress for the same size of orifice increased dramatically, by 300%, when the orifice shape changed from circular to triangular. This can explain why the shear stress in bioprosthetic heart valve was the highest in comparison with those of other heart valve types (Hanle *et al.* 1989).

Table 5-4. Maximum and mean absolute shear stress at different measuring planes

Shape	Hydraulic diameter		Axial position	1D	2D	3D	6D
Triangular	8.5 mm	Maximum value		**231**	133	47	6
		Mean value (Pa)		**104**	73	17	1.8
Annular	4.5 mm	Maximum value		**146**	56	33	6
		Mean value (Pa)		**69**	17	13	2.5
Square	10.4 mm	Maximum value		**130**	78	31	5
		Mean value (Pa)		**51**	35	15	2.2
Circular	12 mm	Maximum value		60	**83**	48	3.5
		Mean value (Pa)		19	**34**	16	4

5.3.3 The effects of the occluder position on shear stress fields

Velocities were measured for three positions of the ball occluder (more details given in *sub-section 5.2.3*). The first position, when the ball was located on the centre line, created two equal areas for forward flow. The second position with the eccentricity of the ball of 1 mm created two unequal areas for forward flow called major and minor orifices. In the third position, due to the ball location being very near to the tube wall, only one major orifice flow was observed.

The 1 mm eccentric orifice generated the highest shear stress and mean absolute value of 185 and 85 Pa, respectively. Whereas the 2 mm eccentric orifice created the lowest shear stress of 138 Pa in comparison with 155 Pa for the 0 mm eccentric and 185 Pa for the 1 mm eccentric orifice (see *Table 5-5*). This result was unexpected and can be explained by the eccentricity of the occluder causing eccentric flow downstream of the orifice, affecting the characteristics of the initial and fully developed jet flow-region. As a result, the initial jet-flow region for differently occluded flows ended at different measuring planes, consequently, maximum shear stress occurred at different planes. For example, the central orifice had two equal areas for forward flow, so that the length of the initial jet-flow region should be larger than those of the 1 and 2 mm eccentric orifices, and the maximum shear stress should occur at a plane behind 1D downstream. The 2 mm eccentric orifice produced the largest disturbance; as a result, mixing layers of jet and vortex regions merged with each other somewhat quicker to generate fully developed jet-flow, than those of the other two orifices. The transition flow region of the 2 mm eccentric orifice occurred somewhere behind the ball. As a result, shear stress at 1D downstream was not larger than those of the other two orifices, because the maximum shear stress of this orifice should occur somewhere behind the ball at about half D downstream of the orifice. The shear stress profile at 1D downstream of the 2 mm eccentric orifice was already in the fully developed jet flow region. Furthermore, the maximum shear stress of each measuring plane in the fully developed jet flow region reduced from about two to three times when the measuring plane was moved further from the orifice by 1D's distance (see *Tables 5-4* and *5-5*). Maximum shear stress of about 210 Pa for the 2 mm eccentric orifice was expected.

Table 5-5. Maximum and mean absolute shear stresses at different measuring planes

Occluder positions		Axial positions	1D	2D	3D	6D
0 mm	Maximum shear stress Mean absolute value (Pa)		**155** **53**	55 22	13 6	8 4
1 mm	Maximum shear stress Mean absolute value (Pa)		**185** **85**	51 17	25 12	6 2.2
2 mm	Maximum shear stress Mean absolute value (Pa)		**138** **58**	43 19	19 8	6 3

As can be seen from these results, the larger eccentricities of the occluder caused larger shear stresses (except when very large eccentricity causes one single jet and eliminates the effect of the minor orifice), this can explain why the shear stress for the tilting valve was very high (almost as high as for bioprosthetic valves), even though the tilting valve had larger effective orifice area (Hanle *et al.* 1989), because in the tilting valve, the tilting disc produced eccentric flow and this increased shear stresses. Maximum shear stress and its mean absolute value occurred at different positions downstream of the orifice dependent on the occluder position and this leads to a conclusion that the comparison of shear stresses at a fixed plane of valves is not fair enough or practical. Like in the pressure drop measurements, the eccentricity of the occluder does not affect as much as the orifice shape and area does.

5.3.4 Summary of flow relationships

The orifice causes stenotic blood flow which leads to two distinct stages of flows downstream of the valve known as initial and fully developed jet flow. These two flow regions produce two corresponding shear stress distributions. Shear stress in the initial region increases when the measuring plane moves further from the orifice and reaches a peak value within the transition flow region. Whereas shear stress in the fully developed jet flow region reduces further from the orifice location. Overall mean absolute shear stress distribution along axial position can be observed in *Figure 5-17*.

Maximum shear stress and its mean absolute value occurs at the same measuring plane - within the transition flow region, and this region is observed at different positions dependent on the orifice hydraulic diameter and occluder position. Smaller hydraulic diameter and larger eccentric orifices produce more disturbed flow, as a result the transition flow region as well as maximum shear stress and its mean absolute value occur at the position closer to the orifice location (see *Figure 5-17* and highlighted data on *Tables 5-4* and *5-5*). This result leads to a conclusion that the comparison of shear stresses of different heart valves at a fixed distance from the valve location in previous studies may lead to mis-evaluating the valve performance.

The magnitude of shear stresses downstream of the valves in each measuring plane is a function of axial velocity profiles and its r.m.s velocities. In the initial jet flow region, minimal and maximal peak shear stresses can be observed in the plug flow region and in the region around the plug flow region, respectively. In the fully developed jet flow region, shear stresses reach peak values where velocities reach peak values (for more detail, see *Appendix 4.2*). These shear stress distributions gave good agreement with Woo *et al.'s* work who measured shear stresses downstream of the Abiomed trileaflet heart valve prosthesis.

As maximum shear stress and its mean absolute value of each orifice occur at the same plane, leading to an ideal that the comparison of heart valve *in-vitro* measurements for maximum mean absolute shear stresses is better than that for maximum shear stresses, because this may reduce measurement error.

The orifice area is the most important factor in reducing shear stresses, but alterations to this are impractical due to the limitation of the valve size and its structure. Changing the orifice shape is a good way to optimise the valve's fluid dynamical performance. The orifice position does not affect shear stress as much as the orifice area and shape do, but this factor can not be neglected.

5.4 The effects of the struts of the ball on velocity and shear stress fields

Two velocity measurement sets were conducted through the annular orifices, the first across the ball and the second across the ball and two struts (see *Figure 5-11 c* and *d*). Because of the presence of these two struts, the velocity profiles at 1, 2 and 3D downstream of the ball were very disturbed and different from those without struts. The velocity profiles at 6D downstream seem to be the same. The velocity profiles without struts got two peak velocities in the regions near to the tube walls corresponding to the centres of two orifice flow areas, and a low velocity region was observed in the centre line of the tube. This distribution of velocities still remained at 3D downstream plane. Whereas, velocity profiles across struts at 1, 2 and 3D downstream planes peaked in the centre of the tube and low velocity regions near to the tube walls. Maximum velocities of 0.37 and 3 m/s were observed at 1D downstream with and without the struts, respectively. The two struts produced two regions of separation and recirculation flow near to the walls of the tube (see *Figure*

5-18). These two regions were low velocity and recirculation flow regions and relatively large (6 mm in diameter at 1D downstream position), and they promote the probability of thrombus formation in the regions near to the struts. This observation gave good agreement with Yoganathan *et al.*'s work (1981) which investigated the caged ball valve. Furthermore, the presence of the two struts produced higher mean tangential velocities and its r.m.s. velocities downstream of the struts than those without struts.

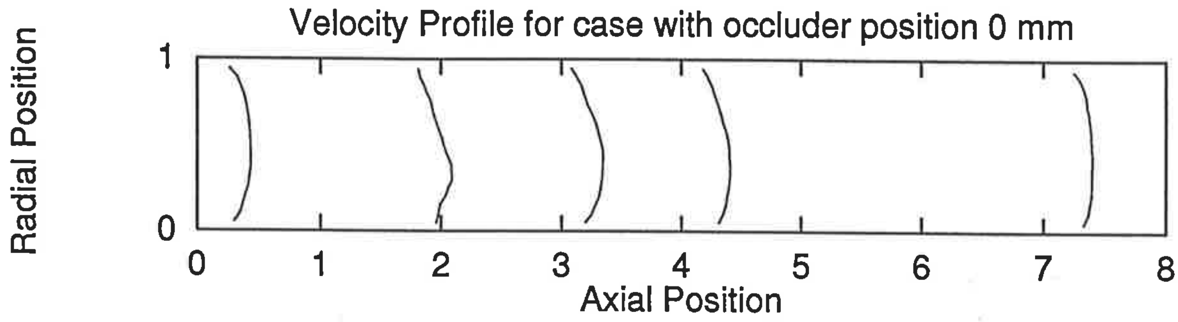

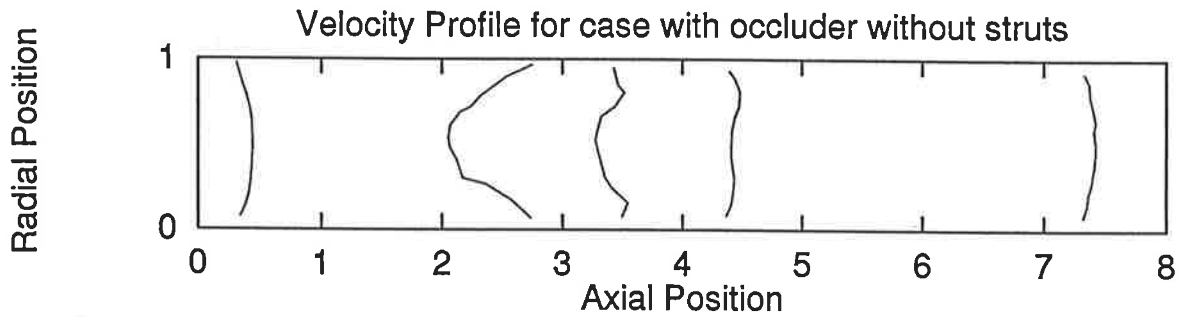

Figure 5-18. Velocity profiles with and without struts

The velocity profiles with struts were different from those without struts leading to different shear stress distributions. Shear stress reached a peak value when the velocity profile curve reached its peak maximum or minimum value in the fully developed jet flow region. Shear stress distribution without struts at 1D downstream looked like the shape of fourth order equation, with two positive peak values at the centre of the two jet-flow areas and one negative in the centre line of the tube (for more detail, see *Appendix 4.5*). A maximum shear stress of 155 Pa was observed at

1D downstream of all two cases, but mean absolute shear stress without struts was larger than that with struts and were 68.7 and 53.4 Pa, respectively (see *Table 5-6).*

As can be seen, the magnitude of the maximum Reynolds shear stress produced by the ball with and without struts was the same, however, the ball with struts produced high velocity gradients near to the tube wall, leading to high wall shear stress which may damage the aorta wall. Furthermore, the ball with struts generated a larger shear stress region (larger mean absolute shear stress) than the ball with struts did. However, the ball with struts produced relatively large stagnation and recirculation flow regions, which are more prone to thrombus formation and tissue overgrowth than areas of high shear stresses (Yoganathan *et al.* 1981).

Table 5-6. Shear stress for case of the occluder with and without the struts

Occluder	Axial positions	1D	2D	3D	6D
With the struts	Maximum shear stress Mean absolute value (Pa)	**155** **53**	55 22	13 6	8 4
Without the struts	Maximum shear stress Mean absolute value (Pa)	**146** **69**	56 17	33 13	6 2.5

5.5 Application to a valve prototype

Since 1960 more than 50 different cardiac valves have been introduced and most of them have been discarded due to lack of clinical success. The most commonly used basic types are caged ball, tilting disk, bileaflet pivoting disc and tissue bioprosthesis. Different valve types have different occluders and produce different flow patterns in the near vicinity downstream of the valve, though valves have the same size but effective orifice areas are different. Furthermore, the flow pattern depends strongly on the structure of valves such as occluder type, shape and position. For example, the caged disk valve proved the most obstructive of all prosthetic valves and the tilting disk valve produced eccentric flow downstream of the valve and caused high velocity gradient.

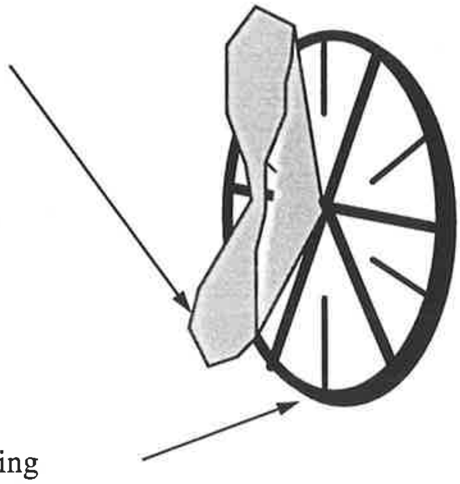

Figure 5-19. Jellyfish valve configuration

In this section, experiments were conducted through a heart valve prototype called a Jellyfish valve, under both steady and pulsatile flow conditions. This valve has the size of 20 mm, and is newly and specially designed for VAD. Unlike other mechanical heart valve prostheses, the Jellyfish valve has a very special occluder in the form of a flexible membrane attached to the centre of a stiff stent (see *Figure 5-19*). This causes minimal obstruction and limited occluder inertia, thus leading to small shear stresses, limited pressure gradients and energy losses (Tran *et al.* 1995). This valve was measured and compared to indicate the effects of the occluder on the fluid mechanics of blood flow through the heart valve prosthesis. Furthermore, pressure drops were measured to compare with the results predicted by this study (from the orifice and occluder configuration).

Jellyfish valve measurements were conducted under the same conditions as the orifice measurements. Steady flow pressure drop measurements were carried out with flowrate range 100 to 417×10^{-6} m^3/s (6 - 25 l/min). LDA velocity measurements were conducted under steady flow conditions with a flowrate of 417×10^{-6} m^3/s and LDA velocity, flowrate, and pressure drop measurements in pulsatile flow conditions were carried with a cardiac output of 91.7×10^{-6} m^3/s (5.5 l/min, peak systolic flowrate is about 417×10^{-6} m^3/s), heart beat rate of 1.2 Hz and aortic pressure of 10.26/16 kPa (80/120 mmHg) (see *Figure 3-6* and *3-7*).

5.5.1 The effects of the flexible membrane and orifice shape on steady pressure drops

Steady pressure drops were measured through the Jellyfish valve with and without the flexible membrane as occluder of the valve, at flowrates of 100 to 417×10^{-6} m^3/s. *Figure 5-20* shows pressure drops in kPa versus square of flowrates. Data points were on the two distinct straight lines. As can be seen from the results, pressure drops through the valve with the membrane were larger by about 12% than those through the valve without the membrane attached in the centre. This occurred probably because of two reasons:

- the obstruction of the membrane when it opens
- oscillation of the flexible membrane.

The first reason seems to be insignificant, because when the valve was open the flexible membrane contracts into the centre line behind the base where the membrane was attached causing a very small obstruction to the flow downstream of the valve. Furthermore, velocity profiles (see *Figure 5-21*) of 1.5D downstream of the valve with and without membrane were almost the same, and this could imply that the membrane, as occluder, caused minimal obstruction of the forward flow through the Jellyfish valve.

The second reason was surely significant, because when the valve was open, the membrane oscillated and generated a wake downstream of the membrane which produced a disproportionately wide zone of disturbance further downstream. This led to increased pressure drag and consequently to a larger pressure drop across the valve. This result gave good agreement with Tansley *et al.*'s work (1986) when they found the connection between the instability of the ball occluder and pressure drops and tried to reduce the instability of the occluder by modifying inlet and outlet flow area, and Yoganathan *et al.*'s work in 1981 when they investigated the ball valve and measured pressure drops across the valve in steady flow when the ball was tied and untied. Pressure drops across the untied ball valve was larger by about 18% than those across the tied ball valve due to the oscillation of the untied ball downstream of this valve.

The effective orifice area of the Jellyfish valve can be calculated using Gorlin and Gorlin formula (1951) (re: *Equation 4-11*).

The discharge coefficient C for each particular valve or orifice may be derived empirically, this is best done by comparison of the calculated areas with the actually measured areas. For the most cases, C = 1 was considered, the effective orifice area of the Jellyfish valve with membrane was calculated from average value at different flowrates:

$$A_{Effective\ with\ membrane} = 2.09 \quad \text{cm}^2$$

In the same way, the average effective orifice area of Jellyfish valve without membrane attached in the centre was calculated:

$$A_{Effective\ without\ membrane} = 2.36 \quad \text{cm}^2.$$

As discussed above, the presence of the membrane gave minimal obstruction to forward flow of the Jellyfish valve, so that the actually measured orifice area of the valve with or without membrane should remain the same and this value is:

$$A_{Actually\ measured} = 1.74 \quad \text{cm}^2.$$

As can be seen from the results of the actually measured and calculated areas, the effective orifice area of the valve with membrane is smaller than that of the valve without membrane by about 12% due to the oscillation of the membrane in forward flow of the valve. The measured orifice area is too small in comparison with the calculated areas, this is unusual and unexpected, because C factor now is about 1.20, whereas C should be ≤ 1.

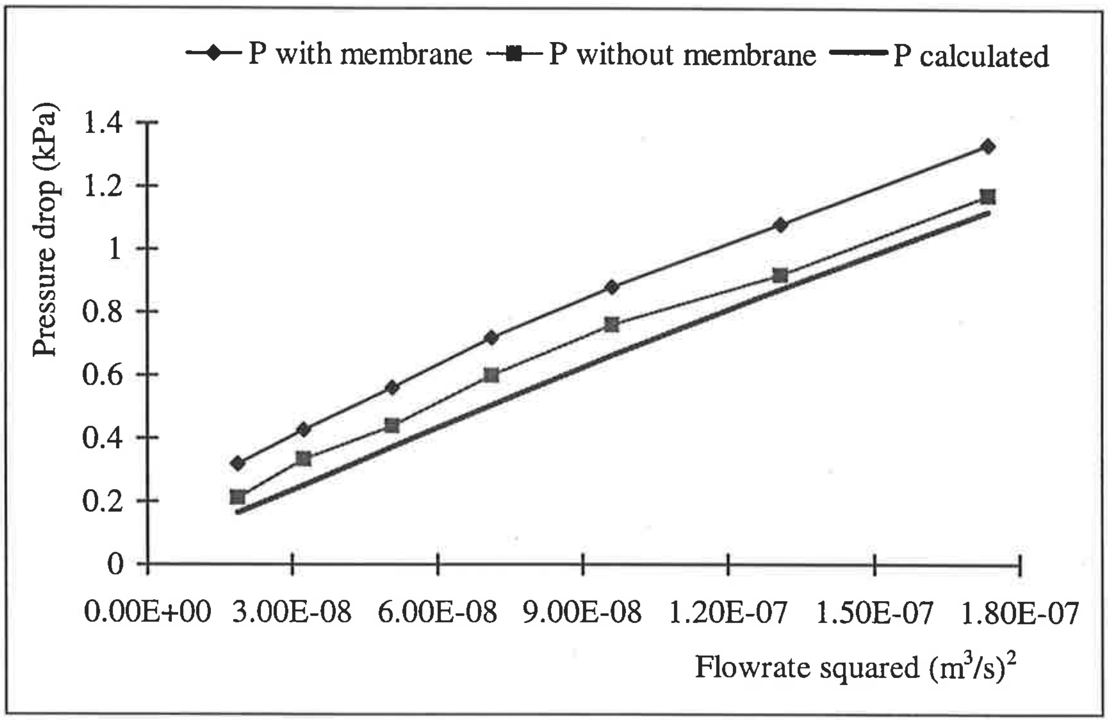

Figure 5-20. Calculated and measured pressure drops versus flowrate squared

Furthermore, pressure drops across the Jellyfish valve were predicted using equations developed in this study. The valve was considered as an annular orifice, so that pressure drops were calculated using *Equation 5-15* considering the shape of the orifice. *Figure 5-20* shows the calculated pressure drops with the measured values versus square of flowrate. As can be seen, the predicted pressure drops stayed within error of 5% in comparison with the results of the valve without membrane and within 15% of the results of the valve with membrane. This means that this formula can be applied and gives good results only for the valve without the oscillation of the occluder. Moreover, actual orifice area of the valve calculated using *Equation 5-17* of this study fitted the measured orifice area with a maximum error of 1.2%.

In conclusion, the flexible membrane as occluder gives minimal obstruction in forward flow through the Jellyfish valve, generating low pressure drops, a maximum pressure drop of 1.33 kPa (10 mmHg) was observed at a flowrate of 417×10^{-6} m^3/s (Tran *et al.* 1994). However, the membrane oscillated in the flow and generated a wake downstream of the valve producing larger pressure drops than those of the valve without membrane. Consequently, a smaller effective orifice area was produced. The Gorlin and Gorlin formula is unreliable for the calculation of effective orifice area of the Jellyfish valve, because this formula did not take the shape coefficient of annular orifice flow (the orifice shape) into account. This value for the annular orifice is 1.22 *(Table 5-3).* Now, the calculated area should be:

$$A_{Calculated} = \frac{A_{Effective}}{C_{Shape}} = \frac{2.1}{1.22} = 1.72\ cm^2$$

This value gives good agreement with the actually measured value and this result can also be calculated using *Equation 5-17* developed in this study, and gives the same result as the *Equation 5-17* took the shape coefficient of the annular orifice into account.

5.5.2 The effects of the flexible membrane on velocity and shear stress fields

Steady velocity measurements were conducted using LDA through the Jellyfish valve, with and without the membrane occluding the valve, at a flowrate of 417×10^{-6} m^3/s. Velocities were recorded at 1D up- and 1.5 and 2.5D downstream of the valve. Velocity profiles at 1D upstream, like the velocity profiles of other orifices were relatively unaffected by the presence of the valve or orifice, and in this study they are not discussed. Shear stresses were calculated using *Equation 4-5* from axial and tangential fluctuating velocity components as axial and tangential velocities were measured.

Figure 5-21 shows the comparison of velocity profiles at 1.5 and 2.5D downstream of the valve with and without membrane. At 1.5D downstream, the two velocity profiles looked almost the same, but the velocity profile of the valve with membrane looked a little bit more disturbed in the left hand side region than that of the valve without membrane. This result implies that the presence of the membrane causes minimal obstruction. However, at 2.5D downstream, the velocity profile of the valve with membrane was different and became flat somewhat quicker than that of the valve without membrane due to the oscillation of the membrane occluder. This result gave an agreement with Yoganathan *et al.*'s, work in 1981 when they investigated velocity fields of the ball valve with tied and untied ball occluder.

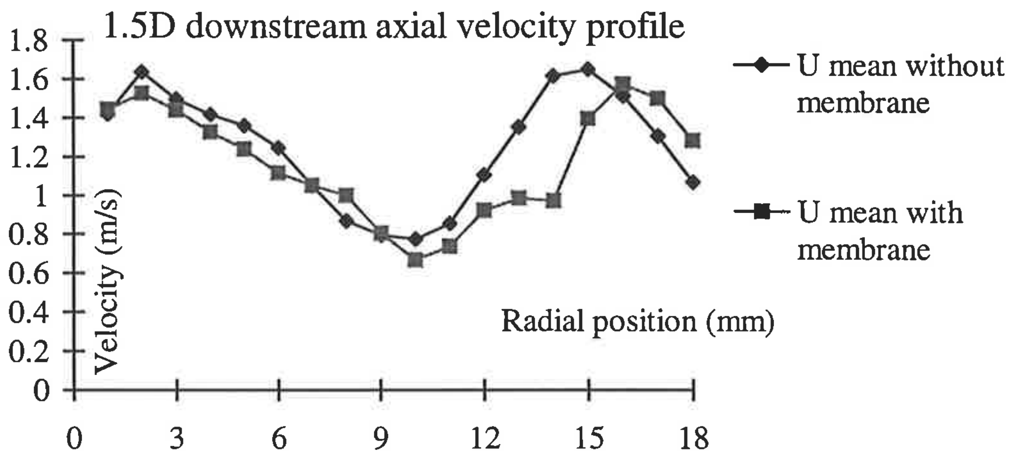

1.

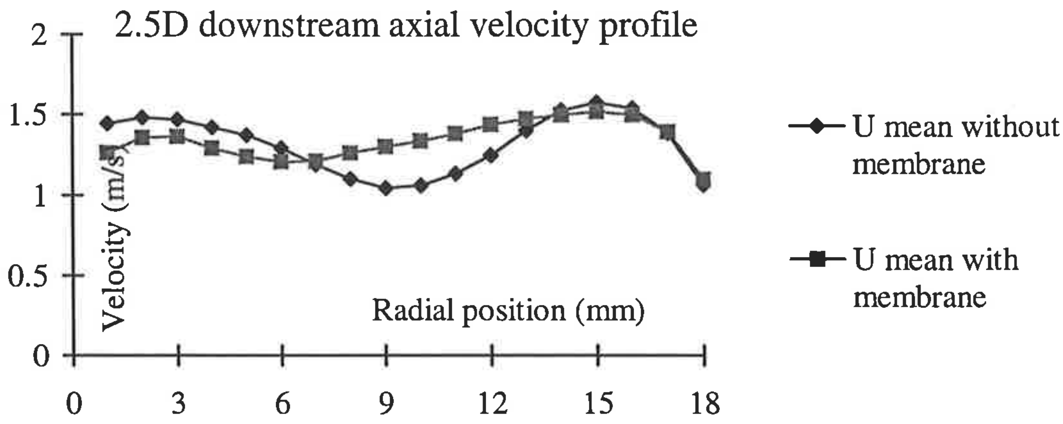

Figure 5-21. Velocity profiles with and without the membrane

Velocity profiles of the valve without the membrane were symmetrical and affected by the presence of the base in the centre where the membrane can be attached, as a result, velocities exhibited a low peak value in the center and two high peak value near to the tube walls. Whereas, velocity profiles of the valve with the membrane attached in the centre were asymmetrical, because the Jellyfish membrane was seen to open into an asymmetrical four-lobed configuration (Tran *et al.* 1995).

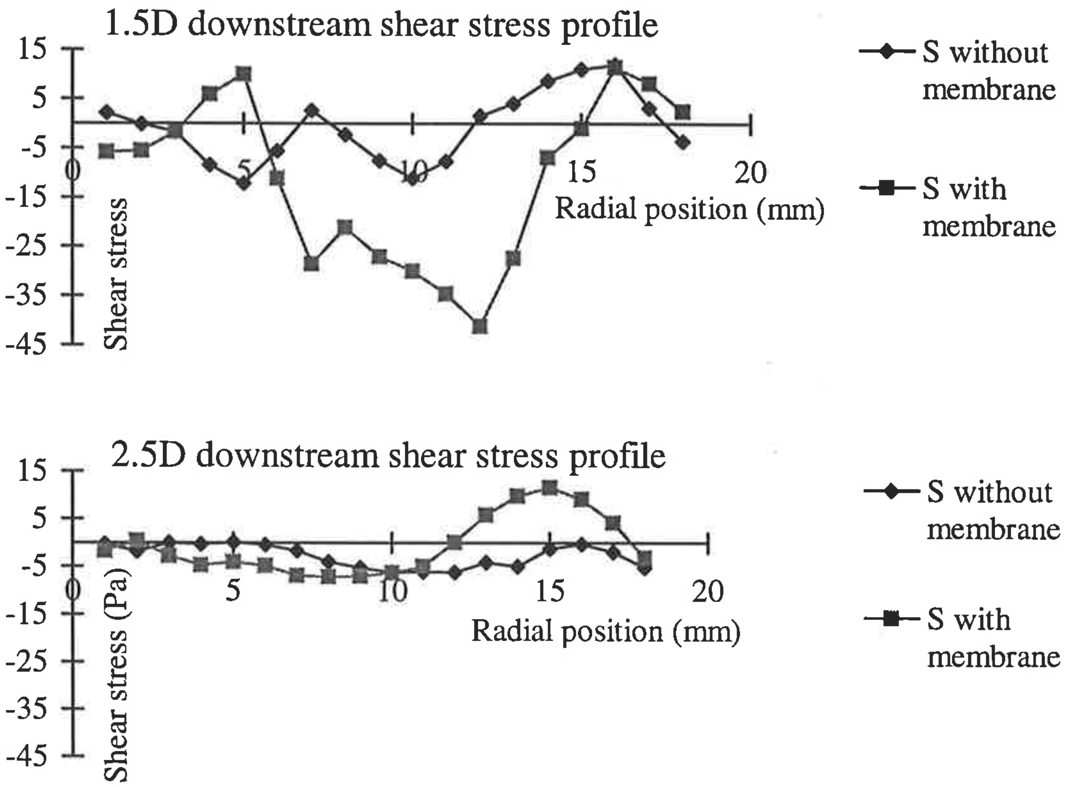

Figure 5-22. Shear stress fields with and without the membrane

As can be seen from the result of shear stress, the shear stresses of the valve with membrane were larger than those of the valve without membrane. At 1.5D downstream, maximum shear stresses of 41 and 12 Pa were observed in the valve with and without the membrane, respectively. As mentioned above, velocity profiles at 1.5D downstream looked almost the same, but shear stresses were significantly different (see *Figure 5-22*). This can be explained in that the membrane oscillated during the valve opening and generated wake in the flow behind the membrane leading to higher shear stresses. This result agreed with the result of the untied ball occluder generating larger shear stress than that of the tied ball occluder (Yoganathan *et al.* 1981).

5.5.3 The effects of the occluder type on pulsatile measurements

The potential advantage of this valve for pulsatile flow conditions is limited occluder inertia and therefore reduced regurgitant flow and energy losses (Tran *et al.* 1995). Pressure drops, flowrate and velocities were measured across the valve under pulsatile flow conditions with the valve located in (the in-vitro equivalent of) the aortic position. All tests were conducted at a heart rate of 1.2 Hz (72 beats/min) with aortic pressure set at 10.26/16 kPa (80/120 mmHg) and a cardiac output of 91.7 $\times 10^{-6}$ m^3/s (5.5 l/min). Instantaneous velocities, pressure drops and flowrate in pulsatile flow were measured over 8 cycles and then analysed for mean and fluctuating values using a 5° bin analysis (see *section 4.2*) to calculate shear stresses, regurgitant flow and energy losses.

Velocities under pulsatile flow conditions were recorded at several positions such as 1D upstream and 1, 1.25, 1.5 and 2D downstream over 8 cycles. Firstly, data was analysed for mean and fluctuating components using *Equation 4-6*, then shear stresses were calculated using *Equation 4-5*. As in steady flow, the maximum shear stress region in pulsatile flow occurred in the near vicinity downstream of the valve, with a maximum shear stress value of 90 Pa near to the same point where it occurred in steady flow. This value is sub-critical for haemolytic damage in comparison with the threshold value of 150 Pa.

Figure 5-23 shows velocity and shear stress of a maximum shear stress point at 1D downstream measuring plane versus a period of systolic time. The magnitude of shear stresses was strongly dependent on the time during systole, and had its peak value near to the peak velocity of that point during systole. This result agreed with other results of previous investigators eg. Woo *et al.* (1983). The peak shear stress value lagged behind the peak velocity value (see *Figure 5-23*), this may be due to the effect of the oscillation of the flexible membrane; when the velocity has reached its peak value and started reducing, the membrane became most unstable and this produced the greatest wake during systole. Consequently, shear stresses at that time were shown to be highest.

Pulsatile pressure drops and flowrate were recorded over 8. Again, these data were analysed using the 5° binning technique (*Equation 4-6*) for mean values and these values were plotted over a cardiac cycle (see *Figure 5-24*). Pressure drops were the difference between pressures in the up- and downstream regions of the valve, and maximum pressure drop of 6 kPa (45 mmHg) was observed. This value was larger than the maximum value generated in steady flow due to the acceleration of pulsatile flow.

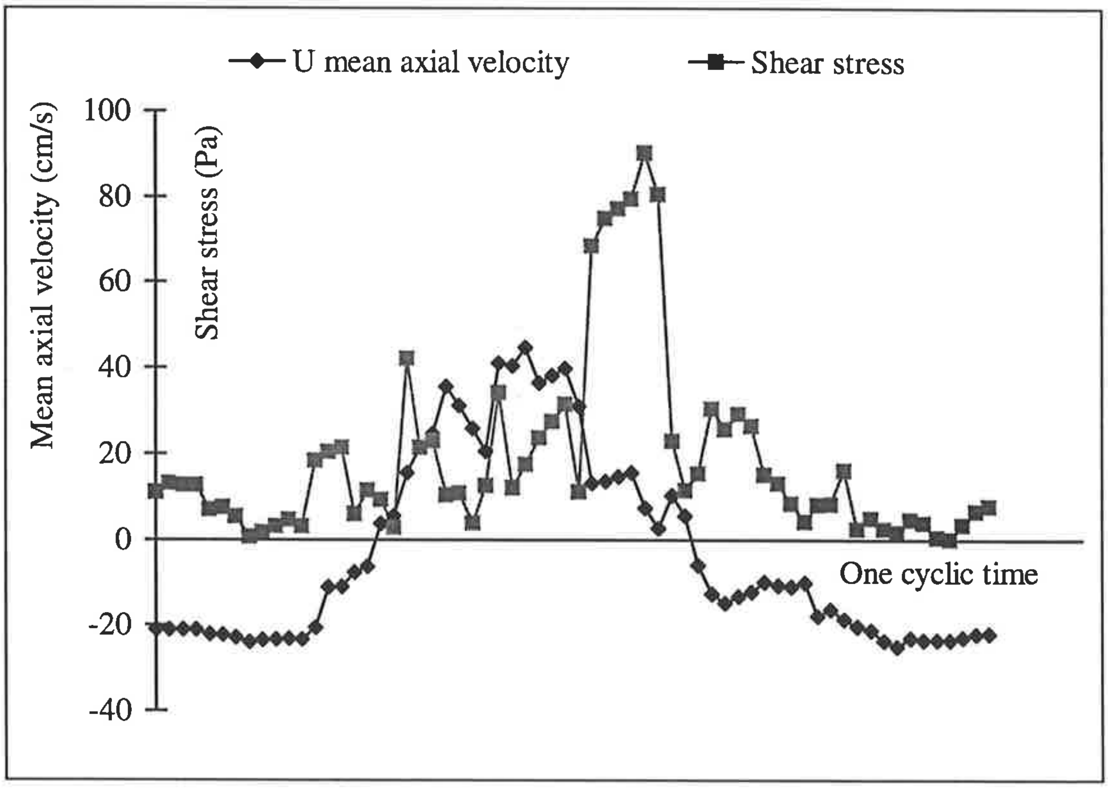

Figure 5-23. Flowrate and shear stress over a cyclic period

Regurgitant flow consisted of the reverse flow when the valve was closing and the leakage when the was closed. Total flow volume was the integral of flowrate over a complete cycle and regurgitant flow volume was integrated over the two stages of the cardiac cycle using *Equations 4-14* and *4-12*, respectively. The ratio of the regurgitant volume to total volume of the jellyfish valve over a cardiac cycle was about 4% in comparison with about 8-12 % and 1-4% of other mechanical and trileaflet bioprosthetic heart valves, respectively (Woo *et al.* 1983 and Tillman *et al.* 1984). It means that regurgitant flow of the Jellyfish heart valve was small in comparison with those of other mechanical heart valves in the literature. This can imply that tissue and membrane occluders are a major factors in reducing regurgitant flow and energy losses.

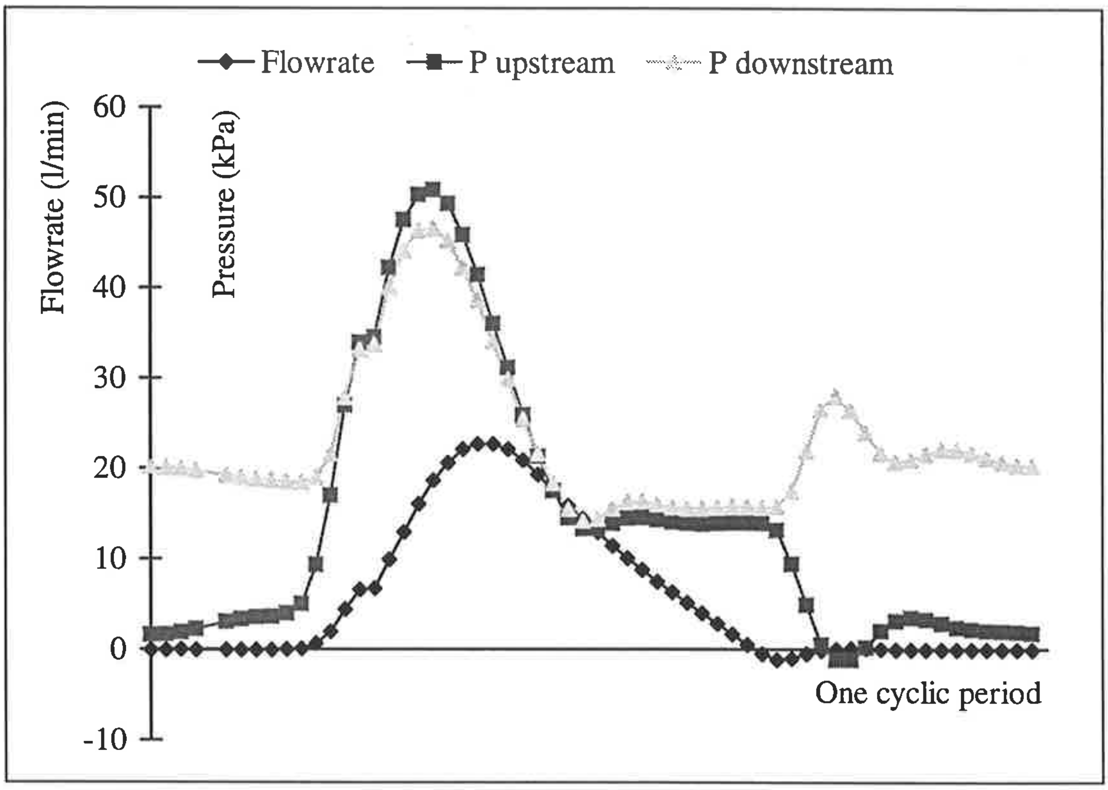

Figure 5-24. Pressure drop and flowrate over a cycle

Energy loss is the product of pressure drops and flowrate (see *Equation 4-16*), it is lost in three distinct stages; (T_1) resistance of forward flow during systole; (T_2) reverse flow during closing and (T_3) leakage flow during closed phase (Teijeira and Mikhail 1992).

Energy loss of the Jellyfish valve was calculated using *Equations 4-16* and *4-17* from the pressure drop and flowrate data analysed by the 5° binning analysis. It was found that energy losses of this valve were very limited (3.5 %) in comparison with those of other heart valves (6-10 %) eg. the ball valves, tilting valves and St. Jude Medical valves (Teijeira and Mikhail 1992). This was interesting in that the energy loss of the first stage (resistance of forward flow during systole) in other mechanical heart valves was about 50 % (40 - 60 %) of the total energy losses (Teijeira and Mikhail 1992). On the other hand, in the Jellyfish valve energy loss generated by the resistance of the occluder in the first stage flow was almost zero. This was probably due to the fact that the flexible membrane occluder of the valve had little inertia - hence produced minimal resistance for forward flow of the valve.

5.5.4 Summary of Jellyfish valve flow

The membrane of the Jellyfish valve oscillated and generated wake downstream of the valve when the valve was open. The oscillation of the membrane affected pressure drops, shear stress and velocity fields eg. increased pressure drops by 12%, maximum shear stresses and mean absolute shear stresses by about 400% (from 15 to 58 Pa and from 12 to 41 Pa, respectively). However, velocity profiles became flat somewhat quicker than those of the valve without membrane, but the presence of the membrane produced a region of stagnation and recirculation of 5 mm in the centre and at 1D downstream of the valve. This may lead to thrombus formation and tissue overgrowth in the near vicinity downstream of the valve (Tran *et al.* 1995).

Though the presence of the flexible membrane caused more disturbance, larger shear stress and pressure drops, these values were relatively smaller than those of other heart valves, and shear stresses were shown to be sub-critical for haemolysis. The use of the flexible membrane occluder could lead to some advantages over other occluder types:

- The membrane produces minimal flow obstruction - hence relatively low shear stresses and pressure gradients.
- The oscillation of the membrane does not effect shear stresses and pressure gradients as much as the orifice area does - hence these values were smaller than those of other heart valves.
- The oscillation of the membrane also reduces the extent of the stagnation and recirculation region and makes the velocity field become redeveloped quicker.
- This causes limited occluder inertia and therefore reduced regurgitant flow in forward flow stage, and energy losses in forward flow and closing stage.

Performance of the Jellyfish valve could be predicted well from the relationships for occluder and orifice flow developed earlier in this chapter.

6. CHAPTER SIX: CONCLUSION

This chapter draws conclusions about two major aspects of this research work, viz: the experimental techniques used, verification of the techniques and justification of selection of the techniques, and also the results gleaned from this study, critique of these results and their significance to the analysis of heart valve fluid mechanics.

6.1 Verification of Experimental Techniques

Flow through a series of orifices and a prototype heart valve prosthesis have been studied in some detail.

Pressure drop across, velocity, shear stress and turbulence measurements in different orifices and a prototype heart valve prosthesis (called the Jellyfish valve) can provide quantitative descriptions of steady flow characteristics of the region downstream of prosthetic heart valves.

Pressure drop measurements were analysed to develop empirical relationships between flow parameters for flow through heart valve prostheses with the aid of dimensional analysis techniques. These techniques can reduce the complexity of experimental programmes and at the same time increase the generality of experimental information. Static pressure distributions along the wall, downstream of the orifice plane, were not produced, as only one downstream pressure-tap plane was used; this was located 6 diameters downstream of the orifice plane.

Turbulence intensity and Reynolds stresses were obtained from LDA velocity measurements. Results gained by LDA such as velocity profile, shear stress, turbulence intensity and velocity fluctuation distributions in the upstream region of fully developed turbulent flow give good agreement with Longwell's work (1966) adding credibility to measurements taken downstream of the orifice plane.

Moreover, mean axial velocity and shear stress distributions downstream of the orifice agree with the theory of turbulent jet flow (Abramovich 1967) and Woo *et al.*'s work (1983), respectively. Measured velocity profiles and shear stresses accorded well with classical turbulent jet theory and good correlation was established between observed pressure gradients, shear stresses and velocity profiles in the flow regions just downstream of orifices and occluders. These findings were used to predict flow properties of a developmental heart valve - there was good agreement between these predictions and measured flow patterns.

Velocity and shear stress profiles gained by LDA were sparse and a full picture of the flow downstream of valves was not possible due to a limited number of measuring planes, but were adequate for the purposes of this study. LDA signals near to the tube walls were very noisy reducing the accuracy of measurements and precluding measurements in the region near to the orifice due to the obstruction of the test section wall caused by the valve or orifice insertion. Furthermore, the difference of the two measurement volume locations, caused by the refractive effects of the curved window through which the laser beams were passed compelled the use of error minimisation techniques to be applied to shear stress results.

The experimental methods adopted exhibited advantages in investigating heart valve flow over other methods, eg. CFD. This was especially so, in evaluating the effects of the occluder, the occluder oscillation, and the presence of the struts on turbulent flow phenomena of valves. The oscillation of the flexible membranous occluder of the Jellyfish valve increased pressure drops and shear stresses and the presence of the struts produced a large stagnation and recirculation region in good agreement with Yoganathan *et al.*'s work (1981). However this occluder motion highlighted the shortcomings of the Gorlin and Gorlin analysis and was a good vehicle for demonstrating the advantages of the orifice area estimation techniques developed in this study.

6.2 Results from this study

Results of this study can provide some clinical significance for further valve design and investigation as follows:

- Pressure drops are compared for prosthetic heart valves by simply measuring the geometries of valves using *Equation 5-15* (which was derived from results from the present study):

$$C_P = \frac{C_{Pr} \times C_{PR} \times C_{PE}}{29.21423} \times \Phi_{Shape}$$

where: $C_{PR} = 0.473249 + 270.05902\, e^{\frac{-r_A}{0.1002386}}$

$$C_{PR} = 5.294376 + 10.382888 e^{\frac{-\mathrm{Re}}{3302.9157}}$$

$$C_{PE} = 5.371233 + 0.004281 \times E^2$$

Φ_{Shape} is the shape factor

r_A is the ratio of orifice area to tube or sewing ring area

Re is Reynolds number

E Eccentricity stated as a percentage.

This procedure can reduce the need to measure pressure drops across valves and produce results which are unaffected by measurement error caused by the flow channel, pressure tap locations, etc.

- An Equation (*5-17*) for calculating actual valve orifice area:

$$A_{Real} = \frac{A_{Effective}}{C_{Position} \times C_{Shape}}$$

where $A_{Effective} = \frac{Q}{44.5 \times \sqrt{\Delta P}}$

Q is flowrate

ΔP	is the pressure drop through the valve
$C_{Position}$	is a position coefficient
C_{Shape}	is a shape coefficient

may assist cardiac surgeons in the selection of suitable valve size for implantation into individual patients.

- Pressure drop measurements across prosthetic heart valves are necessary, but do not provide enough information for valve assessments and comparisons.
- LDA velocity measurements are able to assess two important factors in heart valve investigations, namely axial velocity profiles and shear stress fields. Axial velocity profiles are the dominant factor in heart valve flow over other velocity profiles eg. tangential and radial as these axial velocity profiles provide information about the regions of stagnation and recirculation which promote thrombus formation and tissue overgrowth.
- Axial velocity profiles can also identify the region where maximum shear stress occurs. Furthermore, high axial velocity gradients produce high shear stress giving good agreements with Hanle *et al.*'s work (1989).
- The flow downstream of orifices or valves is jet flow, it consists of three stages: initial jet flow region, fully developed jet flow and finally, redeveloped turbulent flow. In the first stage, plug flow can be observed and the length of the initial jet flow region is about 2d, where d is hydraulic diameter of orifices. Initial regions of annular and triangular orifice flow were not observed in these results, because the first velocity profile downstream of the orifice is located at the position of 1D (19 mm) larger than 2d. The second stage is fully developed jet flow, where plug flow disappears and mean velocity gradients become smaller getting further from the orifice location. Except for the concentric annular orifice, the length of the second stage flow depends inversely on hydraulic diameter of primary orifices. The region between the end of the initial jet flow and the beginning of the second stage is called a transition region. At the end of the second stage, the flow again becomes plug at about 3 to 7D downstream of the

orifice dependent on the hydraulic diameter and the orifice and occluder position where velocity profiles are flat across the entire tube diameter. Beyond this point the flow pattern becomes redeveloped turbulent tube flow and this stage is called the third stage.

- Theory indicates that three flow stages should be observable downstream of the orifices. However, these three stages of heart valves, especially the initial jet flow region, were hardly observed. This was because the length of the initial flow region (2d of valve) ended before the first measuring plane location; also the presence of the valve elements eg. occluder, struts and hinge make the flow more disturbed and patterns more difficult to recognize. The length of each stage flow for the different orifices commenced and ended at different positions downstream of their location. This leads to a conclusion that the comparison of velocity profiles of heart valves at fixed positions, such as at 1 and 2D downstream of prosthetic heart valves, used in previous heart valve studies may lead to comparisons being made of shear stresses between different heart valve types.

- The orifice area is the most important factor in the causation of shear stress, pressure drops and the extent of stagnation and recirculation regions.

- The valve can be optimised by increasing the ratio of orifice area to sewing area (r_A): the result of this study shows that as r_A increases from 0.4 to 0.75, pressure drop and shear stress reduces 10 and 70 fold, respectively. However, it is often infeasible to increase r_A due to the limitation of the valve size and sewing ring requirements: hence r_A must be optimised, whilst maintaining flow area, by adapting the orifice shape and the occluder type and position.

- The orifice shape of the valve when the valve is fully open is the second most important factor in the causation of shear stress and pressure drops. Pressure drops and shear stress at flowrate of 417×10^{-6} m^3/s (25 l/min) change 140% and 300%, respectively when the orifice shape changes from circular triangular. This can explain why pressure drops and shear stresses in bioprosthetic heart valves were highest in comparison with those of other heart valve types of the same size (Hanle *et al.* 1989), as bioprosthetic valves produce a triangular orifice shape when open.

- The eccentricity of the orifice or occluder does not affect pressure drops and shear stresses as much as the orifice area and shape do. However, the eccentricity of the occluder introduces the largest effects on the causation of stagnation and recirculation regions downstream of valves.
- Two flow regions, initial and fully developed jet flow, downstream of the orifices produce two different shear stress distributions implying that axial velocities are dominant over tangential and radial velocities in determining shear stresses. This gives good agreements with other works (Longwell 1966; Tennekes and Lumley 1972; and Gerhart and Gross 1985).
- The comparison of maximum shear stress values produced by each valve sometimes may lead to mis-understanding of valve performance due to the error of measurements, especially shear stress measurements. In order to avoid this problem, mean absolute shear stress of each measuring plane is introduced.
- Maximum turbulent shear stresses along radial positions occur in the region of the sharp axial velocity gradients. Along axial positions maximum turbulent shear stresses depend on the flow region downstream of the orifice. This result gives good agreement with Schwarz *et al.*'s work (1988). Maximum shear stress value and maximum mean absolute shear stress of a measuring plane occur at the same position within the transition flow region downstream of the orifices.

6.3 Recommendations

The recommendations of this study are as follows:

- In order to acquire better heart valve haemodynamic performance, new heart valve designs should have (a) a large ratio of orifice area to sewing ring area, (b) circular orifice shape, (c) a non-central occluder and (d) concentric orifice flow.
- The comparison of maximum velocity gradient and shear stress in heart valve prostheses at a fixed position is not practical. Mean absolute shear stress should be compared within the transition flow region of the valves.
- The use of the flexible membrane as an occluder of valves is promising for future valve design, as this occluder type causes minimal obstruction (maximal orifice area); even though the oscillation of the membrane produces higher pressure drops and shear stresses. However, these values are still smaller than those of other heart valve types, because the orifice area is the most important factor effecting flow parameters. The material of the membrane should be durable and not easily torn under pulsatile flow.
- LDA is a powerful technique for investigating fluid flow of prosthetic heart valves. In order to acquire more accurate and reliable results, especially shear stresses, a larger laser beam intersection angle should be applied producing smaller measurement volume length and reducing the effects of curved windows on the location of the measurement volume. Furthermore, the difference in location (or lack of spatial coincidence) of the two measurement volume locations can be reduced by reducing the refractive index of the tube making the test section wall's refractive index as close to the refractive index of the test section liquid as possible and by reducing wall thickness.

7. REFERENCES

Abramovich, G.N., 1963. *The theory of turbulent jets.* The MIT Press, Massachusetts Institute of Technology, Cambridge, Massachusetts.

ASME, 1935. *History of orifice meters and the calibration, construction, and operation of orifices for metering.* The American Society of Mechanical Engineers.

ASME, 1959. *Fluid meters, their theory and application*, 5^{th} ed. The American Society of Mechanical Engineers.

Barenblatt, G.I., 1987. *Dimensional Analysis.* Gordon and Breach Science Publishers, New York.

Bortolotti, U., Milano, A., Thiene, G., Guerra, F., Mazzucco, A., Valente, M., Talenti, E., and Gallucci, V., 1987. Early mechanical failures of the Hancock pericardial xenograft. *J. Thoracic. Cardiovasc. Surg.,* **94,** 200-207.

Bradshaw, P., 1975. *An introduction to turbulence and its measurement.* Pergamon Press, Oxford.

Carrell, A. and Guthrie, C.C., 1905. The plantation of veins and organs. *Am. Med.*, 10-1101.

Chandran, K.B., Cabell, G.N., Khalighi, B. and Chen C.J., 1984. Pulsatile flow past aortic valve bioprostheses in a model human aorta. *Journal of Biomechanics,* **17,** (8), 609-619.

Chandran, K.B., Khalighi, B. and Chen C.J., 1985a. Experimental study of physiological pulsatile flow past valve prostheses in a model human aorta - I: Caged ball valves. *J. Biomechanics,* **18,** 763-772.

Chandran, K.B., Khalighi, B. and Chen C.J., 1985b. Experimental study of physiological pulsatile flow past valve prostheses in a model human aorta - II: Tilting disc valves and the effects of orientation. *J. Biomechanics,* **18,** 773-780.

Chew, Y.T., Low, H.T., Lee, C.N. and Kwa, S.S., 1993. Laser Anemometry measurements of steady flow past aortic valve prostheses. *Journal of Biomechanical Engineering,* **115,** 290-298.

Clark, W.J., 1965. *Flow measurement,* 1st ed., Pergamon Press, Oxford.

Demikhove, V.P., 1962. Experimental transplantation of vital organs. New York, Consultants' Bureau.

Duff, W.R., 1970. *Fluid dynamics of prosthetic heart valves.* Ph.D. *thesis*, Purdue University, USA.

Durrani, T.S. and Greated C.A., 1977. *Laser system in flow measurement*, Plenum press, New York and London.

Figliola, R.S., 1976. A study of the hemolytic potential of prosthetic heart valve flow on local *in-vitro* stress measurements. *MS thesis*, University of Notre Dame, Indiana.

Figliola, R.S. and Mueller, T.J., 1981. On the hemolytic and thrombogenic potential of occluder prosthetic heart valves from *in-vitro* measurements. *ASME Journal of Biomechanical Engineering,* **103,** 83-90.

Forrester, J.H., Weiting, D.W., Hall, C.W. and Debakey, M.E., 1969. A comparative study of fluid flow resistance of prosthetic heart valves. *Cardiovasc. Res. Cent. Bull.* **7,** 83-99.

Fry, D.L., 1968. Acute vascular endothelial changes associated with increased blood velocity gradients. *Circulation research,* **22,** 165-197.

Gentle, C.R., 1977. A limit to hydraulic design of heart valve prostheses. *Engineering in Medicine,* **6,** (1), 17-2.

Gentle, C.R., 1984. Flow testing of artificial heart valves as an illustration of Bernoulli's equation. *International Journal of Mechanical Engineering Education,* **12,** (4), 281-189.

Gentle, C.R., 1995. Personal correspondence.

Gerhart, P.M. and Gross, R.J., 1985. *Fundamentals of fluid mechanics.* Addison - Wesley Publishing Company.

Gorlin, R. and Gorlin, S.G., 1951. Hydraulic formula for calculation of the area of the stenotic mitral valve, other cardiac valves, and central circulatory shunt. *American Heart Journal,* **41,** (1), 1-29.

Hanle, D.D., Harrison, E.C., Yoganathan, A.P., Allen, D.T. and Corcoran, W.H., 1989. *In-vitro* flow dynamics of four prosthetic aortic heart valves: A comparative analysis. *Journal of Biomechanics*, **22**, (6/7), 597-607.

Harken, D.E., Soroff, H.S., and Taylor, W.J., 1960. Partial and complete prostheses in aortic insufficiency. *J. Thorac. Cardiovasc. Surg.,* 40-744.

Harken, D.E., Taylor, W.J. and Lifemine A.A., 1962. Aortic valve replacement with a caged ball valve. *Am. J. Cardiol,* 9-292.

Hasenkan, J.M., Giersiepen, M. and Reul, H., 1988. Three dimensional visualisation of velocity fields downstream of six mechanical aortic valves in a pulsatile flow model. *Journal of Biomechanics,* **21,** (8), 647-661.

Heiliger, R., 1987. Haemodynamic advantages and disadvantages of mechanical bileaflet valves and tilting disc valves No. 29. *Engineering in Medicine,* **16,** (2), 77-85.

Hellums, J.D. and Brown, C.H., 1977. Blood cell damage by mechanical forces. In: Hwang, N.H.C. and Normann, N.A., *Cardiovascular fluid dynamics*, University Park Press, Baltimore, 799-823.

Henze, A., Carlsson, S. and Björk, V.O., 1973. Mortality and pathology following aortic valve replacement with the Björk-Shiley tilting disc valve. *J. Thorac. Cardiovasc. Surg.,* 7-17.

Horace, J., Columbus, and Ohio, 1916. Experiment in water flow through pipe orifices. In: Cotton, K.C. *ASME, Flow measurement symposium*, 315-350.

Horstkotte, D., Haerten, K., Schulte, H.D., Seipel, L., Krian, A. and Loogen, F., 1983. Hämodynamische Ruhe- und Belastungsunterchungen nach Implantation verchiedener Mitral-Klappenprothesen mit gleichem Außendurchmesser, *Zeitschrift für Kardiologie,* **72,** 385-393. (Referenced by Heiliger, R., 1987.)

Huang, Z.J., Merkle, C.L., Abdallah, S. and Tarbell, J.M., 1994. Numerical simulation of unsteady laminar flow through a tilting disc heart valve: prediction of vortex shedding. *J. Biomechanics,* **27,** (4), 391-402.

Hufnagel, C.A., Harvey, W.P., Rapil, P.J. and Mcdermott, T.F., 1954. Surgical correction of aortic insufficiency. *Surgery,* **35**, 673-683.

Hufnagel, C.A. and Conrad, P.W., 1965. Comparative study of some prosthetic valves for aortic and mitral replacement. *Surgery*, **57**, (1), 205-210.

Hughes, P.E. and How, T.V., 1994. Pulsatile velocity distribution and wall shear rate measurement using pulsed Doppler ultrasound. *J. Biomechanics,* **27,** (1), 103-110.

Jin, W. and Clark, C., 1994. A correlation method for determining the number of sampling cycles required for pulsating flow analysis using LDA. *J. Biomechanics,* **27,** (9), 1179-1181.

Jorgensen, J.E., Campau, D.N. and Baker, D.W., 1973. Physical characteristics and mathematical modelling of the pulsed ultrasonic flowmeter. *Med. Biol. Eng.,* **11,** 404-420.

JSME, 1988. *Visualised flow: Fluid motion in basic and engineering situations revealed by flow visualisation.* The Japan Society of Mechanical Engineering, Pergamon Press.

Kaster, R.L., Lillehei, C.W. and Starek, P.J.K., 1970. The Lillehei-Kaster pivoting disc aortic prosthesis and a comparative study of its pulsatile flow characteristics with four other prostheses. *International Society for Artificial Organs,* **16,** 233-243.

Knoch, M., Reul, H., Kroger, R and Gunter, R., 1988. Model study at mechanical aortic heart valve prostheses - Part I: Steady-state flow fields and pressure loss coefficients. *Journal of Biomechanical Engineering,* **110,** 334-343.

Knott, R., Reul, H., Knoch, M., 1988. In-vitro comparison of aortic heart valve prostheses. *J. Thorac. Cardiovasc. Surg.,* 96-952.

Krucinski, S., Vesely, I., Dokainish, M.A. and Campbell, G., 1992. Numerical simulation of leaflet flexure in bioprosthetic valves mounted on rigid and expansile stents. *J. Biomechanics,* **26,** (8), 929-943.

Lamsman, L.S, Arisan Ergia, M. and Griepp, B.R., 1990. The history of heart and heart - lung transplantation. In: Thompson, M.E. (ed.). *Cardiac transplantation*, 3-19.

Leefe, S.E., Tansley, G.D. and Gentle, C.R., 1986. Pulsatile flow testing of prosthetic heart valve conduits. In: *Heart Valve Engineering*, Mechanical Engineering Press, London, 15-19.

Leverett, L.B., Hellums, J.D., Alfrey, C.P. and Lynch, E.C., 1972. Red blood cell damage by shear stress. *Biophysics Journal,* **12,** 257-273.

Lomas, C.G., 1986. *Fundamentals of hot-wire anemometers*. Cambridge University Press.

Longwell, P.A., 1966. *Mechanics of fluid flow,* Mcgraw - Hill book company.

Lutz, T.W. and Barass, J.P. 1983. Rheological behaviour of human blood and plasma at steady flow and oscillatory flow. *VASA*, **12**, (2) 121-125.

Mann, F.C., Priestley, J.T., Markowitz, J., *et al.* 1933. Transplantation of the intact mammalian heart. *Arch. Surg*., 26-219.

Mazumdar, J.N., 1992. *Biofluid Mechanics.* World Scientific Publishing Co. Pte. Ltd., Singapore.

Mito, K., Ikeda, H., Sumi, M. and Shinohara, S., 1993. Self-mixing effect of the semiconductor laser Doppler method for blood flow measurement. *Medical and Biological Engineering and Computing,* **31,** 308-310.

Nandy, S. and Tarbell, J.M., 1988. Measurement of wall shear stress distal to a tri-leaflet valve in a rigid model of the aortic arch with branch flow. *Journal of Biomechanical Engineering,* **110,** 172-179.

Pathak, Y.V., Boyd, J., and Schoen, F.J., 1990. Prevention of calcification of glutaradehyde pretreated bovine pericardium through controlled release polymeric implants: study of Fe^{3+}, Al^{3+}, protamine sulphate and levamisole. *Biomaterial,* **11,** 718-723.

Purinya, B., Kasyanov, V., Volkolakov, J., Latsis, R. and Tetere, G., 1993. Biomechanical and structural properties of the explanted bioprosthetic valve leaflets. *J. Biomechanics,* **27,** (1), 1-11.

Reitz, B.A., Burton, N.A., Jamieson, S.W., *et al.*, 1980. *J. Thorac. Cardiovasc. Surg.*, 80-360.

Reul, H., Giersiepen, M. and Knott, E., 1987. Laboratory testing of prosthetic heart valves. *Engineering in Medicine,* **16,** (2), 67-76.

Reul, H., Vahlbruch, A., Giersiepen, M., Schmitz-Rode, Th., Hirtz, V., and Effert, S., 1990. The geometry of the aortic root in health at valve disease and after valve replacement. *J. Biomechanics,* **23,** 181-191.

Schoephoerster, R. and Chandran, K.B., 1991. Velocity and turbulence measurements past mitral valve prostheses in a model left ventricle. *J. Biomechanics,* **24,** 549-562.

Schwarz, A.C., Tiederman, W.G. and Phillips, W.M., 1988. Influence of cardiac flowrate on turbulent shear stress from a prosthetic heart valve. *Journal of Biomechanical Engineering,* **110,** 123-128.

Scott, L.J., Sindt, F.C. and Lewis, A.M., 1993. *Flow conditioner location effects in orifice flowmeters.* NIST Technical Note 1356, U.S. Goverment Printing Office, Washington.

Scott, L.J. and Lewis, A.M., 1994. *Flow conditioner tests for three orifice flowmeter sizes.* NIST Technical Note 1367, U.S. Goverment Printing Office, Washington.

Sergio, R.I., Lino, E.C. and Ricardo, P.I., 1985. Comparative computational study of blood flow through prosthetic heart valves using finite element method. *Journal of Biomechanics,* **18,** (2), 97-115.

Slot, M., Koelink, M.H., Scholten, F.G., de Mul, F.F.M., Wejers, A.L., Greve, J., Graaff, R., Dassel, A.C.M., Aarnoudse, J.G. and Tuyman, F.H.B., 1992. Blood flow velocity measurements based on the self-mixing effect in a fibre-coupled semiconductor laser: *in-vivo* and *in-vitro* measurements. *Medical and Biological Engineering and Computing,* **30,** 441-446.

Souttar, H.S., 1925. The surgical treatment of mitral stenosis. *The British Medical Journal*, (2), 603-606.

Starr, A. and Edwards, M.L., 1961. Mitral replacement: Clinical experience with a ball valve prosthesis. *Annals of thoracic surgery,* **154,** 726-740.

Stern, M., 1985. Laser Doppler Velocimetry in blood and multiply scattering fluids: theory. *Applied Optics*, **24,** (13), 1968-1986.

Stevensohn, D.M., Yoganathan, A.P. and Williams, F.P., 1985. Numerical simulation of steady turbulent flow through trileaflet aortic heart valves - II. Results on five models. *Journal of Biomechanics,* **18,** (12), 909-926.

Swanson, W.M., 1984. Comparison of in-vitro valve pressure drop results from different investigators. *Medical Instrumentation,* **18,** (2), 115-117.

Tansley, G.D., Edwards, R.J., Leefe, S.E. and Gentle, C.R., 1986. Ball occluder instability during forward flow through prosthetic heart valve conduits. *Proceeding of the 13th Annual General Meeting of the European Society for Artificial Organs. Life Support System,* **4,** Supplement 2, 169-191.

Tansley G.D., 1988. Computational investigation of turbulent, non-Newtonian flow in heart valve conduits. Ph.D. *thesis*, Trent Polytechnic, Nottingham.

Tansley G.D., Edwards, R.J. and Gentle, C.R., 1988. The role of computational fluid mechanics in the analysis of prosthetic heart valve flow. *Medical and Biological Engineering and Computing,* **26,** 175-185.

Tansley, G.D., 1993. Aspects of non-Newtonian blood flow in prosthetic heart valve studies. *Automedica,* **15,** 207-226.

Teijra, J.F. and Mikhail, A.A., 1992. Cardiac valve replacement with mechanical prostheses: Current status and trends. In: Hwang, N.H.C., Turitto, V.T and Yen, M.R.T. (eds.). *Advances in Cardiovascular Engineering,* 195-227.

Tennekes, H. and Lumley, J.L., 1972. *A first course in turbulence,* The MIT Press, Cambridge, Massachusetts and London, England.

Thalassoudis, K., 1987. Numerical studies of flow through prosthetic heart valves. Ph.D. *thesis*, The University of Adelaide, Adelaide.

Tiederman, W.G., Steinle, M.J. and Phillips W.M., 1986. Two-component laser velocimeter measurements downstream of heart valve prostheses in pulsatile flow. *Journal of Biomechanical Engineering,* **108**, 59-64.

Tillmann, W., Reul, H., Herold, M., Bruss, K.-H. and VanGilse J., 1984. *In-vitro* wall shear stress measurements at aortic valve prostheses. *Journal of Biomechanics,* **17,** (4), 263-279.

Tran V.V., Tansley, G.D. and Morsi, Y.S., 1994. Haemodynamics of a Jellyfish heart valve. *Engineering and the Physical Sciences in Medicine,* 44.

Tran V.V., Tansley, G.D., .Morsi, Y.S. and Larson, M.C., 1995. LDA evaluation of a prototype Jellyfish artificial heart valve. *Proceeding of The Six Asian Congress of Fluid Mechanics,* Singapore.

TSI, 1994. Model 9800 series fiberoptic probes, *Instruction manual.* TSI Incorporated.

TSI, 1985. Model 1990C counter-type signal processor, *Instruction manual.* TSI Incorporated.

TSI, 1986. Model 9180 frequency shift system, *Instruction manual.* TSI Incorporated.

Walker, J.D., Tiederman, W.G. and Phillips, W.M., 1989. Effects of tilting disc, heart valve orientation on flow through a curved aortic model. *Journal of Biomechanical Engineering,* **111,** 228-232.

Wang, C.P., 1977. Laser anemometry. *Am. Sci.* **65,** 289-293.

Weiting, D.W., 1969. *Dynamic flow characteristics of heart valves.* Ph.D. *thesis,* Texas University, USA.

Woo, Y.R., Williams, F.P. and Yoganathan, A.P., 1983. *In-vitro* fluid dynamic characteristics of the biomed trileaflet heart valve prosthesis. *Journal of Mechanical Engineering,* **105,** 338-345.

Yoganathan, A.P., 1978. Cardiovascular fluid mechanics. Ph.D. *thesis*, California Institute of Technology, Pasadena.

Yoganathan, A.P., Corcoran, W.H. and Harrison, E.C., 1978. Wall shear stress measurement in the near vicinity of aortic prosthetic heart valves. *Journal of Bioengineering*, **2**, 369-379.

Yoganathan, A.P., Corcoran, W.H. and Harrison, E.C., 1979a. Pressure drops across prosthetic aortic heart valves under steady and pulsatile flow - *In-vitro* measurements. *Journal of Biomechanics,* **12,** 153-164.

Yoganathan, A.P., Reamer, H.H. Corcoran, W.H. and Harrison, E.C., 1979b. A Laser Doppler Anemometer to study velocity fields in the vicinity of prosthetic heart valves. *Med. & Biol. Eng. & Comput.,* **17**, 38-44.

Yoganathan, A.P., Corcoran, W.H., Harrison, E.C. and Carl, J.R. 1979c. *In-vitro* measurements in the vicinity of the Björk-Shiley aortic prosthesis using laser Doppler anemometer. *Med. & Biol. Eng. & Comput.,* **17**, 453-459.

Yoganathan, A.P., Reamer, H.H., Corcoran, W.H., Harrison, E.C., Shulman, I.A. and Parnassus, W., 1981. The Starr-Edwards aortic ball valve: Flow characteristics, thrombus formation, and tissue overgrowth. *International Society for Artificial Organs,* **5,** (1), 6-17.

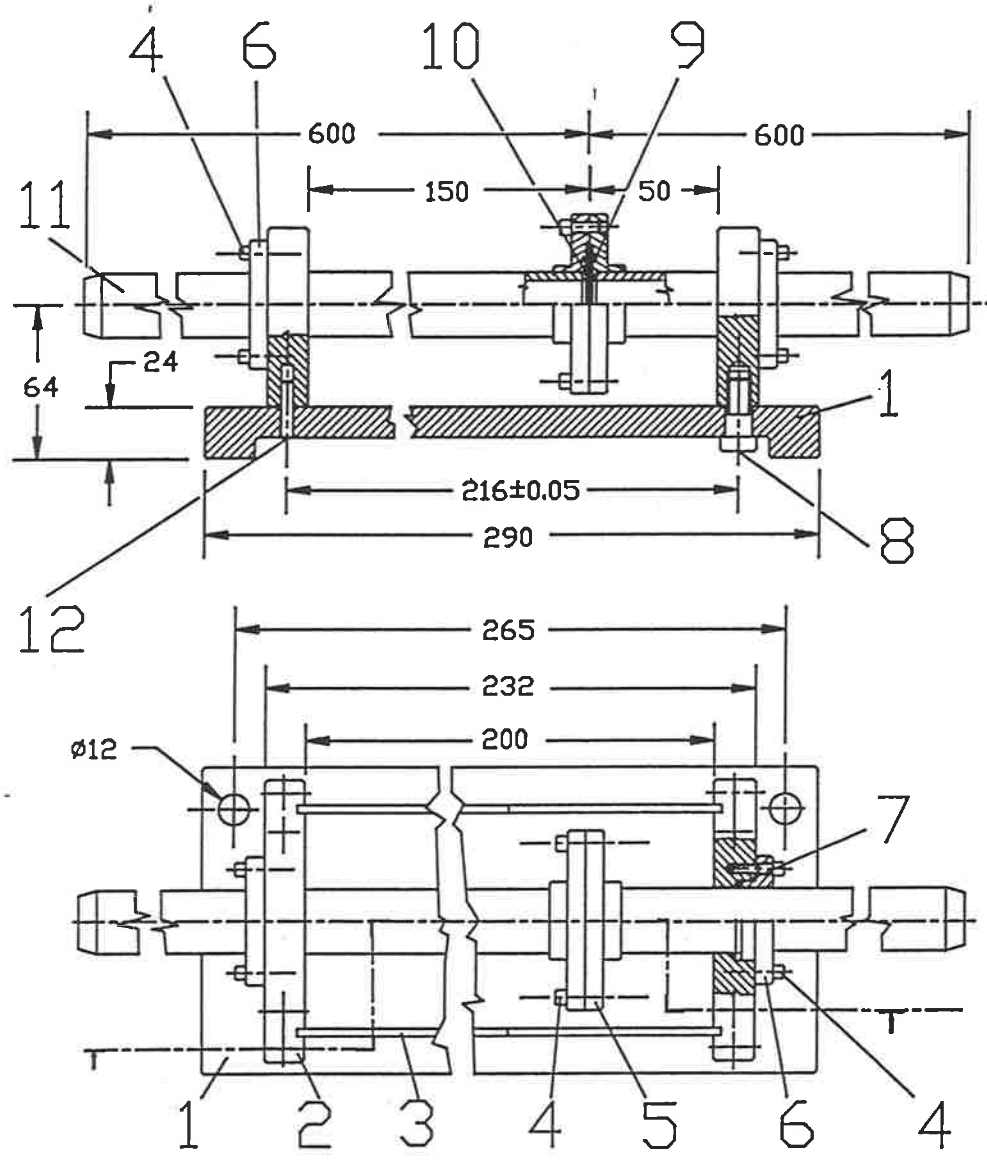

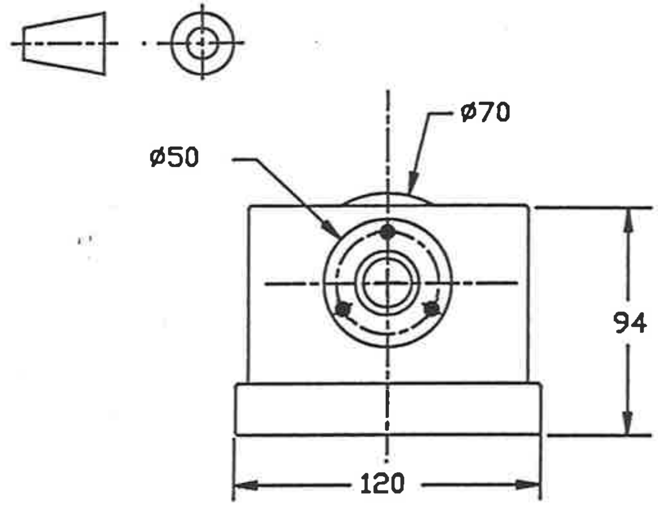

I	Q	Description	Material	Ref No	Draw No
12	4	Locating bin	Stainless	NDI	
11	2	ø19 tube	Acrylic		105
10	8	Orifice plate	Acrylic		104
9	2	O ring seal		NDI	BS218
8	4	Socket screw M8	Stainless	NDI	
7	2	O ring seal		NDI	BS214
6	2	Fixing plate	Acrylic		103
5	2	Orifice house	Acrylic		102
4	9	Socket screw M5	Stainless	NDI	
3	2	Glass shroud	Glass		101C
2	2	End plaate	Acrylic		101B
1	1	Base	Acrylic		101A

Drawn by	The University of Adelaide Mech. Eng. Dept.	
Checked		
Scale 1:2	Title: Base box	Draw No 94-1

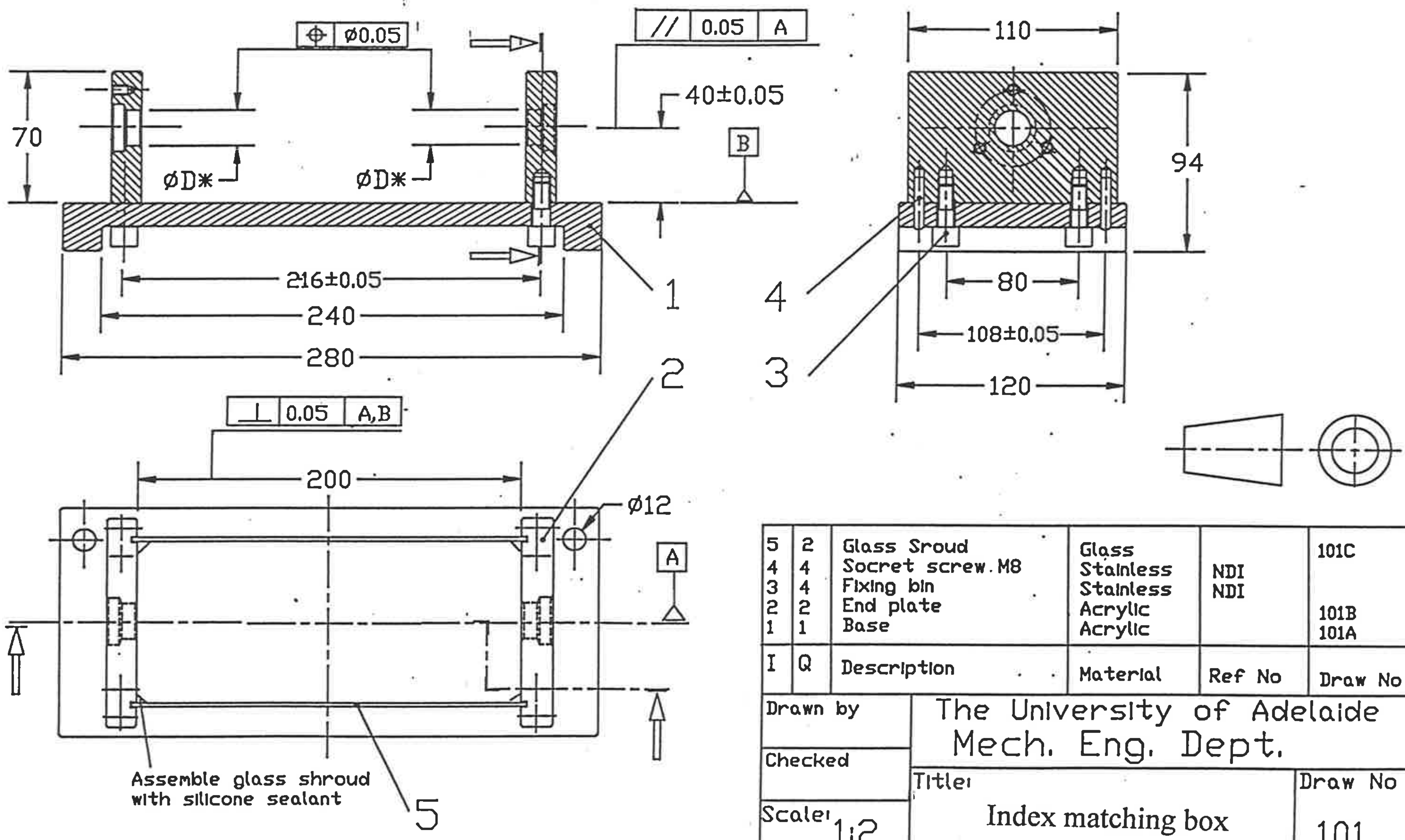

5	2	Glass Sroud	Glass		101C
4	4	Socret screw. M8	Stainless	NDI	
3	4	Fixing bin	Stainless	NDI	
2	2	End plate	Acrylic		101B
1	1	Base	Acrylic		101A
I	Q	Description	Material	Ref No	Draw No

Drawn by	The University of Adelaide Mech. Eng. Dept.	
Checked		
Scale: 1:2	Title: Index matching box	Draw No 101

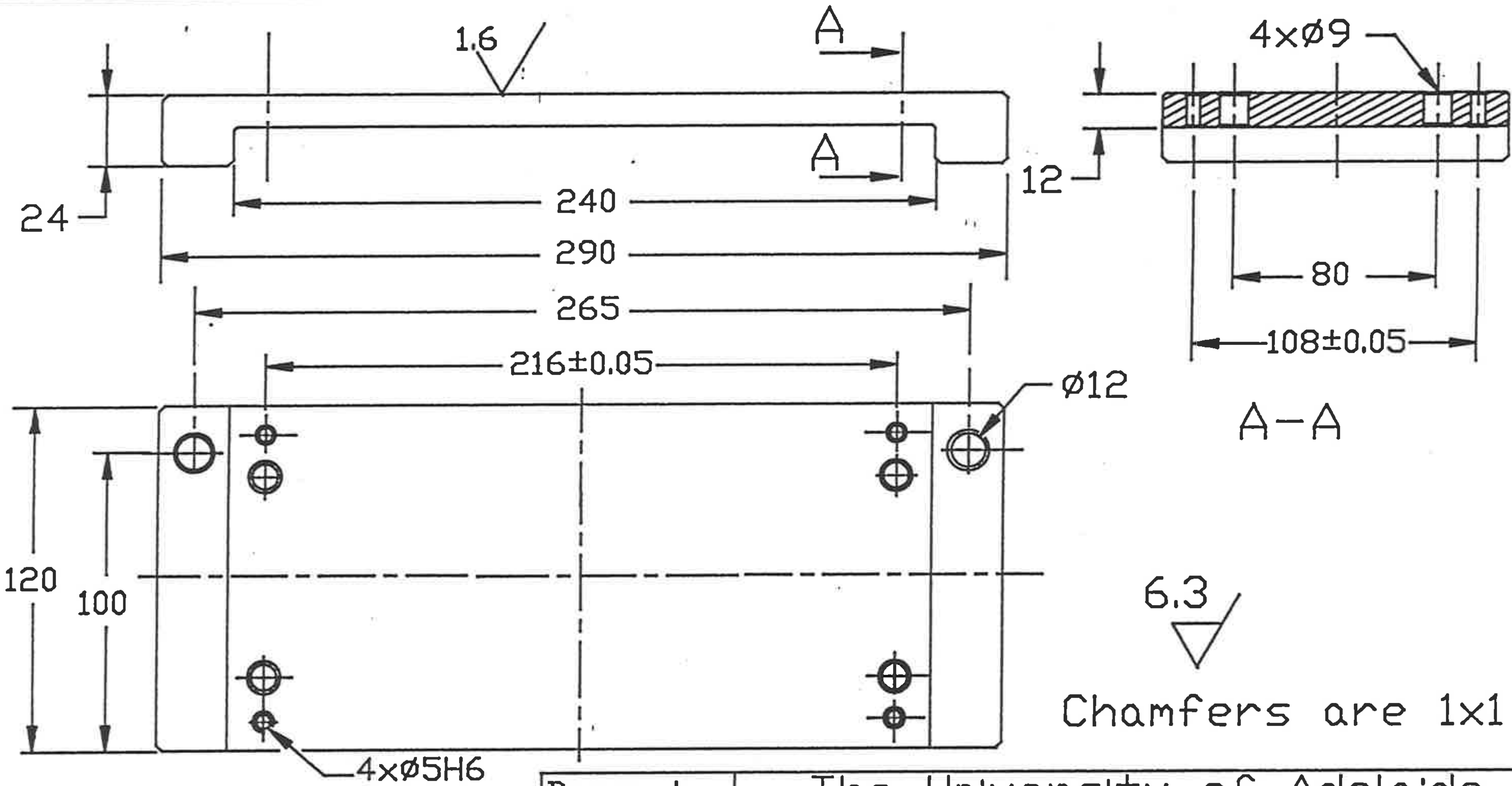

Drawn by	The University of Adelaide Mech. Eng. Dept.	
Checked		
Scale 1:2	Title Base	Draw No 101A

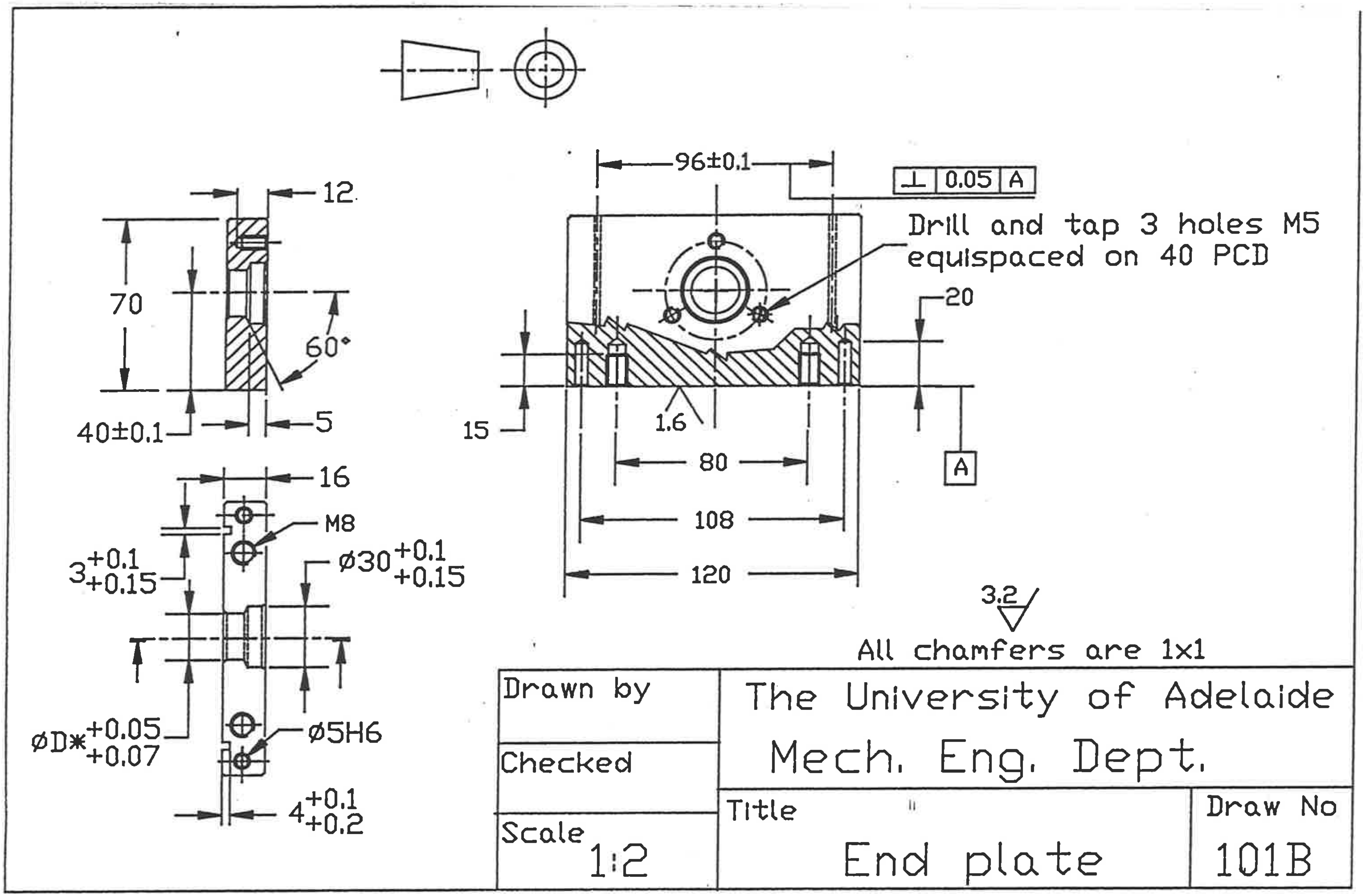

12
70
60°
5
40±0.1
16
M8
3 +0.1 +0.15
ø30 +0.1 +0.15
øD* +0.05 +0.07
ø5H6
4 +0.1 +0.2
96±0.1
⊥ 0.05 A
Drill and tap 3 holes M5
equispaced on 40 PCD
20
15
1.6
80
108
120
A
3.2
All chamfers are 1x1
Drawn by
Checked
Scale 1:2
The University of Adelaide
Mech. Eng. Dept.
Title
End plate
Draw No
101B

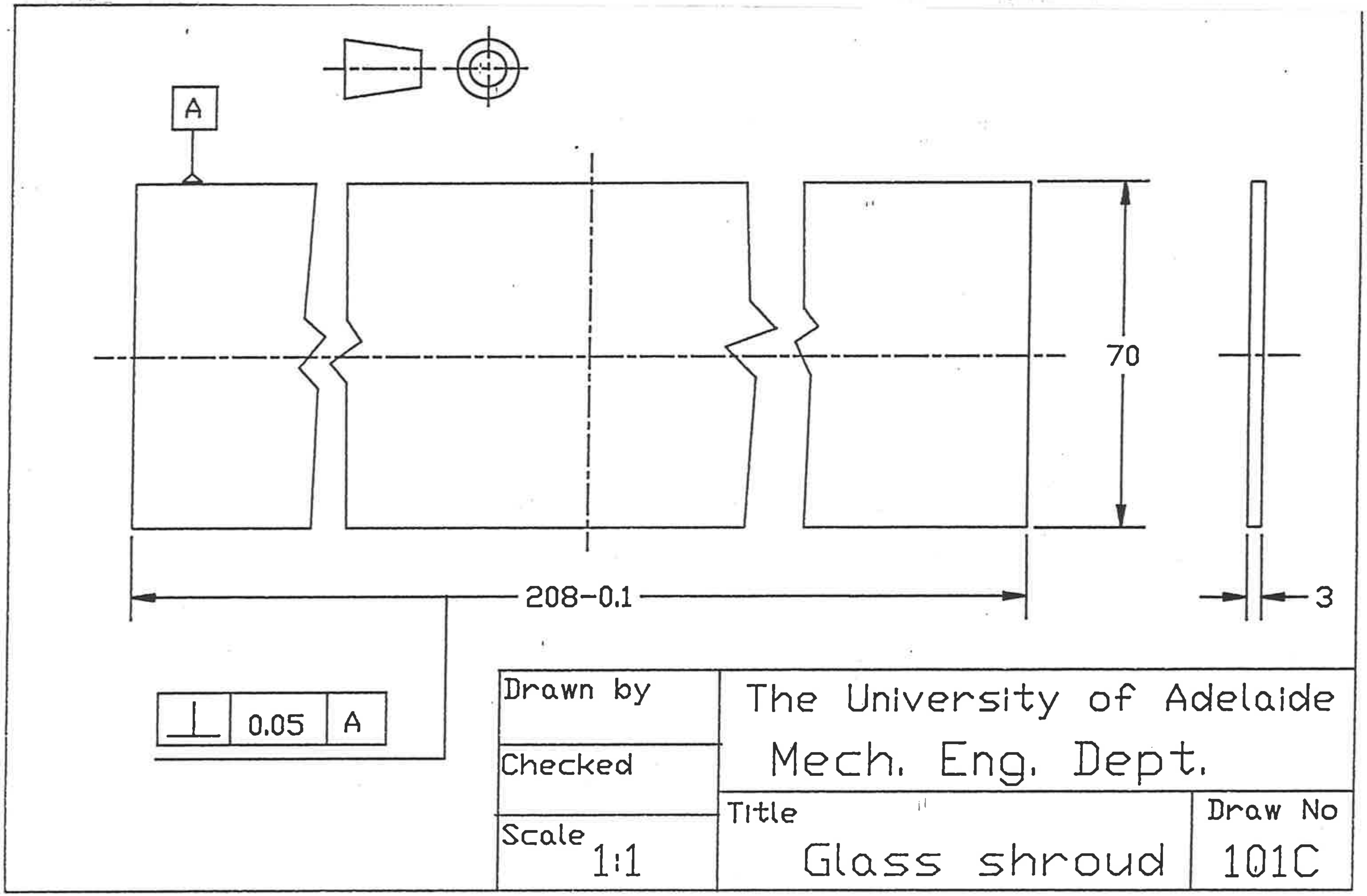
A
70
208-0.1
3
0.05
A
Drawn by
Checked
Scale 1:1
The University of Adelaide
Mech. Eng. Dept.
Title
Glass shroud
Draw No
101C

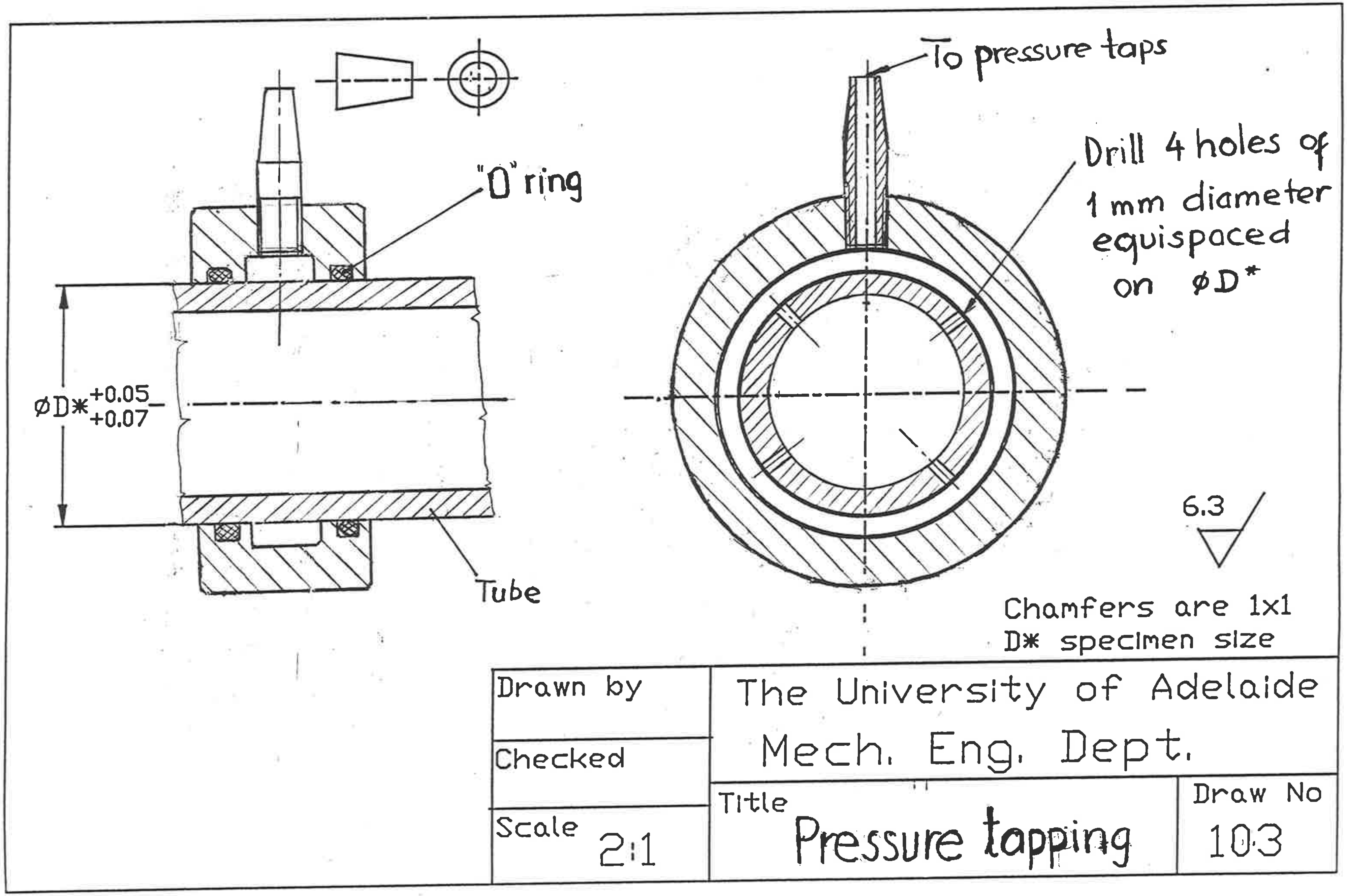
"O" ring
To pressure taps
Drill 4 holes of 1 mm diameter equispaced on ⌀D*
⌀D* +0.05 +0.07
Tube
6.3
Chamfers are 1x1
D* specimen size
Drawn by
Checked
Scale 2:1
The University of Adelaide
Mech. Eng. Dept.
Title Pressure tapping
Draw No 103

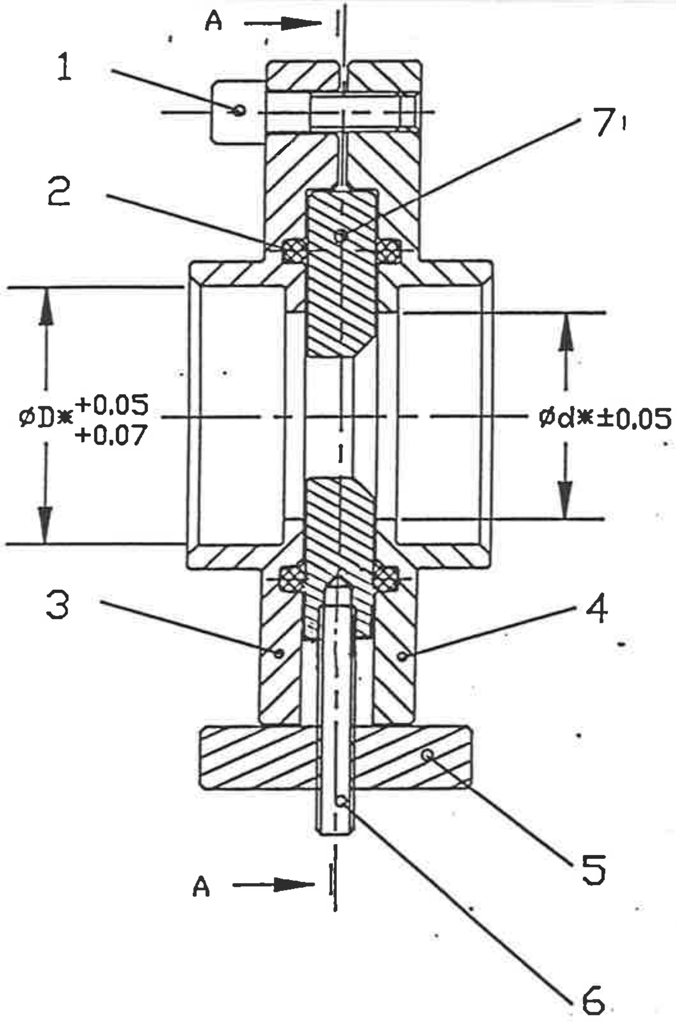

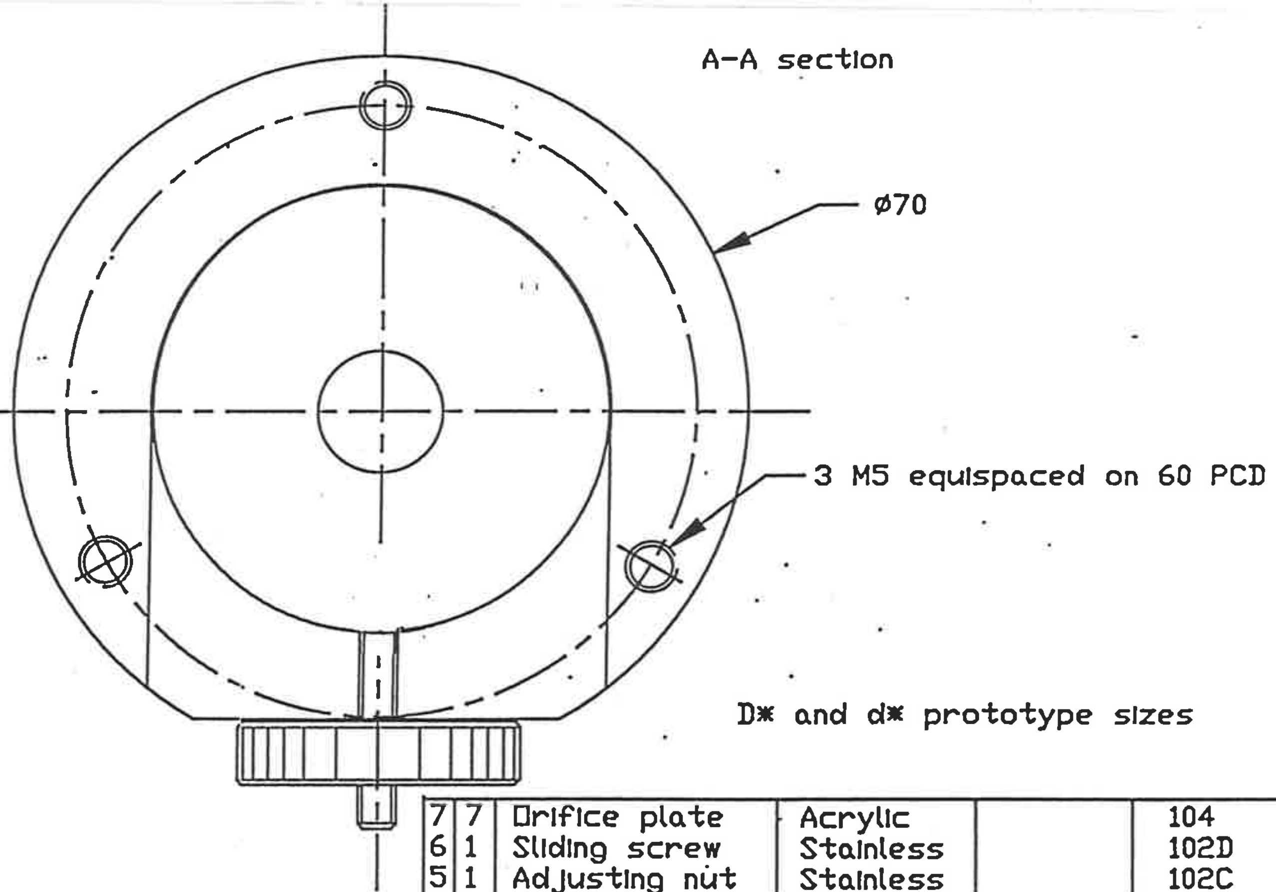

I	Q	Description	Material	Ref No	Draw No
7	7	Orifice plate	Acrylic		104
6	1	Sliding screw	Stainless		102D
5	1	Adjusting nut	Stainless		102C
4	1	House plate 2	Acrylic		102B
3	1	House plate 1	Acrylic		102A
2	2	O ring seal		NDI	BS218
1	3	Socket screw.	Stainless	NDI	

Drawn by	The University of Adelaide Mech. Eng. Dept.,	
Checked		
Scale 2:1	Title: Orifice house	Draw No 102

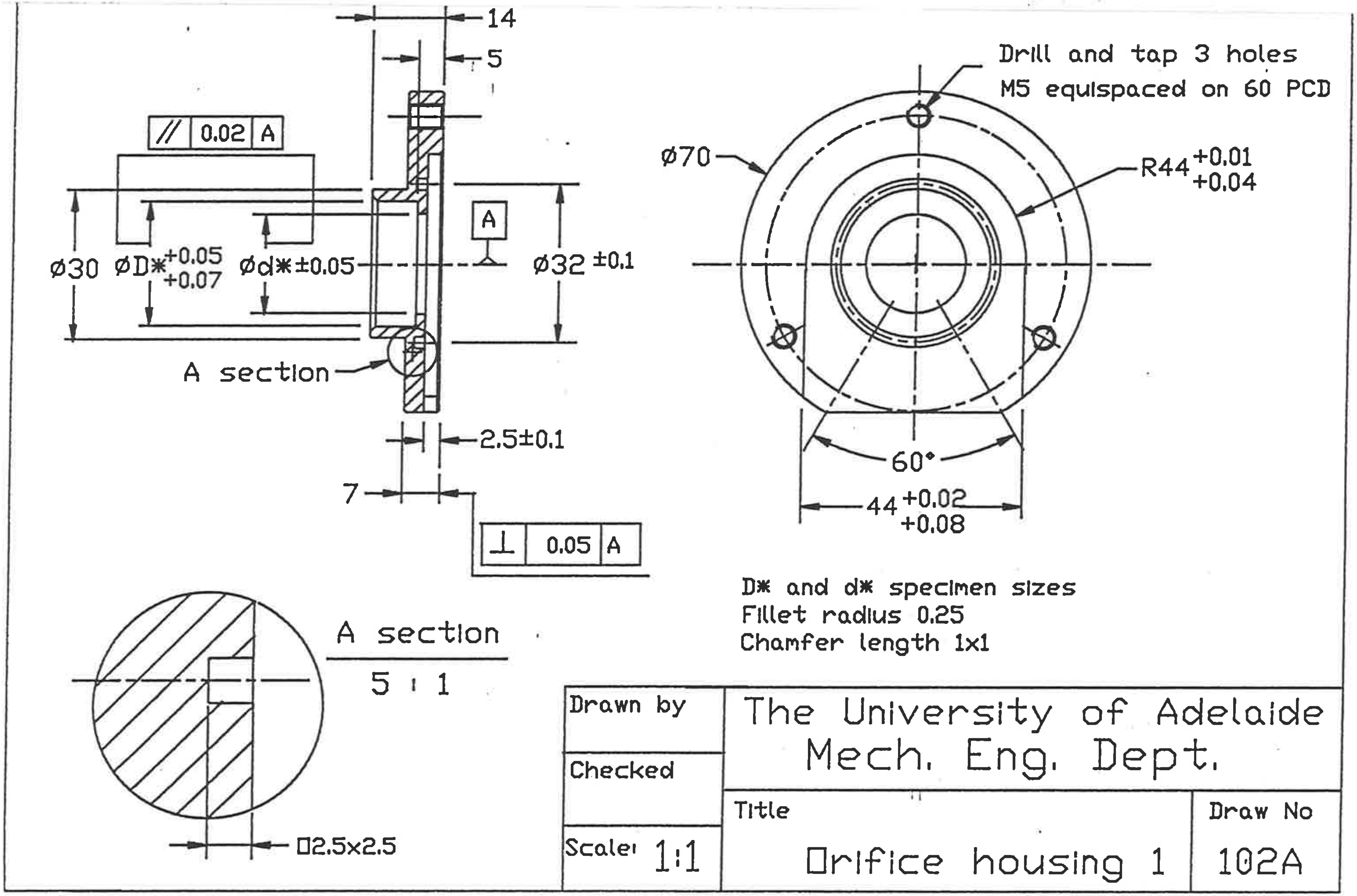
14
5
// 0.02 A
A
Ø30
ØD* +0.05 +0.07
Ød* ±0.05
Ø32 ±0.1
A section
2.5±0.1
7
⊥ 0.05 A
Drill and tap 3 holes
M5 equispaced on 60 PCD
Ø70
R44 +0.01 +0.04
60°
44 +0.02 +0.08
D* and d* specimen sizes
Fillet radius 0.25
Chamfer length 1x1
A section
5 : 1
□2.5x2.5
Drawn by
Checked
Scale: 1:1
The University of Adelaide
Mech. Eng. Dept.
Title
Orifice housing 1
Draw No
102A

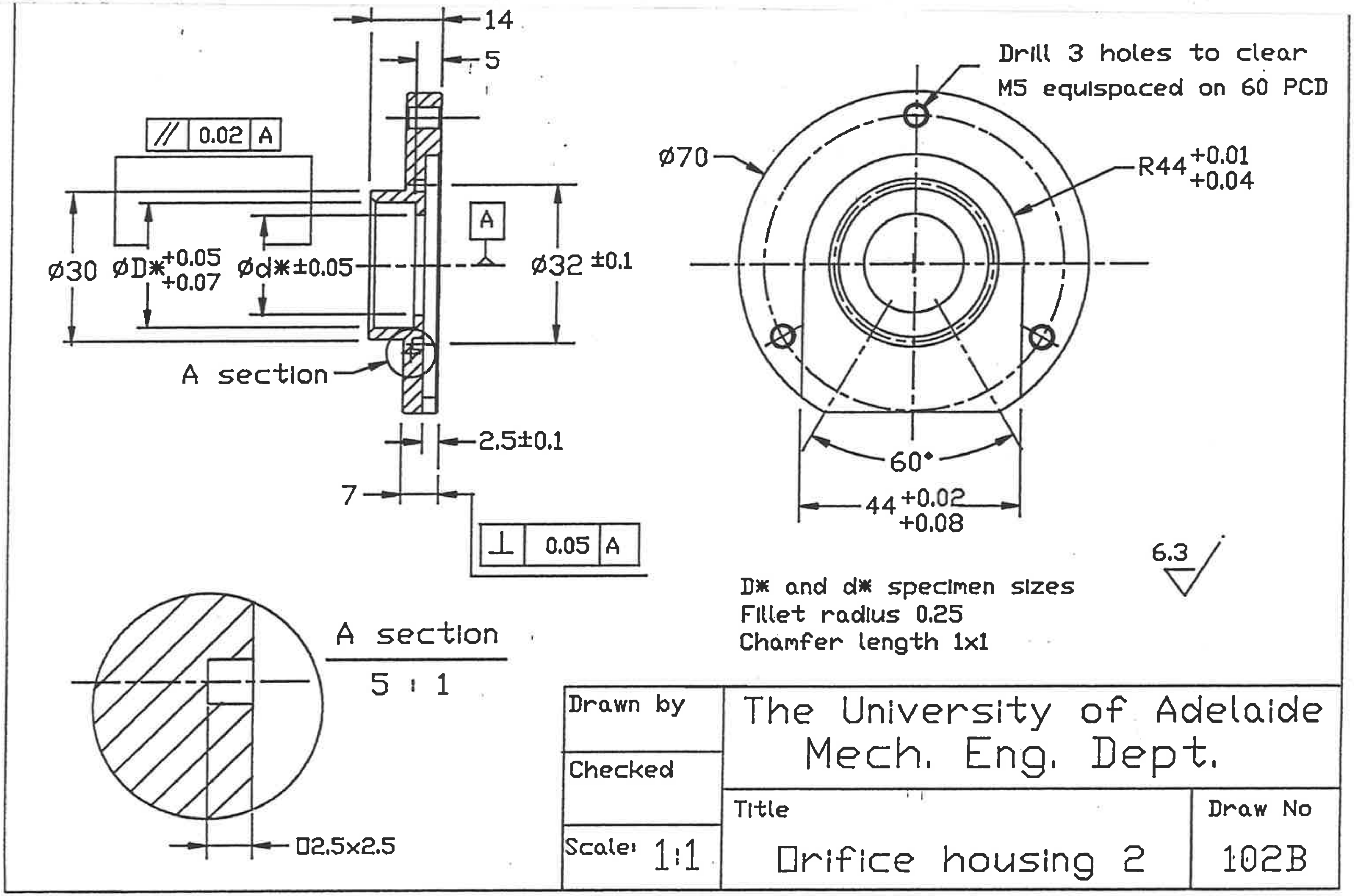
14
5
// 0.02 A
A
Ø30
ØD* +0.05 +0.07
Ød* ±0.05
Ø32 ±0.1
A section
2.5±0.1
7
⊥ 0.05 A
Drill 3 holes to clear
M5 equispaced on 60 PCD
Ø70
R44 +0.01 +0.04
60°
44 +0.02 +0.08
6.3
D* and d* specimen sizes
Fillet radius 0.25
Chamfer length 1x1
A section
5 : 1
□2.5x2.5
Drawn by
Checked
Scale: 1:1
The University of Adelaide
Mech. Eng. Dept.
Title
Orifice housing 2
Draw No
102B

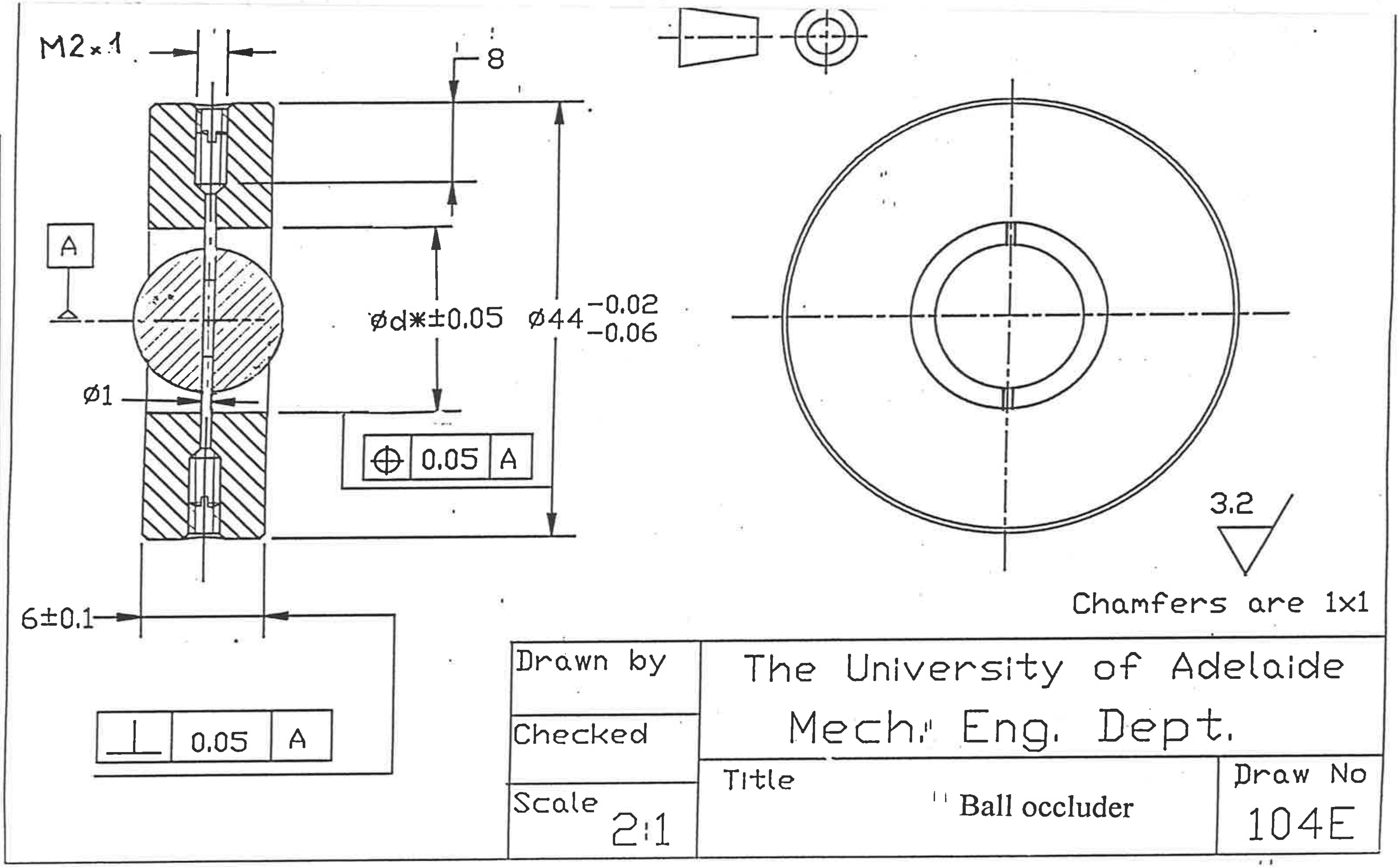
M2×1
8
A
ød*±0.05
ø44 −0.02 −0.06
ø1
0.05 A
6±0.1
0.05 A
3.2
Chamfers are 1x1
Drawn by
Checked
Scale 2:1
The University of Adelaide
Mech. Eng. Dept.
Title
Ball occluder
Draw No
104E

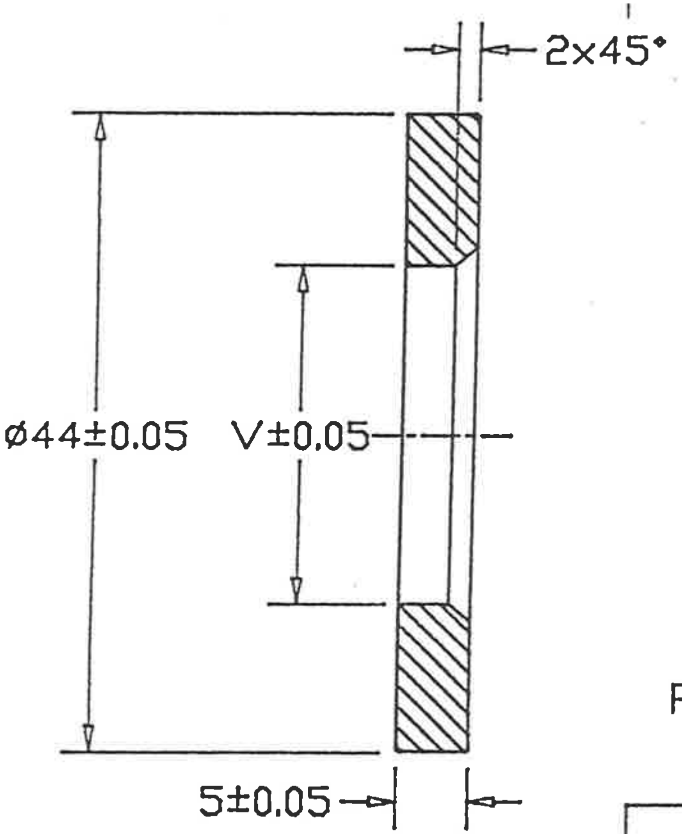

Orifices are:

1. Square
2. Triangular
3. Circular

V Values:

Shape	Notation	Values (mm)
Square	VxV	10.2X10.2
Triangular	VxVxV	16x16x16
Circular	Ø V	12 13.5 15 16.5

Fillet radius: 0.5 mm

	Mech. Eng. Dept.	
Scale: 2:1	Title: Orifice plate	Draw. No 105

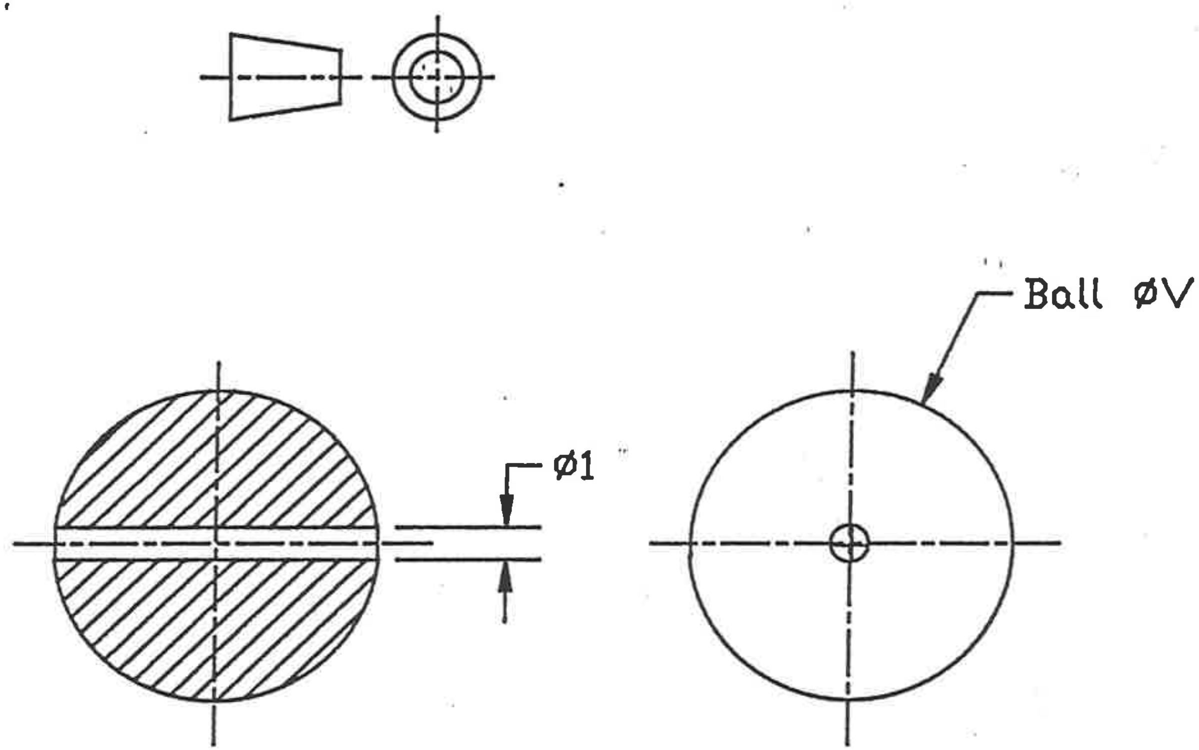

ØV values:

ØV	9.4
	14.5

Drawn by	The University of Adelaide Mech. Eng. Dept.	
Checked		
Scale 1:1	Title Ball occluder	Draw No 107

8.2 Appendix two

Tran, V.V., Tansley, G.D. and Morsi, Y.S., 1994.

Haemodynamics of a Jellyfish heart valve

Conference abstracts of EPSM'94 (Engineering and the Physical Sciences in Medicine), Perth, Western Australia. 12th - 15th, September 1994, 44.

HAEMODYNAMICS OF A JELLYFISH HEART VALVE

Tran Van Vinh[1], Geoff D. Tansley[2] and Yos S. Morsi[3]

[1]Department of Mechanical Engineering, The University of Adelaide, SA 5005
[2]School of Engineering, Flinders University, GPO Box 2100 Adelaide 5001
[3]School of Mechanical and Manufacturing Engineering, Swinburne University of Technology, GPO Box 218, Hawthorn, Victoria 3122

Introduction All prosthetic heart vales exhibit haemodynamic inadequacies in that they are liab to thrombus formation, tissue overgrowth, haemolysis, etc. This work examines a new artifici heart valve viz the Jellyfish valve designed by Professor Umezu of Waseda University ar Professor Imachi of The University of Tokyo. This study aims to provide haemodynam information about this newly designed valve and to give an indicator of dysfunction potentials f this prosthesis through the determination of velocity profiles, shear stresses and pressure drops.

Methods Steady and pulsatile-flow experiments were conducted to examine the fluid flow régin through the Jellyfish artificial heart valve using Laser Doppler Anemometry (LDA). The LD technique has become the most popular method in recent years for the determination of she phenomena in flow through heart valve prostheses. A two component Laser Doppl Anemometer was used to determine the velocity and turbulence parameters of inlet flow and flo downstream of the valve; these along with the pressure drops across the valve were compare those of other valves.

Results Pressure drops across the valve compared favourably with those of other heart valv (>10 mmHg), and the Jellyfish valve was shown to exhibit sub-critical values of shear stress >150 Pa, see figure 2); but a large stagnation region was exhibited immediately downstream

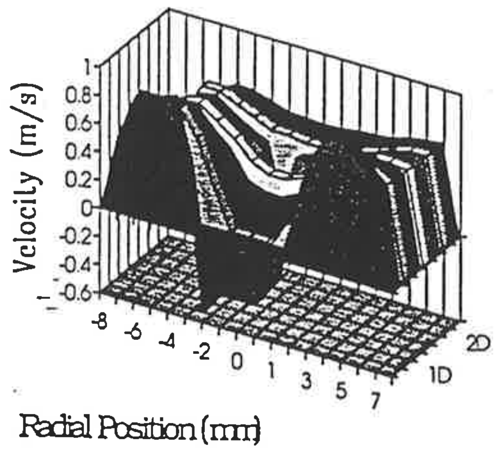

Figure 1. Steady-flow velocity profiles downstream of the valve

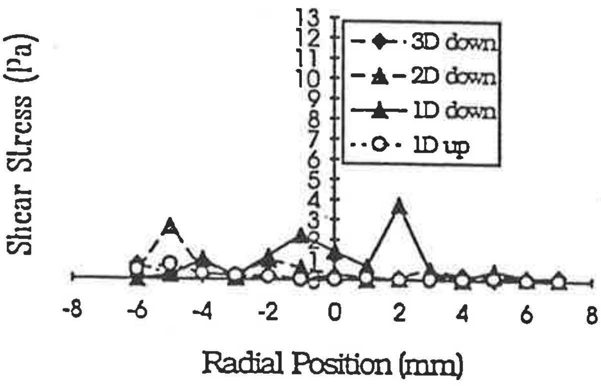

Figure 2. Turbulent shear stresses upstream and downstream of the valve

of the valve (see figure 1) - this could have implications for excessive thrombus formation an tissue overgrowth.

Conclusions These preliminary studies show that the Jellyfish valve exhibits good flui dynamical properties, though possible thrombogenisity of the valve needs further investigation.

Tran, V.V., Tansley, G.D., Morsi, Y.S. and Larson, C.M., 1995.

LDA evaluation of a prototype Jellyfish artificial heart valve.

Proceedings of The Sixth Asian Congress Of Fluid Mechanics. May 22-26, 1995, Singapore, 1030-1034.

THE SIXTH ASIAN CONGRESS OF FLUID MECHANICS
May 22-26, 1995, Singapore

LDA EVALUATION OF A PROTOTYPE JELLYFISH ARTIFICIAL HEART VALVE

Tran Van Vinh, Geoff D. Tansley*, Yos S. Morsi** and Christine M. Larson**

Department of Mechanical Engineering, The University of Adelaide, South Australia
*School of Engineering, Flinders University of South Australia, Adelaide, Australia
**School of Mechanical & Manufacturing Engineering, Swinburne University of Technology, Hawthorn, Victoria, Australia

ABSTRACT - Experiments were conducted under steady flow conditions to examine the fluid flow régime through a prototype Jellyfish artificial heart valve. A two component Laser Doppler Anemometer (LDA) was used to determine the velocity and turbulence parameters of flow at inlet and downstream of the valve. The velocity profiles and turbulence shear stress parameters are presented and compared with critical threshold values for blood trauma. The Jellyfish valve was shown to exhibit sub-critical values of shear stress and very limited jetting under steady flow conditions.

1. Introduction

Contemporary Total Artificial Hearts (TAH's) and Ventricular Assist Devices (VAD's) rely on passive non-return valves for the control of flow direction; but most mechanical valves exhibit less than optimal performance in that they present ring thrombus (clotting near the valve/seat interface due to flow disturbances near abrupt surface discontinuities), regurgitant flow due to inertial properties of the occluder, haemolysis (the destruction of red cells under high shear stresses), and in rare cases, mechanical failure due to water hammer and erosion.

Many centres around the world are researching ways of improving heart valve design through a re-examination of the fluid dynamics of these devices. Of particular influence are the magnitudes of shear stress and shear rate developed in the vicinity of heart valves; these parameters are commonly measured with Laser Doppler Anemometers (LDA) or are predicted using Computational Fluid Dynamics (CFD). Both of these techniques have been instrumental in the quantum leaps forward made recently in fluid dynamics. As a result of such developments, a number of new valve design concepts are now being examined by many researchers world wide. Flow phenomena of particular interest are:

- shear stresses - a threshold level of Reynolds stress for haemolysis in a free jet is around 400 - 500 N/m^2 [1,2], though blood trauma is both time and stress dependent and damage can occur at values as low as 150 N/m^2 close to a prosthetic surface [2],
- velocity profile - shear stresses developed in impingent jets are very high. Jets forming downstream of an artificial heart valve are deleterious to a valve's proper functioning,
- shear rate - low shear rates exacerbate thrombus formation [3] and can lead to valve dysfunction or embolism.

There is a healthy volume of literature which reports fluid dynamical studies of heart valves, e.g.: Yoganathan *et al.* reported on studies of Björk-Shiley[4] and Starr-Edwards [5]valves, Tillman *et al.* [6], using flush mounted shear stress probes examined three different types of mechanical valves and found a peak value of 120 - 140 N/m^2 at the large orifice of a Björk-Shiley valve, 12-15 N/m^2 at the large orifice of a Lillehei-Kaster valve and 85 N/m^2 at the valve ring of a Starr-Edwards valve.

In this study a new type of valve known as a Jellyfish valve - which was developed by Professor Imachi at the University of Tokyo - is being examined by groups at Adelaide, Flinders and Swinburne Universities.

The Jellyfish valve is unique in design; incorporating a thin flexible membranous occluder attached centrally to a rigid frame. The potential advantages this valve could offer are:

- minimal flow disturbance - hence relatively low shear stresses and pressure gradients,
- limited occluder inertia and therefore reduced regurgitant flow,
- reduced cost - this is important, since the cost of valves is a significant proportion of the total cost of VAD's and TAH's.

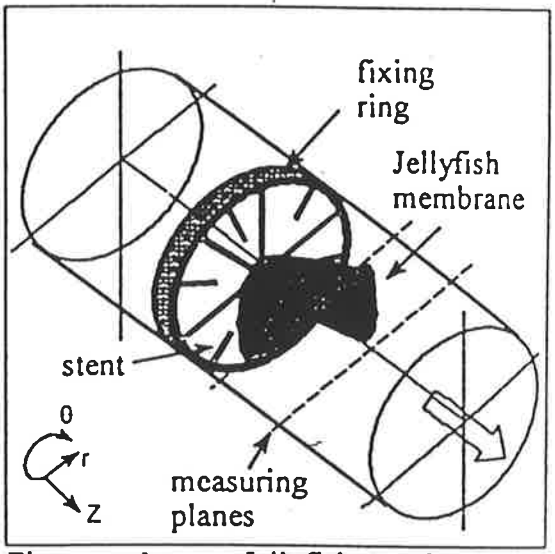

Figure 1 Jellyfish valve and measurement planes

2. Experimental Facilities

Steady flow LDA measurements were carried out in Adelaide using the 488 nm and 514.5 nm beams from a 5 Watt Spectra Physics 165 argon-Ion laser driving a TSI 9100-7 Laser Doppler Anemometer. Optics included two Bragg cells, a beam expander (to 82.5 mm beam spacing) and a 450 mm lens mounted on TSI 9400 traverse. Steady flow generated by a small centrifugal pump circulated through a size 20 Jellyfish valve* and was returned, via a turbine flow-meter to an open sump. Experiments with a flow rate of 10.7 - 10.9 l/min are reported here. The valve was inserted into a plane acrylic tube (refractive index 1.48 and internal diameter 19 mm) which was then placed in an index matching enclosure filled with medical grade paraffin. The LDA seeding particles used were 11 μm metallic coated spheres.

Two velocity components (v_z and v_Θ) and stress measurements were recorded at two planes upstream of the valve, at 1 diameter (19 mm) and 2 diameters (38 mm) upstream of the valve seating ring, and at five positions downstream of the valve, at 1, 1¼, 1½, 2 and 3 diameters downstream of the seating ring, providing a good picture of the structure and subsequent development of the flow (see Figure 1). Measurements were made in cross sectional planes in 1 mm increments across the radius of the test section at each of the above

* The outer diameter of the valve ring was 20 mm, the inner diameter was 18mm

Yoganathan, A.P., 1978. Cardiovascular fluid mechanics. Ph.D. *thesis*, California Institute of Technology, Pasadena.

Yoganathan, A.P., Corcoran, W.H. and Harrison, E.C., 1978. Wall shear stress measurement in the near vicinity of aortic prosthetic heart valves. *Journal of Bioengineering*, **2**, 369-379.

Yoganathan, A.P., Corcoran, W.H. and Harrison, E.C., 1979a. Pressure drops across prosthetic aortic heart valves under steady and pulsatile flow - *In-vitro* measurements. *Journal of Biomechanics,* **12,** 153-164.

Yoganathan, A.P., Reamer, H.H. Corcoran, W.H. and Harrison, E.C., 1979b. A Laser Doppler Anemometer to study velocity fields in the vicinity of prosthetic heart valves. *Med. & Biol. Eng. & Comput.,* **17**, 38-44.

Yoganathan, A.P., Corcoran, W.H., Harrison, E.C. and Carl, J.R. 1979c. *In-vitro* measurements in the vicinity of the Björk-Shiley aortic prosthesis using laser Doppler anemometer. *Med. & Biol. Eng. & Comput.,* **17**, 453-459.

Yoganathan, A.P., Reamer, H.H., Corcoran, W.H., Harrison, E.C., Shulman, I.A. and Parnassus, W., 1981. The Starr-Edwards aortic ball valve: Flow characteristics, thrombus formation, and tissue overgrowth. *International Society for Artificial Organs,* **5,** (1), 6-17.

planes. Between 15-18 of these sites per plane yielded valid data - data was not always available near to the tube walls or near to the Jellyfish membrane. Index matching between the flowing liquid and the test cell was not carried out limiting measurements to the axial (z) and tangential (θ) directions. Some difficulties were encountered due to the use of acrylic which is highly absorbent around the 500 μm wavelength.

3. Data Analysis

Reynolds shear stresses are calculated from 1024 coincident data points collected in each of the two directions as:

$$\tau_R = \frac{1}{K}\sum_{i=1}^{K} v_z' v_\theta' = \overline{v_z' v_\theta'} = \overline{v_z v_\theta} - \overline{v_z}\,\overline{v_\theta} \tag{1}$$

where

$$v = \bar{v} + v', \qquad \bar{v} = \sum_{i=1}^{K} \frac{v}{K}$$

4. Results and Discussion

Under steady-flow conditions, the Jellyfish membrane was seen to open into an asymmetric four-lobed configuration; measurement planes were orientated such that they either dissected the lobes or passed between the lobes. Velocity profiles are depicted in

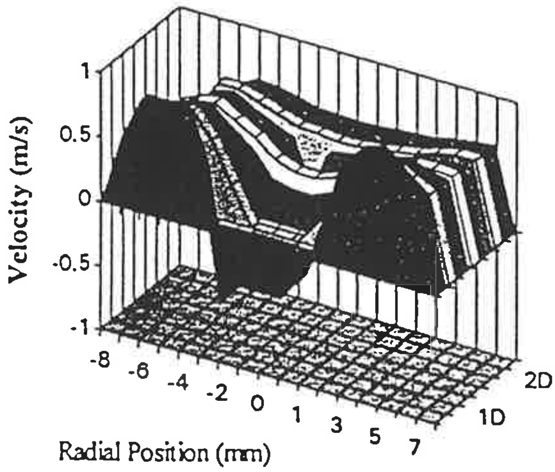

Figure 2 Velocity profiles between lobes

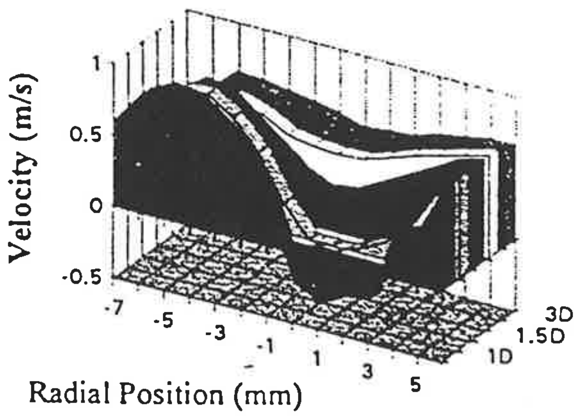

Figure 3 Velocity profile dissecting lobes

Figures 2 and 3 for both of these measurement orientations; each shows a series of velocity profiles for successive steps downstream of the valve. The plots reveal areas subjected to annular jetting and regions of pronounced flow reversals at 1 diameter downstream which gradually decays until the velocity profile is almost flat 3 diameters downstream. Maximum flow velocities are evident at a 5 mm radial location in both the between lobes measurements (0.968 m/s) and dissecting lobe measurements (0.897 m/s).

Figures 4 and 5 show the shear stress profiles in the series of measurement planes downstream of the valve; again measurements between the lobes and dissecting the lobes are indicated. Reynolds shear. stress values were calculated using equation 1.

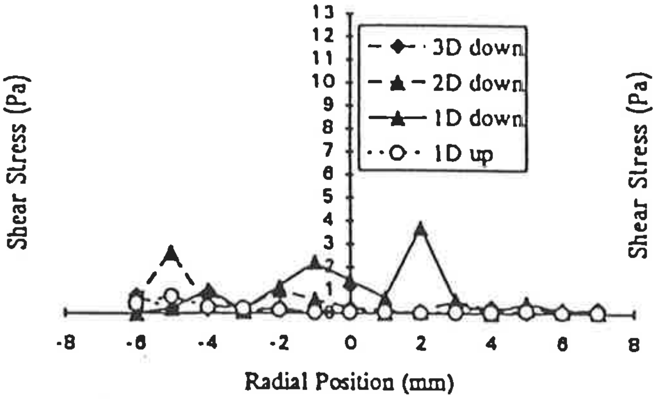

Figure 4 Shear stress profiles between lobes

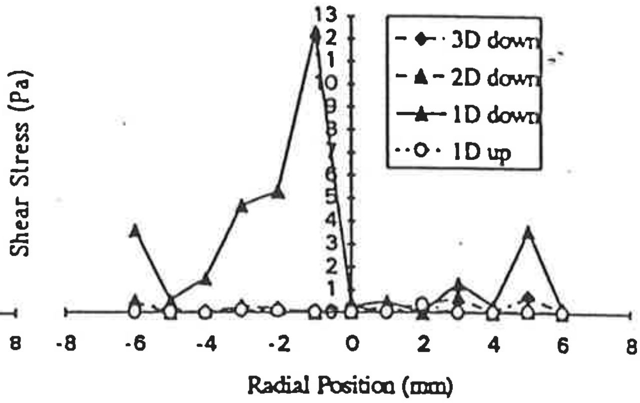

Figure 5 Shear stress profiles dissecting lobes

5. Conclusion

LDA has been used to determine the fluid flow and turbulence parameters inside an artificial heart valve. It was found that the magnitude of shear stresses were of the order of 1-14 N/m^2 which is sub-critical for haemolytic damage. Velocity profiles downstream of the valve show only limited jetting - restricting shear stress development at the flow vessel wall (where haemolysis is exacerbated and where endothelial damage would occur if the valve were placed into a natural aorta). Regions close to the valve (in the central recirculation region and near the valve ring) are the most likely regions to display thrombosis; these were not examined during this study due to difficulties of (control volume) access. Since turbulence in the valve is anisotropic, shear stresses calculated from $v_\theta'$and v_r' will be of a greater magnitude.

6. References

1 Imachi, K. et al. 1988. A newly designed jellyfish valve for an artificial heart blood pump. *Transactions of the American Society for Artificial Internal Organs*, 34 726-728

2 Tansley, G.D., Edwards, R.J. and Gentle, C.R. 1988. Role of computational fluid dynamics in the analysis of prosthetic heart valve flow. *Medical and Biological Engineering and Computing*, 26, 175-185

3 Dintenfass, L. 1964. Rheological approach to thrombosis and atherosclerosis, *Angiology*, 15, 333-343

4 Yoganathan, A.P., Corcoran, W.H., Harrison, E.C. and Car, J.R. 1979. Measurements in the near vicinity of the Björk-Shiley aortic prosthesis using LDA. Medical and Biological Engineering and Computing, 17, 453-459

5 Yoganathan, A.P., Reamer, H.M., Harrison, E.C., Shulman, I.A. and Parnassus, W. 1981. The Starr-Edwards aortic ball valve: flow characteristics, thrombus formation and tissue overgrowth. *Artificial Organs*, 5, 6-17

6 Tillman, W., Reul, H., Herold, M, Bruss, K.H. and van Glise, J. 1984. In-vitro wall shear measurements at aortic valve prostheses, *Journal of Biomechanics*, **4**, 263-279

7 Einav, S., Stolero, D., Avidor, J.M., Elad, D. and Talbot, L. 1988. LDA evaluation of wall shear stress distribution along the cusp of a tri-leaflet prosthetic heart valve. In: *Proceedings of the 4th International Symposium on the Application of Laser Anemometry to Fluid Mechanics, Lisbon, Portugal,* 7.21.1-7.21.3

8 Einav, S., Stolero, D., Avidor, J.M., Elad, D. and Talbot, L. 1990. In vitro measurements of the velocity field in the core of tri-leaflet prosthetic valves. In: *Laser Anemometry - Proceedings of the 3rd International Conference, Los Angeles, California, USA*, 523-532

Nomenclature

V_z	mean velocity along the flow axis (z)
V_r	mean velocity in the radial direction
V_Θ	mean velocity in the tangential direction
v_z, v_r, v_Θ	local instantaneous velocity components
$v_z v_\Theta$	mean product of v_z and v_Θ
v_z', v_Θ'	fluctuations about the local v_z and v_Θ components of velocity
σ_z	standard deviation of the v_z component
τ_R	Reynolds Shear Stress
T	coincident time window
K	number of samples in a record

8.3 Appendix three: Pressure drop measurements

PRESSURE DROPS - RAW DATA

1. Measured and calculated pressure drops across different orifices

P are pressure drops in mm Hg, eg. P(d12) are pressure drops across 12 mm diameter orifice
d is the orifice diameter in mm
Annular, square and triangular are different shaped orifices with equivalent area of the 12 mm circular orifice.

Measured

l/min	P(d16.5)	P(d15)	P(d13.5)	P(d12)	P(d10.4)	P(Annular	P(Square)	P(Triangular)
24.25	4.2	7.8	18.6	40.6		30	51.5	55.6
21	3.3	6.4	14.1	30.8	80.6	22.4	39.2	42.7
18	2.6	4.7	10.3	22.4	59.3	16.4	28.7	31.5
15	2	3.4	7.1	15.4	40.9	11.9	20.2	21.7
12	1.5	2.4	4.8	10	26.4	7.8	13.1	14.1
9	1	1.7	3.1	6.2	15.1	4.8	8	8.4
6	0.6	1.2	1.6	3.1	7.1	2.5	3.9	4.4

Calculated

l/min	P(d16.5)	P(d15)	P(d13.5)	P(d12)	P(d10.4)	P(Annular	P(Square)	P(Triangular)
24.25	4.602302	7.527849	16.66459	40.99515		30.99233	52.67877	57.14724
21	3.455065	5.651347	12.51053	30.7761	78.94001	23.26673	39.54729	42.90189
18	2.545595	4.163755	9.217408	22.67497	58.1608	17.14228	29.13734	31.60891
15	1.781533	2.914002	6.450798	15.86907	40.7038	11.99701	20.39175	22.12148
12	1.164478	1.904703	4.216488	10.37263	26.60556	7.841708	13.32883	14.45945
9	0.69273	1.133078	2.508324	6.170517	15.82724	4.664911	7.929114	8.601701
6	0.354127	0.579234	1.282265	3.154393	8.090948	2.384721	4.053396	4.397224

Maximum error of 1.94 mmHg

2. Pressure drops across a circular orifice of 12 mm diameter at various eccentricities.

P are pressure drops in mm Hg, eg. P(e=1) are pressure drops across the orifice mounted at 1mm eccentricity
e is the eccentricity in mm

Measured

l/min	P(e=0)	P(e=0.5)	P(e=1)	P(e=1.5)	P(e=2)	P(e=2.5)	P(e=3)	P(e=3.5)
24.25	40.6	41	41.7	42.9	44.1	45.9	47.9	50.6
21	30.8	31.2	31.8	32.8	33.8	34.9	36.8	38.9
18	22.4	22.6	22.9	23.8	24.9	25.6	27.1	28.6
15	15.4	15.9	16	16.4	17	17.9	18.5	19.8
12	10	10.3	10.5	10.9	11.1	11.6	12.3	13.3
9	6.2	6.4	6.5	6.6	6.7	6.9	7.3	7.7
6	3.1	3.2	3.4	3.4	3.4	3.4	3.5	3.8

Calculated

l/min	P(e=0)	P(e=0.5)	P(e=1)	P(e=1.5)	P(e=2)	P(e=2.5)	P(e=3)	P(e=3.5)
24.25	41.07	41.29642	41.97567	43.11033	44.69955	46.73902	49.23132	52.17645
21	30.8323	31.00227	31.5122	32.36402	33.55709	35.08817	36.9592	39.17019
18	22.71638	22.84161	23.21731	23.84491	24.72393	25.85199	27.23051	28.8595
15	15.89804	15.98569	16.24862	16.68785	17.30303	18.0925	19.05726	20.19731
12	10.39157	10.44886	10.62072	10.90782	11.30992	11.82595	12.45655	13.20173
9	6.181784	6.215864	6.318103	6.488891	6.728097	7.035074	7.410211	7.853507
6	3.160153	3.177575	3.22984	3.317147	3.439431	3.596359	3.78813	4.014745

Maximum error of 1.58 mm Hg

3. Measured and calculated pressure drops across a ball occluder with various eccentricities.

P are pressure drops in mm Hg
e is the eccentricity, eg. e=1 means 1 mm eccentricity

Measured

l/min	Pe=0	Pe=0.5	Pe=1	Pe=1.5	Pe=2
24.25	30	31.6	31.7	32.7	34.5
21	22.4	23.1	23.7	24.2	25.7
18	16.4	17.1	17.4	17.7	18.9
15	11.9	12.2	12.4	12.6	13.4
12	7.8	8.3	8.5	8.5	9
9	4.8	4.9	5.1	5.3	5.5
6	2.5	2.5	2.6	2.7	2.8

Calculated

l/min	Pe=0	Pe=0.5	Pe=1	Pe=1.5	Pe=2
24.25	30.99233	31.28635	32.16736	33.63588	35.69174
21	23.26673	23.48745	24.14885	25.25131	26.7947
18	17.14228	17.3049	17.7922	18.60446	19.74159
15	11.99701	12.11083	12.45186	13.02032	13.81614
12	7.841708	7.916099	8.139014	8.51058	9.030756
9	4.664911	4.709165	4.841773	5.062812	5.372257
6	2.384721	2.407344	2.475134	2.58813	2.74632

Maximum error of 1.2 mm Hg

8.4 Appendix four: LDA velocity data

Notations:

X:	Axial position (tube diameter)
Y:	Radial position (mm)
U MEAN:	Axial mean velocity (m/s)
U RMS:	R.M.S. axial velocity (m/s)
U TURBU:	Axial turbulence intensity
W MEAN:	Tangential mean velocity (m/s)
W RMS:	R.M.S. tangential velocity (m/s)
W TURBU:	Tangential turbulence intensity
uw:	Product of axial and tangential fluctuating velocities (m^2/s^2)

A. 4.1. Typical velocity profile in upstream region

VELOCITY IN UPSTREAM REGION
X: Axial position
Y: Radial position (mm)

X	Y	U MEAN	U RMS	U TURBU	W MEAN	W RMS	W TURBU	uw
1D up-stream	1	1.173449	0.208232	17.74529	-0.01265	0.005137	0.437809	-0.00013
	2	1.374797	0.13997	10.18113	-0.01254	0.005699	0.414549	-0.00034
	3	1.458564	0.120613	8.269293	-0.01349	0.005449	0.373605	-0.00031
	4	1.543701	0.107682	6.975562	-0.01787	0.022098	1.431471	-0.00029
	5	1.640309	0.086948	5.300682	-0.03272	0.07275	4.435137	-0.00023
	6	1.679676	0.069232	4.121766	-0.01654	0.055096	3.280159	-0.00013
	7	1.719911	0.052917	3.076706	-0.0167	0.044466	2.585346	0.000159
	8	1.727269	0.048163	2.788378	-0.01446	0.035814	2.07342	-0.00008
	9	1.720813	0.048876	2.84028	-0.01467	0.034408	1.99954	0.000006
	10	1.706575	0.055046	3.225533	-0.01245	0.036691	2.149955	0.000286
	11	1.68486	0.061981	3.678728	-0.00833	0.042187	2.503902	0.00036
	12	1.657942	0.068716	4.14467	-0.00806	0.047046	2.837627	0.000466
	13	1.623301	0.077202	4.75584	-0.0097	0.053601	3.301968	0.000758
	14	1.575847	0.090397	5.736437	-0.00944	0.064365	4.084487	0.000835
	15	1.495926	0.109244	7.302743	-0.00054	0.073803	4.933569	0.000857
	16	1.397421	0.120975	8.657001	0.00433	0.085848	6.143296	0.000698
	17	1.275121	0.156962	12.30961	0.003873	0.096953	7.603453	0.00055
	18	1.024328	0.282227	27.55242	-0.0033	0.098037	9.570908	0.000578

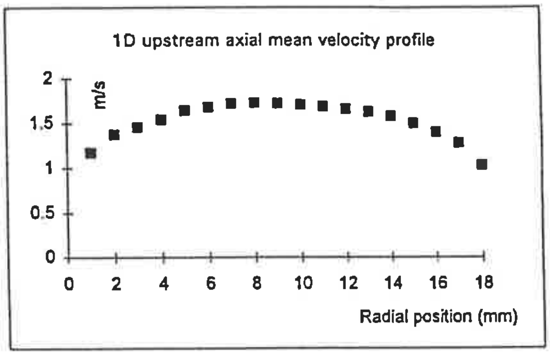

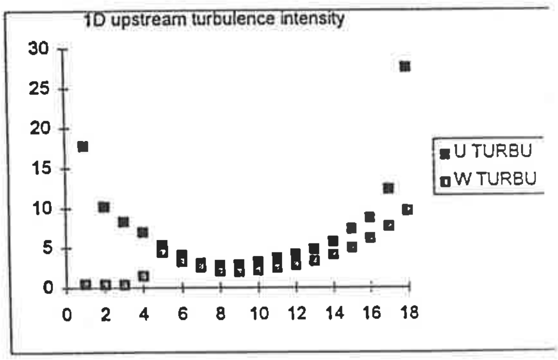

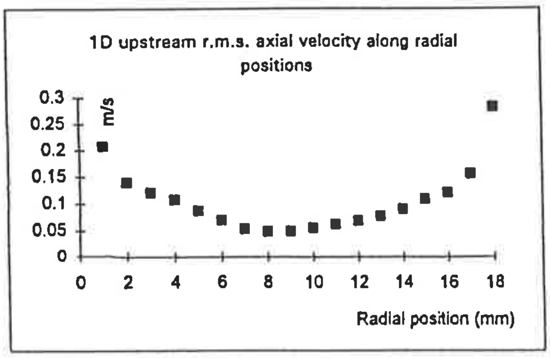

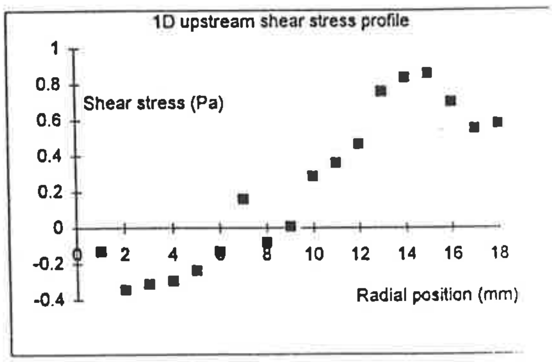

A. 4.2. Velocity data across circular orifices

SHEAR STRESS AND TURBULENCE INTENSITY IN 12 mm CIRCULAR ORIFICE

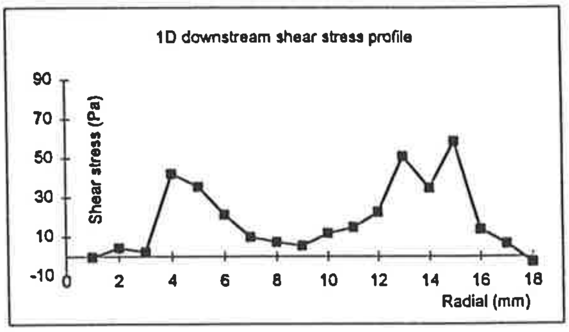

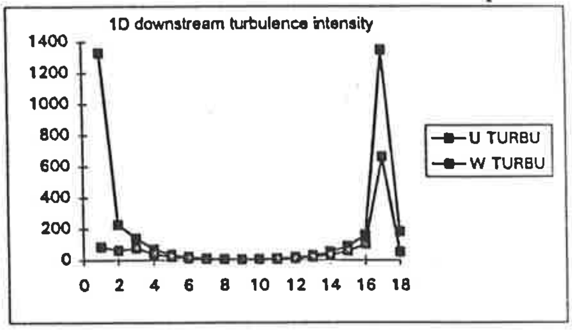

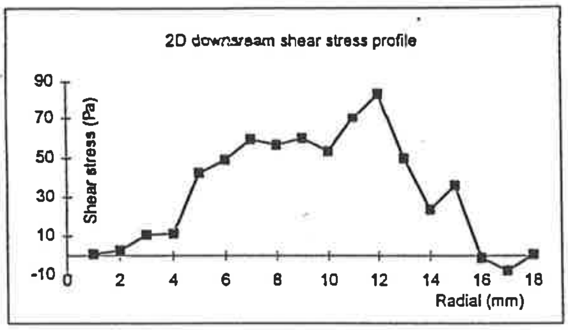

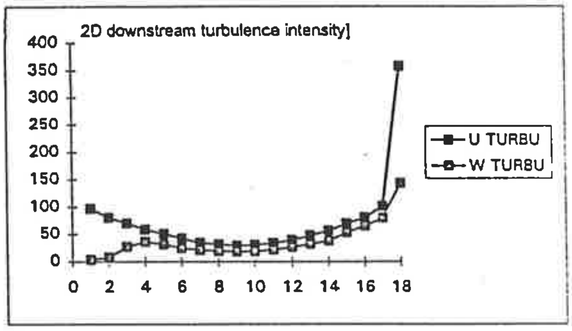

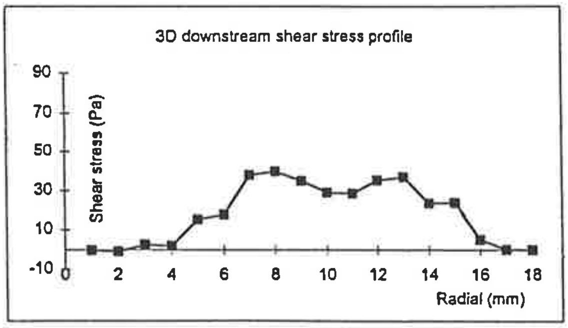

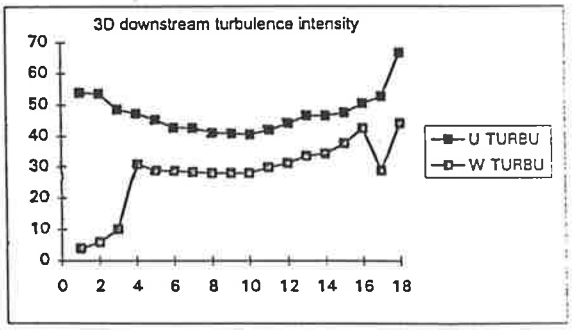

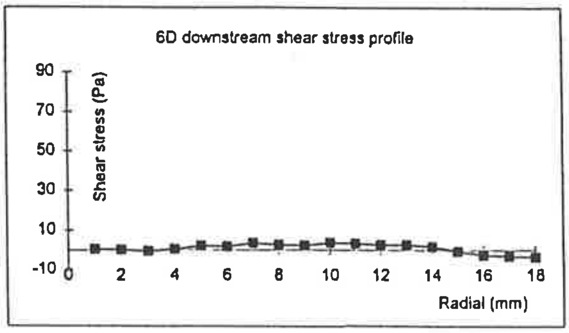

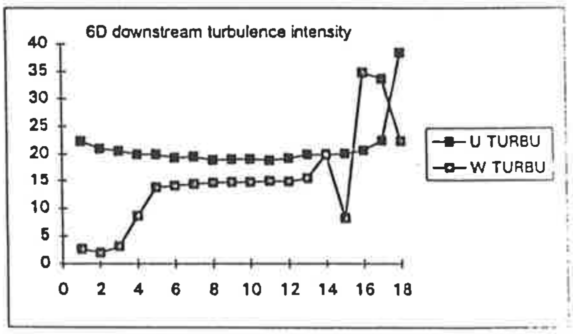

VELOCITY RAW DATA - CIRCULAR ORIFICE OF 12 mm DIAMETER

X	Y	U MEAN	U RMS	U TURBU	W MEAN	W RMS	W TURBU	uw
1D dow	1	0.065174	0.865056	1327.307	-0.0742	0.05475	84.00691	-0.00035
stream	2	0.451859	1.034646	228.9757	-0.08	0.285375	63.15591	0.004366
	3	0.800294	1.127128	140.8394	-0.06471	0.615945	76.96485	0.002166
	4	1.759705	1.216632	69.13841	-0.03647	0.691238	39.28146	0.04194
	5	2.912282	1.055412	36.24003	-0.02471	0.611353	20.99223	0.035297
	6	3.669674	0.778022	21.20138	-0.02057	0.471493	12.84835	0.021206
	7	4.045124	0.424892	10.50382	-0.03128	0.309146	7.642447	0.009844
	8	4.147513	0.246327	5.939159	-0.03011	0.226354	5.457594	0.007219
	9	4.137476	0.207638	5.018468	-0.0349	0.205632	4.969977	0.005227
	#	4.142973	0.266048	6.421673	-0.02911	0.2261	5.457431	0.011644
	#	4.067698	0.422201	10.37937	-0.01706	0.295479	7.264046	0.014635
	#	3.760401	0.737019	19.59947	-0.00751	0.459324	12.21477	0.022356
	#	3.245793	0.962489	29.65342	-0.01392	0.598717	18.44593	0.05072
	#	2.325441	1.23114	52.94223	-0.01265	0.738686	31.76544	0.034697
	#	1.352009	1.194837	88.37492	-0.01237	0.804595	59.51107	0.058477
	#	0.627879	1.026442	163.4776	-0.03783	0.65403	104.1649	0.013737
	#	-0.06285	0.84705	1347.732	-0.04156	0.416355	662.4578	0.006395
	#	-0.37313	0.682653	182.9523	-0.04233	0.200505	53.73573	-0.00295

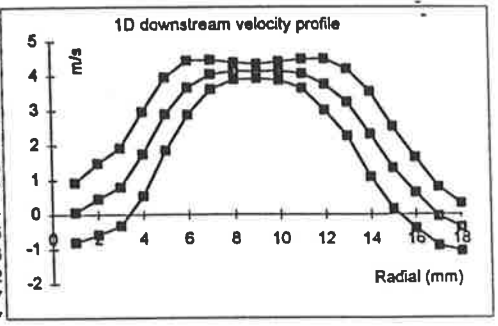

X	Y	U MEAN	U RMS	U TURBU	W MEAN	W RMS	W TURBU	uw
2D dow	1	0.781545	0.758719	97.07938	-0.0363	0.027605	3.532083	0.000772
stream	2	1.069632	0.86188	80.57721	-0.07285	0.081235	7.594623	0.002701
	3	1.315811	0.926247	70.39361	-0.04358	0.359918	27.35335	0.01061
	4	1.637462	0.962712	58.79295	-0.02426	0.590971	36.09068	0.011241
	5	2.018151	1.020618	50.57193	-0.01305	0.631258	31.27903	0.04242
	6	2.409187	1.014144	42.09487	-0.00703	0.6043	25.08316	0.049006
	7	2.777305	0.951034	34.24307	0.012031	0.586413	21.11447	0.059474
	8	2.963384	0.936531	31.60345	-0.01875	0.568999	19.201	0.056595
	9	3.047834	0.8927	29.28964	-0.01532	0.561535	18.42406	0.059919
	#	2.965726	0.892849	30.10558	-0.00759	0.555099	18.71715	0.053309
	#	2.799488	0.953341	34.05413	-0.02236	0.607955	21.71664	0.070803
	#	2.499126	0.97745	39.11166	-0.01642	0.662593	26.513	0.083237
	#	2.126452	1.010866	47.53769	-0.01791	0.679543	31.95664	0.049727
	#	1.75557	0.989027	56.33651	-0.0259	0.673938	38.38855	0.023661
	#	1.308765	0.908242	69.39689	-0.02759	0.696105	53.18797	0.035872
	#	1.051912	0.846146	80.43885	-0.03653	0.685924	65.20743	-0.00126
	#	0.735933	0.749246	101.809	-0.04118	0.58568	79.58334	-0.00757
	#	0.118977	0.425142	357.3304	-0.05408	0.17085	143.5986	0.000716

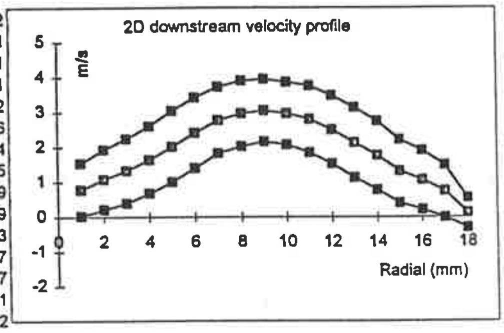

X	Y	U MEAN	U RMS	U TURBU	W MEAN	W RMS	W TURBU	uw
3D dow	1	1.154399	0.62274	53.94491	-0.0501	0.045075	3.904609	-0.00021
stream	2	1.243324	0.66614	53.57734	-0.07367	0.073746	5.93132	-0.00084
	3	1.419125	0.687844	48.4696	-0.05108	0.143171	10.08866	0.002715
	4	1.466036	0.690919	47.12838	-0.03037	0.452483	30.86439	0.001916
	5	1.629677	0.73485	45.09179	-0.01548	0.468801	28.76648	0.01534
	6	1.74474	0.742978	42.58388	-0.01914	0.500504	28.68644	0.017806
	7	1.841182	0.782673	42.50928	-0.0114	0.520486	28.26913	0.03799
	8	1.892763	0.772725	40.82525	-0.00865	0.529794	27.99048	0.039972
	9	1.903413	0.773832	40.65494	0.01369	0.532069	27.95339	0.035182
	#	1.928088	0.778892	40.39712	-0.03209	0.53951	27.98161	0.02935
	#	1.836995	0.769152	41.87013	-0.01349	0.546291	29.73831	0.028726
	#	1.713705	0.753457	43.96655	-0.01682	0.53272	31.08588	0.035512
	#	1.603677	0.744506	46.42492	-0.00718	0.537116	33.49278	0.037264
	#	1.505878	0.699219	46.43265	-0.00281	0.515201	34.21268	0.023668
	#	1.401053	0.662684	47.29897	-0.03129	0.524589	37.4425	0.02412
	#	1.256097	0.631916	50.30787	-0.04361	0.531476	42.31173	0.00511
	#	1.145353	0.601376	52.50567	-0.0331	0.330035	28.81515	0.000182
	#	0.896116	0.595621	66.4669	-0.02634	0.39383	43.94857	-6.1E-05

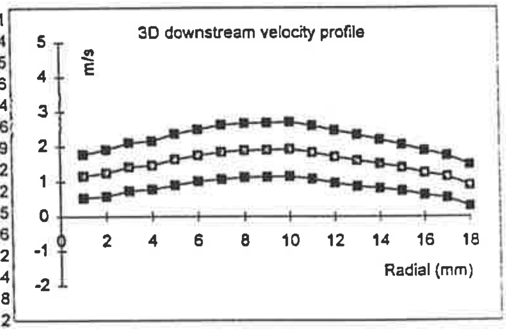

X	Y	U MEAN	U RMS	U TURBU	W MEAN	W RMS	W TURBU	uw
6D dow	1	1.339227	0.298554	22.29304	-0.03961	0.035944	2.683903	0.000488
stream	2	1.395997	0.291917	20.91099	-0.04356	0.02819	2.019378	0.000161
	3	1.408698	0.288616	20.48813	-0.05112	0.044085	3.129471	-0.00053
	4	1.400189	0.279073	19.9311	-0.0679	0.121466	8.674947	0.000521
	5	1.40302	0.279571	19.92641	-0.0512	0.193353	13.78117	0.002146
	6	1.404956	0.270937	19.2844	-0.02723	0.198834	14.15235	0.001865
	7	1.399481	0.273065	19.51187	-0.02726	0.203359	14.53106	0.003435
	8	1.409514	0.266054	18.8756	-0.0315	0.208161	14.76825	0.002547
	9	1.404895	0.266885	18.99679	-0.0276	0.208718	14.85646	0.002238
	#	1.395537	0.266132	19.07025	-0.02623	0.208155	14.91575	0.003706
	#	1.401556	0.263834	18.82437	-0.02681	0.211244	15.07211	0.003252
	#	1.403371	0.269241	19.18529	-0.02436	0.209682	14.94133	0.002682
	#	1.399716	0.277458	19.82249	-0.03053	0.217994	15.57414	0.002624
	#	1.397131	0.276199	19.76898	-0.06127	0.278189	19.91147	0.001555
	#	1.397268	0.280197	20.05322	-0.03748	0.115456	8.262999	-0.0008
	#	1.370979	0.283293	20.6636	-0.03825	0.475946	34.71576	-0.00259
	#	1.298648	0.290682	22.38347	-0.02745	0.436921	33.64429	-0.00311
	#	1.03457	0.39663	38.33772	-0.04138	0.231151	22.34276	-0.00354

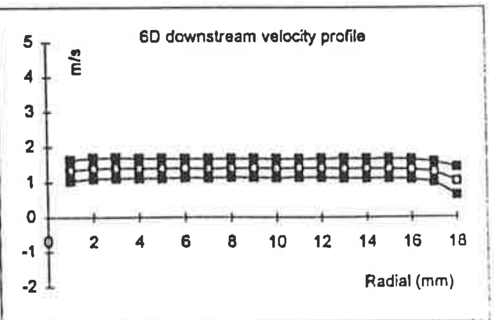

VELOCITY RAW DATA - CIRCULAR ORIFICE OF 13.5 mm DIAMETER

X	Y	U MEAN	U RMS	U TURBU	W MEAN	W RMS	W TURBU	uw
2D dow	1	0.297692	0.687126	230.8177	-0.07742	0.050929	17.10796	-0.0015
stream	2	0.222889	0.679445	304.8353	-0.03524	0.420986	188.8768	-0.04172
	3	0.90434	0.85619	94.67567	-0.04029	0.447415	49.47416	0.01276
	4	1.555504	0.901849	57.97795	-0.02834	0.475794	30.5878	0.037881
	5	2.300758	0.759232	32.9992	-0.03025	0.421773	18.3319	0.019319
	6	2.807866	0.472797	16.83831	-0.04572	0.306515	10.91629	0.024279
	7	2.965836	0.32523	10.96589	-0.05553	0.22799	7.687207	0.014975
	8	3.034035	0.201849	6.65281	-0.05958	0.167028	5.505147	0.008977
	9	3.019146	0.145435	4.817088	-0.05198	0.136163	4.509976	0.003059
	#	3.033321	0.145538	4.797977	-0.04626	0.134665	4.43952	0.003994
	#	2.989831	0.160471	5.367229	-0.04579	0.146109	4.886856	0.003265
	#	2.938085	0.261461	8.899014	-0.03416	0.208866	7.108912	0.006666
	#	2.730394	0.478915	17.54016	-0.02015	0.300063	10.98974	0.005995
	#	2.295371	0.735144	32.02726	-0.00813	0.429797	18.7245	0.008083
	#	1.702335	0.848835	49.86297	-0.00582	0.516657	30.34987	0.019492
	#	1.039513	0.819573	78.84196	-0.01845	0.549275	52.83963	0.015079
	#	0.445088	0.68521	153.9492	-0.04772	0.172261	38.70263	-0.00234
	#	0.136927	0.529912	387.004	-0.03754	0.085565	62.48985	-0.00066

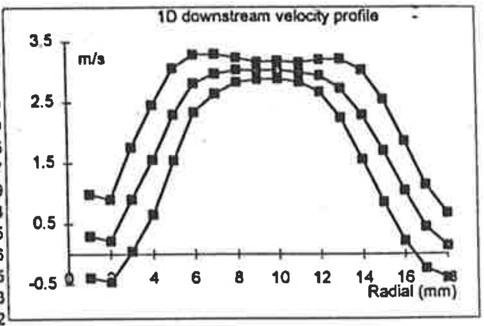

X	Y	U MEAN	U RMS	U TURBU	W MEAN	W RMS	W TURBU	uw
3D dow	1	0.852119	0.555334	65.17099	-0.03775	0.026424	3.100967	0.000599
stream	2	1.04212	0.593636	56.96423	-0.07947	0.106364	10.20646	0.003776
	3	1.237756	0.642624	51.9185	-0.06433	0.271845	21.96273	0.000749
	4	1.399811	0.678699	48.48505	-0.00996	0.411099	29.36815	0.014691
	5	1.687158	0.71038	42.10514	-0.00905	0.420992	24.9527	0.021808
	6	2.00187	0.689398	34.43771	-0.01429	0.422492	21.10488	0.044494
	7	2.176584	0.672531	30.89848	-0.02172	0.386002	17.73429	0.044606
	8							
	9	2.474344	0.519071	20.97815	-0.02071	0.335059	13.54135	0.045033
	#	2.477691	0.506385	20.43779	-0.02275	0.338262	13.65229	0.042235
	#	2.387913	0.546415	22.88256	-0.01619	0.372448	15.59723	0.035297
	#	2.239061	0.574925	25.67708	-0.01422	0.377754	16.87108	0.026344
	#	2.010169	0.634941	31.58643	-0.00557	0.423777	21.08164	0.02101
	#	1.736445	0.665629	38.33287	0.000971	0.446823	25.73203	0.009554
	#	1.478713	0.651782	44.07766	-0.00582	0.467262	31.59921	0.021327
	#	1.209618	0.601483	49.72503	-0.06759	0.303803	25.11565	0.006027
	#	0.96443	0.54324	56.32758	-0.03093	0.029351	3.043343	0.000634
	#	0.126918	0.330499	260.4025	-0.0282	0.025674	20.22873	-0.001

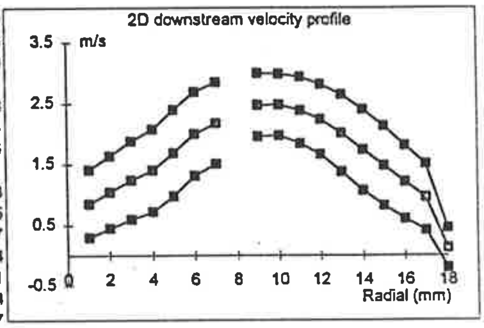

X	Y	U MEAN	U RMS	U TURBU	W MEAN	W RMS	W TURBU	uw
3D dow	1	1.114755	0.45515	40.82962	-0.05369	0.04425	3.96952	0.000481
stream	2	1.193177	0.452057	37.88688	-0.10741	0.280803	23.53402	0.012577
	3	1.369679	0.515384	37.62806	-0.05645	0.221206	16.15018	-0.0045
	4	1.425127	0.519776	36.47224	-0.03275	0.337175	23.65931	0.016463
	5	1.527902	0.551142	36.07184	-0.02048	0.349155	22.8519	0.017567
	6	1.661226	0.551574	33.20285	-0.01534	0.359265	21.62651	0.021285
	7	1.763419	0.555888	31.52331	-0.02382	0.370499	21.01028	0.025212
	8	1.831076	0.55865	30.50939	-0.03155	0.364798	19.92261	0.032814
	9	1.859679	0.55188	29.67608	-0.01974	0.365229	19.63938	0.026482
	#	1.878312	0.55225	29.40141	-0.02783	0.364631	19.41268	0.031653
	#	1.857561	0.54626	29.40739	-0.0128	0.369502	19.8918	0.02353
	#	1.740471	0.537638	30.89035	-0.00299	0.374601	21.52296	0.021747
	#	1.664761	0.537418	32.28197	-0.01482	0.373465	22.43356	0.018065
	#	1.528387	0.524263	34.30172	-0.0051	0.369331	24.16474	0.013809
	#	1.417954	0.494407	34.86764	-0.01937	0.368819	26.01065	0.012529
	#	1.303751	0.474378	36.38565	-0.04028	0.078323	6.007523	0.000023
	#	1.157805	0.446048	38.5253	-0.02908	0.025366	2.190846	-5.2E-05
	#	0.936707	0.470943	50.27642	-0.03885	0.058619	6.257971	-0.00021

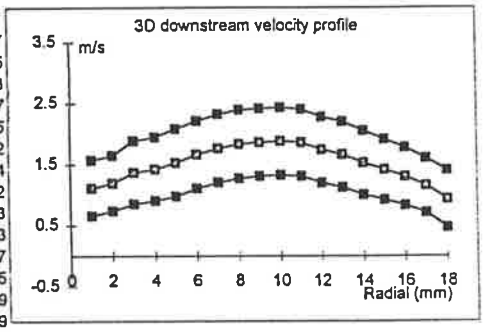

X	Y	U MEAN	U RMS	U TURBU	W MEAN	W RMS	W TURBU	uw
6D dow	1	1.332445	0.261011	19.5889	-0.02489	0.01028	0.771517	0.000038
stream	2	1.39418	0.257544	18.47283	-0.02458	0.009482	0.680093	-2.8E-05
	3	1.397197	0.253545	18.14669	-0.03865	0.033081	2.367651	-7.4E-05
	4	1.413767	0.260088	18.39681	-0.07338	0.137329	9.713692	0.000701
	5	1.420317	0.250875	17.66329	-0.05551	0.166342	11.71158	0.000711
	6	1.42405	0.251405	17.65422	-0.0365	0.178604	12.54199	0.002314
	7	1.428457	0.243158	17.02243	-0.03429	0.183861	12.87128	0.00403
	8	1.437462	0.24534	17.0676	-0.03083	0.18558	12.91029	0.004534
	9	1.437124	0.242065	16.84373	-0.03439	0.18614	12.95225	0.004347
	#	1.439605	0.242773	16.86389	-0.02516	0.188504	13.09411	0.003148
	#	1.445763	0.249691	17.27051	-0.03048	0.179794	12.43596	0.003835
	#	1.425164	0.24921	17.48638	-0.03182	0.183874	12.90196	0.003538
	#	1.428999	0.250303	17.51593	-0.04308	0.167753	11.73917	0.002977
	#	1.412157	0.254285	18.00682	-0.04396	0.08909	6.308759	-2.4E-05
	#	1.401327	0.257783	18.39564	-0.03818	0.091874	6.556178	-0.00035
	#	1.360885	0.254263	18.68361	-0.04191	0.061071	4.487625	-7E-06
	#	1.282141	0.274007	21.37103	-0.03773	0.047811	3.728969	-0.0003
	#	1.04609	0.359151	34.33269	-0.03771	0.046095	4.406389	-0.0013

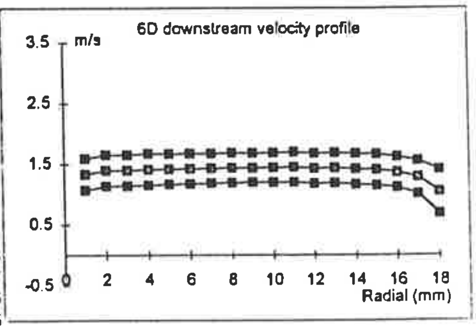

SHEAR STRESS AND TURBULENCE INTENSITY IN 13.5 mm DIAMETER CIRCULAR ORIFICE

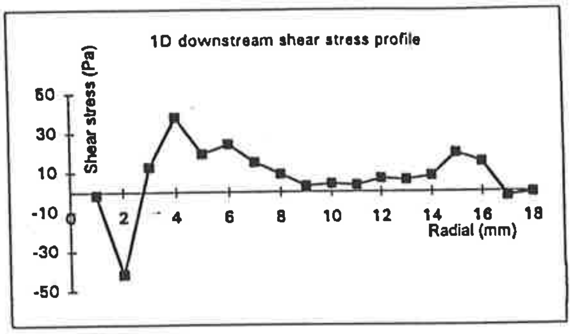

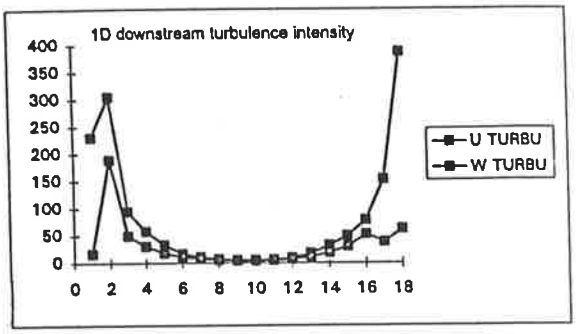

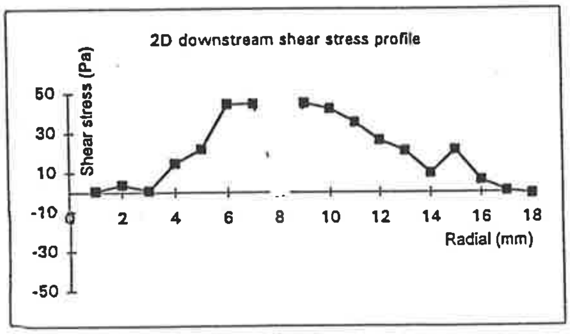

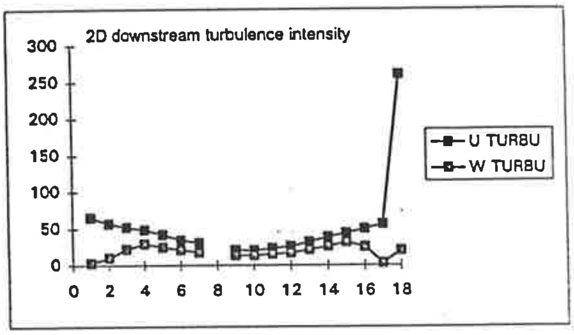

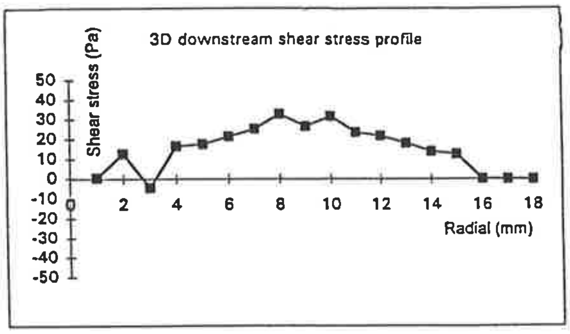

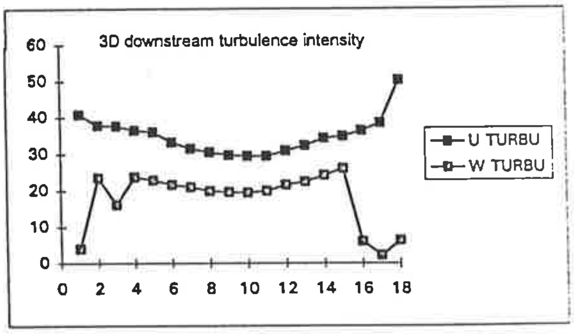

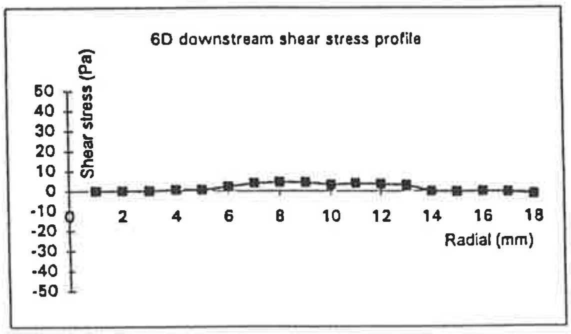

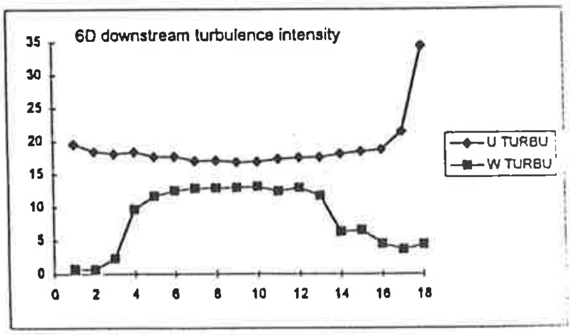

VELOCITY RAW DATA - CIRCULAR ORIFICE OF 15 mm DIAMETER

X	Y	U MEAN	U RMS	U TURBU	W MEAN	W RMS	W TURBU	uw
1D dow	1	0.606987	0.439205	72.35811	-0.10186	0.08033	13.23415	0.003348
stream	2	0.632885	0.505216	79.82752	-0.05337	0.236224	37.32489	0.001741
	3	1.156432	0.528492	45.70021	-0.05499	0.270141	23.35984	0.010413
	4	1.615792	0.48551	30.0478	-0.04751	0.26287	16.26882	0.005117
	5	1.964946	0.330204	16.80474	-0.05148	0.193239	9.834335	0.006318
	6	2.165293	0.167571	7.738947	-0.04382	0.126079	5.822742	0.001658
	7	2.224977	0.097417	4.378346	-0.03672	0.079945	3.593053	0.000253
	8	2.262867	0.072115	3.186893	-0.03702	0.0603	2.664773	0.000495
	9	2.24809	0.060684	2.699365	-0.03562	0.051699	2.299678	0.000403
	#	2.263469	0.066535	2.939533	-0.03208	0.050837	2.245999	0.000497
	#	2.259519	0.065896	2.916362	-0.03031	0.052588	2.327407	0.000608
	#	2.254193	0.090798	4.027977	-0.02937	0.06556	2.90834	0.000829
	#	2.17641	0.119405	5.486336	-0.02713	0.089733	4.12298	0.001901
	#	2.083574	0.261358	12.54374	-0.02456	0.160319	7.694433	0.004741
	#	1.74331	0.434626	24.93106	-0.01349	0.258929	14.85273	0.000388
	#	1.286924	0.517585	40.21877	-0.01648	0.32203	25.02321	-0.00262
	#	0.820318	0.458445	55.88634	-0.03775	0.064173	7.822996	-0.00028
	#	0.489944	0.359905	73.45825	-0.02982	0.036298	7.408535	-1.1E-05

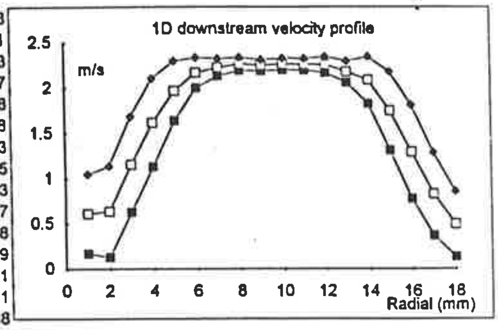

X	Y	U MEAN	U RMS	U TURBU	W MEAN	W RMS	W TURBU	uw
2D dow	1	0.959641	0.351425	36.62049	-0.07878	0.065157	6.789707	0.000212
stream	2	1.156079	0.377547	32.65754	-0.08772	0.091117	7.881538	0.001627
	3	1.285762	0.398731	31.01124	-0.05483	0.220735	17.16761	0.00668
	4	1.459622	0.400085	27.41019	-0.0463	0.350741	24.02959	0.007219
	5	1.701172	0.382258	22.4703	-0.0273	0.258439	15.19182	0.006404
	6	1.904786	0.316182	16.59936	-0.03842	0.199298	10.46303	0.008607
	7	2.054157	0.232953	11.34055	-0.03674	0.155117	7.551385	0.006717
	8	2.135	0.166475	7.797431	-0.03297	0.121141	5.674029	0.003082
	9	2.166457	0.121429	5.60498	-0.03066	0.09851	4.547053	0.002004
	#	2.168515	0.110493	5.095335	-0.03475	0.094548	4.360031	0.002551
	#	2.149406	0.133834	6.226565	-0.03098	0.108554	5.050399	0.004014
	#	2.084266	0.187216	8.982334	-0.03059	0.135997	6.524956	0.004251
	#	1.963134	0.269871	13.74694	-0.03224	0.172842	8.804376	0.004435
	#	1.783992	0.340801	19.10329	-0.01645	0.225562	12.64366	0.002003
	#	1.51683	0.372818	24.57874	-0.02438	0.262408	17.29976	0.000936
	#	1.278152	0.372129	29.11465	-0.0644	0.273471	21.39582	-0.00365
	#	1.071314	0.33619	31.38112	-0.03383	0.036376	3.395466	-0.00091
	#	-0.00336	0.127825	3803.617	-0.02333	0.006683	198.8658	-0.00013

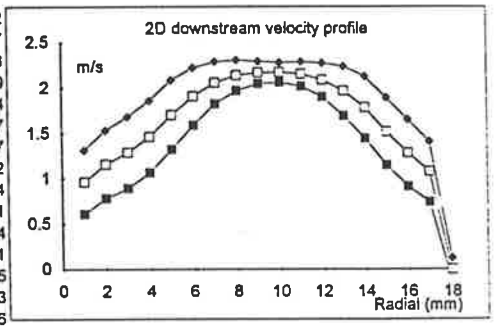

X	Y	U MEAN	U RMS	U TURBU	W MEAN	W RMS	W TURBU	uw
3D dow	1	1.116815	0.259228	23.21134	-0.08513	0.111156	9.952918	-0.00028
stream	2	1.107792	0.311759	28.14235	-0.09241	0.2186	19.73296	0.009479
	3	1.352636	0.329298	24.34489	-0.08824	0.125958	9.312043	0.000855
	4	1.425292	0.333616	23.40684	-0.03909	0.238391	16.72574	0.00417
	5	1.565285	0.347404	22.1943	-0.03432	0.218461	13.95664	0.003646
	6	1.718116	0.342351	19.92597	-0.03033	0.209069	12.16848	0.007469
	7	1.861927	0.309172	16.60494	-0.02745	0.186586	10.02112	0.006837
	8	1.980042	0.253757	12.81574	-0.03016	0.164377	8.301703	0.008578
	9	2.032799	0.219554	10.80058	-0.0304	0.151798	7.467415	0.007769
	#	2.034285	0.211297	10.3868	-0.02898	0.147658	7.258496	0.006614
	#	1.99734	0.22998	11.51434	-0.02536	0.159057	7.963435	0.00593
	#	1.914975	0.262098	13.68677	-0.02659	0.179106	9.352928	0.005814
	#	1.78958	0.294072	16.43244	-0.02149	0.199987	11.17508	0.00457
	#	1.633932	0.310062	18.97641	-0.02622	0.217957	13.33944	0.003652
	#	1.466362	0.31359	21.38556	-0.03026	0.22818	15.56093	0.001532
	#	1.313599	0.303354	23.09337	-0.03889	0.092392	7.033496	-0.0016
	#	1.161708	0.282829	24.34595	-0.03126	0.057752	4.971293	-0.0006
	#	0.928583	0.333925	35.96066	-0.02963	0.027139	2.922626	-0.00037

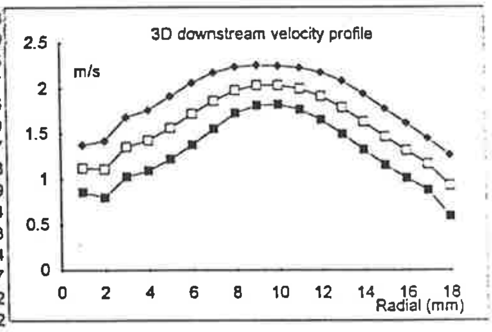

X	Y	U MEAN	U RMS	U TURBU	W MEAN	W RMS	W TURBU	uw
6D dow	1	1.269033	0.218661	17.23052	-0.03739	0.037125	2.925458	-4.3E-05
stream	2	1.340943	0.21711	16.19084	-0.02764	0.015563	1.160621	-1.2E-05
	3	1.403731	0.222404	15.84374	-0.04927	0.038834	2.766483	0.000011
	4	1.456457	0.236739	16.25445	-0.09025	0.097246	6.676888	-7.9E-05
	5	1.494171	0.234494	15.6939	-0.05487	0.140936	9.432365	0.000828
	6	1.547063	0.236945	15.31577	-0.03667	0.155926	10.07884	0.002625
	7	1.604215	0.232135	14.47029	-0.02797	0.16072	10.0186	0.002742
	8	1.645824	0.233678	14.19825	-0.0309	0.160255	9.737057	0.002979
	9	1.658058	0.224244	13.52451	-0.02657	0.159895	9.643504	0.003712
	#	1.653957	0.226489	13.69374	-0.02954	0.16326	9.870864	0.004152
	#	1.640307	0.228443	13.92682	-0.02774	0.163195	9.949047	0.002925
	#	1.602871	0.230215	14.36268	-0.02644	0.162831	10.1587	0.00291
	#	1.548475	0.230643	14.89483	-0.03737	0.144104	9.306196	0.001651
	#	1.492079	0.223434	14.97467	-0.0493	0.095331	6.38911	-0.00102
	#	1.424171	0.222335	15.61156	-0.02861	0.032149	2.257414	-0.00035
	#	1.359105	0.220959	16.25768	-0.03987	0.063282	4.656116	-0.00092
	#	1.240474	0.22379	18.04067	-0.03407	0.046276	3.730516	-0.00102
	#	0.986104	0.337198	34.19436	-0.03708	0.048654	4.934005	-0.00133

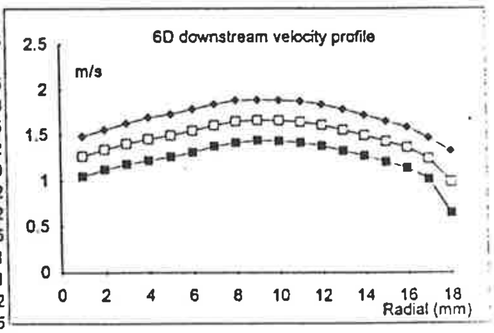

SHEAR STRESS AND TURBULENCE INTENSITY IN 15 mm DIAMETER CIRCULAR ORIFICE

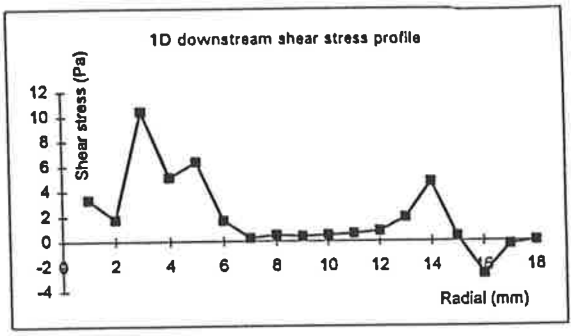

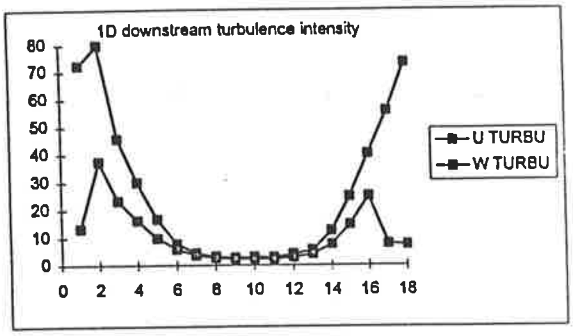

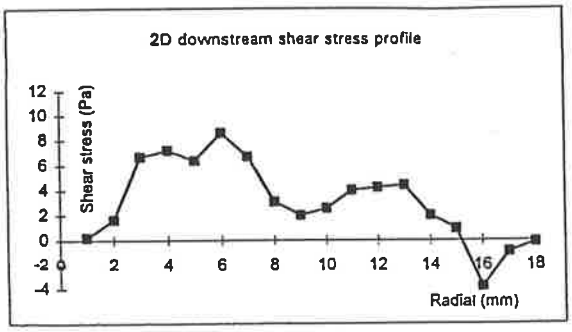

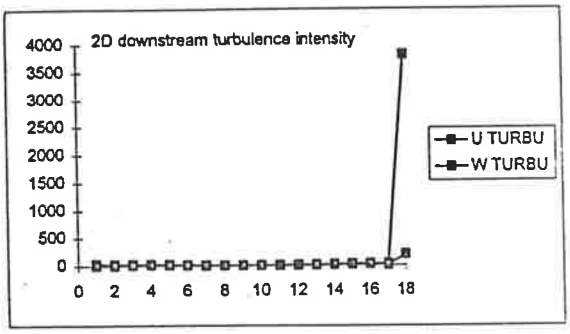

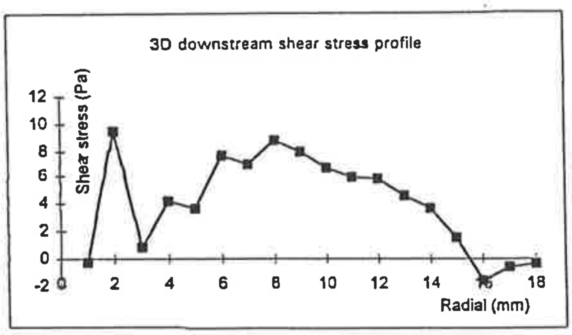

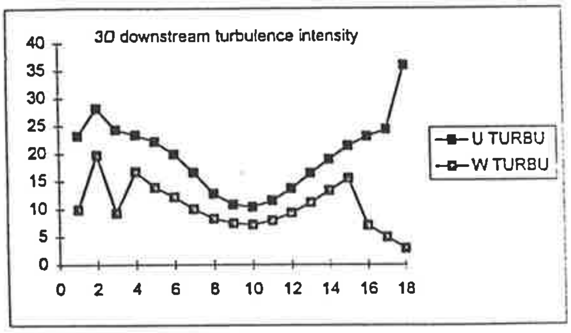

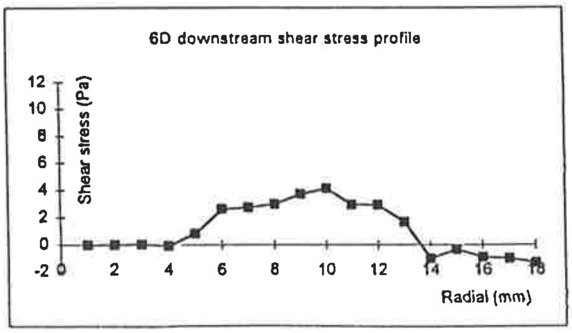

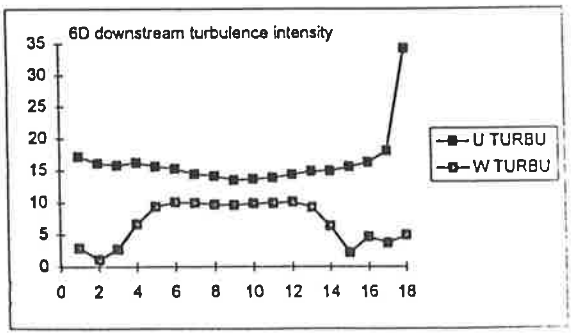

VELOCITY RAW DATA - CIRCULAR ORIFICE OF 16.5 mm DIAMETER

X	Y	U MEAN	U RMS	U TURBU	W MEAN	W RMS	W TURBU	uw
1D dow	1	1.014955	0.304551	30.00634	-0.04398	0.024832	2.446587	0.00043
stream	2	1.308494	0.288139	22.02064	-0.08452	0.075021	5.733361	0.000111
	3	1.178835	0.362348	30.73782	-0.07857	0.101572	8.616302	-0.00168
	4	1.616685	0.147093	9.098419	-0.06273	0.108909	6.736536	-0.00083
	5	1.712538	0.104328	6.092023	-0.04542	0.075394	4.402457	-0.00018
	6	1.792765	0.081176	4.527984	-0.03549	0.059538	3.321012	0.000005
	7	1.833545	0.069887	3.811598	-0.03443	0.047843	2.609329	-9.8E-05
	8	1.858722	0.049353	2.6552	-0.03303	0.042686	2.296538	-0.00016
	9	1.846044	0.045949	2.489059	-0.03133	0.040148	2.17481	-0.00017
	#	1.838017	0.05125	2.788357	-0.02853	0.041106	2.236411	-0.00017
	#	1.836378	0.058069	3.162172	-0.0254	0.045482	2.476727	-0.00012
	#	1.827975	0.069432	3.798311	-0.02501	0.05427	2.968868	0.000089
	#	1.779808	0.078698	4.421718	-0.02592	0.060101	3.376804	0.000247
	#	1.728356	0.105961	6.130759	-0.02335	0.072744	4.20887	0.000432
	#	1.600438	0.164487	10.27761	-0.02234	0.104093	6.50401	-0.00017
	#	1.38792	0.255832	18.43278	-0.06944	0.201416	14.5121	-0.00567
	#	0.893341	0.323207	36.17956	-0.02769	0.028425	3.181834	-0.00017
	#	0.715125	0.290052	40.55961	-0.03356	0.054626	7.638645	-0.00087

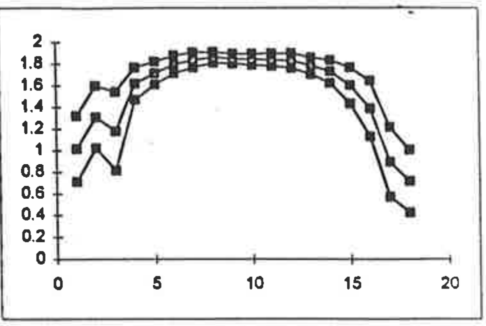

X	Y	U MEAN	U RMS	U TURBU	W MEAN	W RMS	W TURBU	uw
2D dow	1	1.104665	0.225033	20.37116	-0.05179	0.043711	3.956952	0.00002
stream	2	1.283605	0.223524	17.41373	-0.07	0.058518	4.5589	0.000233
	3	1.39371	0.228034	16.36168	-0.06674	0.122623	8.79833	-0.00034
	4	1.548065	0.18492	11.94522	-0.04559	0.122428	7.908426	0.000549
	5	1.672126	0.118209	7.069368	-0.04417	0.08937	5.344721	0.000506
	6	1.74957	0.085786	4.903255	-0.03897	0.066334	3.791463	-4.8E-05
	7	1.799925	0.061835	3.4354	-0.03737	0.05238	2.910095	0.000089
	8	1.827673	0.045112	2.468291	-0.03332	0.043285	2.368286	0.000147
	9	1.838135	0.040653	2.211626	-0.03315	0.041049	2.233206	0.000189
	#	1.834596	0.04408	2.402707	-0.03407	0.041538	2.264157	0.000192
	#	1.819967	0.053244	2.925568	-0.03175	0.045108	2.478497	0.000331
	#	1.796628	0.066842	3.720401	-0.04193	0.057068	3.17639	0.000493
	#	1.747889	0.092361	5.284146	-0.04068	0.071098	4.067629	0.000576
	#	1.656495	0.146541	8.846444	-0.03544	0.089814	5.421916	0.000199
	#	1.481193	0.215184	14.52777	-0.04366	0.141753	9.570169	-0.00021
	#	1.288596	0.2315	17.9653	-0.03983	0.063551	4.931775	-0.00182
	#	1.09061	0.224701	20.60325	-0.03578	0.045123	4.137391	-0.00138
	#	0.234114	0.378319	161.5962	-0.02568	0.016237	6.935346	-0.00099

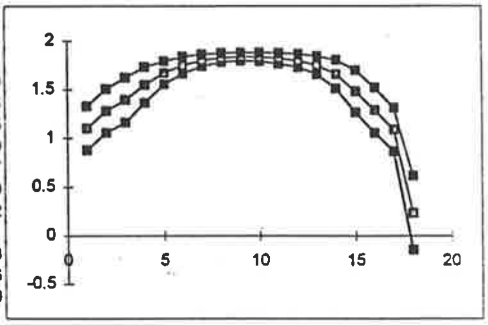

X	Y	U MEAN	U RMS	U TURBU	W MEAN	W RMS	W TURBU	uw
3D dow	1	1.085412	0.184197	16.97028	-0.04696	0.031803	2.930037	0.00006
stream	2	1.230763	0.196796	15.98976	-0.08034	0.074321	6.038631	-0.00038
	3	1.372481	0.192401	14.01849	-0.07208	0.111044	8.090714	-4E-06
	4	1.468785	0.181409	12.35094	-0.05785	0.128021	8.716125	0.000501
	5	1.620304	0.144071	8.89161	-0.03888	0.101879	6.28764	0.000173
	6	1.715512	0.100296	5.846417	-0.03923	0.07587ᵅ	4.423129	0.000256
	7	1.782563	0.071145	3.99114	-0.03576	0.055959	3.139228	0.000094
	8	1.820416	0.051303	2.818229	-0.03334	0.046179	2.536743	0.000109
	9	1.832737	0.045152	2.463616	-0.03195	0.042885	2.33997	0.000245
	#	1.828735	0.049652	2.715078	-0.02956	0.043188	2.361642	0.000273
	#	1.808581	0.06095	3.370066	-0.03016	0.049718	2.749026	0.000399
	#	1.768115	0.080904	4.575733	-0.03237	0.061751	3.492493	0.000661
	#	1.701077	0.121053	7.116273	-0.02949	0.080608	4.738616	0.000684
	#	1.591248	0.161539	10.15174	-0.03086	0.10118	6.358557	0.000284
	#	1.432914	0.187371	13.07624	-0.05622	0.131662	9.188412	-0.00194
	#	1.278724	0.193963	15.16845	-0.03214	0.039399	3.081095	-0.00071
	#	1.12359	0.20436	18.18812	-0.0377	0.03807	3.38824	-0.00087
	#	0.867035	0.288904	33.32093	-0.03414	0.03644	4.20284	-0.00074

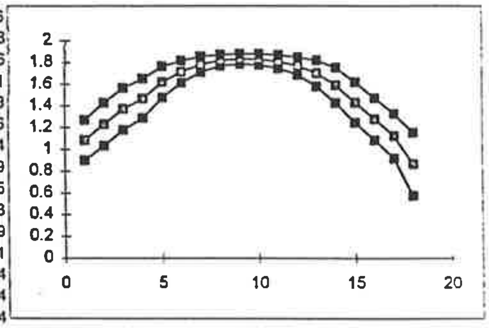

X	Y	U MEAN	U RMS	U TURBU	W MEAN	W RMS	W TURBU	uw
6D dow	1	1.160911	0.167795	14.4537	-0.0277	0.018508	1.594244	-1.4E-05
stream	2	1.265735	0.161532	12.76188	-0.03211	0.019908	1.572866	-4.3E-05
	3	1.37512	0.158902	11.5555	-0.03427	0.033228	2.416345	-3.1E-05
	4	1.442678	0.170587	11.82436	-0.07474	0.11761	8.152199	-0.00069
	5	1.551907	0.149229	9.615848	-0.07671	0.087187	5.618052	-0.0004
	6	1.622941	0.132814	8.183551	-0.03773	0.0916	5.644055	0.000134
	7	1.699648	0.114031	6.709109	-0.03743	0.078321	4.608079	0.000369
	8	1.762942	0.084954	4.818883	-0.0331	0.064802	3.675772	0.000405
	9	1.781055	0.074751	4.197003	-0.03153	0.062142	3.489038	0.000691
	#	1.766336	0.082425	4.666449	-0.03465	0.063003	3.566874	0.000888
	#	1.73476	0.098932	5.702919	-0.03003	0.074328	4.284656	0.000697
	#	1.667178	0.122018	7.318813	-0.03218	0.086502	5.188506	0.00099
	#	1.586719	0.139188	8.77209	-0.04358	0.120387	7.587162	0.000164
	#	1.489552	0.152371	10.22935	-0.0513	0.085099	5.71304	-0.0013
	#	1.381368	0.162328	11.75126	-0.04131	0.092966	6.730021	-0.00148
	#	1.274338	0.164473	12.90658	-0.03105	0.03858	3.027442	-0.0004
	#	1.136644	0.184051	16.19254	-0.02872	0.028959	2.547784	-0.00039
	#	0.874458	0.308282	35.25404	-0.03095	0.0384	4.391313	-0.00075

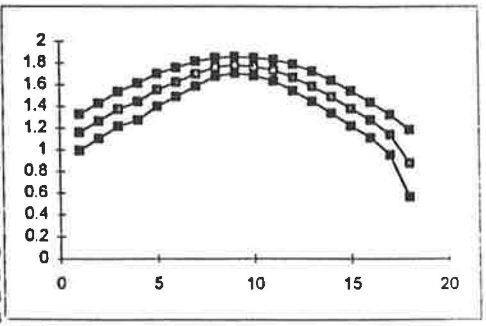

SHEAR STRESS AND TURBULENCE INTENSITY IN 16.5 mm DIAMETER CIRCULAR ORIFICE

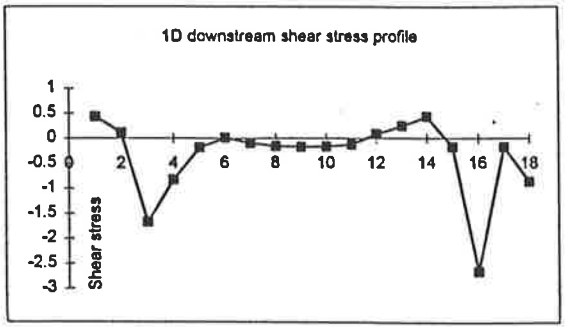

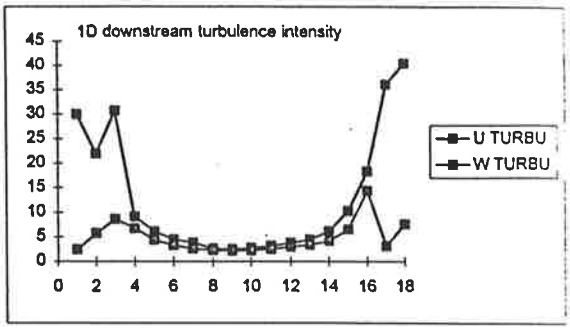

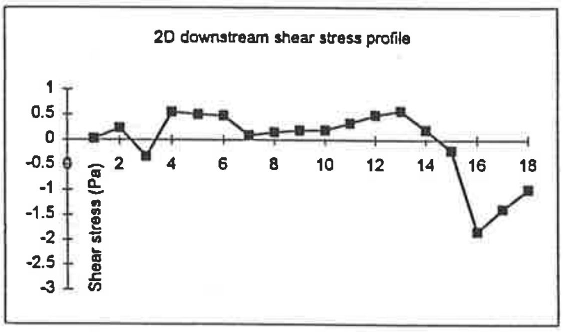

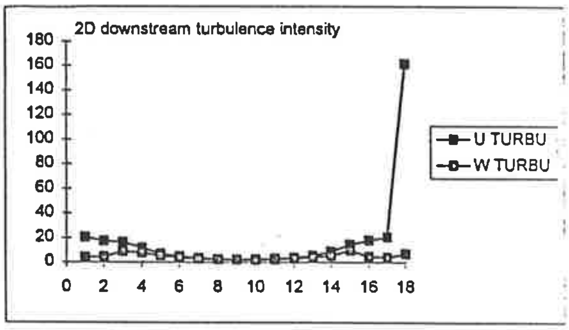

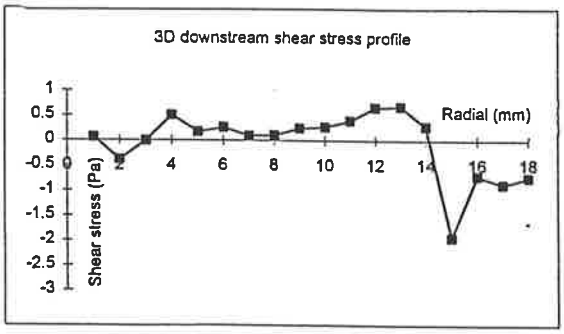

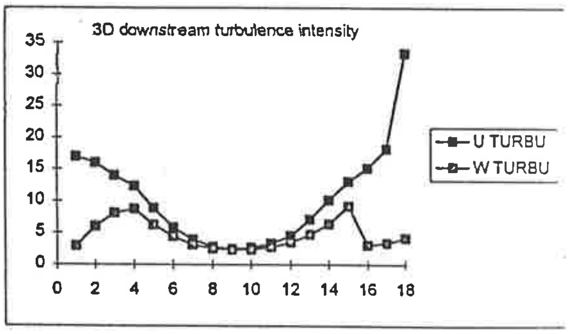

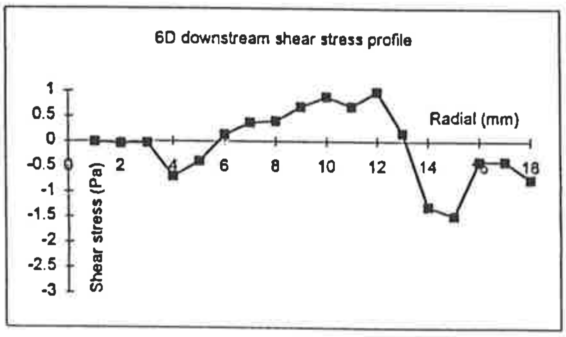

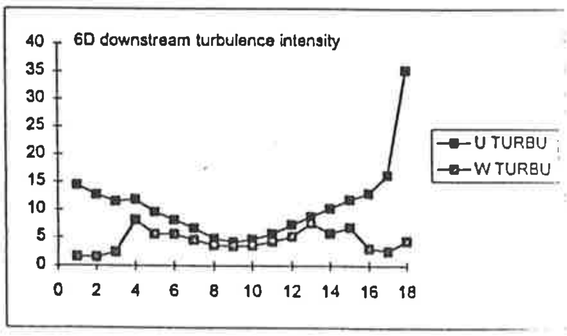

A. 4.3. Velocity data across different shape orifices

VELOCITY RAW DATA - CIRCULAR ORIFICE OF 12 mm DIAMETER

X	Y	U MEAN	U RMS	U TURBU	W MEAN	W RMS	W TURBU	uw
1D dow	1	0.065174	0.865056	1327.307	-0.0742	0.05475	84.00691	-0.00035
stream	2	0.451859	1.034646	228.9757	-0.08	0.285375	63.15591	0.004366
	3	0.800294	1.127128	140.8394	-0.06471	0.615945	76.96485	0.002166
	4	1.759705	1.216632	69.13841	-0.03647	0.691238	39.28146	0.04194
	5	2.912282	1.055412	36.24003	-0.02471	0.611353	20.99223	0.035297
	6	3.669674	0.778022	21.20138	-0.02057	0.471493	12.84835	0.021206
	7	4.045124	0.424892	10.50382	-0.03128	0.309146	7.642447	0.009844
	8	4.147513	0.246327	5.939159	-0.03011	0.226354	5.457594	0.007219
	9	4.137476	0.207638	5.018468	-0.0349	0.205632	4.969977	0.005227
	#	4.142973	0.266048	6.421673	-0.02911	0.2261	5.457431	0.011644
	#	4.067698	0.422201	10.37937	-0.01706	0.295479	7.264046	0.014635
	#	3.760401	0.737019	19.59947	-0.00751	0.459324	12.21477	0.022356
	#	3.245793	0.962489	29.65342	-0.01392	0.598717	18.44593	0.05072
	#	2.325441	1.23114	52.94223	-0.01265	0.738686	31.76544	0.034697
	#	1.352009	1.194837	88.37492	-0.01237	0.804595	59.51107	0.058477
	#	0.627879	1.026442	163.4776	-0.03783	0.65403	104.1649	0.013737
	#	-0.06285	0.84705	1347.732	-0.04156	0.416355	662.4578	0.006395
	#	-0.37313	0.682653	182.9523	-0.04233	0.200505	53.73573	-0.00295

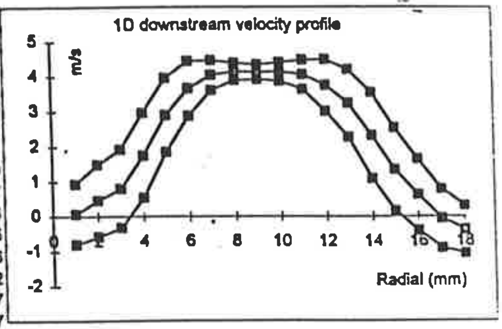

X	Y	U MEAN	U RMS	U TURBU	W MEAN	W RMS	W TURBU	uw
2D dow	1	0.781545	0.758719	97.07938	-0.0363	0.027605	3.532083	0.000772
stream	2	1.069632	0.86188	80.57721	-0.07285	0.081235	7.594623	0.002701
	3	1.315811	0.926247	70.39361	-0.04358	0.359918	27.35335	0.01061
	4	1.637462	0.962712	58.79295	-0.02426	0.590971	36.09068	0.011241
	5	2.018151	1.020618	50.57193	-0.01305	0.631258	31.27903	0.04242
	6	2.409187	1.014144	42.09487	-0.00703	0.6043	25.08316	0.049006
	7	2.777305	0.951034	34.24307	0.012031	0.586413	21.11447	0.059474
	8	2.963384	0.936531	31.60345	-0.01875	0.568999	19.201	0.056595
	9	3.047834	0.8927	29.28964	-0.01532	0.561535	18.42406	0.059919
	#	2.965726	0.892849	30.10558	-0.00759	0.555099	18.71715	0.053309
	#	2.799488	0.953341	34.05413	-0.02236	0.607955	21.71664	0.070803
	#	2.499126	0.97745	39.11166	-0.01642	0.662593	26.513	0.083237
	#	2.126452	1.010866	47.53769	-0.01791	0.679543	31.95664	0.049727
	#	1.75557	0.989027	56.33651	-0.0259	0.673938	38.38855	0.023661
	#	1.308765	0.908242	69.39689	-0.02759	0.696105	53.18797	0.035872
	#	1.051912	0.846146	80.43885	-0.03653	0.685924	65.20743	-0.00126
	#	0.735933	0.749246	101.809	-0.04118	0.58568	79.58334	-0.00757
	#	0.118977	0.425142	357.3304	-0.05408	0.17085	143.5986	0.000716

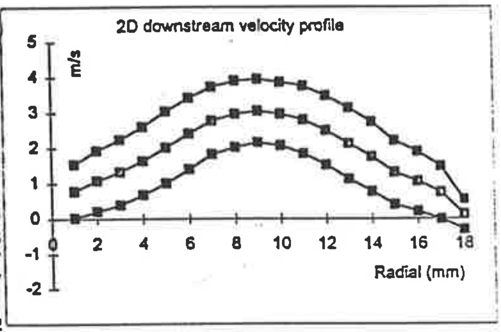

X	Y	U MEAN	U RMS	U TURBU	W MEAN	W RMS	W TURBU	uw
3D dow	1	1.154399	0.62274	53.94491	-0.0501	0.045075	3.904609	-0.00021
stream	2	1.243324	0.66614	53.57734	-0.07367	0.073746	5.93132	-0.00084
	3	1.419125	0.687844	48.4696	-0.05108	0.143171	10.08866	0.002715
	4	1.466036	0.690919	47.12838	-0.03037	0.452483	30.86439	0.001916
	5	1.629677	0.73485	45.09179	-0.01548	0.468801	28.76648	0.01534
	6	1.74474	0.742978	42.58388	-0.01914	0.500504	28.68644	0.017806
	7	1.841182	0.782673	42.50928	-0.0114	0.520486	28.26913	0.03799
	8	1.892763	0.772725	40.82525	-0.00865	0.529794	27.99048	0.039972
	9	1.903413	0.773832	40.65494	0.01369	0.532069	27.95339	0.035182
	#	1.928088	0.778892	40.39712	-0.03209	0.53951	27.98161	0.02935
	#	1.836995	0.769152	41.87013	-0.01349	0.546291	29.73831	0.028726
	#	1.713705	0.753457	43.96655	-0.01682	0.53272	31.08588	0.035512
	#	1.603677	0.744506	46.42492	-0.00718	0.537116	33.49278	0.037264
	#	1.505878	0.699219	46.43255	-0.00281	0.515201	34.21268	0.023668
	#	1.401053	0.662684	47.29897	-0.03129	0.524589	37.4425	0.02412
	#	1.256097	0.631916	50.30787	-0.04361	0.531476	42.31173	0.00511
	#	1.145353	0.601376	52.50567	-0.0331	0.330035	28.81515	0.000182
	#	0.896116	0.595621	66.4669	-0.02634	0.39383	43.94857	-6.1E-05

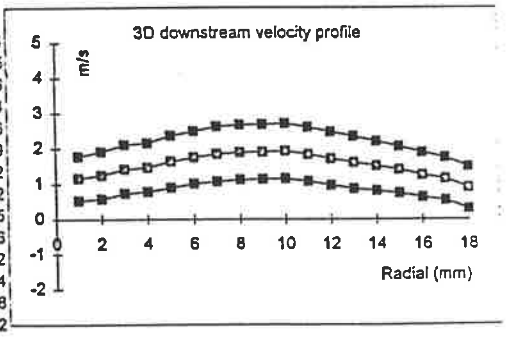

X	Y	U MEAN	U RMS	U TURBU	W MEAN	W RMS	W TURBU	uw
6D dow	1	1.339227	0.298554	22.29304	-0.03961	0.035944	2.683903	0.000488
stream	2	1.395997	0.291917	20.91099	-0.04356	0.02819	2.019378	0.000161
	3	1.408698	0.288616	20.48813	-0.05112	0.044085	3.129471	-0.00053
	4	1.400189	0.279073	19.9311	-0.0679	0.121466	8.674947	0.000521
	5	1.40302	0.279571	19.92641	-0.0512	0.193353	13.78117	0.002146
	6	1.404956	0.270937	19.2844	-0.02723	0.198834	14.15235	0.001865
	7	1.399481	0.273065	19.51187	-0.02726	0.203359	14.53106	0.003435
	8	1.409514	0.266054	18.8756	-0.0315	0.208161	14.76825	0.002547
	9	1.404895	0.266885	18.99679	-0.0276	0.208718	14.85646	0.002238
	#	1.395537	0.266132	19.07025	-0.02623	0.208155	14.91575	0.003706
	#	1.401556	0.263834	18.82437	-0.02681	0.211244	15.07211	0.003252
	#	1.403371	0.269241	19.18529	-0.02436	0.209682	14.94133	0.002682
	#	1.399716	0.277458	19.82249	-0.03053	0.217994	15.57414	0.002624
	#	1.397131	0.276199	19.76898	-0.06127	0.278189	19.91147	0.001555
	#	1.397268	0.280197	20.05322	-0.03748	0.115456	8.262999	-0.0008
	#	1.370979	0.283293	20.6636	-0.03826	0.475946	34.71576	-0.00259
	#	1.298648	0.290682	22.38347	-0.02745	0.436921	33.64429	-0.00311
	#	1.03457	0.39663	38.33772	-0.04138	0.231151	22.34276	-0.00354

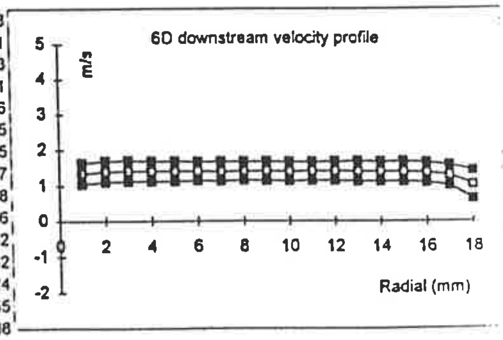

SHEAR STRESS AND TURBULENCE INTENSITY IN 12 mm CIRCULAR ORIFICE

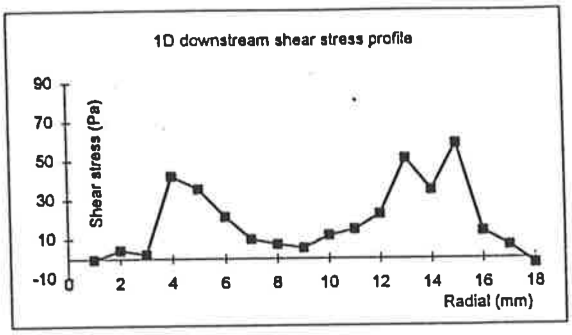

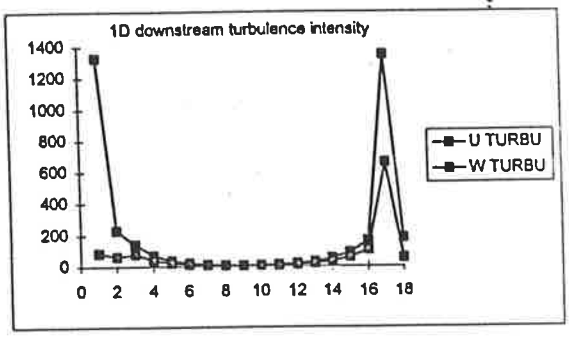

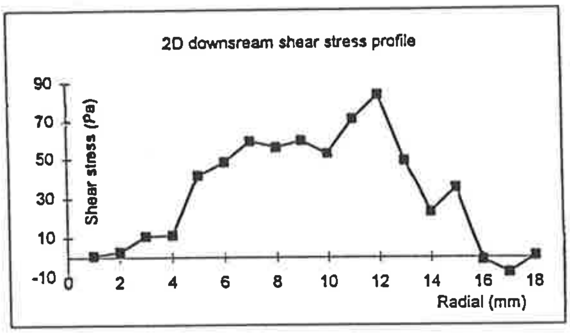

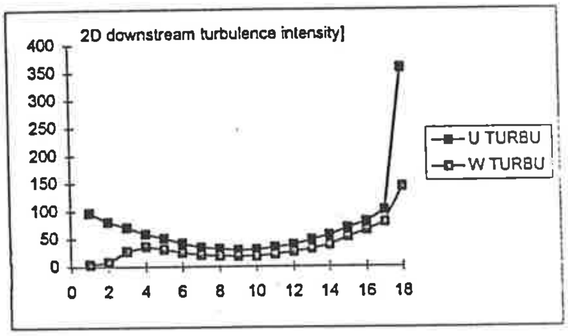

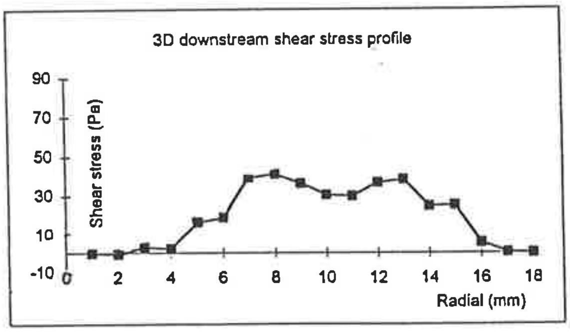

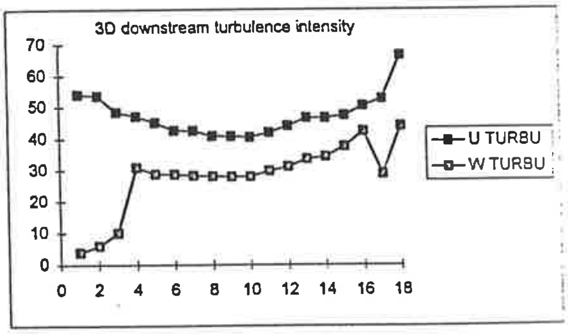

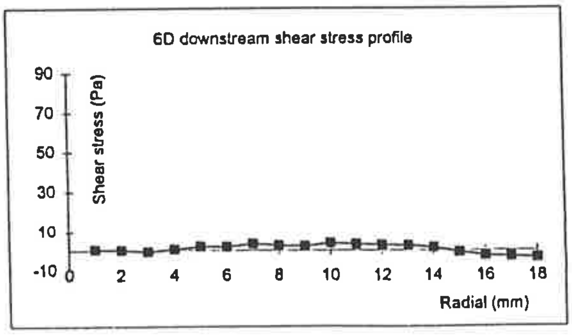

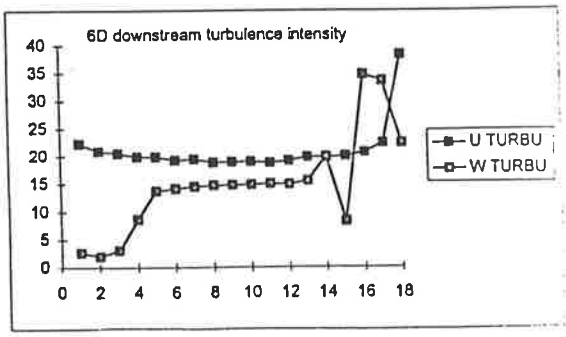

VELOCITY RAW DATA - CONCENTRIC ANNULAR ORIFICE

X	D	U MEAN	U RMS	U TURBU	W MEAN	W RMS	W TURBU	uw
1D dow	1	-0.17763	0.546149	307.4663	-0.09059	0.062871	35.3948	-0.0018
stream	2	-0.09713	0.540223	556.1886	-0.03758	0.066871	68.84695	-0.00066
	3	-0.04198	0.58049	1382.839	-0.02329	0.123628	294.5047	-0.0054
	4	0.162122	0.593131	365.8553	-0.04155	0.413768	255.2205	-0.01104
	5	0.261599	0.59163	226.1597	-0.05407	0.531864	203.3129	-0.03875
	6	0.366684	0.594241	162.0581	-0.16807	0.547002	149.1753	-0.07313
	7	0.34888	0.61817	177.1871	-0.25244	0.591151	169.4424	-0.09918
	8	0.344105	0.653481	189.9075	-0.35448	0.618844	179.8416	-0.13521
	9	0.242036	0.66919	276.4838	-0.3792	0.649657	268.4132	-0.15509
	10	0.107388	0.650112	605.3869	-0.34475	0.648602	603.9808	-0.14986
	11	0.018675	0.640627	3430.429	-0.28789	0.620767	3324.08	-0.11728
	12	-0.15028	0.582681	387.7362	-0.08574	0.606888	403.8445	-0.07168
	13	-0.285	0.535999	188.0683	0.057775	0.564718	198.1451	-0.03566
	14	-0.34829	0.529583	152.054	0.127928	0.523177	150.2148	0.00592
	15	-0.47239	0.461189	97.62959	0.106085	0.487478	103.1948	0.028103
	16	-0.57648	0.454433	78.82864	0.010319	0.466895	80.9903	0.018806
	17	-0.69858	0.427639	61.2156	-0.00558	0.403158	57.71122	0.007521
	18	-0.76574	0.376761	49.20232	-0.01289	0.379178	49.51797	0.006417

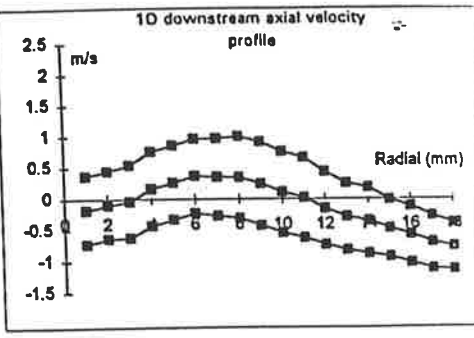

X	D	U MEAN	U RMS	U TURBU	W MEAN	W RMS	W TURBU	uw
2D dow	1	0.767004	0.434286	56.6211	-0.03393	0.020754	2.705893	0.000226
stream	2	0.984557	0.491491	49.91997	-0.0618	0.17474	17.74812	-0.00377
	3	1.110798	0.460273	41.4362	-0.05297	0.273397	24.6127	-0.00526
	4	1.23115	0.476792	38.72736	-0.06463	0.387508	31.47532	-0.00865
	5	1.302208	0.493839	37.9232	-0.07159	0.395379	30.36219	-0.01628
	6	1.339574	0.464899	34.70498	-0.06886	0.430128	32.1093	-0.01529
	7	1.355769	0.475957	35.10607	-0.09906	0.44107	32.53282	-0.01922
	8	1.373024	0.498839	36.33138	-0.1285	0.468518	34.12306	-0.03382
	9	1.375118	0.513429	37.33709	-0.19123	0.475335	34.56682	-0.05494
	10	1.324226	0.509163	38.44986	-0.19235	0.475851	35.93427	-0.0484
	11	1.230585	0.508396	41.31335	-0.15347	0.48343	39.28461	-0.05331
	12	1.151675	0.498095	43.24963	-0.13668	0.480676	41.73715	-0.043
	13	1.013941	0.493018	48.6239	-0.08096	0.479898	47.33003	-0.03261
	14	0.873253	0.478996	54.85193	-0.04499	0.453271	51.90606	-0.01273
	15	0.755036	0.442605	58.62034	0.01608	0.423506	56.09078	-0.00621
	16	0.671017	0.440519	65.64941	0.00365	0.423998	63.18735	-0.02088
	17	0.503887	0.420591	83.46922	0.038498	0.386643	76.73208	-0.01634
	18	0.320521	0.376816	117.5638	0.034621	0.347594	108.4465	-0.00401

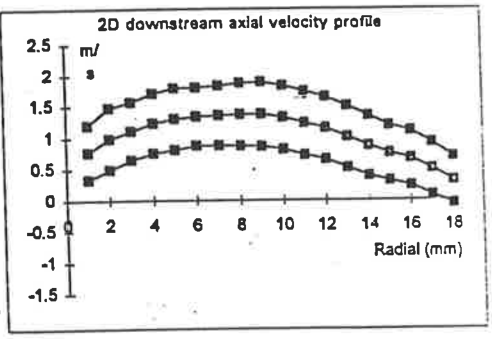

X	D	U MEAN	U RMS	U TURBU	W MEAN	W RMS	W TURBU	uw
3d dow	1	1.249469	0.343047	27.45546	-0.03236	0.023056	1.845259	0.000025
stream	2	1.394569	0.348369	24.98042	-0.07054	0.056668	4.063463	0.000084
	3	1.493036	0.351012	23.50999	-0.06516	0.16751	11.21945	-0.00101
	4	1.534344	0.345613	22.52511	-0.05529	0.325243	21.19753	0.003914
	5	1.595483	0.35619	22.32492	-0.04467	0.304988	19.11568	0.00459
	6	1.625086	0.357262	21.98422	-0.04309	0.314255	19.33777	0.007302
	7	1.647529	0.362067	21.97635	-0.0297	0.327251	19.86316	0.007306
	8	1.624733	0.362906	22.33637	-0.02594	0.335276	20.63579	0.006759
	9	1.616379	0.369165	22.83902	-0.01335	0.338343	20.93215	0.012111
	10	1.575047	0.374009	23.74587	-0.01385	0.33892	21.51811	0.012747
	11	1.517144	0.372804	24.57274	-0.04006	0.335874	22.13855	0.006358
	12	1.412861	0.378315	26.77651	-0.03215	0.322852	22.85093	0.009453
	13	1.328987	0.373373	28.09457	-0.03101	0.32452	24.41863	0.004007
	14	1.243705	0.350955	28.21854	-0.02164	0.309703	24.90168	0.005808
	15	1.125674	0.330762	29.3835	-0.01139	0.285928	25.40058	0.003384
	16	1.029047	0.323426	31.42967	0.008788	0.289035	28.08762	0.004943
	17	0.892751	0.321426	36.00394	0.010754	0.287804	32.23788	0.007151
	18	0.717136	0.336754	46.95821	-0.00539	0.263926	36.80275	0.010675

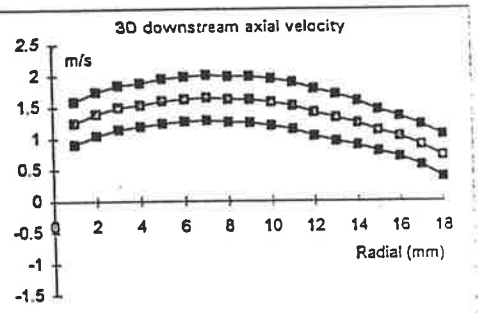

X	D	U MEAN	U RMS	U TURBU	W MEAN	W RMS	W TURBU	uw
6d dow	1	1.315779	0.375651	28.54969	-0.06188	0.106081	8.062188	-0.00188
stream	2	1.460953	0.23221	15.8944	-0.02506	0.011948	0.817829	0.000064
	3	1.505798	0.221799	14.72965	-0.02557	0.012684	0.842313	-4.8E-05
	4	1.554886	0.217279	13.97392	-0.03056	0.023961	1.541004	0.000183
	5	1.577778	0.213265	13.51677	-0.0602	0.078713	4.988876	0.000846
	6	1.585026	0.217338	13.71195	-0.02149	0.178691	11.27368	0.006739
	7	1.585368	0.214699	13.54256	-0.01201	0.162891	10.27467	0.006571
	8	1.601495	0.223912	13.98141	-0.00732	0.168492	10.52094	0.007907
	9	1.583866	0.215288	13.59254	-0.00882	0.167504	10.57567	0.004704
	10	1.567906	0.216068	13.78068	-0.01154	0.164249	10.47569	0.006207
	11	1.558798	0.216924	13.91611	-0.00648	0.172331	11.05541	0.005371
	12	1.518536	0.221563	14.59057	-0.00552	0.17143	11.28915	0.00608
	13	1.484591	0.216342	14.57252	-0.0072	0.169219	11.39836	0.003392
	14	1.430946	0.21839	15.26191	-0.0231	0.168879	11.8019	0.004337
	15	1.391134	0.213224	15.32735	-0.0352	0.170003	12.22045	0.004224
	16	1.33046	0.213487	16.04612	-0.07076	0.317	23.82636	-0.00395
	17	1.191884	0.241224	20.23889	-0.0537	0.222926	18.70365	-0.00433
	18	0.99099	0.312128	31.49656	-0.0547	0.155167	15.65776	-0.00253

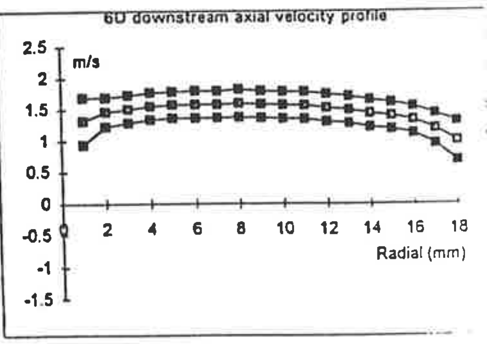

SHEAR STRESS AND TURBULENCE INTENSITY IN IN A CONCENTRIC ANNULAR ORIFICE

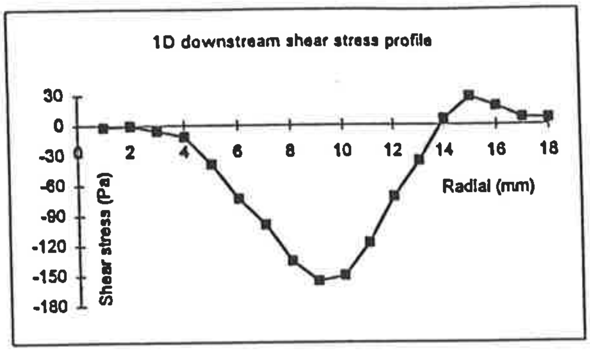

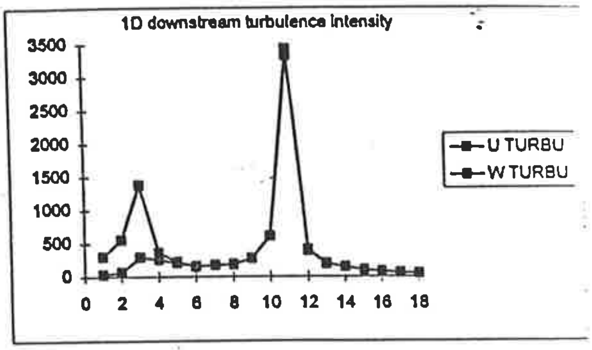

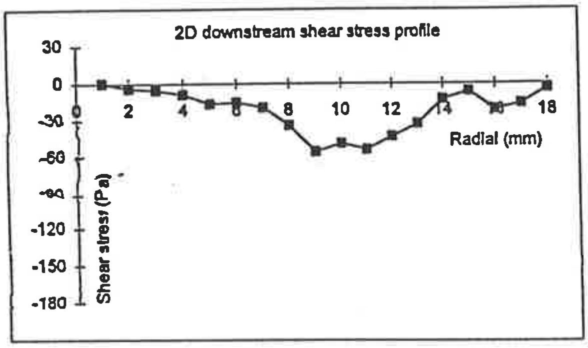

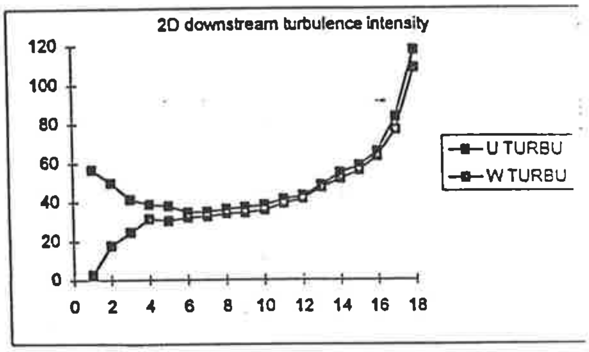

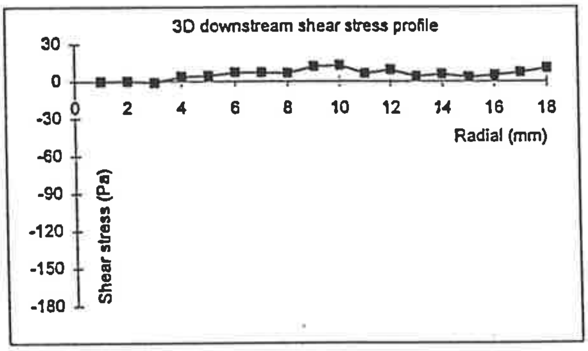

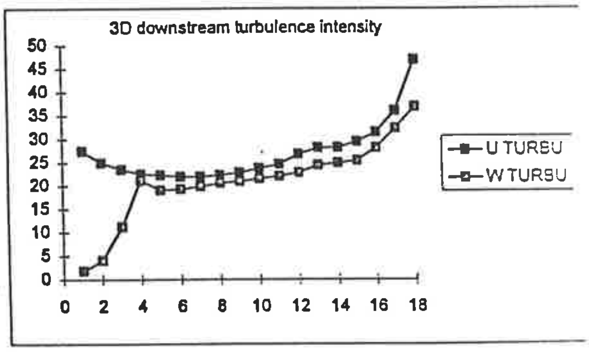

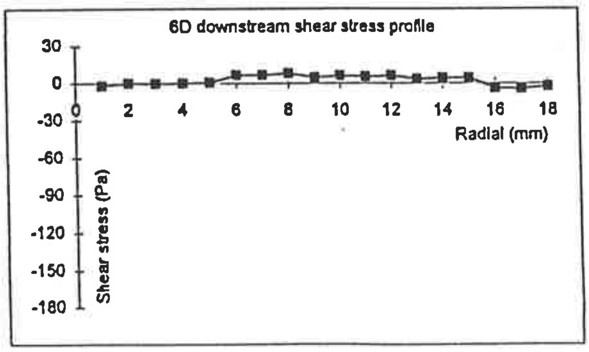

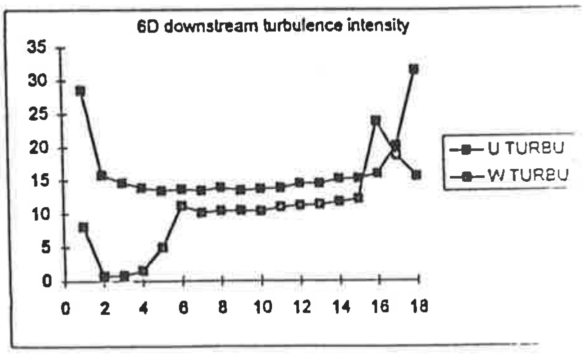

VELOCITY RAW DATA - SQUARE ORIFICE

X	Y	U MEAN	U RMS	U TURBU	W MEAN	W RMS	W TURBU	uw
1D dow	1	0.365251	1.337668	366.2323	-0.05307	0.028232	7.729434	0.001792
stream	2	0.851543	1.446191	169.8318	-0.08229	0.085442	10.03378	0.008218
	3	1.459511	1.514451	103.7642	-0.05348	0.393522	26.96259	0.029561
	4	1.819679	1.521691	83.62414	-0.03021	0.755332	41.50907	0.129703
	5	2.753826	1.45254	52.74624	-0.03226	0.780144	28.32947	0.118283
	6	3.579524	1.174673	32.81647	-0.04642	0.70369	19.65876	0.115673
	7	4.018399	0.994429	24.7469	-0.04667	0.572283	14.24157	0.054142
	8	4.378886	0.650566	14.85688	-0.05821	0.420856	9.611026	0.065172
	9	4.443493	0.464131	10.44518	-0.04071	0.370502	8.338082	0.040829
	#	4.381822	0.517896	11.81918	-0.03011	0.378864	8.646271	0.036056
	#	4.248428	0.684481	16.11139	-0.0184	0.460975	10.85048	0.040179
	#	3.9318	0.98727	25.10988	-0.01617	0.595147	15.13675	0.060767
	#	3.452192	1.162061	33.66155	0.008276	0.734141	21.26593	0.058403
	#	2.640971	1.407836	53.3075	0.01328	0.844023	31.95883	0.049948
	#	2.027383	1.453127	71.675	0.02756	0.83114	40.99572	0.074594
	#	1.195236	1.442376	120.6771	-0.01078	0.656527	54.92864	0.017916
	#	0.50687	1.347521	265.8515	-0.04681	0.332061	65.512	0.008538
	#	0.108247	1.113673	1028.821	-0.03673	0.342994	316.8613	-0.00158

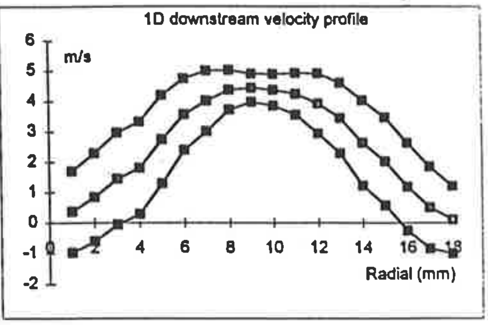

X	Y	U MEAN	U RMS	U TURBU	W MEAN	W RMS	W TURBU	uw
2D dow	1	0.830173	0.872962	105.1543	-0.04409	0.026048	3.137711	0.001152
stream	2	1.078822	0.949268	87.99119	-0.0615	0.044497	4.124635	0.001118
	3	1.198652	0.956579	79.80463	-0.10136	0.46657	38.92459	0.010401
	4	1.444188	1.044528	72.32631	-0.0498	0.581421	40.25938	0.049576
	5	1.811416	1.069132	59.02188	0.002118	0.667515	36.85047	0.047378
	6	2.178123	1.100563	50.52807	-0.01463	0.684154	31.41027	0.063847
	7	2.487885	1.129937	45.41756	-0.00648	0.663145	26.65498	0.058831
	8	2.684524	1.083398	40.35717	-0.04196	0.67928	25.30356	0.077884
	9	2.858805	1.091493	38.18003	-0.00276	0.676023	23.64704	0.073726
	#	2.80333	1.091514	38.93631	-0.01648	0.678618	24.20757	0.07688
	#	2.660919	1.066819	40.09211	-0.01458	0.698328	26.24387	0.057467
	#	2.381687	1.101728	46.25831	0.005209	0.717716	30.13478	0.063144
	#	2.095978	1.055337	50.35056	0.000266	0.745208	35.5542	-0.00136
	#	1.740997	1.051907	60.4198	-0.01941	0.706334	40.57064	0.024906
	#	1.501176	0.997523	66.44946	-0.05222	0.637787	42.48581	0.00387
	#	1.170227	0.95829	81.88921	-0.05981	0.466885	39.89695	0.011097
	#	0.911532	0.884118	96.99255	-0.06928	0.316233	34.69244	0.006919
	#	0.613448	0.787433	128.3619	-0.04737	0.305527	49.80497	0.000885

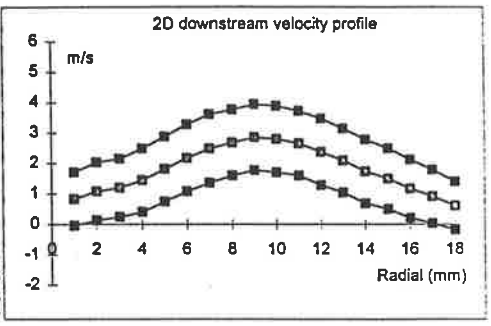

X	Y	U MEAN	U RMS	U TURBU	W MEAN	W RMS	W TURBU	uw
3D dow	1	1.149719	0.590951	51.39958	-0.05056	0.032402	2.818238	0.000346
stream	2	1.218987	0.642569	52.72155	-0.08986	0.09382	7.696561	0.002753
	3	1.302936	0.60491	46.42667	-0.05617	0.375701	28.83496	-0.00324
	4	1.425738	0.655626	45.98505	-0.03123	0.407043	28.54962	0.000635
	5	1.488361	0.695266	46.71351	-0.01823	0.455104	30.57752	0.033555
	6	1.533287	0.696332	45.41433	-0.01821	0.482746	31.48436	0.011788
	7	1.76982	0.754756	42.64592	-0.01296	0.507299	28.66387	0.029144
	8	1.788341	0.734412	41.06667	-0.01872	0.501421	28.03833	0.022092
	9	1.821466	0.737971	40.51523	-0.0256	0.520626	28.58279	0.031327
	#	1.8071	0.745154	41.23482	-0.01706	0.516674	28.59133	0.025102
	#	1.762205	0.744167	42.22929	-0.00061	0.515826	29.27161	0.027827
	#	1.670611	0.719209	43.05064	-0.00974	0.512372	30.66971	0.023347
	#	1.597438	0.708024	44.32248	-0.00824	0.511077	31.99356	0.019715
	#	1.509562	0.670696	44.42987	-0.00996	0.489543	32.42946	0.012912
	#	1.401626	0.663161	47.31369	-0.05551	0.424623	30.29506	0.013755
	#	1.294139	0.645935	49.91234	-0.06683	0.30517	23.58094	0.003332
	#	1.191447	0.596328	50.05071	-0.01963	0.662465	55.6017	-0.00324
	#	0.959874	0.590174	61.48455	-0.0406	0.351018	36.56918	-0.00167

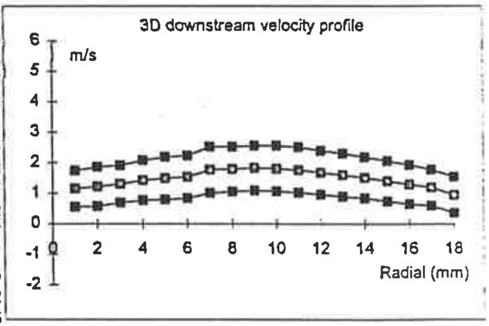

X	Y	U MEAN	U RMS	U TURBU	W MEAN	W RMS	W TURBU	uw
6D dow	1	1.329602	0.293744	22.09261	-0.03311	0.026402	1.985715	0.00002
stream	2	1.385313	0.27983	20.19979	-0.03596	0.022323	1.611436	0.000182
	3	1.394897	0.272813	19.55792	-0.03696	0.02718	1.948509	0.000065
	4	1.397978	0.272963	19.52553	-0.08207	0.107303	7.675611	0.001229
	5	1.404898	0.266437	18.96485	-0.0474	0.175747	12.5096	0.001469
	6	1.4106	0.263119	18.65295	-0.03198	0.197166	13.97745	0.004741
	7	1.401354	0.254889	18.18876	-0.0312	0.198086	14.1353	0.003307
	8	1.411688	0.255564	18.10341	-0.03002	0.194477	13.7762	0.00285
	9	1.410519	0.253025	17.93846	-0.02828	0.201058	14.25416	0.002243
	#	1.40768	0.246965	17.54415	-0.02189	0.201471	14.31228	0.001871
	#	1.417901	0.253953	17.91046	-0.02645	0.202904	14.31019	0.002111
	#	1.414833	0.260716	18.42731	-0.02797	0.199726	14.11655	0.002724
	#	1.414901	0.269026	19.01376	-0.04072	0.233282	16.4875	0.003195
	#	1.406119	0.271698	19.32257	-0.06073	0.238349	16.95082	0.000471
	#	1.403454	0.280929	20.01697	-0.04548	0.355154	25.30573	-0.00249
	#	1.384207	0.280711	20.27954	-0.05011	0.380747	27.50648	-0.00436
	#	1.293133	0.292734	22.63761	-0.04805	0.22976	17.76771	-0.00292
	#	1.031008	0.370316	35.91787	-0.05738	0.363781	35.28399	-0.00939

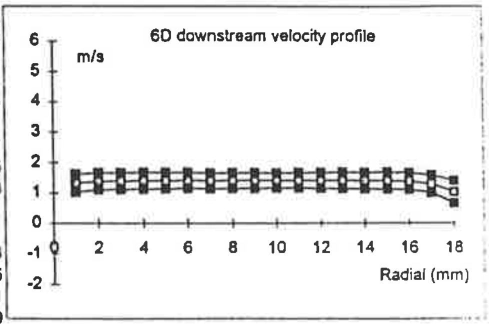

SHEAR STRESS AND TURBULENCE INTENSITY IN SQUARE ORIFICE

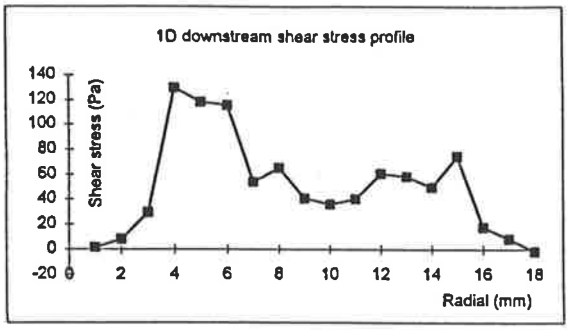

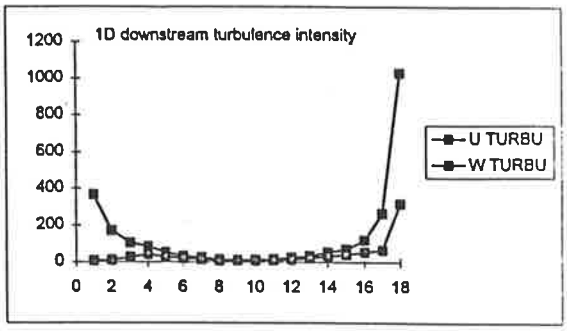

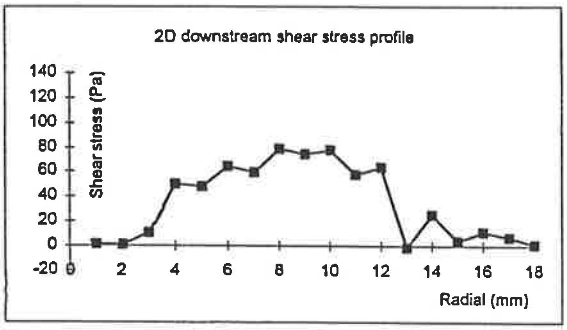

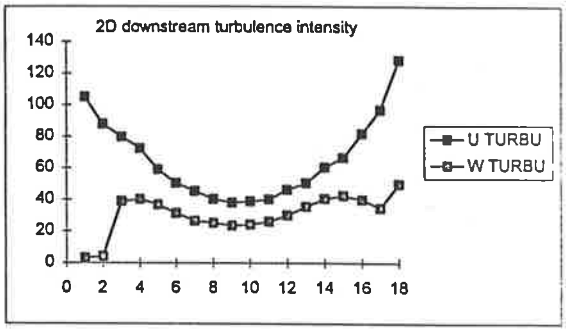

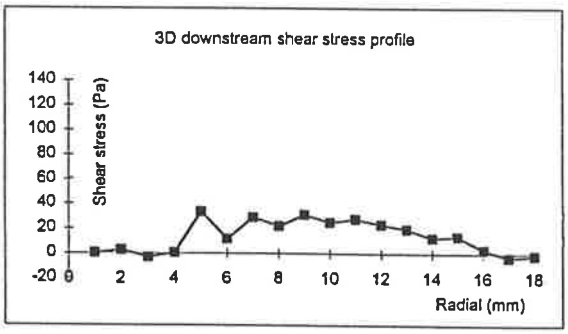

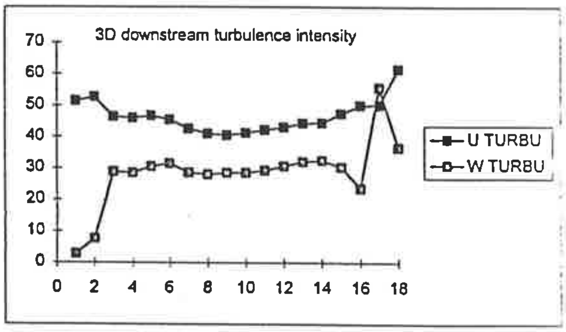

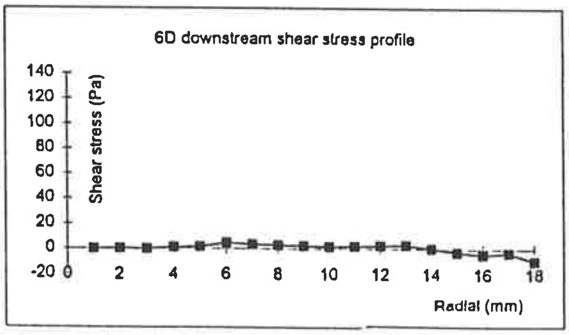

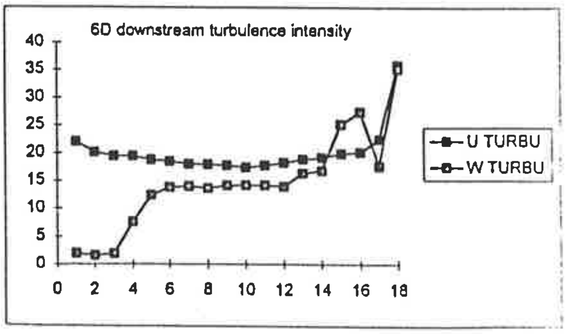

VELOCITY RAW DATA - TRIANGULAR ORIFICE

X	Y	U MEAN	U RMS	U TURBU	W MEAN	W RMS	W TURBU	uw
1D dow	1	-0.06228	1.002639	1610	-0.10132	0.067993	109.1806	-0.00017
stream	2	0.096251	1.125677	1169.518	-0.14166	0.391262	406.5004	-0.00605
	3	0.278572	1.184481	425.198	-0.02235	0.595298	213.6968	0.022956
	4	0.930075	1.423577	153.0604	0.001312	0.720337	77.44933	0.120119
	5	1.979212	1.587737	80.22067	0.057512	0.740763	37.42718	0.143676
	6	2.885513	1.549527	53.70025	0.056835	0.715679	24.80248	0.178332
	7	3.764141	1.267783	33.68053	0.069626	0.590647	15.69141	0.168695
	8	3.982409	1.175266	29.51143	-0.01062	0.582642	14.63039	0.21706
	9	4.019941	1.066858	26.53915	-0.03288	0.598732	14.89405	0.201673
	#	3.829597	1.211748	31.64165	-0.0797	0.677708	17.69659	0.230745
	#	3.480422	1.333369	38.31057	-0.05546	0.737515	21.1904	0.147442
	#	3.09602	1.564003	50.51658	-0.0262	0.789445	25.49871	0.040264
	#	2.45844	1.896333	77.13562	0.014885	0.863419	35.12059	-0.0124
	#	2.097462	1.945677	92.7634	0.001216	0.885685	42.22649	0.061586
	#	2.122377	1.818477	85.68115	-0.04662	0.843179	39.72804	0.160313
	#	0.982522	1.898805	193.2584	0.020925	0.827983	84.27119	0.077466
	#	1.17137	1.956977	167.0674	-0.00595	0.495865	42.33202	0.042081
	#	0.582331	1.866804	320.5744	-0.03464	0.288404	49.52585	0.043803

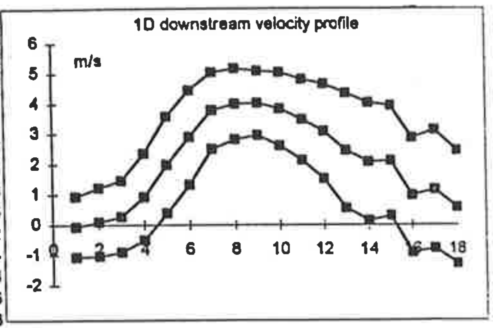

X	Y	U MEAN	U RMS	U TURBU	W MEAN	W RMS	W TURBU	uw
2D dow	1	0.840502	0.958929	114.0901	-0.07721	0.048564	5.77801	0.000777
stream	2	1.166748	1.029153	88.20699	-0.10984	0.322026	27.60026	-0.01695
	3	1.069727	1.00269	93.7332	-0.07189	0.40293	37.66665	-0.00645
	4	1.314133	1.081651	82.30911	0.012831	0.629514	47.90337	0.006395
	5	1.637085	1.133782	69.25616	0.027239	0.667831	40.79394	0.045733
	6	1.852916	1.174714	63.39815	0.029519	0.683361	36.8803	0.074186
	7	2.155118	1.210636	56.17492	0.040515	0.708138	32.85844	0.133337
	8	2.351941	1.168612	49.68714	0.023781	0.699024	29.72117	0.107164
	9	2.34126	1.177384	50.28848	0.043257	0.72352	30.90302	0.102196
	#	2.310003	1.179714	51.06982	0.050887	0.73471	31.80557	0.110108
	#	2.168725	1.183053	54.55061	0.054209	0.762982	35.18113	0.103056
	#	1.954625	1.201088	61.44852	0.02224	0.74352	38.03903	0.100095
	#	1.839948	1.246458	67.74422	0.07122	0.740353	40.23773	0.103286
	#	1.588408	1.290656	81.25465	0.014343	0.723748	45.56435	0.111271
	#	[illegible]	1.279657	77.05609	0.058338	0.69667	41.95079	0.126926
	#	1.431964	1.368106	95.5405	-0.01568	0.64104	44.76646	0.106842
	#	1.457599	1.419304	97.37268	-0.04263	0.423388	29.04691	0.040188
	#	0.967913	1.260619	130.241	-0.03933	0.378781	39.13379	0.018155

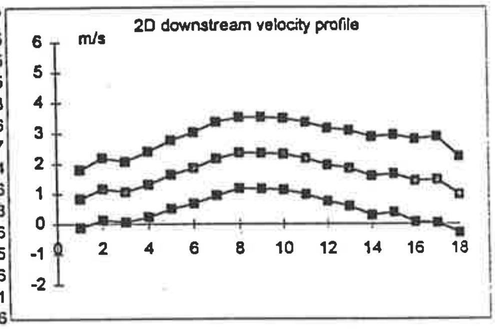

X	Y	U MEAN	U RMS	U TURBU	W MEAN	W RMS	W TURBU	uw
3D dow	1	1.030522	0.578223	56.10973	-0.09624	0.10434	10.125	0.000925
stream	2	1.162572	0.585824	50.39034	-0.09845	0.326883	28.1172	0.014515
	3	1.352276	0.722589	53.43506	-0.03768	0.371558	27.47647	-0.01364
	4	1.370942	0.704479	51.38652	-0.03894	0.425846	31.06226	0.003725
	5	1.45095	0.692438	47.7231	-0.01127	0.451431	31.11281	0.009143
	6	1.514741	0.698804	46.13356	-0.01171	0.468802	30.94934	0.013256
	7	1.564541	0.708988	45.31607	-0.02629	0.465607	29.75997	0.020035
	8	1.583789	0.685725	43.29647	-0.01378	0.48848	30.84248	0.014023
	9	1.572892	0.701972	44.62936	-0.02786	0.483938	30.76739	0.019277
	#	1.550505	0.695175	44.83541	-0.02842	0.49408	31.86572	0.029981
	#	1.539583	0.719696	46.74614	-0.00502	0.48612	31.57476	0.020638
	#	1.475394	0.716808	48.58418	-0.01304	0.48652	32.9756	0.024317
	#	1.496491	0.758363	50.6761	-0.00779	0.484871	32.40054	0.022699
	#	1.422389	0.788943	55.46606	-0.02642	0.470913	33.10716	0.030181
	#	1.53961	0.813231	52.8206	-0.02398	0.4928	32.00814	0.046903
	#	1.359607	0.803268	59.08085	-0.04647	0.45641	33.56925	0.017029
	#	1.322793	0.818648	61.88779	-0.03588	0.503795	38.08566	0.005989
	#	1.009049	0.735229	72.86361	-0.04505	0.35524	35.20544	0.002288

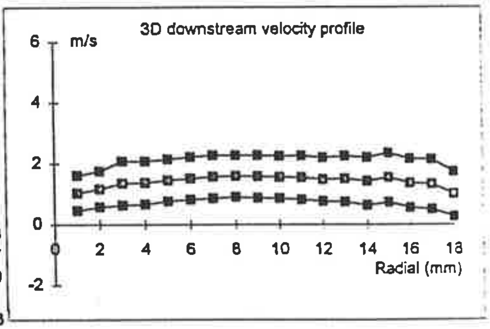

X	Y	U MEAN	U RMS	U TURBU	W MEAN	W RMS	W TURBU	uw
6D dow	1	1.259676	0.359294	28.52276	-0.03487	0.042126	3.344225	0.001598
stream	2	1.370286	0.336614	24.56522	-0.03331	0.020586	1.502311	0.000141
	3	1.397944	0.332794	23.80599	-0.06053	0.05381	3.849258	0.00034
	4	1.381575	0.326044	23.59942	-0.08553	0.093594	6.77444	0.000563
	5	1.41213	0.324189	22.95747	-0.07407	0.176395	12.49139	-0.0004
	6	1.422038	0.309217	21.74464	-0.0513	0.213024	14.98016	0.000684
	7	1.410352	0.305369	21.65201	-0.03794	0.219216	15.54335	-6.4E-05
	8	1.420444	0.295779	20.82299	-0.03439	0.218345	15.37164	0.001592
	9	1.430391	0.287022	20.06595	-0.03799	0.226721	15.85027	-0.00215
	#	1.425711	0.299191	20.98539	-0.02463	0.232049	16.27601	0.001805
	#	1.454078	0.311569	21.42723	-0.04177	0.227565	15.65009	0.003318
	#	1.461002	0.305868	20.93549	-0.02805	0.223594	15.30414	0.003374
	#	1.41524	0.32387	22.88443	-0.06083	0.274501	19.39609	0.000161
	#	1.433445	0.332891	23.22314	-0.05957	0.385088	26.86451	0.004425
	#	1.393906	0.343436	24.53838	-0.05341	0.319218	22.90094	-0.00146
	#	1.373297	0.347325	25.2913	-0.03643	0.494813	36.03105	0.001121
	#	1.309523	0.359606	27.46084	-0.02658	0.658945	50.31946	0.002361
	#	0.796079	0.528794	66.42475	-0.05437	0.430859	54.12264	-0.00602

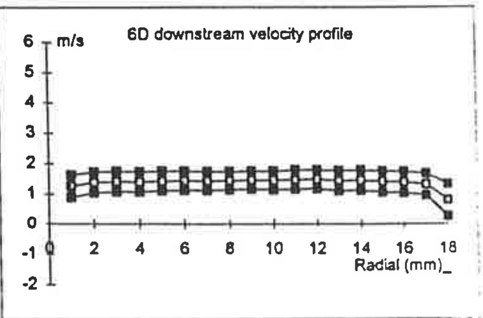

SHEAR STRESS AND TURBULENCE INTENSITY IN TRIANGULAR ORIFICE

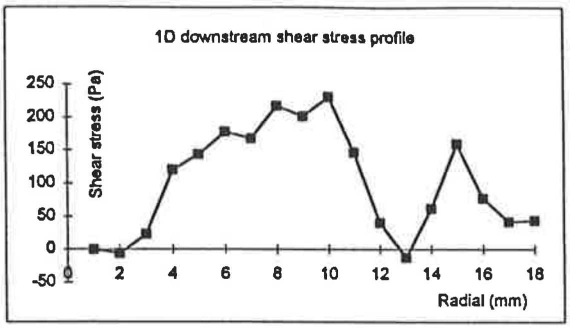

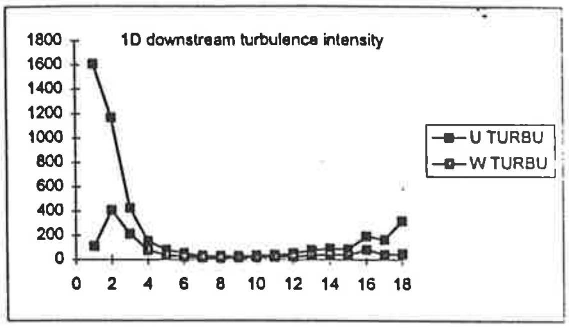

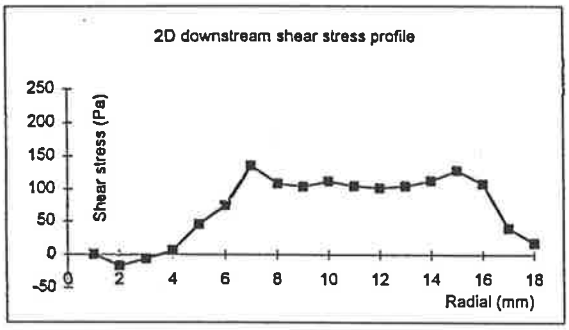

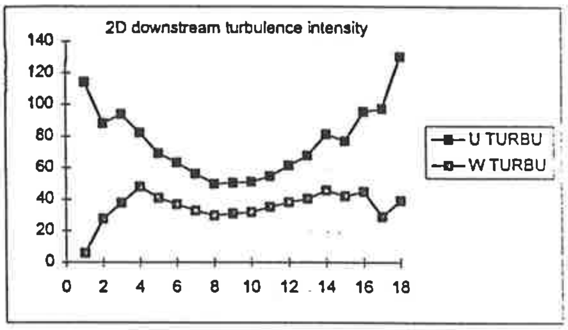

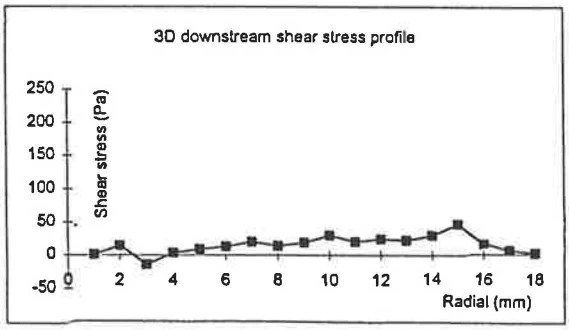

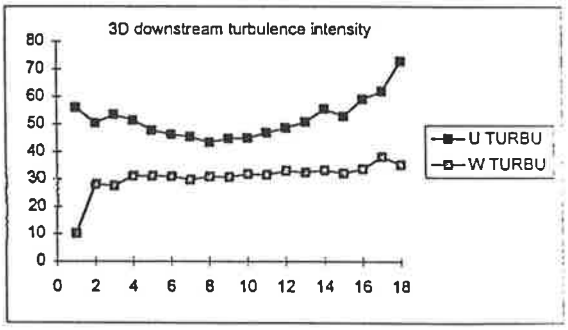

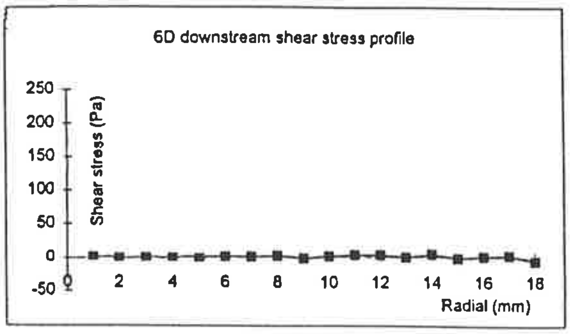

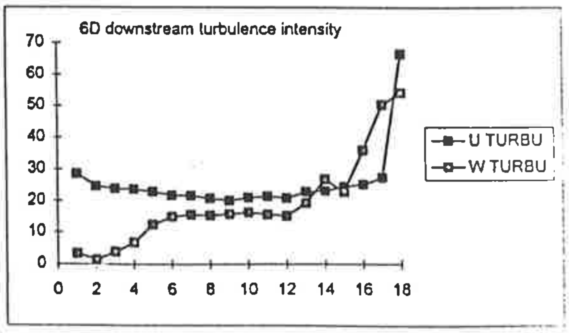

A. 4.4. Velocity data across different occluder positions

VELOCITY RAW DATA - CONCENTRIC ANNULAR ORIFICE

X	D	U MEAN	U RMS	U TURBU	W MEAN	W RMS	W TURBU	uw
1D dow	1	-0.17763	0.546149	307.4663	-0.09059	0.062871	35.3948	-0.0018
stream	2	-0.09713	0.540223	556.1886	-0.03758	0.066871	68.84695	-0.00066
	3	-0.04198	0.58049	1382.839	-0.02329	0.123628	294.5047	-0.0054
	4	0.162122	0.593131	365.8553	-0.04155	0.413768	255.2205	-0.01104
	5	0.261599	0.59163	226.1597	-0.05407	0.531864	203.3129	-0.03875
	6	0.366684	0.594241	162.0581	-0.16807	0.547002	149.1753	-0.07313
	7	0.34888	0.61817	177.1871	-0.25244	0.591151	169.4424	-0.09918
	8	0.344105	0.653481	189.9075	-0.35448	0.618844	179.8416	-0.13521
	9	0.242036	0.66919	276.4838	-0.3792	0.649657	268.4132	-0.15509
	10	0.107388	0.650112	605.3869	-0.34475	0.648602	603.9808	-0.14986
	11	0.018675	0.640627	3430.429	-0.28789	0.620767	3324.08	-0.11728
	12	-0.15028	0.582681	387.7362	-0.08574	0.606888	403.8445	-0.07168
	13	-0.285	0.535999	188.0683	0.057775	0.564718	198.1451	-0.03566
	14	-0.34829	0.529583	152.054	0.127928	0.523177	150.2148	0.00592
	15	-0.47239	0.461189	97.62959	0.106085	0.487478	103.1948	0.028103
	16	-0.57648	0.454433	78.82864	0.010319	0.466895	80.9903	0.018806
	17	-0.69858	0.427639	61.2156	-0.00558	0.403158	57.71122	0.007521
	18	-0.76574	0.376761	49.20232	-0.01289	0.379178	49.51797	0.006417

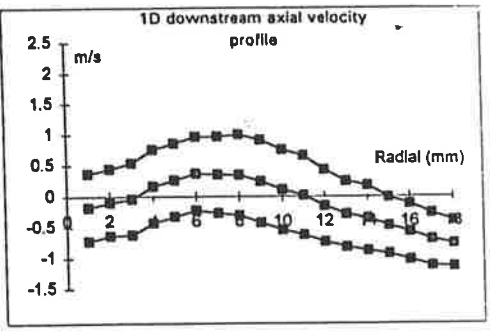

X	D	U MEAN	U RMS	U TURBU	W MEAN	W RMS	W TURBU	uw
2D dow	1	0.767004	0.434286	56.6211	-0.03393	0.020754	2.705893	0.000226
stream	2	0.984557	0.491491	49.91997	-0.0818	0.17474	17.74812	-0.00377
	3	1.110798	0.460273	41.4362	-0.05297	0.273397	24.6127	-0.00526
	4	1.23115	0.476792	38.72736	-0.06463	0.387508	31.47532	-0.00865
	5	1.302208	0.493839	37.9232	-0.07159	0.395379	30.36219	-0.01628
	6	1.339574	0.464899	34.70498	-0.06886	0.430128	32.1093	-0.01529
	7	1.355769	0.475957	35.10607	-0.09906	0.44107	32.53282	-0.01922
	8	1.373024	0.498839	36.33138	-0.1285	0.468518	34.12306	-0.03382
	9	1.375118	0.513429	37.33709	-0.19123	0.475335	34.56682	-0.05494
	10	1.324226	0.509163	38.44986	-0.19235	0.475851	35.93427	-0.0484
	11	1.230585	0.508396	41.31335	-0.15347	0.48343	39.28461	-0.05331
	12	1.151675	0.498095	43.24963	-0.13668	0.480676	41.73715	-0.043
	13	1.013941	0.493018	48.6239	-0.08096	0.479898	47.33003	-0.03261
	14	0.873253	0.478996	54.85193	-0.04499	0.453271	51.90606	-0.01273
	15	0.755036	0.442605	58.62034	0.01608	0.423506	56.09078	-0.00621
	16	0.671017	0.440519	65.64941	0.00365	0.423998	63.18735	-0.02088
	17	0.503887	0.420591	83.46922	0.038498	0.386643	76.73208	-0.01634
	18	0.320521	0.376816	117.5638	0.034621	0.347594	108.4465	-0.00401

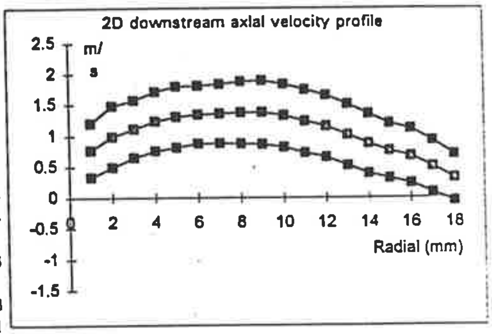

X	D	U MEAN	U RMS	U TURBU	W MEAN	W RMS	W TURBU	uw
3d dow	1	1.249469	0.343047	27.45546	-0.03236	0.023056	1.845259	0.000026
stream	2	1.394569	0.348369	24.98042	-0.07054	0.056668	4.063463	0.000084
	3	1.493036	0.351012	23.50999	-0.06516	0.16751	11.21945	-0.00101
	4	1.534344	0.345613	22.52511	-0.05529	0.325243	21.19753	0.003914
	5	1.595483	0.35619	22.32492	-0.04467	0.304988	19.11568	0.00459
	6	1.625086	0.357262	21.98422	-0.04309	0.314255	19.33777	0.007302
	7	1.647529	0.362067	21.97635	-0.0297	0.327251	19.86316	0.007306
	8	1.624733	0.362906	22.33637	-0.02594	0.335276	20.63579	0.006759
	9	1.616379	0.369165	22.83902	-0.01335	0.338343	20.93215	0.012111
	10	1.575047	0.374009	23.74587	-0.01385	0.33892	21.51811	0.012747
	11	1.517144	0.372804	24.57274	-0.04006	0.335874	22.13855	0.006358
	12	1.412861	0.378315	26.77651	-0.03215	0.322852	22.85093	0.009453
	13	1.328987	0.373373	28.09457	-0.03101	0.32452	24.41863	0.004007
	14	1.243705	0.350955	28.21854	-0.02164	0.309703	24.90168	0.005808
	15	1.125674	0.330762	29.3835	-0.01139	0.285928	25.40058	0.003384
	16	1.029047	0.323426	31.42967	0.008788	0.289035	28.08762	0.004943
	17	0.892751	0.321426	36.00394	0.010754	0.287804	32.23788	0.007151
	18	0.717136	0.336754	46.95821	-0.00539	0.263926	36.80275	0.010675

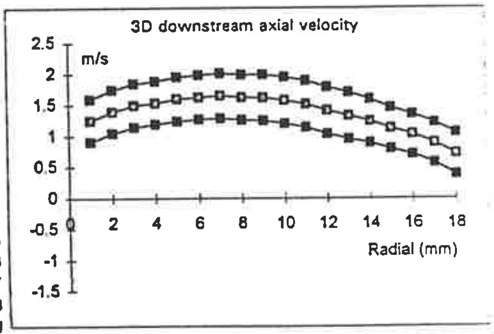

X	D	U MEAN	U RMS	U TURBU	W MEAN	W RMS	W TURBU	uw
6d dow	1	1.315779	0.375651	28.54969	-0.06188	0.106081	8.062188	-0.00188
stream	2	1.460953	0.23221	15.8944	-0.02506	0.011948	0.817829	0.000064
	3	1.505798	0.221799	14.72965	-0.02557	0.012684	0.842313	-4.8E-05
	4	1.554886	0.217279	13.97392	-0.03056	0.023961	1.541004	0.000183
	5	1.577778	0.213265	13.51677	-0.0602	0.078713	4.988876	0.000846
	6	1.585026	0.217338	13.71195	-0.02149	0.178691	11.27368	0.006739
	7	1.585368	0.214699	13.54256	-0.01201	0.162891	10.27467	0.006571
	8	1.601495	0.223912	13.98141	-0.00732	0.168492	10.52094	0.007907
	9	1.583866	0.215288	13.59254	-0.00882	0.167504	10.57567	0.004704
	10	1.567906	0.216068	13.78068	-0.01154	0.164249	10.47569	0.006207
	11	1.558798	0.216924	13.91611	-0.00648	0.172331	11.05541	0.005371
	12	1.518536	0.221563	14.59057	-0.00552	0.17143	11.28915	0.00608
	13	1.484591	0.216342	14.57252	-0.0072	0.169219	11.39836	0.003392
	14	1.430946	0.21839	15.26191	-0.0231	0.168879	11.8019	0.004337
	15	1.391134	0.213224	15.32735	-0.0352	0.170003	12.22045	0.004224
	16	1.33046	0.213487	16.04612	-0.07076	0.317	23.82636	-0.00395
	17	1.191884	0.241224	20.23889	-0.0537	0.222926	18.70365	-0.00433
	18	0.99099	0.312128	31.49656	-0.0547	0.155167	15.65776	-0.00253

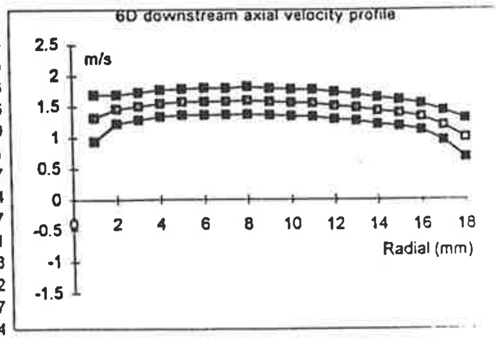

SHEAR STRESS AND TURBULENCE INTENSITY IN IN A CONCENTRIC ANNULAR ORIFICE

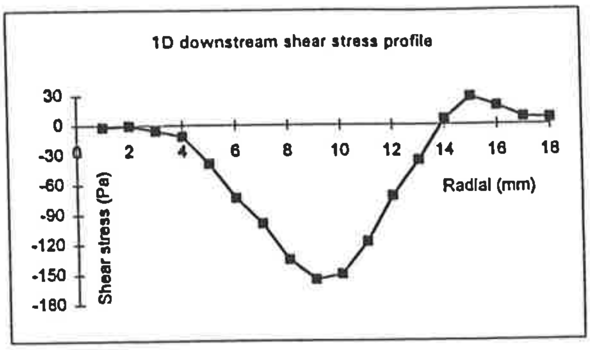

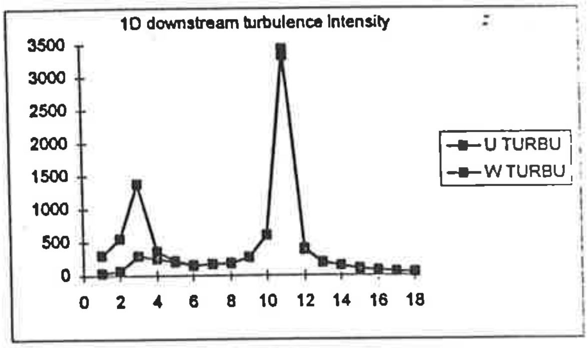

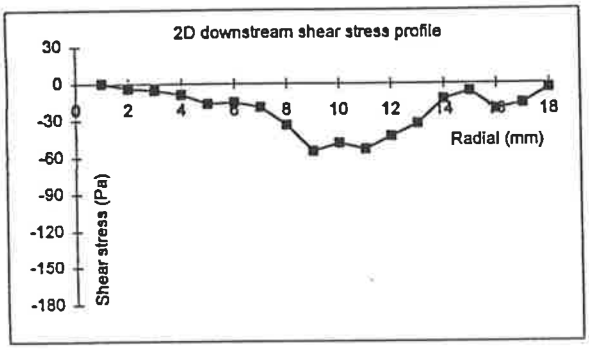

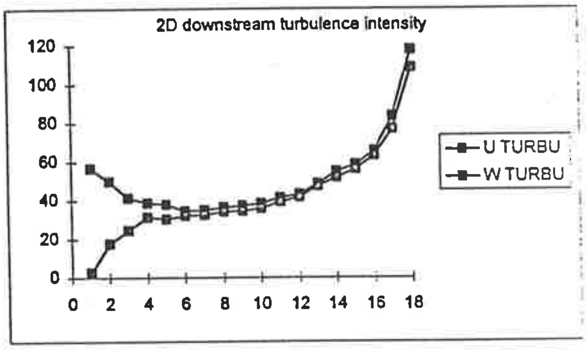

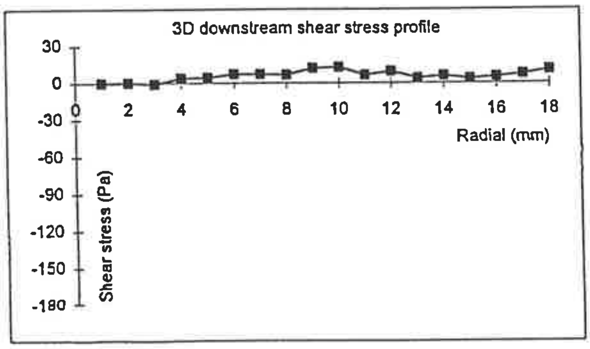

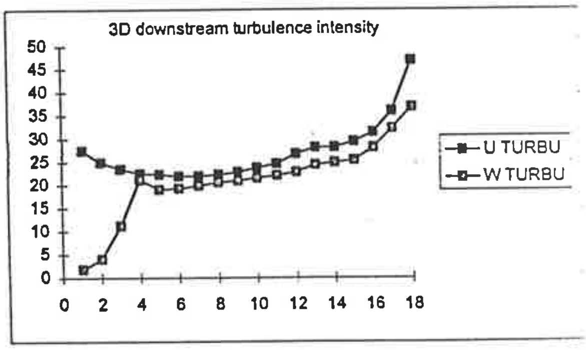

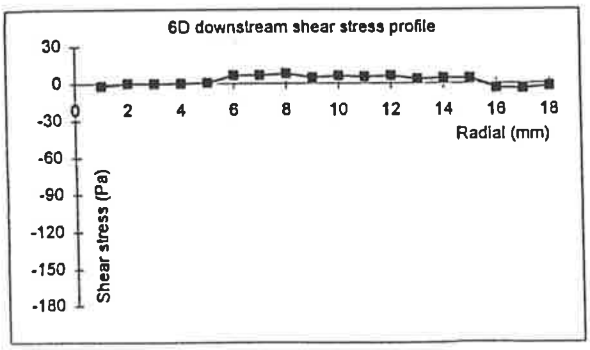

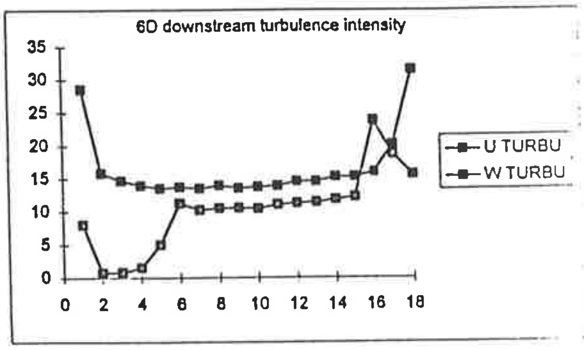

VELOCITY RAW DATA - 1mm ECCENTRIC BALL OCCLUDER

X	Y	U MEAN	U RMS	U TURBU	W MEAN	W RMS	W TURBU	uw
1D dow	1	-0.82398	0.397122	48.19538	-0.04742	0.033315	4.043176	-0.00036
stream	2	-0.74086	0.408001	55.07121	-0.06945	0.103103	13.9167	-0.00162
	3	-0.82794	0.366205	44.23071	-0.01523	0.139668	16.86928	0.004895
	4	-0.25011	0.472618	188.9645	-0.05515	0.1573	62.89255	0.000722
	5	-0.29077	0.471498	162.1536	-0.0142	0.509396	175.1868	0.014926
	6	-0.15169	0.510594	336.6016	-0.05594	0.57492	379.0074	-0.01194
	7	0.081406	0.571735	702.3272	-0.06716	0.661735	812.8848	-0.05971
	8	0.242712	0.592641	244.1746	-0.09593	0.708453	291.89	-0.07932
	9	0.348465	0.604653	173.5193	-0.12817	0.702134	201.4938	-0.08978
	#	0.502599	0.615926	122.5483	-0.19172	0.697708	138.8201	-0.1048
	#	0.689385	0.644824	93.53606	-0.22454	0.674322	97.81506	-0.11259
	#	0.866897	0.677926	78.20143	-0.27943	0.678838	78.30673	-0.1306
	#	1.0035	0.697523	69.50904	-0.25942	0.673922	67.15714	-0.16656
	#	0.993306	0.698229	70.29343	-0.19384	0.634561	63.88366	-0.1849
	#	0.865939	0.706358	81.57129	-0.09439	0.593675	68.55851	-0.17012
	#	0.74125	0.675328	91.10665	0.004531	0.541877	73.10304	-0.15061
	#	0.864087	0.66426	76.87426	-0.01206	0.523798	60.61865	-0.13316
	#	0.850164	0.642555	75.58015	-0.0766	0.468381	55.09303	-0.11454

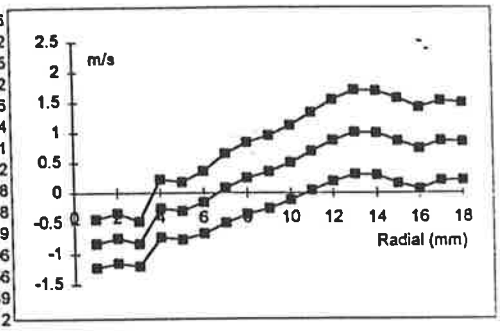

X	Y	U MEAN	U RMS	U TURBU	W MEAN	W RMS	W TURBU	uw
2D dow	1	0.466349	0.45335	97.21251	-0.03032	0.017984	3.856365	0.000446
stream	2	0.712323	0.501087	70.34552	-0.04556	0.040615	5.701742	0.000164
	3	0.806851	0.514204	63.7297	-0.09974	0.358848	44.47512	0.012925
	4	1.00509	0.518505	51.58794	-0.07446	0.450632	44.83497	0.016103
	5	1.223041	0.545734	44.62107	-0.05894	0.450842	36.86239	0.003085
	6	1.306276	0.566684	43.38162	-0.05634	0.491735	37.64402	0.003859
	7	1.467529	0.564531	38.46812	-0.06984	0.525978	35.84105	-0.00353
	8	1.535287	0.555587	36.18784	-0.05183	0.535388	34.87216	-0.00624
	9	1.568305	0.535738	34.16031	-0.04863	0.521931	33.27994	-0.00767
	#	1.564722	0.507599	32.44023	-0.00923	0.497994	31.82639	-0.00474
	#	1.544442	0.488548	31.63269	-0.0237	0.478601	30.98859	-0.00669
	#	1.510054	0.476559	31.55908	-0.01064	0.443986	29.402	-0.00899
	#	1.498165	0.476228	31.7874	-0.03038	0.433398	28.92856	-0.01955
	#	1.437781	0.470378	32.71557	-0.03476	0.424861	29.54977	-0.03377
	#	1.343158	0.497211	37.01808	-0.02744	0.407778	30.35969	-0.03796
	#	1.267054	0.502529	39.66121	-0.00972	0.398624	31.46072	-0.05124
	#	1.111872	0.48509	43.62825	-0.0219	0.382186	34.37324	-0.04795
	#	0.853555	0.458273	53.68993	-0.03325	0.342415	40.11636	-0.03422

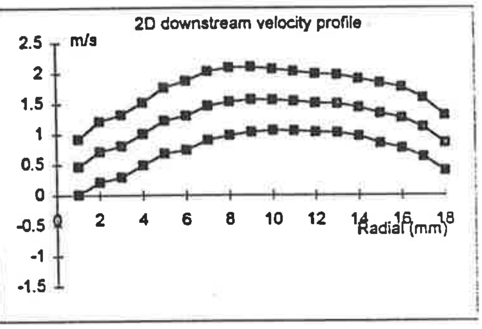

X	Y	U MEAN	U RMS	U TURBU	W MEAN	W RMS	W TURBU	uw
3D dow	1	1.114351	0.395545	35.4955	-0.03893	0.026483	2.376538	0.000463
stream	2	1.23499	0.406375	32.9051	-0.0376	0.024275	1.96562	0.000445
	3	1.369353	0.418617	30.5704	-0.08328	0.100589	7.345745	0.001413
	4	1.425765	0.415456	29.13918	-0.04011	0.343183	24.07008	0.013304
	5	1.52868	0.423366	27.69489	-0.03503	0.34981	22.88313	0.015686
	6	1.624135	0.441281	27.17024	-0.0247	0.366759	22.58181	0.025447
	7	1.703263	0.44848	26.33066	-0.01272	0.38457	22.57843	0.025301
	8	1.742769	0.445701	25.57428	-0.01094	0.389591	22.3547	0.020307
	9	1.769091	0.432701	24.45892	-0.00496	0.393376	22.23605	0.025627
	#	1.742154	0.443639	25.46495	0.000144	0.396888	22.78148	0.021107
	#	1.695408	0.435764	25.70261	0.015024	0.387457	22.85332	0.016034
	#	1.662906	0.429269	25.81437	-0.00859	0.363509	21.85988	0.007665
	#	1.577724	0.420469	26.65036	-0.01098	0.353943	22.43376	0.00505
	#	1.520549	0.421735	27.7357	-0.01835	0.332412	21.86133	-0.00305
	#	1.421074	0.423611	29.80922	-0.02217	0.326748	22.993	-0.01023
	#	1.33292	0.399879	30.00026	-0.03161	0.32484	24.37059	-0.00906
	#	1.171702	0.403749	34.45831	-0.02327	0.310017	26.45869	-0.00938
	#	0.952485	0.390503	40.99837	-0.04968	0.3006	31.55957	-0.0073

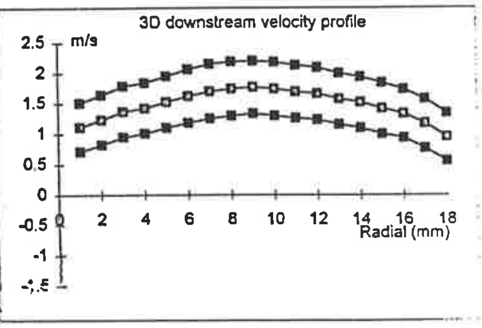

X	Y	U MEAN	U RMS	U TURBU	W MEAN	W RMS	W TURBU	uw
6D dow	1	1.446868	0.234408	16.20104	-0.05328	0.035151	2.429466	0.000155
stream	2	1.528924	0.217895	14.25154	-0.02617	0.036681	2.399114	-0.00017
	3	1.558131	0.218184	14.00294	-0.02626	0.020721	1.329842	-8.9E-05
	4	1.577675	0.21704	13.75693	-0.02464	0.068182	4.321693	-0.00051
	5	1.594527	0.215083	13.48881	-0.03577	0.031425	1.970803	-5.3E-05
	6	1.593466	0.219061	13.74744	-0.05266	0.112714	7.073503	0.001916
	7	1.579645	0.225185	14.25543	-0.02735	0.167966	10.63315	0.004131
	8	1.550518	0.233265	15.0443	-0.02715	0.178338	11.50185	0.003892
	9	1.520656	0.23704	15.58804	-0.02653	0.181386	11.92814	0.002739
	#	1.482891	0.239537	16.1534	-0.02672	0.184937	12.4714	0.002978
	#	1.454824	0.246919	16.97242	-0.02813	0.185047	12.71952	0.002698
	#	1.398738	0.247012	17.65963	-0.02895	0.189123	13.52101	0.000924
	#	1.345101	0.257632	19.15338	-0.02952	0.193982	14.42134	0.001635
	#	1.314785	0.249269	18.9589	-0.02414	0.199538	15.1765	0.001592
	#	1.247336	0.248661	19.93535	-0.03789	0.208198	16.6914	-0.00238
	#	1.195137	0.241892	20.23968	-0.04493	0.294321	24.62651	-0.00313
	#	1.098167	0.252943	23.03323	-0.04258	0.308079	28.05394	-0.00692
	#	0.908437	0.306495	33.73873	-0.05226	0.18995	20.90956	-0.00455

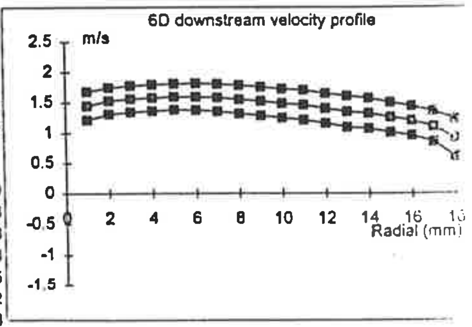

SHEAR STRESS AND TURBULENCE INTENSITY IN 1 mm ECCENTRIC BALL OCCLUDER

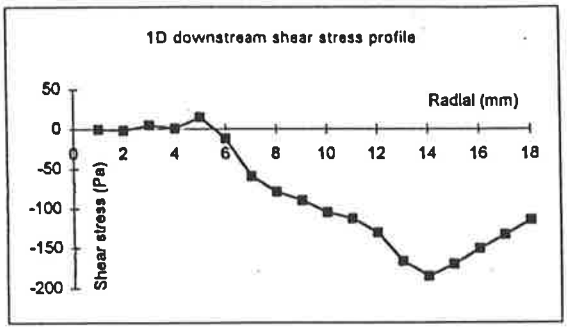

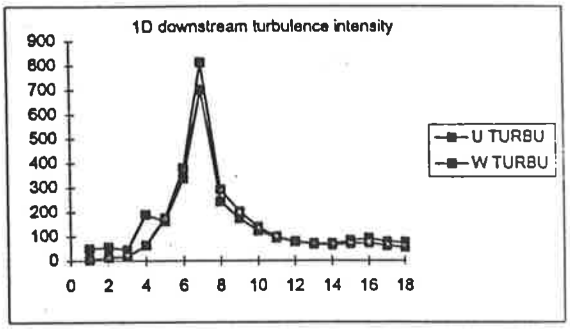

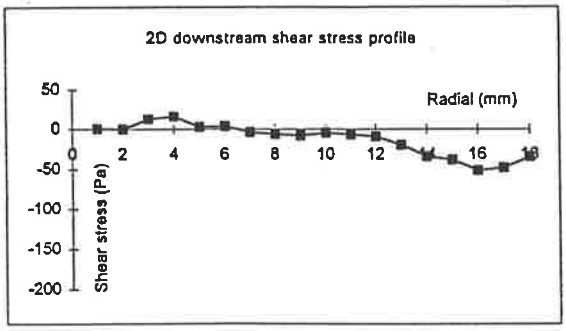

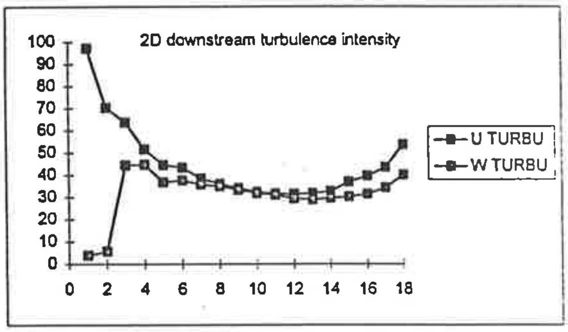

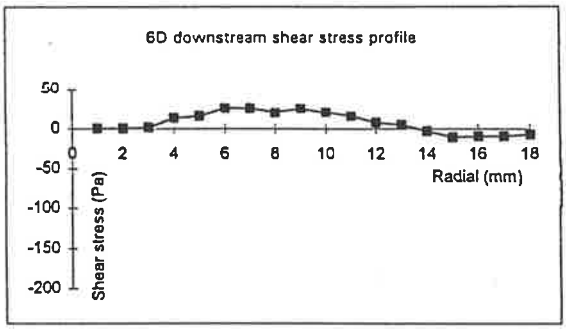

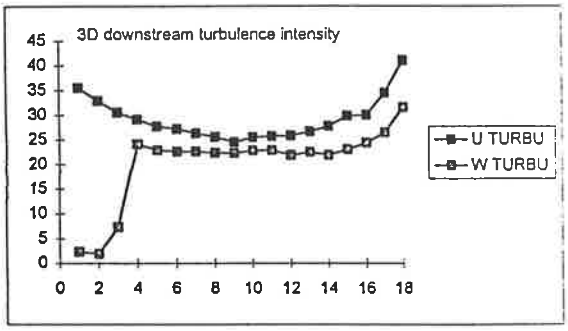

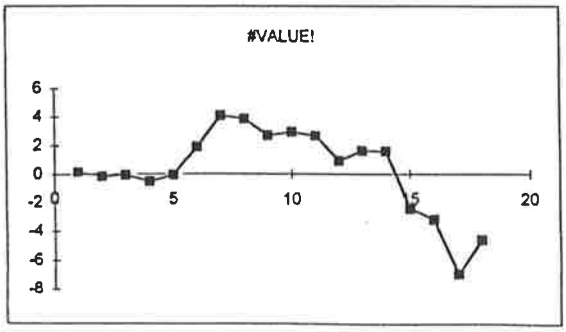

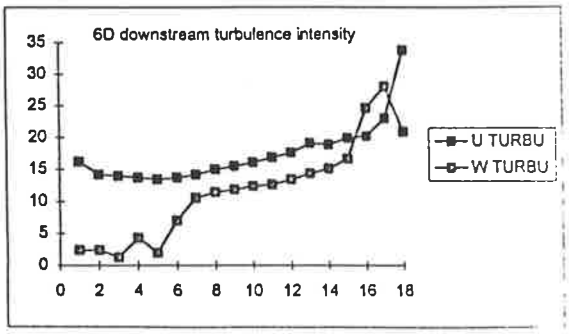

VELOCITY RAW DATA - 2 mm ECCENTRIC BALL OCCLUDER

X	Y	U MEAN	U RMS	U TURBU	W MEAN	W RMS	W TURBU	uw
1D dow	1	-0.54985	0.577471	105.0228	-0.04796	0.041571	7.56048	0.000611
stream	2	-0.29099	0.603369	207.3539	-0.02615	0.019604	6.737289	-0.00017
	3	-0.02763	0.6342	2295.341	-0.0539	0.08478	306.8432	-0.00037
	4	0.225388	0.644398	285.9067	-0.1435	0.393515	174.5947	-0.00016
	5	0.505621	0.688493	136.1678	-0.29113	0.687694	136.0099	-0.04627
	6	0.756879	0.75349	99.55226	-0.28556	0.794838	105.0153	-0.10826
	7	0.901804	0.768241	85.18932	-0.26464	0.829759	92.01093	-0.11401
	8	0.932309	0.778151	83.46494	-0.14179	0.863332	92.60145	-0.12825
	9	0.868189	0.766345	88.26932	-0.02518	0.873116	100.5675	-0.082
	#	0.740509	0.736318	99.43395	-0.00261	0.827517	111.7497	-0.06655
	#	0.44771	0.690748	154.2846	0.002034	0.742776	165.9055	-0.03865
	#	0.119166	0.654207	548.9878	-0.03844	0.641435	538.2698	-0.03251
	#	-0.24577	0.616703	250.9268	-0.04427	0.538928	219.2814	-0.04457
	#	-0.53887	0.569105	105.6115	0.012218	0.484129	89.84218	-0.04981
	#	-0.70917	0.544168	76.73357	0.08445	0.452977	63.87468	-0.03969
	#	-0.46921	0.705126	150.2789	0.063922	0.527507	112.4241	-0.06309
	#	0.152665	0.83213	545.0693	-0.08511	0.616958	404.1257	-0.13814
	#	0.386071	0.790992	204.8824	-0.25267	0.467899	121.1949	-0.09807

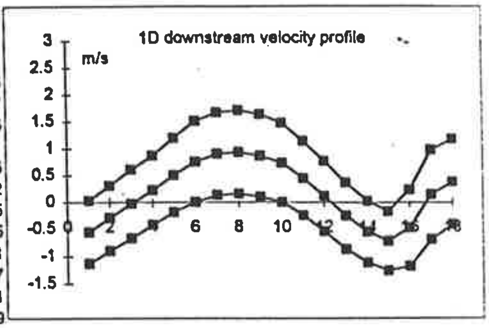

X	Y	U MEAN	U RMS	U TURBU	W MEAN	W RMS	W TURBU	uw
2D dow	1	0.918172	0.587286	63.96252	-0.05619	0.055218	6.013949	0.001445
stream	2	1.10334	0.60177	54.54077	-0.03434	0.03133	2.839538	0.000205
	3	1.32056	0.667795	50.5691	-0.03134	0.029739	2.251992	-0.00017
	4	1.52366	0.670252	43.98961	-0.05236	0.109986	7.21855	0.000093
	5	1.639697	0.683918	41.71005	-0.01287	0.607812	37.06858	0.016965
	6	1.811368	0.69338	38.27935	0.016502	0.64224	35.45605	0.014154
	7	1.913399	0.726834	37.98652	0.04298	0.683814	35.7382	0.01663
	8	1.912855	0.728393	38.07886	0.072467	0.703719	36.78891	0.037955
	9	1.838086	0.734724	39.97223	0.057785	0.721813	39.26984	0.022797
	#	1.741782	0.724542	41.59773	0.037082	0.723383	41.53122	0.017029
	#	1.550678	0.713095	45.98601	-0.02296	0.709526	45.75583	-0.0013
	#	1.302858	0.7171	55.04052	-0.03015	0.666348	51.14505	-0.01026
	#	1.035791	0.693632	66.96639	-0.04837	0.589644	56.92693	-0.03245
	#	0.697125	0.623557	89.44698	-0.07659	0.516213	74.04883	-0.04287
	#	0.434879	0.560859	128.9691	-0.09623	0.473466	108.8732	-0.03565
	#	0.211555	0.503586	238.04	-0.10003	0.444808	210.2562	-0.04111
	#	0.050711	0.450478	888.3177	-0.11614	0.399869	788.5186	-0.03498
	#	-0.03147	0.407914	1296.112	-0.11478	0.30977	984.2675	-0.01857

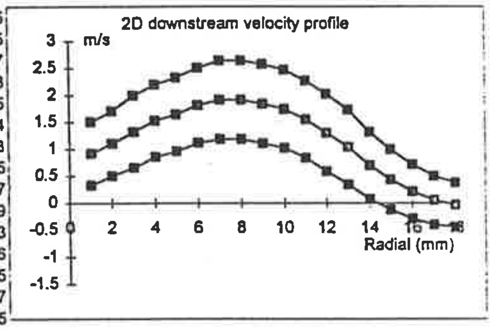

X	Y	U MEAN	U RMS	U TURBU	W MEAN	W RMS	W TURBU	uw
3D dow	1	1.354082	0.439381	32.44865	-0.02807	0.021113	1.559196	0.00005
stream	2	1.452461	0.439864	30.28403	-0.0461	0.05006	3.446572	0.000224
	3	1.557544	0.463484	29.75736	-0.03671	0.033524	2.152354	0.000648
	4	1.627299	0.479677	29.4769	-0.05451	0.076847	4.722379	0.00078
	5	1.660862	0.499656	30.08417	-0.0396	0.409052	24.62891	-0.0029
	6	1.709385	0.508559	29.75101	-0.01983	0.419706	24.55306	-0.00822
	7	1.765491	0.524664	29.71775	-0.02817	0.439009	24.86613	-0.0127
	8	1.800801	0.54259	30.13049	-0.0057	0.463764	25.75323	-0.01317
	9	1.800688	0.539735	29.97379	-0.03583	0.474322	26.34113	-0.00706
	#	1.752832	0.55027	31.39322	-0.03017	0.486371	27.74774	-0.01674
	#	1.690853	0.568958	33.64918	-0.02275	0.502538	29.72098	-0.01686
	#	1.544727	0.575363	37.24692	-0.02759	0.492566	31.8869	-0.01916
	#	1.390448	0.561963	40.41599	-0.03902	0.49317	35.46843	-0.0125
	#	1.25306	0.534733	42.67414	-0.04376	0.481987	38.46476	-0.01739
	#	1.065489	0.497281	46.67162	-0.05538	0.462939	43.44845	-0.00287
	#	0.938322	0.454107	48.3956	-0.01666	0.433993	46.25208	0.004582
	#	0.818392	0.421089	51.45326	-0.03115	0.367919	44.95631	-0.00346
	#	0.657472	0.40845	62.12436	-0.03008	0.156991	23.87801	-0.00175

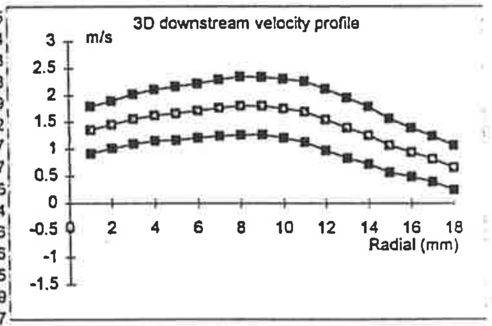

X	Y	U MEAN	U RMS	U TURBU	W MEAN	W RMS	W TURBU	uw
6D dow	1	1.434509	0.330067	23.00902	-0.07561	0.078057	5.441389	0.000176
stream	2	1.542288	0.228756	14.83224	-0.03594	0.036959	2.396397	-0.00021
	3	1.555448	0.218102	14.0218	-0.03979	0.097987	6.299614	-0.00072
	4	1.562884	0.215909	13.8148	-0.03791	0.102637	6.567127	-0.00014
	5	1.556591	0.213537	13.71823	-0.04437	0.066142	4.249187	-0.00058
	6	1.54411	0.213239	13.80981	-0.05958	0.078902	5.109881	-0.00115
	7	1.521472	0.217688	14.3077	-0.03964	0.157283	10.33752	-0.00199
	8	1.506339	0.22404	14.87317	-0.03254	0.168984	11.21822	-0.00512
	9	1.478063	0.230911	15.62254	-0.03928	0.181171	12.25731	-0.00572
	#	1.443384	0.236769	16.40375	-0.03809	0.184046	12.75101	-0.0064
	#	1.412914	0.23773	16.82551	-0.03872	0.190306	13.46906	-0.00432
	#	1.379849	0.239371	17.34759	-0.03936	0.192067	13.91941	-0.00481
	#	1.347421	0.245291	18.20452	-0.06534	0.205849	15.27725	-0.00378
	#	1.301393	0.237799	18.27268	-0.06921	0.213171	16.38022	-0.00305
	#	1.272792	0.23469	18.439	-0.07097	0.238403	18.73069	-0.00561
	#	1.242954	0.235651	18.95892	-0.04675	0.20299	16.33128	-0.00352
	#	1.149893	0.252508	21.95928	-0.04826	0.190974	16.60798	-0.0046
	#	0.959839	0.310809	32.38142	-0.04853	0.152605	15.89901	-0.0048

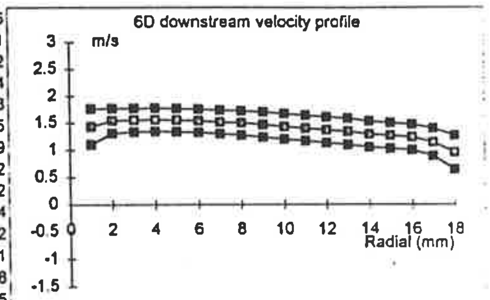

SHEAR STRESS AND TURBULENCE INTENSITY IN 2 mm ECCENTRIC BALL OCCLUDER